

MoDOT

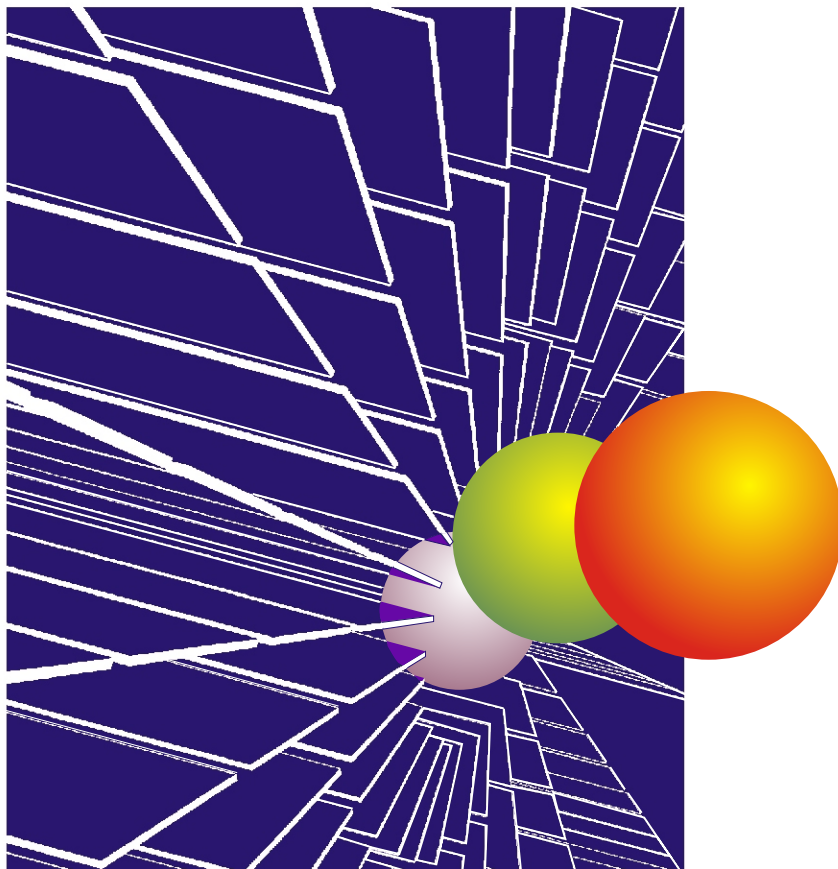
Research, Development and Technology

University of Missouri-Rolla

RDT 04-021

Structural Integrity of RC Columns Wrapped with FRP Sheet Subjected to Various Environmental Conditions Including Corrosion

RI 99-007
RI 99-007B



September, 2004

TECHNICAL REPORT DOCUMENTATION PAGE

1. Report No. RDT 04-021	2. Government Accession No.	3. Recipient's Catalog No.	
4. Title and Subtitle Structural Integrity of RC Columns Wrapped with FRP Sheet Subjected to Various Environmental Conditions Including Corrosion		5. Report Date November 2004	
		6. Performing Organization Code University of Missouri-Rolla	
7. Author(s) Abdeldjelil Belarbi, John J. Myers, K. Chandarshekhara, Steve E. Watkins, and Sang-Wook Bae		8. Performing Organization Report No. RDT 04-021/ RI 99-007, RI 99-007B	
9. Performing Organization Name and Address University of Missouri-Rolla Dept. of Civil, Architectural, and Environmental Engineering 211 Butler-Carlton Hall Rolla, Missouri 65409-0030		10. Work Unit No.	
		11. Contract or Grant No.	
12. Sponsoring Agency Name and Address Missouri Department of Transportation Research, Development and Technology Division P. O. Box 270-Jefferson City, MO 65102		13. Type of Report and Period Covered Final Report, May, 1 2000 - Nov. 17, 2004	
		14. Sponsoring Agency Code MoDOT	
15. Supplementary Notes The investigation was conducted in cooperation with the U. S. Department of Transportation.			
16. Abstract <p>Although the short-term performance of reinforced concrete (RC) columns wrapped with fiber reinforced polymer (FRP) composite materials has been widely studied, research studies on the long-term performance are limited. The objective of this study was to evaluate the effects of various environmental conditions on the long-term behavior of RC columns wrapped with FRP sheets.</p> <p>The experimental program comprised two parts; ambient environmental effect tests and corrosion tests. The environmental conditions considered in the ambient environmental tests included (1) freeze-thaw cycles, (2) high-temperature cycles, (3) high-humidity cycles, (4) ultraviolet (UV) radiation, and (5) saline solution; while the corrosion tests dealt with the corrosion of steel reinforcement embedded in RC columns wrapped with FRP sheets. RC columns were wrapped with carbon fiber reinforced polymer (CFRP) sheets and glass fiber reinforced polymer (GFRP) sheets and conditioned under the environmental conditions listed. After the environmental conditioning, uni-axial compression tests were conducted in order to evaluate the effects on the mechanical properties, such as column capacity, stiffness, and ductility.</p> <p>The test results showed that the mechanical properties were affected due to the environmental conditioning and the corrosion of steel reinforcement, and the effects varied according to the types of environmental conditions. Based on these results, improved design guidelines for the RC columns wrapped with FRP sheet were proposed. The proposed design guidelines included an analytical model and reduction factors to account for the effects of various environmental conditions.</p>			
17. Key Words Corrosion of Steel Reinforcement FRP Sheets Freeze-Thaw Cycles High-Humidity Cycles High-Temperature Cycles RC Columns Saline Solution		18. Distribution Statement No restrictions. This document is available to the public through National Technical Information Center, Springfield, Virginia 22161	
19. Security Classification (of this report) Unclassified	20. Security Classification (of this page) Unclassified	21. No. of Pages 211	22. Price

FINAL REPORT

RDT 04-021

Structural Integrity of RC Columns Wrapped with FRP Sheet Subjected to Various Environmental Conditions Including Corrosion

Prepared for the

Missouri Department of Transportation

by

Principal Investigators:

Dr. Abdeldjelil Belarbi, Professor

Department of Civil, Architectural, and Environmental Engineering

Dr. John J. Myers, Assistant Professor

Department of Civil, Architectural, and Environmental Engineering

Dr. K. Chandrashekhara, Professor

Department of Mechanical Engineering

Dr. Steve E. Watkins, Associate Professor

Department of Electrical and Computer Engineering

Graduate Research Assistant:

Sang-Wook Bae, Ph.D. Candidate

Department of Civil, Architectural, and Environmental Engineering

University of Missouri-Rolla

November 2004

ABSTRACT

Although the short-term performance of reinforced concrete (RC) columns wrapped with fiber reinforced polymer (FRP) composite materials has been widely studied, research studies on the long-term performance are limited. The objective of this study was to evaluate the effects of various environmental conditions on the long-term behavior of RC columns wrapped with FRP sheets.

The experimental program comprised two parts; ambient environmental effect tests and corrosion tests. The environmental conditions considered in the ambient environmental tests included (1) freeze-thaw cycles, (2) high-temperature cycles, (3) high-humidity cycles, (4) ultraviolet (UV) radiation, and (5) saline solution; while the corrosion tests dealt with the corrosion of steel reinforcement embedded in RC columns wrapped with FRP sheets. RC columns were wrapped with carbon fiber reinforced polymer (CFRP) sheets and glass fiber reinforced polymer (GFRP) sheets and conditioned under the environmental conditions listed. After the environmental conditioning, uni-axial compression tests were conducted in order to evaluate the effects on the mechanical properties, such as column capacity, stiffness, and ductility.

The test results showed that the mechanical properties were affected due to the environmental conditioning and the corrosion of steel reinforcement, and the effects varied according to the types of environmental conditions. Based on these results, improved design guidelines for the RC columns wrapped with FRP sheet were proposed. The proposed design guidelines included an analytical model and reduction factors to account for the effects of various environmental conditions.

ACKNOWLEDGEMENT

This research project was supported by Missouri Department of Transportation, UMR University Transportation Center, and Manufacturing Research & Training Center. Their support is gratefully acknowledged, with special note of appreciation to Missouri Department of Transportation, the lead funding source of this project.

TABLE OF CONTENTS

	Page
ABSTRACT.....	iii
ACKNOWLEDGEMENT	iv
LIST OF ILLUSTRATIONS.....	xi
LIST OF TABLES.....	xv
NOMENCLATURE	xviii
SECTION	
1. INTRODUCTION	1
1.1. BACKGROUND	1
1.1.1. Fiber Reinforced Polymer Composite Materials	1
1.1.2. Applications of FRP Composite Materials in Civil Engineering Infrastructures.....	1
1.1.3. Repair/Rehabilitation of RC Columns by FRP Sheet Wrapping.....	2
1.1.4. Durability Issue of RC Columns Wrapped with FRP Sheets	3
1.1.5. Corrosion of Steel Reinforcements of RC Columns Wrapped with FRP Sheets	4
1.2. OBJECTIVES OF THIS STUDY.....	5
1.3. RESEARCH PLAN AND METHODOLOGY	5
1.3.1. Ambient Environmental Effect Tests.....	6
1.3.2. Corrosion Tests	6
1.4. ORGANIZATION OF THE REPORT	7
2. LITERATURE REVIEW	8
2.1. GENERAL.....	8
2.2. ENVIRONMENTAL CONDITIONS AFFECTING THE DURABILITY OF FRP COMPOSITE.....	8
2.2.1. Moisture Effects.....	8
2.2.2. Alkali Effects	9
2.2.3. Thermal Effects.....	10
2.2.4. Creep and Stress Rupture.....	10
2.2.5. Fatigue.....	10
2.2.6. Fire	11

2.2.7. Ultraviolet Radiation.....	11
2.3. RECENT RESEARCH STUDIES RELATED TO LONG-TERM DURABILITY OF FRP COMPOSITE SYSTEMS	11
2.3.1. Freeze and Freeze-Thaw Conditions	12
2.3.2. Wet-Dry Cycles and Corrosion of Steel Reinforcements.....	13
2.3.3. Combined Environmental Conditions	15
2.3.4. Creep and Fatigue	16
2.3.5. Field Study	17
2.4. RESEARCH STUDIES ON THE DURABILITY OF RC COLUMNS WRAPPED WITH FRP COMPOSITE MATERIALS	17
2.5. SUMMARY.....	17
3. EXPERIMENTAL PROGRAM.....	19
3.1. GENERAL.....	19
3.2. AMBIENT ENVIRONMENTAL EFFECT TESTS	19
3.2.1. Small-Scale RC Column Tests.....	19
3.2.1.1 Test matrix	19
3.2.1.2 Materials used	21
3.2.1.2.1 Concrete	21
3.2.1.2.2 Steel reinforcements.....	23
3.2.1.2.3 FRP sheets.....	24
3.2.1.3 Specimen detail and manufacturing.....	25
3.2.1.4 Environmental conditioning.....	26
3.2.1.5 Test set-up and instrumentation	28
3.2.2. Mid-Scale RC Column Tests	30
3.2.2.1 Test matrix	30
3.2.2.2 Materials used	31
3.2.2.3 Specimen detail and manufacturing.....	31
3.2.2.4 Test set-up and instrumentation	33
3.2.2.5 Environmental conditioning.....	33
3.3. CORROSION TESTS.....	34
3.3.1. Small-Scale RC Column Tests.....	34
3.3.1.1 Test matrix	34
3.3.1.2 Materials used	36
3.3.1.3 Specimen detail and manufacturing.....	36
3.3.1.4 Accelerated corrosion process	36
3.3.1.5 Repair of the columns damaged by the accelerated corrosion process.....	41
3.3.1.5.1 Conventional method.....	41

3.3.1.5.2 CFRP sheet wrapping after epoxy injection into cracks	44
3.3.1.5.3 CFRP sheet wrapping without epoxy injection into cracks	44
3.3.1.6 Test set-up and instrumentation	44
3.3.2. Mid-Scale RC Column Tests	46
3.3.2.1 Test matrix	46
3.3.2.2 Materials used	46
3.3.2.3 Specimen detail and manufacturing	47
3.3.2.4 Accelerated corrosion process	49
3.3.2.5 Repair of the columns damaged by the accelerated corrosion process	49
3.3.2.6 Environmental conditioning	49
3.3.2.7 Test set-up and instrumentation	49
4. TEST RESULTS AND DISCUSSIONS	50
4.1. GENERAL	50
4.2. DEFINITIONS OF MECHANICAL PROPERTIES OF FRP CONFINED COLUMNS	50
4.3. AMBIENT ENVIRONMENTAL EFFECT TESTS	52
4.3.1. Small-Scale RC Column Tests	52
4.3.1.1 Behavior of the control columns	54
4.3.1.1.1 Failure load, P_u	55
4.3.1.1.2 Failure modes	55
4.3.1.2 Effects of freeze-thaw cycles on the FRP wrapped columns	57
4.3.1.3 Effects of combined environmental cycles on the FRP wrapped columns	59
4.3.1.4 Effects of saline solution on the FRP wrapped columns	62
4.3.1.5 Effects of high-temperature cycles with UV radiation and high-humidity cycles on the FRP wrapped columns	66
4.3.1.6 Strain reduction factor, R_c	68
4.3.1.7 Strength reduction factor, ϕ_{env}	71
4.3.1.7.1 Strength reduction factor, ϕ_{FT}	72
4.3.1.7.2 Strength reduction factor, ϕ_{Na}	73
4.3.1.7.3 Strength reduction factor, ϕ_H	74
4.3.2. Mid-Scale RC Column Tests	74
4.3.2.1 Failure mode	74
4.3.2.2 Effects of freeze-thaw cycles on the FRP wrapped columns	77

4.3.2.3 Effects of combined environmental cycles on FRP wrapped columns.....	78
4.3.3. Summary and Conclusions	78
4.4. CORROSION TESTS.....	82
4.4.1. Definition of Corrosion Rate	82
4.4.2. Small-Scale RC Column Tests.....	83
4.4.2.1 Results of accelerated corrosion process	84
4.4.2.1.1 Corrosion rate.....	84
4.4.2.1.2 Corrosion damages due to the accelerated corrosion process.....	91
4.4.2.2 Results of failure tests.....	98
4.4.2.2.1 Failure modes.....	98
4.4.2.2.2 Failure load	102
4.4.2.3 Area reduction factor, ϕ_{cor}	112
4.4.2.3.1 Area reduction factor, ϕ_{cor1}	112
4.4.2.3.2 Area reduction factor, ϕ_{cor2}	112
4.4.2.3.3 Relationship between area reduction factors, ϕ_{cor1} and ϕ_{cor2}	113
4.4.2.3.4 Determination of area reduction factor, ϕ_{cor}	114
4.4.2.4 Decrease in ultimate tensile strain of CFRP sheets	116
4.4.3. Mid-Scale RC Column Tests	118
4.4.3.1 Results of accelerated corrosion process	118
4.4.3.1.1 Corrosion rate.....	118
4.4.3.1.2 Corrosion damages due to the accelerated corrosion process.....	119
4.4.3.1.3 Radial strains.....	120
4.4.3.2 Results of failure tests.....	122
4.4.3.2.1 Failure modes.....	122
4.4.3.2.2 Failure load, P_u	123
4.4.4. Summary and Conclusions	125
5. ANALYTICAL MODEL	127
5.1. GENERAL.....	127
5.2. ELASTIC BEHAVIOR OF CONCRETE CONFINED BY FRP SHEET.....	127
5.3. VARIABLE POISSON'S RATIO OF CONCRETE CONFINED BY FRP SHEET.....	131
5.4. MANDER ET AL.'S MODEL FOR STEEL CONFINED CONCRETE	132

5.5. A STEP BY STEP APPLICATION OF MANDER ET AL.'S MODEL TO FRP CONFINED CONCRETE	134
5.6. COMPARISON OF THE PREDICTIONS BY THE PROPOSED ANALYTICAL MODEL WITH EXPERIMENTAL RESULTS	137
5.6.1. Small-Scale RC Columns in this Study	137
5.6.2. Xiao and Wu (2000).....	140
5.6.3. Toutanji (1999)	141
5.6.4. Ilki and Kumbasar (2002)	141
5.6.5. Samaan et al. (1998)	142
5.6.6. Karbhari and Gao (1997)	143
5.7. SUMMARY AND CONCLUSIONS	145
6. DESIGN GUIDELINES	146
6.1. GENERAL	146
6.2. SCOPE AND LIMIT	146
6.3. DESIGN EQUATIONS	146
6.4. MATERIAL PROPERTIES	147
6.4.1. Concrete	147
6.4.2. Steel Reinforcement.....	148
6.4.3. FRP Sheet.....	148
6.5. STRENGTH REDUCTION FACTOR, ϕ_{env}	149
6.6. COMPRESSIVE STRENGTH OF FRP CONFINED CONCRETE, f'_{cc}	149
6.7. REDUCED CROSS-SECTIONAL AREA OF STEEL REINFORCEMENTS, $(A_{st})_{cor}$, AND AREA REDUCTION FACTOR, ϕ_{cor1}	149
6.8. EQUIVALENT AREA, A_{eqv} , AND AREA REDUCTION FACTOR, ϕ_{cor2}	150
6.9. COMPARISON OF EXPERIMENTAL RESULTS AND PREDICTIONS CALCULATED BY THE PROPOSED DESIGN GUIDELINES.....	151
6.9.1. Mid-Scale RC Columns of Ambient Environmental Effect Tests	152
6.9.1.1 Material properties of mid-scale RC columns wrapped with FRP sheets	152
6.9.1.1.1 Concrete	152

6.9.1.1.2 Steel reinforcements.....	153
6.9.1.1.3 FRP sheets.....	153
6.9.1.2 Compressive strength, f'_{cc} , of the mid-scale RC columns.....	153
6.9.1.3 Performance of strength reduction factor, ϕ_{env}	155
6.9.2. Mid-Scale RC Columns of Corrosion Tests	157
6.9.2.1 Material properties of mid-scale RC columns wrapped with CFRP sheets	157
6.9.2.1.1 Concrete	157
6.9.2.1.2 Steel reinforcement	157
6.9.2.1.3 Aluminum pipe	157
6.9.2.1.4 FRP sheets.....	157
6.9.2.2 Compressive strength f'_{cc} of mid-scale RC columns.....	158
6.9.2.3 Area reduction factors ϕ_{cor1} and ϕ_{cor2}	158
6.9.2.4 Reduced cross-sectional area of steel reinforcement, $(A_{st})_{cor}$, and equivalent area, A_{eqv}	159
6.9.2.5 Axial compressive capacity P_n	160
6.10. SUMMARY AND CONCLUSIONS	162
7. CONCLUSIONS AND RECOMMENDATIONS FOR FUTURE RESEARCH.....	163
7.1. SUMMARY OF RESEARCH WORK.....	163
7.2. CONCLUSIONS.....	164
7.2.1. Ambient Environmental Effect Tests.....	164
7.2.2. Corrosion Tests	166
7.2.3. Analytical Model	167
7.2.4. Design Guidelines.....	167
7.3. GENERAL CONCLUSION	167
7.4. RECOMMENDATIONS FOR FUTURE RESEARCH.....	168
APPENDIX A.....	169
APPENDIX B	179
BIBLIOGRAPHY	185

LIST OF ILLUSTRATIONS

Figure	Page
3.1. Experimental Results of Tensile Tests of Number 3 Reinforcing Bars.....	24
3.2. Details of Small-Scale RC Column	25
3.3. Small-Scale RC Columns after FRP Wrapping	25
3.4. Combined Environmental Cycle.....	26
3.5. Freeze-Thaw Cycle	27
3.6. High-Temperature Cycle	27
3.7. High-Humidity Cycle.....	28
3.8. Test Set-Up and Instrumentation of Small-Scale RC Columns.....	29
3.9. Detail of Mid-Scale Column.....	32
3.10. Mid-Scale RC Columns after FRP Sheet Wrapping.....	32
3.11. Test Set-Up and Instrumentation of Mid-Scale Column	33
3.12. Details of Small-Scale RC Columns for Corrosion Test	37
3.13. Schematic Drawing of Corrosion Process of Steel Reinforcement in Concrete.....	38
3.14. Schematic Drawing of the Accelerated Corrosion Process	39
3.15. Laboratory Set-Up of the Accelerated Corrosion Process.....	40
3.16. Column R-COV after the Second Stage of the Accelerated Corrosion Process.....	42
3.17. Removing of Corrosion-Damaged Concrete Cover by Pneumatic Hammer.....	42
3.18. Column R-COV after Removing of Corrosion-Damaged Concrete Cover.....	43
3.19. Procedure of Epoxy Injection Method.....	45
3.20. Experimental Results of Tensile Test of Aluminum 6061-T6 Bars and Bi-Linear Model.....	47
3.21. Details of Mid-Scale RC Columns for Corrosion Tests	48
3.22. Steel Cages and Aluminum Pipes Used for the Mid-Scale RC Columns of Corrosion Tests.....	48
3.23. Column M-CONT in Testing.....	49
4.1. Typical Load - Axial Strain Curve of FRP Wrapped Columns.....	50
4.2. Applied Load vs. Axial Strain Curves of the Group 1 Columns	55
4.3. Average Failure Load, P_u , of Group 1 Columns.....	56
4.4. Columns S-CONT, S-C1-CONT, and S-G1-CONT after Failure	56
4.5. Average Failure Load, P_u , of Group 2 Columns.....	57

4.6. Average Axial Rigidity in the Plastic Region, $(EA)_2$, of Group 2 Columns.....	58
4.7. Average Ductility Index, μ , of Group 2 Columns.....	59
4.8. Average Failure Load, P_u , of Group 3 Columns.....	60
4.9. Average Axial Rigidity in the Plastic Region, $(EA)_2$, of Group 3 Columns.....	61
4.10. Average Ductility Index, μ , of Group 3 Columns.....	61
4.11. Average Failure Load, P_u , of Group 4 Columns.....	63
4.12. Average Axial Rigidity in the Plastic Region, $(EA)_2$, of Group 4 Columns.....	65
4.13. Average Ductility Index, μ , of Group 4 Columns.....	65
4.14. Average Failure Load, P_u , of Group 5 Columns.....	67
4.15. Average Axial Rigidity in the Plastic Region, $(EA)_2$, of Group 5 Columns.....	67
4.16. Average Ductility Index, μ , of Group 5 Columns.....	68
4.17. Ratio of Measured Ultimate Tensile Strains to Ultimate Tensile Strain Provided by Manufacturer (CFRP Sheet).....	69
4.18. Ratio of Measured Ultimate Tensile Strains to Ultimate Tensile Strain Provided by Manufacturer (GFRP Sheet).....	69
4.19. Applied Load vs. Axial Strain Curves of Mid-Scale RC Columns Wrapped with CFRP Sheets.....	75
4.20. Applied Load vs. Axial Strain Curves of Mid-Scale RC Columns Wrapped with GFRP Sheets.....	76
4.21. Typical Failure Mode of Mid-Scale Columns.....	76
4.22. Typical Corrosion Current vs. Time Curves.....	83
4.23. Typical Steel Loss vs. Time Curves.....	83
4.24. Corrosion Current vs. Time Curves of Columns R-CON and C-CON4.....	84
4.25. Steel Loss vs. Time Curves of Columns R-CON and C-CON4.....	85
4.26. Corrosion Current vs. Time Curves of Columns C-CON4 and C-CFRP1.....	86
4.27. Steel Loss vs. Time Curves of Columns C-CON4 and C-CFRP1.....	87
4.28. Cracks in the CFRP Sheets Due to the Accelerated Corrosion Process.....	88
4.29. Corrosion Current Variations of Columns C-CFRP1 and C-CFRP3 during the Accelerated Corrosion Process.....	89
4.30. Calculated Steel Loss of Columns C-CFRP1 and C-CFRP3 during the Accelerated Corrosion Process.....	90
4.31. Steel Loss vs. Time Curves during the Third Stage.....	91
4.32. Corrosion Damaged Longitudinal and Spiral Reinforcements.....	92

4.33. Cracks of Unwrapped and CFRP Wrapped Columns Due to the Accelerated Corrosion Process	94
4.34. Internal Crack Patterns of Control Column and Corrosion Damaged Columns.....	96
4.35. Radial Strain vs. Time Curves of Columns C-CFRP1 and C-CFRP3	97
4.36. Radial Strain vs. Percentile Loss of Cross-Sectional Area of Steel Reinforcements.....	98
4.37. Failure Modes of Unwrapped Columns.....	100
4.38. Failure Modes of the Columns Strengthened by CFRP Sheet Wrapping before Beginning of the Accelerated Corrosion Process.....	101
4.39. Failure Modes of the Corrosion-Damaged Columns Repaired by CFRP Sheet Wrapping after the Accelerated Corrosion Process.....	101
4.40. Typical Load vs. Axial Strain Curves of all Tested Columns	102
4.41. Average Failure Load, P_u , and Equivalent Area, A_{eqv} , of Columns C-CONT and C-CON4.....	106
4.42. Typical Load vs. Axial Strain Curves of Columns C-CONT and C-CON4.....	106
4.43. Average Failure Load, P_u , and Equivalent Area, A_{eqv} , of Columns C-CON4 and C-CFRP2	107
4.44. Typical Load vs. Axial Strain Curves of Columns C-CON4 and C-CFRP2.....	108
4.45. Average Failure Load, P_u , and Equivalent Area, A_{eqv} , of Columns C-CON3 and C-CFRP1	109
4.46. Typical Load vs. Axial Strain Curves of Columns C-CON3 and C-CFRP1	110
4.47. Average Failure Load, P_u , and Equivalent Area, A_{eqv} , of Columns C-CFRP1, C-CFRP2, C-CFRP3 and C-CFRP4.....	111
4.48. Relationship between ϕ_{cor1} and ϕ_{cor2}	113
4.49. Ratio of $(\epsilon_r)_{total} / \epsilon_{fu}$	118
4.50. Current vs. Time Curves of Columns M-COR-CFRP, M-CFRP-COR and M-COR-CFRP-COR	119
4.51. Steel Loss vs. Time Curves of Columns M-COR-CFRP, M-CFRP-COR and M-COR-CFRP-COR	120
4.52. Cracks Due to the Accelerated Corrosion Process	121
4.53. Radial Strain of CFRP Wrapped Mid-Scale RC Columns	121
4.54. Failure Modes of Mid-Scale RC Columns.....	122
4.55. Axial Load vs. Axial Strain Curves of Mid-Scale RC Columns	124

5.1. Coordinate System of Concrete Cylinder Confined by FRP Sheet along with Stress and Strain Components	128
5.2. Equilibrium of Forces in Concrete Cylinder Wrapped with FRP Jacket.....	129
5.3. Steel Confinement Model by Mander et al. (1988)	133
5.4. Proposed Axial Stress-Strain Response Model.....	135
5.5. Flow Chart for the Proposed FRP Confined Model.....	136
5.6. Comparison of Compressive Strength, f'_{cc} , between Experimental Results and Predictions by Analytical Models	138
5.7. Comparison of Axial Stress vs. Strain Curve of Column S-C1-CONT Obtained from Experiments and the Proposed Analytical Model.....	139
5.8. Comparison of Axial Stress vs. Strain Curve of Column S-G1-CONT Obtained from Experiments and the Proposed Analytical Model.....	139

LIST OF TABLES

Table	Page
3.1. Test Matrix for Small-Scale RC Columns	20
3.2. Groups and Objectives of Small-Scale RC Columns	21
3.3. Mixture Proportion of the Concrete for Small-Scale Columns	22
3.4. Mechanical Properties of FRP Sheets.....	24
3.5. Thirty-Year Average Temperatures in Missouri.....	29
3.6. Test Matrix for Mid-Scale RC Columns.....	30
3.7. Test Matrix of Small-Scale RC Columns for Corrosion Tests	35
3.8. Compressive Strength of Concrete Used for Small-Scale RC Columns for Corrosion Tests.....	36
3.9. Stages of Accelerated Corrosion Process	41
3.10. Mixture Proportion of the Concrete for the Repair of Column R-COV	44
3.11. Test Matrix of Mid-Scale RC Columns for Corrosion Tests.....	46
4.1. Failure Load, P_u , of Small-Scale RC Columns.....	52
4.2. Axial Rigidity in the Plastic Region, $(EA)_2$, of Small-Scale RC Columns	53
4.3. Ductility Index, μ , of Small-Scale RC Columns	54
4.4. Strength Reduction Factor, ϕ_{FT}	72
4.5. Strength Reduction Factor, ϕ_{Na}	73
4.6. Strength Reduction Factor, ϕ_H	74
4.7. Failure Load, P_u , of Mid-Scale RC Columns.....	75
4.8. Comparison of Failure Load, P_u , of Freeze-Thaw Conditioned Mid-Scale RC Columns with Control Columns	78
4.9. Comparison of Failure Load, P_u , of Mid-Scale RC Columns Conditioned under the Combined Environmental Cycles with Control Columns	78
4.10. Percentile Changes in Mechanical Properties Due to the Environmental Conditioning Used in this Study	81
4.11. Percentile Loss of Cross-Sectional Area of Steel Reinforcement Determined by Faraday's Law	92
4.12. Comparison of the Percentile Loss of Cross-Sectional Area of Steel Reinforcement Determined by Tensile Test with that Determined by Faraday's Law	93

4.13. Crack Width Measured with Crack Scope.....	95
4.14. Failure Load, P_u , and Failure Modes of Small-Scale RC Columns of Corrosion Tests.....	99
4.15. Ratio of the Equivalent Area of Corrosion-Damaged Columns to those of Control Columns.....	104
4.16. Area Reduction Factors, ϕ_{cor2} , of Columns C-CFRP1, C-CFRP2, C-CFRP3, and C-CFRP4 and Experimental Programs Applied to the Columns.....	115
4.17. Proposed Area Reduction Factor, ϕ_{cor2}	115
4.18. Radial Strains, ε_r , Measured during the Accelerated Corrosion Process and during the Compressive Failure Test.....	117
4.19. Failure Load, P_u , and Failure Modes.....	123
5.1. Mechanical Properties of Small-Scale RC Columns	137
5.2. Comparison of the Compressive Strength between Experimental Results and Predictions by Analytical Models.....	138
5.3. Comparison of Experimental Results of Xiao and Wu (2000) and Predictions by the Proposed Analytical Model.....	140
5.4. Comparison of Experimental Results of Toutanji (2000) and Predictions by the Proposed Analytical Model	141
5.5. Comparison of Experimental Results of Ilki and Kumbasar (2002) and Predictions by the Proposed Analytical Model.....	142
5.6. Comparison of Experimental Results of Samaan et al. (1998) and Predictions by the Proposed Analytical Model.....	143
5.7. Comparison of Experimental Results 1 of Karbhari and Gao (1997) and Predictions by the Proposed Analytical Model.....	144
5.8. Comparison of Experimental Results 2 of Karbhari and Gao (1997) and Predictions by the Proposed Analytical Model	145
6.1. Strength Reduction Factor, ϕ_{env}	149
6.2. Area Reduction Factors, ϕ_{cor1} and ϕ_{cor2}	150
6.3. Mechanical Properties of Concrete for Mid-Scale RC Columns.....	152
6.4. Radial Strains of FRP Sheet.....	153
6.5. Compressive Strengths of Concrete Confined by FRP Sheets of Mid-Scale RC Columns	154
6.6. Strength Reduction Factors, ϕ_{env} , for Mid-Scale RC Columns Exposed to Environmental Cycles.....	156

6.7. Comparison of Compressive Strengths between Experimental Results and Predictions by the Proposed Design Guidelines	156
6.8. Mechanical Properties of Concrete for Mid-Scale RC Columns	157
6.9. Design Ultimate Tensile Strain of CFRP Sheet	158
6.10. Compressive Strength, f'_{cc} , of Mid-Scale RC Columns Wrapped with CFRP Sheet Calculated by the Proposed Analytical Model	158
6.11. Area Reduction Factors, ϕ_{cor1} and ϕ_{cor2} used for Mid-Scale RC Columns	159
6.12. Reduced Cross-Sectional Area of Steel Reinforcement, $(A_{st})_{cor}$, and Equivalent Area, A_{eqv}	160
6.13. Comparisons of Failure Load, P_u and Predictions by the Proposed Design Guidelines, P_n	161

NOMENCLATURE

A_{eqv}	equivalent area
A_g	gross area of cross-section
A_m	atomic mass
A_{st}	cross-sectional area of steel reinforcement
$(A_{st})_{cor}$	reduced cross-sectional area of steel reinforcement
$A_{st}Loss_{Faraday}$	steel loss calculated by Faraday's law
$A_{st}Loss_{Test}$	steel loss determined by tensile test
D_c	diameter of concrete cylinder or RC circular column
$(EA)_1$	axial rigidity in the elastic region
$(EA)_2$	axial rigidity in the plastic region
E_c	elastic modulus of concrete
E_f	elastic modulus of FRP sheet
E_j	confining modulus of FRP confined concrete
E_{sec}	secant elastic modulus of FRP confined concrete
f_a	stress in axial direction
f_c'	compressive strength of concrete
f_{co}'	compressive strength of unconfined concrete
f_{cc}'	compressive strength of FRP confined concrete
f_{fu}	design tensile strength of FRP sheet
f_r	stress in radial direction
f_s	stress of steel reinforcement

f_y	yield strength of steel reinforcement
f_θ	stress in circumferential direction
F	Faraday's constant
I	electric current (amp)
I_{ave}	average electric current during time increment Δt
P_1	load at which the plastic region begins
P_u	failure load
R	electric resistivity (Ω)
R_c	strain reduction factor
t	time
Δt	time increment
t_f	thickness of FRP sheet
T_g	glass transition temperature
V	electric potential (V)
ν_c	Poisson's ratio of concrete
ν_c'	variable Poisson's ratio
Δw	incremental steel loss
w	accumulated steel loss
z	valency
ε_1	axial strain at load P_1

ε_a	strain in axial direction
ε_{co}	peak strain of unconfined concrete
ε_{cc}	peak strain of FRP confined concrete
ε_f	strain of FRP sheet
ε_{fu}	ultimate tensile strain of FRP sheet provided by the manufacturer
ε_{fu}^*	design ultimate tensile strain of FRP sheet
$(\varepsilon_r)_{corrosion}$	pre-strain of FRP sheet induced by corrosion of steel reinforcement
$(\varepsilon_r)_{failuretest}$	radial strain measured at failure during the compressive test
$(\varepsilon_r)_{total} = (\varepsilon_r)_{corrosion} + (\varepsilon_r)_{failuretest}$	
ε_u	axial strain at failure load P_u
ε_y^*	axial strain at which transition zone begins
ϕ_{cor}	area reduction factor
ϕ_{cor1}	area reduction factor for steel reinforcement
ϕ_{cor2}	area reduction factor for concrete
ϕ_{env}	strength reduction factor for environmental effects
ϕ_{FT}	strength reduction factor for freeze-thaw cycles
ϕ_{Na}	strength reduction factor for saline solution effects
ϕ_H	strength reduction factor for high-temperature cycles with UV radiation and high-humidity cycles
μ	ductility index

1. INTRODUCTION

1.1. BACKGROUND

1.1.1. Fiber Reinforced Polymer Composite Materials. Fiber reinforced polymer (FRP) composite materials consist of fibers embedded in or bonded to a matrix with distinct interfaces between them. In this form, both fibers and matrix retain their physical and chemical identities, but they produce a combination of properties that cannot be achieved with either of the constituents acting alone. In general, fibers are the principal load-carrying members, while the surrounding matrix keeps them in the desired location and orientation, acts as a load transfer medium between them, and protects them from environmental effects.

Commercially, the principal fibers come in various types of glass and carbon as well as aramid (Kevlar). Other fibers, such as boron, silicon carbide, and aluminum oxide, are used in limited quantities. All fibers can be incorporated into a matrix either in continuous lengths or in discontinuous (chopped) lengths. A polymer, used as a matrix, is defined as a long-chain molecule containing one or more repeating units of atoms, joined together by strong covalent bonds (Mallick, 1993). Polymers are divided into two broad categories: thermoplastics and thermosets. Among the thermoset polymeric materials are epoxies and polyesters, which are widely used, mainly because of the ease of processing.

FRP composite materials exhibit high tensile strength in the fiber direction although they are not always rigid as metals. Because of their low specific gravities, the strength-weight ratios of FRP composite materials are markedly superior to those of metallic materials. In addition, an advantage attributed to FRP composite materials is their non-corroding behavior. For these reasons, FRP composite materials have emerged as a major class of structural material and are either used or being considered as substitutions for metals in many weight-critical components in aerospace, automotive, marine application and other industries.

1.1.2. Applications of FRP Composite Materials in Civil Engineering Infrastructures. Although FRP composites are relatively a new class of materials in the field of civil engineering, there has been rapid growth in the use of them for civil

engineering application during the last decade. Today, they are commercially available in various forms: reinforcing bars, prestressing tendons, pre-cured laminates/shells, and fiber sheets. The applications include the repair/rehabilitation of existing reinforced concrete (RC) structures, seismic retrofitting of columns and bridge piers, and construction of pedestrian bridges and vehicular bridges. Particularly, the repair/rehabilitation of structurally deficient RC structures using FRP composite materials has been successfully demonstrated for the past years through many laboratory works and field applications (Nanni, 2000).

Currently, the repair/rehabilitation of RC structures using FRP composite focuses mainly on the externally bonded reinforcements to the concrete surface. This is because the speed and ease of the installation of this technology lead to the decrease in overall cost resulting from labor and site constraint. Similar to steel plate bonding, this technology, known as wet lay-up technique, involves adhering thin, flexible fiber sheets to the concrete surface with a thermoset resin to increase shear and flexural capacity of RC beams and RC slabs, and to increase confinement of RC columns.

1.1.3. Repair/Rehabilitation of RC Columns by FRP Sheet Wrapping.

Jacketing an RC column with steel primarily improves column performance, not because the steel itself carries some fraction of the axial load applied to the column, but rather because it provides lateral confining pressure to the column. The confining pressure places the concrete in a tri-axial state of stress, altering the load-deformation characteristics of concrete. Thus, a properly designed steel jacketing can greatly improve not only column strength in compression, flexure, and shear, but also its ductility.

Although steel jacketing has been proven to be an effective measure for retrofitting and has been widely used in practice, the engineering community is currently looking for alternatives. This is because the use of steel in the outdoor environment may cause problems associated with corrosion, resulting in the increase in maintenance cost as well as the degradation of the structural integrity. The distinct advantage of FRP sheet wrapping over steel jacketing is its inherent non-corrosive characteristic. In addition, one of the disadvantages of steel jacketing is the heavy weight of material itself. Because FRP sheets are lightweight, the ease of the installation of the FRP sheet makes it more attractive. Thus, as an alternative to the steel jacketing, the repair/rehabilitation of RC

columns by FRP sheet wrapping has been successfully tested over the past years, the information on the short-term performance is easily available, and the design recommendation is constantly being updated (ACI 440, 2002; Kabhari and Gao, 1997; Moran and Pantelides, 2002; Nanni et al., 1993).

FRP sheet wrapping of RC columns has found mainly two different fields of applications in repair and strengthening of existing RC columns and bridge piers: (1) repair and seismic upgrade and (2) repair of corrosion-damaged members. However, the long-term performance of RC columns wrapped with FRP sheets is not yet fully understood. As a result, engineers in the field tend to hesitate to use the FRP composite materials, even if they are well aware of their advantages. Thus, it is necessary to evaluate the durability of RC columns wrapped with FRP sheets.

1.1.4. Durability Issue of RC Columns Wrapped with FRP Sheets. Most RC columns in need of the repair/rehabilitation have been exposed to harsh environments. They include wide temperature and humidity fluctuation, rain and snow, and freeze-thaw conditions, as well as chemicals like de-icing salt. All these environmental conditions may affect the durability of the FRP composite system. Although FRP composites have potentially very good durability under the civil infrastructure environment, there still exist unanswered questions related to their long-term performance. Although there is a longer history of the use of the FRP composite materials in other areas such as aerospace, performance assess of the application in the areas is not directly applicable since RC structures externally strengthened with FRP sheets behave as an assembly. Thus, it is necessary to investigate the long-term performance of the RC columns wrapped with FRP sheet as a system.

The mechanisms that control the durability of FRP composite materials include chemical or physical changes of the polymeric matrix, loss of adhesion or debonding at the fiber/matrix interface, and reduction of the fiber strength and modulus (Mallick, 1993). Environment plays a crucial role in changing the properties of FRP composite materials. The environments that affect the durability of FRP composite materials can be divided mainly into two categories: ambient environment and loading environment. Considering the ambient environment, it has been revealed that both fibers and matrix may be affected by moisture, temperature, ultraviolet (UV) radiation, ozone, and the

presence of degrading chemicals such as salt or alkalis. For the loading environment, repeated load and sustained load may cause fatigue and creep, respectively. Of course, none of the environmental conditions is independent of each other but interact together. However, this study mainly focuses on the effect of ambient environmental conditions.

1.1.5. Corrosion of Steel Reinforcements of RC Columns Wrapped with FRP Sheets. In addition to the direct effects of the environmental conditions on the FRP composite systems as described previously, corrosion of steel reinforcements is another key issue affecting the long-term performance of the RC columns wrapped with FRP composite sheets.

Premature deterioration of RC structures due to the corrosion of steel reinforcements is a significant problem. Particularly, with the extensive use of de-icing salt under the cold weather, key bridge components, such as bridge piers, are vulnerable to corrosion of steel reinforcements. However, the conventional repair method, consisting of removing contaminated concrete cover and patching low permeable materials, has several limitations. Load transfer and structural issue is one of the problems of the conventional method. Removing the corrosion damaged concrete cover causes load redistribution while the exposed steel reinforcements may be deformed since the bond between the reinforcements and concrete is lost. Thus, a support system is needed for structures being repaired and a complete traffic interruption is also required. In addition, it is common to see second and even third generation repairs if the structure remains in the same corrosive environment after repair. Consequently, engineers are looking for an innovative and cost-effective repair solution.

Wrapping an RC column with FRP composite sheets has been tested for the repair of the corrosion damage (Pantazopoulou et al., 2001). This is because FRP composite sheet was thought to serve as a diffusion barrier to inhibit the ingress of chlorides, moisture and oxygen, and thus decrease the post-repair corrosion rate.

However, the effect of FRP composite sheet wrapping on the corrosion process is not yet fully understood. Although the wraps may reduce the ingress of new chloride ions and moisture into the concrete, they may also trap the existing moisture and chloride ions. In addition, there is a possibility that chloride ion, moisture, and oxygen can ingress into the concrete through the unwrapped portion of the column, resulting in continuous

corrosion. Furthermore, once an RC column is wrapped with FRP composite sheets, it is impossible to detect the symptoms of the continuous corrosion using the currently available non-destructive corrosion monitoring techniques such as the half-cell potential method and the polarization measurement method (Carino, 1999). Thus, it is necessary to investigate the post-repair corrosion rate of the steel reinforcements of RC columns wrapped with FRP sheets under corrosive environment. Nonetheless, limited research has been done in this area.

1.2. OBJECTIVES OF THIS STUDY

The objectives of this study are;

1. To collect and review the literature, research findings, performance data, and current practices related to the design, construction, and inspection of RC columns wrapped with FRP sheets.
2. To investigate the effect of various environmental conditions (ambient and corrosive environments) on RC columns wrapped with FRP sheets in order to evaluate the long-term performance through experimental study.
3. To propose design guidelines that include the strength reduction factors to account for various environmental effects on RC columns wrapped with FRP sheets, as well as an advanced analytical model to determine the compressive strength of concrete confined by FRP sheets.
4. To validate the performance of the proposed design guidelines.

1.3. RESEARCH PLAN AND METHODOLOGY

This study consisted of two test programs; one was to study the effects of ambient environmental conditions and the other was to study the effect of corrosion of steel reinforcements. The former is referred to as “ambient environmental effect tests” and the latter is referred to as “corrosion tests” throughout the report.

Two different scales of RC columns were used in the tests; small-scale and mid-scale RC columns. Small-scale RC column tests were performed for the extensive parametric study of various environmental conditions, while mid-scale RC column tests were conducted to validate the performance of the proposed design guidelines.

Design guidelines were proposed based on the test results of the small-scale RC columns. The proposed design guidelines included an advanced analytical model to predict the axial stress-strain relationship of the concrete confined by FRP composite, reduction factors experimentally determined from the small-scale RC column tests, and design equations to determine the axial compression capacity of the RC columns wrapped with FRP sheets. The performance of the proposed design guidelines was validated through the mid-scale RC column tests.

Test set-ups of environmental conditionings of the two tests (i.e., ambient environmental effect tests and corrosion tests) were different because the mechanisms of degradations of FRP wrapped RC columns are different according to the environmental conditions. The following sections present brief descriptions of the procedure of each test.

1.3.1. Ambient Environmental Effect Tests. The RC columns used in this test were wrapped with two different types of FRP sheets (CFRR and GFRP sheets) using the wet lay-up technique, which is most often used in the field when applying the sheet types of FRP composites. Then, the columns were placed in the environmental chamber for environmental conditioning. Once the environmental conditioning was completed, uniaxial compression tests were carried out to obtain load vs. axial strain curves of the columns.

1.3.2. Corrosion Tests. In this test, RC columns were wrapped with CFRP sheets. CFRP sheet was selected instead of GFRP sheet because CFRP sheet is an electric conductor while GFRP sheet is not. In addition, the thickness of CFRP sheet is much smaller than that of GFRP sheet. Thus, it has been thought that RC columns wrapped with CFRP sheets would be more vulnerable to corrosive environment than the ones wrapped with GFRP sheets.

Corrosion of steel reinforcements occurs over a long period of time, such as several years, in the field. In order to simulate the corrosion process in a laboratory and to induce the corrosion damage to the RC columns within a relatively short period of time, an accelerated corrosion regime was designed. The accelerated corrosion process consisted of imposing 6 V of electric potential between steel reinforcement cages (i.e., anode) and an internal cathode under wet-dry cycles using saline solution. During the

accelerated corrosion process, corrosion rate was monitored to evaluate the effect of CFRP sheet wrapping. After completion of the accelerated corrosion process, failure tests were conducted to obtain load vs. axial strain curves of the columns.

1.4. ORGANIZATION OF THE REPORT

Section 1 addresses the background, objectives, and research plan of this study. Section 2 presents a literature review on the durability of the FRP composites, current issues regarding the durability of civil infrastructures strengthened with FRP composites, and research studies on the durability of RC columns wrapped with FRP composites. Section 3 describes the experimental program of small-scale RC columns and mid-scale RC columns. Section 4 presents the test results and discussions. Section 5 proposes an analytical model to predict the behavior of axially loaded circular concrete columns wrapped with FRP sheet. Section 6 presents design guidelines for RC columns wrapped with FRP sheets and validate its performance. Section 7 summarizes the obtained results, and lists observations, conclusions and general remarks on the recommendations for future research.

2. LITERATURE REVIEW

2.1. GENERAL

This section presents an overview of research studies related to the long-term durability of RC columns wrapped with FRP sheets. First, the major environmental conditions that affect the durability of the FRP composite material itself are addressed briefly. Second, recent research studies regarding the durability of FRP composite systems are discussed in order to highlight key issues in this research field. Finally, research studies on the durability of RC columns wrapped with FRP composite are reviewed and outlined.

2.2. ENVIRONMENTAL CONDITIONS AFFECTING THE DURABILITY OF FRP COMPOSITE

The purpose of this section is to introduce the primary factors that may affect the long-term performance of FRP composite systems in the field of civil engineering. The discussions establish the basis for the need to conduct this study.

According to various research studies conducted to date, there are seven major factors related to the durability of FRP applications in civil infrastructures, which include: (1) moisture effects, (2) alkali effects, (3) thermal effects, (4) creep and stress-rupture, (5) fatigue, (6) fire, and (7) ultraviolet (UV) radiation effects.

2.2.1. Moisture Effects. Under high humidity conditions or water environments, most FRP composites absorb moisture by means of instantaneous surface absorption followed by diffusion through the resin. The primary effect of the absorption is on the resin itself, resulting in a change in its physical and chemical characteristics. The presence of water can plasticize a polymer and lower the glass transition temperature, T_g , at which the material shows a transition from glassy to rubbery behavior (Kumar and Gupta, 1998; Schutte, 1994). This reduction in the glass transition temperature, T_g , makes the polymer softer; thus, it can increase creep deformations. This is a physical change that is reversible when it dries. However, chemical changes induced by moisture

are irreversible. For some of the polymers, moisture can cause hydrolysis¹ when resin is fully cured (Kajorncheappunngam et al., 2002). The result can be a permanent change in the molecular weight between cross-links with an attendant change in both the stiffness and the strength of the polymer.

Moisture and chemicals have also been shown in the case of aramid and glass fibers to cause degradation at the fiber level. For glass fibers, degradation is initiated by moisture extracting ions from the fiber, thereby altering its structure; while, aramid fibers absorb moisture, which can result in accelerated fibrillation² under specific conditions (Karbhari et al., 2003). It is, however, possible to protect these fibers to a significant degree from rapid attack through selection of appropriate resin systems, processing conditions, and application of gel coats and protective coatings.

Volume change or swelling is another possible effect of moisture ingress. Similar to thermal effects, it can cause the stress between fibers and resin (Millick, 1993), resulting microcracks. Swelling can also lead to the loss of bond between the fiber and resin. However, the extent of possible delamination due to the loss of bond is largely dependent on the nature of the sizing or coupling agent³.

2.2.2. Alkali Effects. There are a variety of sources of alkaline effects on FRP composites used in civil infrastructures, including alkaline chemicals, contaminated soil, and concrete. Among these, our primary concern is the pore water in concrete, which has a pH of 12.5 ~ 13.5 because the FRP composite can be directly exposed to this condition when it is used as an internal reinforcement of concrete structure.

Glass fibers can be severely affected by direct exposure to alkaline environments through pitting, hydroxylation⁴, hydrolysis, and leaching⁵, resulting in the reduction in

¹ Hydrolysis: the reaction of a substance with water or its ion

² Fibrillation: the phenomenon wherein a filament or fiber shows further evidence of basic fibrous structure or fibrillar crystalline nature, by a longitudinal opening-up of the filament under rapid, excessive tensile or shearing stresses. Separate fibrils can then often be seen in the main filament trunk.

³ Coupling agent: a chemical substance capable of reacting with both the reinforcement and the resin matrix of a composite material. It may also bond inorganic fillers or fibers to organic resins to form or promote a stronger bond at the interface.

⁴ Hydroxylation: to introduce hydroxyl into a compound

strength and modulus (Karbhari et al., 2003; Stone et al., 2002). Although resin protects the fibers from the environmental effects, the alkaline solution can reach the fibers by absorption and diffusion through the surrounding resin.

2.2.3. Thermal Effects. Thermal effects include changes in response due to the temperature above cure temperature, freezing and freeze-thaw conditions, and temperature cycles. It is known that sub-zero temperatures would result in matrix stiffening/hardening, matrix microcracking, and fiber-matrix bond degradation (Karbhari et al., 2003). Furthermore, under the freeze-thaw conditions, saline solution can accelerate the degradation because of the formation and expansion of salt crystals as well as the effects of moisture.

As for the thermal expansion coefficients, those of GFRP are similar to that of concrete while those of CFRP and AFRP are so different. Moreover, the coefficients of resins can be different in orders of magnitude.

2.2.4. Creep and Stress Rupture. Creep is defined as the increase in strain with time at a constant stress level. Many polymeric resins exhibit large creep strains at low stress level under ambient room temperature. The creep strain of polymeric resin is largely dependent on the temperature, stress level, and moisture level. The thermosetting polymeric resins exhibit lower creep strain than thermoplastic polymeric resins do because of their highly cross-linked structure (Mallick, 1993). Aramid and glass fibers are susceptible to creep, while carbon fibers exhibit little or no creep (Karbhari et al., 2003). The creep nature of aramid and glass fibers can be affected by moisture level and alkaline attack.

Stress rupture is defined as the failure of a material under sustained constant load. Aramid and glass fibers and their composites exhibit failure by stress rupture while carbon fibers are relatively less prone to stress rupture (Mallick, 1993).

2.2.5. Fatigue. Fatigue is defined as the physical phenomenon that causes a material to fail after the repeated application of a condition (e.g., mechanical load) at a level less than the ultimate resistance of the material. Key to the understanding of fatigue

⁵ Leaching: the process of extraction of a component from a mixture by treating the mixture with a solvent which will dissolve the component but has no effect on the remaining portions of the mixture.

is to understand the degradation processes that reduce the strength of the material. Degradation processes can be mechanical or environmental and are not independent of each other but interact with each other.

2.2.6. Fire. An important concern in organic matrix composites is the possibility of fire, resulting in the spread of flame, release of heat and toxic byproduct, and potential structural collapse. The organic resins that comprise up to 50 % by weight of composite structures are combustible in the event of exposure to a fire source.

2.2.7. Ultraviolet Radiation. Ultraviolet (UV) radiation that reaches the Earth's surface comprises 6 % of the total solar radiant flux and has wavelengths between 0.114 and 0.157 micro inches. In this range of wavelength, most of the polymeric materials undergo degradation due to the dissociation⁶ of chemical bonds (Roylance and Roylance, 1976; George et al., 1997). However, the most deleterious effect of UV exposure is probably not due to the actual UV damage, which is limited to the top surface, but it is due to the potential for increased ingress of moisture and other agents via the damaged regions.

2.3. RECENT RESEARCH STUDIES RELATED TO LONG-TERM DURABILITY OF FRP COMPOSITE SYSTEMS

Since concrete structures strengthened with FRP composite materials behave as a system, the assessment of long-term performance of FRP composite material itself, which was briefly discussed in the previous section, may not be directly applicable to FRP composite systems. Therefore, this section is aimed at addressing recent research studies on the long-term durability of FRP composite systems in order to highlight key issues in this field.

Most research studies with regard to the long-term durability of concrete structures strengthened with FRP composite have focused on the following five environmental conditions: (1) freeze and freeze-thaw conditions, (2) wet-dry cycles and corrosion of steel reinforcements, (3) combined environmental conditions, (4) creep and fatigue, and (5) field study.

⁶ Dissociation: as applied to heterogeneous equilibria, it is the transformation of one phase into two or more new phases of different composition.

2.3.1. Freeze and Freeze-Thaw Conditions. The majority of research studies regarding the long-term durability of RC structures strengthened with FRP composite materials have been conducted with focus on the effect of freeze-thaw cycles. This is because the freeze-thaw action has been thought to be the most harmful to concrete structures and FRP composite materials as well.

Soudki and Green (1997) studied the change in response of the concrete confined by FRP composite sheets after exposure to 50 freeze-thaw cycles, which was a modified version of ASTM C 666 (standard test method for resistance of concrete to rapid freezing and thawing). They used standard cylinders ($\phi 6 \times$ of 12 in.) wrapped with CFRP sheets. During the freeze-thaw cycles, warm water at +65 °F was used to thaw the specimens. The result showed that the compressive strength of concrete cylinders wrapped with 1 layer of CFRP sheet decreased by approximately 15 % due to the exposure to the freeze-thaw cycles. Toutanji and Balaguru (1999) reported similar results. They tested small-scale unreinforced concrete columns of 3 in. in diameter and 12 in. in height wrapped with different types of FRP sheets, in uni-axial compression, after exposure to 300 freeze-thaw cycles in accordance with ASTM C 666. During the freeze-thaw cycles, salt solution was used to thaw the specimens. They reported that after exposure to the freeze-thaw cycles, compressive strength decreased by 28 % and 19 % for GFRP and CFRP wrapped columns, respectively. However, they concluded that the decrease in compressive strength was primarily due to the effect of the freeze-thaw cycles on the concrete itself in the end (top and bottom portion) of the column, which was directly exposed to the freeze-thaw cycles rather than the degradation coming from FRP composite materials.

Karbhari et al. (2000) also studied the behavior of the FRP wrapped columns subjected to 200 freeze-thaw cycles. They used standard cylinders ($\phi 6 \times$ of 12 in.) to evaluate the change in ultimate strength. The standard cylinders were wrapped with CFRP and GFRP sheets with different configurations. The freeze-thaw cycles, in their test, were different from the ASTM C 666-97 in that the temperature range was wider and no thawing water was used. They reported that the freeze-thaw cycles used in their study had no significant deteriorative effect on the strength of the FRP confined concrete regardless of the configurations and types of the FRP sheets. Rather, the cylinders

wrapped with CFRP sheets exhibited a slight increase in compressive strength due to the exposure to the freeze-thaw cycles. In an earlier study performed by Karbhari and Eckel (1994), similar results were observed. They placed the standard cylinders ($\phi 6 \times$ of 12 in.) wrapped with different FRP sheets under extremely low temperature, 0°F, instead of freeze-thaw cycles, to simulate the cold climate. The result showed that a slight increase in ultimate strength was observed regardless of types of the FRP sheets. They concluded that the increase was due to the matrix hardening effect.

Baumert et al. (1996) tested RC beams strengthened with CFRP sheets to investigate the effect of cold region climate at -17 °F. They concluded that the extremely low temperature did not affect the CFRP sheets in a negative way. Furthermore, the specimens exposed to the low temperature showed higher failure load when compared to specimens kept at room temperature.

Green et al. (2000) conducted a research study to investigate the reduction in bond between FRP sheets and concrete surface due to freeze-thaw cycles through pull-out tests and four-point bending tests. The freeze-thaw cycles were performed according to ASTM C 310-71 (test for resistance of concrete specimens to slow freezing in air and thawing in water). They reported that the freeze-thaw cycling did not reduce the load carrying capacity of the joint between the CFRP plate and the concrete when the joints were either in pure shear or in a combination of shear and flexure.

2.3.2. Wet-Dry Cycles and Corrosion of Steel Reinforcements. RC structures may lose their structural integrity to a significant degree due to the corrosion of steel reinforcements when exposed to wet-dry cycles in combination with chloride ions such as seawater and de-icing salt in the winter season. Although FRP composites are considered to be an effective solution to the strengthening and/or rehabilitation of RC structures as an alternative of steel, their effectiveness on the rehabilitation of corrosion damaged RC structures has not yet been fully studied. This is because when FRP composite material is used as an external reinforcement, it can entrap the existing moisture chloride ions, and it can also serve as diffusion barrier of moisture ingress into the concrete inside the FRP composite material. When being used as internal reinforcement, the FRP composite can be deteriorated by the high alkaline environment of concrete. Furthermore, as described in the previous section, the effect of moisture on the FRP composite material itself cannot

be neglected. Thus, it is highly important to study the durability of the FRP composite systems subjected to wet-dry cycles or corrosive environment.

Toutanji and Gómez (1997) studied the effect of wet-dry cycles using seawater on the behavior of unreinforced concrete beams strengthened with different types of FRP sheets. The specimens were conditioned by 300 wet-dry cycles and tested in four point bending. The ultimate failure load of the specimens exposed to the wet-dry cycles was lower than that of the control specimens. The authors concluded that the reduction in the ultimate failure load might be attributed to the degradation of the epoxy resin used, which lead to the weakening of the bond between concrete and FRP sheets. In addition, they stated that the extent of the reduction was dependent on the types of epoxy resin used. Toutanji (1999a) also tested standard cylinders ($\phi 6 \times$ of 12 in.) wrapped with different types of FRP sheets using two kinds of epoxy resin. They reported that the ultimate strength of GFRP wrapped specimens was reduced by 10 to 18 % after exposure to the wet-dry cycles when using type A epoxy (modified amine/epoxy resin blend). In the case where type B epoxy (polyxylpropylenediamine hardener/epoxy resin) was used, insignificant loss (less than 3 %) of ultimate strength was reported. For CFRP wrapped specimens, the decrease in ultimate strength was less than 5 % regardless of types of epoxy used.

Researchers at the University of Toronto in Canada have been conducting extensive studies on the repair of corrosion damaged RC columns by FRP composite wrapping (Pantazopoulou et al., 1996; Lee, 1998). Their latest research studies (Pantazopoulou et al., 2001) focused on the post-repair corrosion rate. In their test, small-scale RC columns were conditioned under the accelerated corrosion process consisting of impressed electric current and wet-dry cycles until cracks and spalling of cover concrete occurred. The corrosion-damaged specimens were repaired by several methods, including (1) the conventional method consisting of removal of damaged concrete and patching low permeable grout, (2) GFRP wrapping after cleaning the damaged surface without removal of the damaged concrete, and (3) GFRP wrapping on the top of the alkali-resistant coating, Type-K grout, or expansive grout. After the repair of corrosion-damaged specimens, the specimens were re-conditioned under the accelerated corrosion process to evaluate the post-repair corrosion rate of each repair

method. They concluded that the most effective method in terms of reducing the corrosion rate was the GFRP wrapping after cleaning the damaged surface without removal of damaged concrete; this was the simplest and easiest of the repair methods considered. The use of the grouts (either Type K or expansive grout) before GFRP wrapping could not improve the performance of the repaired specimens in terms of the post-corrosion rate because the GFRP wraps entrapped the existing moisture in the grout, resulting in the decrease of electric resistivity of the concrete.

Masoud et al. (2001) investigated the behavior of RC beams strengthened with CFRP sheets under corrosive environment. The specimens were subjected to an accelerated corrosion process consisting of impressed current and wet-dry cycles. Longitudinal cracks were observed after the accelerated corrosion process for both strengthened specimens and unstrengthened specimen; however, the crack widths of the strengthened specimens were significantly smaller than those of the unstrengthened specimens. The results also revealed that the fatigue life of the specimens strengthened with CFRP sheets was greatly improved even after the accelerated corrosion process when compared to the corrosion damaged unstrengthened specimens.

Okba et al. (2003) tested 'lollipop' specimens to investigate the change in bond strength between steel reinforcements and concrete wrapped with either CFRP or GFRP sheets. They reported that wrapping a concrete column with FRP sheets decreased the corrosion rate but could not stop the corrosion of steel reinforcements. Furthermore, the bond strength decreased when the corrosion level exceeded 25 % of cross-sectional loss of the steel reinforcements. However a slight increase in bond strength was found at low corrosion level.

FRP composite rods are considered to be an alternative to steel reinforcements because of their non-corrosive characteristic. However, FRP composite materials can be deteriorated by the high alkaline environment of fresh concrete. Stone et al. (2002) studied the degradation of GFRP rods due to an alkaline solution, which simulate the concrete pore water. They reported that after 42 days exposure to the alkaline solution, the tensile strength and the tensile modulus of the GFRP rods decreased by 9 to 40 % and 7 to 25 %, respectively, depending on the types of the rods.

2.3.3. Combined Environmental Conditions. In the real world, structures

undergo various environmental conditions throughout the seasonal changes. Thus, there is a need for assessment of durability of FRP composite systems under the combined environmental conditions, which include freeze-thaw cycles, wet-dry cycles, high-temperature cycles, UV radiation, and saline solutions. Research studies on this subject have been conducted extensively at the University of Missouri-Rolla. Myers et al. (2001) investigated the effect of combined environmental cycles on the bond of FRP sheets to concrete. In their test, pre-cracked RC beams, strengthened with three different types of FRP sheets, were conditioned under the combined environmental cycles consisting of freeze-thaw cycles, high-temperature cycles, high-humidity cycles, and UV radiation. During the environmental conditioning, the specimens were subjected to sustained load. The results showed that all the specimens exposed to the combined environmental cycles exhibited the reduction of flexural stiffness. The authors concluded that the reduction was due to the degradation of the bond between FRP sheets and concrete surface after exposure to the environmental cycles.

Micelli et al. (2000) tested concrete cylinders wrapped with FRP sheets in uniaxial compression after exposure to the combined environmental cycles. They reported that specimens wrapped with GFRP sheets exhibited reduction of the compressive strength by 20 % after conditioning under the environmental cycles, when compared to the unconditioned specimens, while CFRP wrapped specimens did not show the decrease in compressive strength. It was also reported that the use of saline solution during the environmental cycles aggravated the degradation of the compressive strength.

2.3.4. Creep and Fatigue. A considerable amount of research studies regarding the fatigue behavior of RC structures strengthened with FRP composite materials have been carried out by several researchers (Adimi et al., 2000; Heffernan, 1997; Mohsen and Thomas, 1998; Richard and Geoffrey, 1999; Senthilnath, 2001; Shahawy and Beitelman, 1999; Yang and Nanni, 2003). However, the research on the creep behavior of RC structures strengthened with FRP composite material is very rare.

Recently, Senthilnath (2001) investigated the performance of CFRP strengthened RC beams in the presence of delamination and lap splices under fatigue loading. Delaminations usually occur when FRP sheets are attached to the surface of RC structural element. The researchers constructed RC beams strengthened with CFRP sheets, which

contained intentionally fabricated delaminations with different sizes (5.9 in., 3.9 in., and 2.0 in. in diameter). The results indicated that the delaminations used in this test did not significantly affect the fatigue performance of the specimens although the size of the delamination increased insignificantly. The stiffness of CFRP strengthened beams with the delaminations decreased by 4 % after 2 million cycles of repeated loading when compared to the stiffness at the beginning of the repeated loading.

Breña et al. (2002) tested eight RC beams externally strengthened with CFRP composites under the fatigue load. In their test, load amplitudes generated stresses representative of service-load in a bridge. The CFRP composites used in the strengthening were three types: pultruded plate, woven fabric, and unidirectional fiber. The test results showed that the bond between the composite laminates and the concrete surface was not degraded.

2.3.5. Field Study. The field applications of FRP composite materials in civil infrastructures date from the early 1990s. Therefore, field data on the long-term durability are not abundant. However, the use of FRP composite materials for strengthening of RC structures has been successfully demonstrated to date.

2.4. RESEARCH STUDIES ON THE DURABILITY OF RC COLUMNS WRAPPED WITH FRP COMPOSITE MATERIALS

Although several research studies have been conducted to investigate the durability of concrete columns wrapped with FRP composite materials, as described in the previous section, most of the research studies used unreinforced concrete cylinders rather than RC columns. Thus, it is necessary to investigate the behavior of FRP wrapped RC columns exposed to various environmental conditions.

2.5. SUMMARY

As reviewed in this section, there are a lot of factors affecting durability of RC structures strengthened with FRP composite materials. Furthermore, the factors are not independent of each other. As a result, the evaluation of the effects of the factors on the long-term performance of RC structures strengthened with FRP composite materials needs extensive parametric studies, covering all the primary factors. Although the durability of RC columns strengthened with FRP composite materials has been

investigated, most of the research projects were conducted using small-scale specimens focusing on a single factor such as freeze-thaw cycles and wet-dry cycles. The purpose of this study, therefore, was to investigate the combined effects of environmental conditions using different scales of RC columns.

3. EXPERIMENTAL PROGRAM

3.1. GENERAL

The purpose of this experimental program was to evaluate the effects of various environmental conditions and consequently to provide evidential basis of design guidelines. The experimental program was separated into two main parts: ambient environmental effect tests and corrosion tests. Each test was conducted using two different scales of RC columns, i.e., small-scale RC columns and mid-scale RC columns. In the ambient environmental effect tests, various environmental conditions such as high-temperature cycles, high-humidity cycles, UV radiation, and freeze-thaw cycles were discussed. The objective of the corrosion tests was to investigate how effectively FRP wrapping can protect the RC columns from steel reinforcement corrosion.

3.2. AMBIENT ENVIRONMENTAL EFFECT TESTS

3.2.1. Small-Scale RC Column Tests. The objective of this test was to investigate the effects of various environmental conditions on the RC columns wrapped with FRP sheets through extensive parametric studies. The test results were used to develop design guidelines for RC columns wrapped with FRP sheets under various environmental conditions.

3.2.1.1 Test matrix. In order to investigate the effect of various environmental conditions, it was necessary to conduct a wide range of parametric studies. Thus, a total of thirty-six small-scale RC columns were included, although only a total of six mid-scale RC columns were considered in the original proposal of this study. Table 3.1 presents the test matrix. As shown in Table 3.1, the main test parameters included numbers of FRP sheet layers, types of FRP sheets, and types of environmental conditions. The environmental conditions were divided into six types: room temperature, freeze-thaw cycles, high-temperature cycles, high-humidity cycles, UV radiation, and saline solution effect.

The specimens in Table 3.1 are identified by groups of letters and a number separated by hyphens. Each of these descriptive groups gives information about some aspect of the specimens in this order: (1) column size (S for small-scale), (2) FRP sheet

type (C and G for CFRP and GFRP sheet, respectively), (3) number of FRP layer (1 and 2 for one layer and two layer, respectively) and (4) environmental condition type (CONT, F/Th and CE for control, freeze-thaw and combined environmental cycles, respectively). The symbol Na in the specimen identification refers to specimens immersed in saline solution during the environmental conditioning.

Table 3.1. Test Matrix for Small-Scale RC Columns

Specimen	Test parameters								Number of specimens
	FRP layer	FRP type	Description of environmental conditioning						
			Room temperature	Freeze-thaw cycles	High-temperature cycles	UV radiation	High-humidity cycles	Saline solution	
S-CONT	0	None	X						3
S-C1-CONT	1	CFRP	X						3
S-G1-CONT	1	GFRP	X						3
S-C2-CONT	2	CFRP	X						3
S-C1-F/Th	1	CFRP		X					3
S-C1-CE	1	CFRP		X	X	X	X		3
S-C2-CE	2	CFRP		X	X	X	X		3
S-G1-F/Th	1	GFRP		X					3
S-G1-CE	1	GFRP		X	X	X	X		3
S-C1-Na-F/Th	1	CFRP		X				X	3
S-G1-Na-F/Th	1	GFRP		X				X	3
S-C1-Na-CE	1	CFRP		X	X	X	X	X	3
Total									36

A total of thirty-six small-scale RC columns were used in this test. They were categorized into five groups, as shown in Table 3.2, in order to evaluate the effect of each environmental condition through comparative study. The objective of Group 1 was to investigate the effect of confinement by FRP sheets. Group 2 was used to investigate the effect of the freeze-thaw cycles. Group 3 was used to investigate the effect of the

combined environmental cycles. Group 4 was used to investigate the effect of saline solution during the exposure to environmental conditioning. Group 5 was used to investigate the effect of the high-temperature cycles with UV radiation and the high-humidity cycles.

Table 3.2. Groups and Objectives of Small-Scale RC Columns

	Specimens Purposes
Group 1	S-CONT, S-C1-CONT, S-G1-CONT and S-C2-CONT <i>to investigate the effect of confinement by FRP sheet</i>
Group 2	S-C1-CONT, S-C1-F/Th, S-G1-CONT and S-G1-F/Th <i>to investigate the effect of the freeze-thaw cycles</i>
Group 3	S-C1-CONT, S-C2-CONT, S-C1-CE , S-C2-CE, S-G1-CONT and S-G1-CE <i>to investigate the effect of the combined environmental cycles</i>
Group 4	S-C1-F/Th, S-C1-Na-F/Th, S-C1-CE, S-C1-Na-CE, S-G1-F/Th and S-G1-Na-F/Th <i>to investigate the effect of saline solution during the exposure to environmental conditioning</i>
Group 5	S-C1-F/Th, S-C1-CE, S-G1-F/Th and S-G1-CE <i>to investigate the effect of the high-temperature cycles with UV radiation and the high-humidity cycles</i>

3.2.1.2 Materials used. The properties of concrete, steel reinforcements, and FRP sheets used in this study are addressed in the following sections.

3.2.1.2.1 Concrete. In order to simulate the long-term performance of RC columns within a relatively short time in a laboratory, it was necessary to accelerate the degradation rate of concrete, in addition to a proper design of environmental cycles. In an attempt to accelerate the degradation rate of concrete, the concrete was produced according to the mixture proportion shown in Table 3.3. The mixture proportion was designed to have a target 28-day strength of 3,000 psi and air content of 9 %. Considering that most RC bridge piers in need of repair/rehabilitation were constructed 20 years ago, the target strength was determined to be 3,000 psi, which was the strength of the concrete usually used for the construction of RC bridge piers in North America at

that time. Determination of the target air content was based on the following.

Table 3.3. Mixture Proportion of the Concrete for Small-Scale Columns (unit: lb/yd³)

W/C	Cement	Water	Coarse aggregate	Fine aggregate	Air Entraining agent (fl. oz.)
0.62	490	303	1,274	1,821	5

ACI 318-02 specifies that the recommended air content of normal weight and lightweight concrete is 7.5 % when exposed to severe freezing and thawing or de-icing chemicals. It implies that with the air content of 7.5 %, degradation of concrete due to freezing and thawing or de-icing chemicals could be minimized. In other words, the air content of less than or greater than 7.5 % could result in more severe damage to concrete due to freezing and thawing or due to de-icing chemicals. Thus, the air content of the concrete used in this test needed to be less than or greater than 7.5 %. Permeability was one of the important concerns when designing the mixture proportion because the same mixture proportion would be used in the corrosion tests for comparison purposes. In the corrosion tests, it was important to supply sufficient water necessary for the corrosion process of steel reinforcements embedded in the concrete. Thus, the concrete with high permeability was necessary so that moisture and chloride ions could easily ingress into the concrete. Higher permeability of concrete can be obtained by higher air content. Consequently, the target air content of the mixture proportion was to be more than 7.5 % instead of less than 7.5 %. Therefore, the target air content was determined to be 9.0 %.

The measured air content of the produced concrete for the ambient environmental tests was 11 %, while that of the concrete for the corrosion tests was 9 %. The strength of the concrete used for the ambient environmental tests was 1,800 psi at the age of 500 days, while that of the concrete used for the corrosion tests was slightly over 3,000 psi at the age of 840 days based on the test results of standard cylinders ($\phi 6 \times 12$ in.). It should be noted that the same mixture proportion was used to produce the concrete for both ambient environmental tests and corrosion tests. Thus, the lower strength of the concrete

used for the ambient environmental tests when compared to that of the concrete used for the corrosion tests could be attributed to the higher air content.

The reason for the different percentages in the air content produced by the same mixture proportion could be due to the inherent difficulty in handling the concrete mixer. In fact, it was very difficult to keep the air content constant through different batches of concrete because the control of water/cement ratio using the ransome type concrete mixer used in this test was not as accurate as needed for the testing of concrete material properties. Rather, the mixer was originally designed for the mass production of concrete for the testing of RC structures in which the concrete strength is not regarded as a test parameter. For example, it was necessary to spray additional water to soak the dried surface of the mixer. Otherwise, the mixing water would be absorbed onto the surface, resulting in a decrease in the designed water/cement ratio. On the other hand, water/cement ratio would increase in the case where too much water is used to soak the surface of the mixer. Thus, it was highly possible in this test that the additional water to soak the surface increased the water/cement ratio and consequently the air content.

Despite the low strength, it was believed that the test results of small-scale RC columns made of this low strength concrete could be used to anticipate the long-term performance of the normal strength concrete, since the overall axial compressive behavior of low strength concrete wrapped with FRP sheets is not significantly different from that of normal and high strength concrete (Xiao and Wu, 2000).

3.2.1.2.2 Steel reinforcements. Number 3 and grade 60 reinforcing bars were used for longitudinal reinforcements, while steel wires with diameter of 0.147 in. were used for spiral reinforcements. Tensile tests of number 3 reinforcing bars were performed and the obtained stress vs. strain curves are presented in Figure 3.1. Based on the test results, a bi-linear stress-strain model for the reinforcing bar was derived, as shown in Equations (3-1) through (3-2),

$$f_s = E_s \varepsilon_s \text{ when } f_s \leq f_y \quad (3-1)$$

$$f_s = f_y + 286 \left(\varepsilon_s - \frac{f_y}{E_s} \right) \text{ ksi when } f_s \geq f_y \quad (3-2)$$

where, yield strength, f_y , is 70 ksi, tensile strength, f_u , is 98 ksi, and elastic modulus, E_s , is 30,400 ksi.

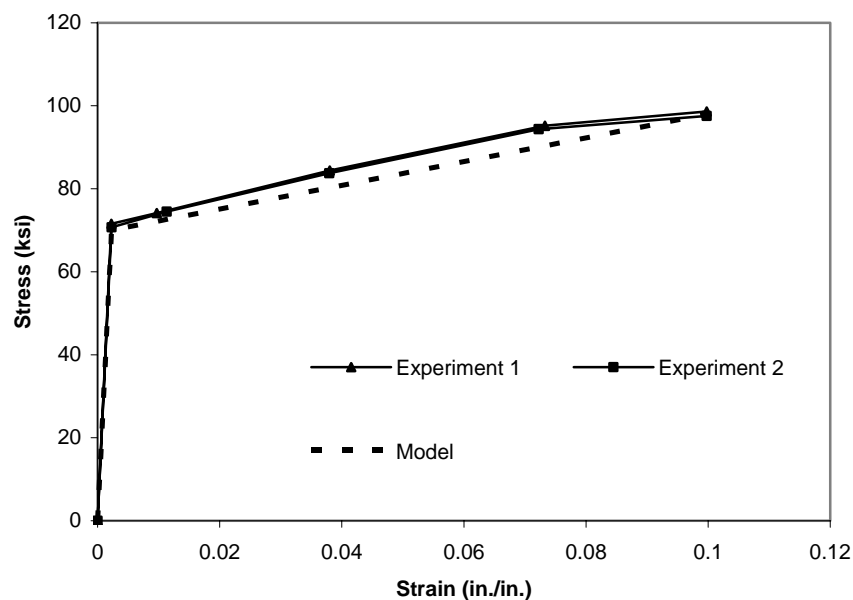


Figure 3.1. Experimental Results of Tensile Tests of Number 3 Reinforcing Bars

3.2.1.2.3 FRP sheets. Two types of FRP sheets, namely, MbraceTM CF High Tensile Carbon Fiber and MbraceTM EG900 E-Glass Fiber, were used in this study. The mechanical properties obtained from the manufacturer are shown in Table 3.4 (Master Builders Inc, 1998). The epoxy-based resin, namely, MbraceTM primer and saturant, were used for the first coating and for impregnating the dry fibers.

Table 3.4. Mechanical Properties of FRP Sheets

Fiber Type	Thickness (in.)	Tensile Strength (ksi)	Ultimate Tensile strain (in./in.)	Tensile modulus (ksi)
Carbon (CFRP)	0.0065	550	0.017	33,000
Glass (GFRP)	0.0139	220	0.021	10,500

3.2.1.3 Specimen detail and manufacturing. The diameter of the small-scale RC columns was 6 in. and the height was 18 in. Three number 3 reinforcing bars were used for longitudinal reinforcements. The details of the column are presented in Figure 3.2 and Figure 3.3 shows a photograph of the small-scale RC columns after the FRP sheet wrapping.

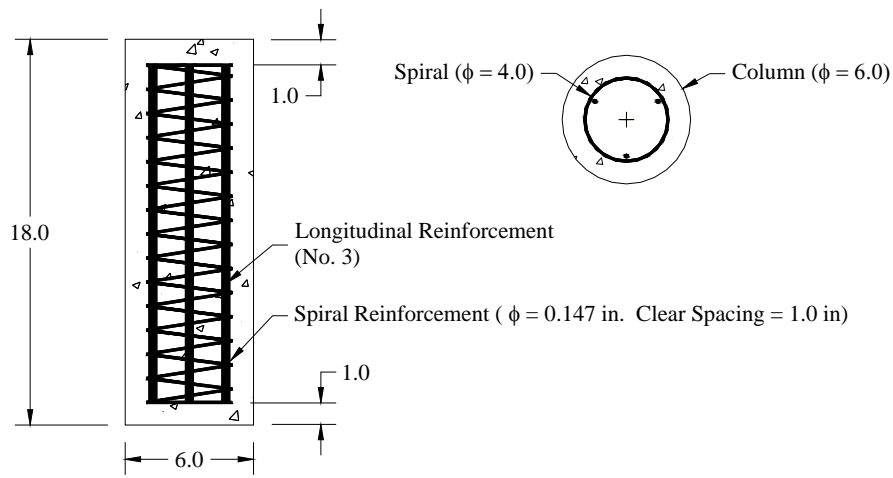


Figure 3.2. Details of Small-Scale RC Column

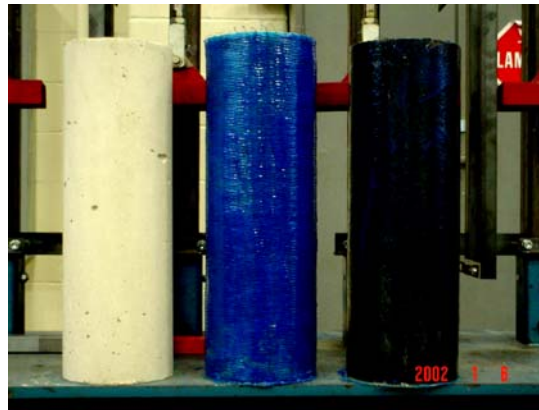


Figure 3.3. Small-Scale RC Columns after FRP Wrapping
(From left to right: Unwrapped, GFRP, CFRP wrapped column)

The columns were manufactured in the materials laboratory at the University of Missouri-Rolla and were cured under the ambient environment prior to the environmental conditioning phase. FRP sheets were applied by wet-lay up technique; first, a coat of primer was applied to ensure good bond between the FRP sheets and concrete surface, and second, saturant was used to saturate the FRP sheets and bond the FRP sheets to the concrete surface. The FRP sheets were applied along the height of columns. The fibers were oriented at 90-degree angle relative to the primary vertical axis of the column.

3.2.1.4 Environmental conditioning. In this study, the combined environmental cycle, as shown in Figure 3.4, was used for environmental conditioning of the small-scale and mid-scale RC columns. The combined environmental cycle was designed to simulate the seasonal change throughout one year in the Midwest region of North America. For that purpose, 30 freeze-thaw cycles were included in the combined environmental cycles in order to simulate the rapid temperature change over the day and night during the winter season. 20 high-temperature cycles were also included in order to account for the rapid variation of temperature over the day and night in the summer season while high-humidity cycles were for the rapid variation of humidity during the change of season from spring to summer and from summer to fall. UV radiation was applied at the constant temperature of 120 °F during the high-temperature cycles. In addition, 5 % saline solution was used to simulate de-icing salt used in the winter season.

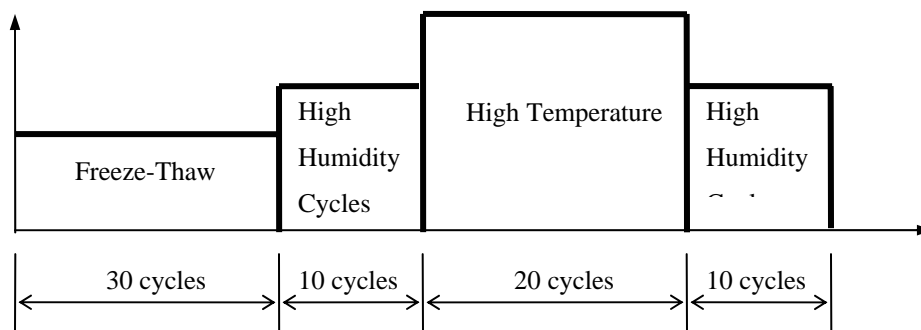


Figure 3.4. Combined Environmental Cycle

Each environmental cycle in the combined environmental cycle is described in Figures 3.5 through 3.7. The freeze-thaw cycles shown in Figure 3.5 consisted of one-hour freeze at 0 °F and one-hour thaw at 50 °F, and 30 min. ramping up and down. The high temperature cycles shown in Figure 3.6 consisted of one-hour low temperature of 80 °F, one-hour high temperature of 120 °F, and 20 min. ramping up and down. Ultraviolet radiation was applied at the temperature of 120 °F during the high temperature cycles. The ultraviolet lamps were positioned in the environmental chamber and they exposed the columns to an irradiance of $6.80 \times 10^{-2} \text{ W/cm}^2$ in a spectral band of 300-800 nm. The high humidity cycle shown in Figure 3.7 consisted of 20-min. 60 % R.H. at 60 °F, 20-min. 100 % R.H. at 80 °F, and 30 min. ramping up and down.

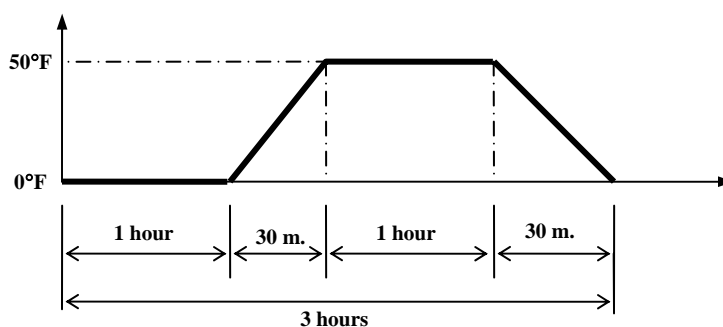


Figure 3.5. Freeze-Thaw Cycle

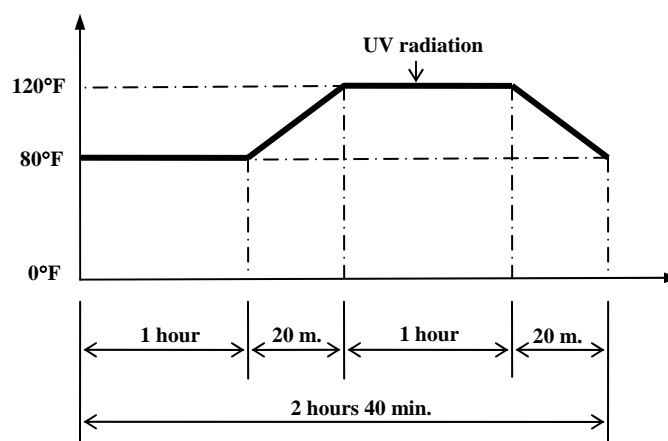


Figure 3.6. High-Temperature Cycle

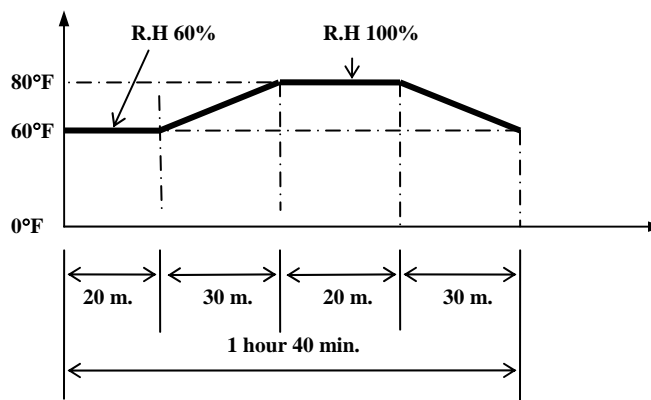


Figure 3.7. High-Humidity Cycle

This combined environmental cycle was repeated ten times so that it could simulate 10 years of outdoor exposure. Since temperatures used in this combined environmental cycles were far more severe than the average temperatures measured in the Midwest of North America (see Table 3.5), the combined environmental cycles could lead to more severe result than in nature. Thus, the combined environmental cycles used in this study could represent more than 10 years of outdoor exposure.

The environmental conditioning was conducted using an environmental chamber. The environmental chamber, located in the Engineering Research Laboratory at the University of Missouri-Rolla, has the interior dimensions of 12 ft by 12 ft in area and 7.4 ft in height. This facility is unique in its large scale, and thus even mid-scale RC columns of this study could be placed. Furthermore, temperature and humidity can be controlled automatically through the central control panel that can program the profiles of the environmental cycles as well as UV radiation.

3.2.1.5 Test set-up and instrumentation. All the columns were tested in uniaxial compression after the environmental conditioning. The load was applied using a hydraulic universal testing machine at a constant loading rate of approximately 0.5 kips/sec. Two linear variable differential transformers (LVDTs) were used to measure the longitudinal deformation, as shown in Figure 3.8. The gage length of the LVDTs was 12 in. covering two-thirds of the height of the columns. To monitor the radial strain of

the columns, strain gages were attached to the surface of the FRP sheet at the mid-height of the columns. Applied load was measured by a load cell with a capacity of 500 kips.

Table 3.5. Thirty-Year Average Temperatures in Missouri (°F)

Month	Highest Temperature		Lowest Temperature	
	1998	30 year Avg.	1998	30 year Avg.
1	42.8	6.2	27.9	9.4
2	48.9	7.5	34.6	11.8
3	48.1	-5.2	33.4	0.4
4	64.5	-2.1	44.8	1.1
5	81.5	7.4	60.3	7.2
6	84.5	1.7	64.6	3.4
7	86.5	-2.1	70	3.8
8	88.9	2.2	68.6	4.8
9	84.8	6	63.8	6.8
10	69.9	2.3	48.9	3.4
11	59.4	5.8	40.3	5.7
12	46.5	6.2	26.7	-3.5

Measurement of temperature has been done in the Columbia, Missouri.

(<http://www.missouri.edu/~soilwww/weather.htm>)

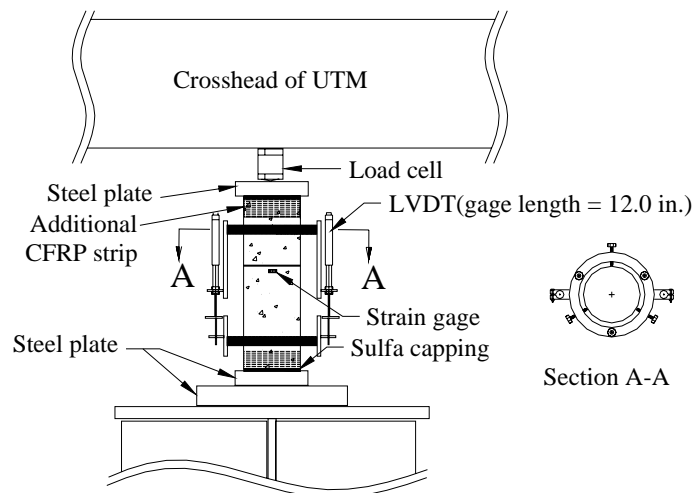


Figure 3.8. Test Set-Up and Instrumentation of Small-Scale RC Columns

3.2.2. Mid-Scale RC Column Tests. Mid-scale column tests were performed to verify the proposed design guidelines. Since the proposed guidelines were developed based on the test results of the small-scale columns with relatively lower strength of concrete, it was necessary to verify the performance through the comparison with the experimental results of different scale RC columns made of normal strength concrete.

3.2.2.1 Test matrix. Table 3.6 presents the test matrix of the mid-scale RC columns. As shown in Table 3.6, the main parameters included the FRP sheet types and environmental conditioning types. In the small-scale RC column tests, the number of FRP sheet layers was a parameter. However, in this test, the number of FRP sheet layers was limited to one layer because of the limit of loading equipment capacity; the predicted failure load of the mid-scale RC columns wrapped with 2 layers of CFRP sheet appeared to exceed the maximum capacity of the hydraulic universal testing machine. The environmental conditions used in this test were identical to those of the small-scale columns except that saline solution was not used during the environmental conditionings.

Table 3.6. Test Matrix for Mid-Scale RC Columns

Specimen	Test parameters							Number of specimens
	FRP layer	FRP type	Description of environmental conditioning					
			Room temperature	Freeze-thaw cycles	High-temperature cycles	UV radiation	High-humidity cycles	
M-C1-CONT	1	CFRP	X					1
M-G1-CONT	1	GFRP	X					1
M-C1-F/Th	1	CFRP		X				1
M-G1-F/Th	1	GFRP		X				1
M-C1-CE	1	CFRP		X	X	X	X	1
M-G1-CE	1	GFRP		X	X	X	X	1
Total								6

The test columns in Table 3.6 are identified by groups of letters and a number separated by hyphens. Each of these descriptive groups gives information about some aspect of the columns in this order: (1) column size (M for mid-scale), (2) FRP sheet type (C and G for CFRP and GFRP sheet, respectively), (3) number of FRP layer (1 for one layer) and (4) environmental conditioning type (CONT, F/Th and CE for control, freeze-thaw, and combined environmental cycles, respectively).

Six columns were fabricated for the parametric study. They were categorized into two groups in order to evaluate the effect of each environmental condition for comparative study: Group 1 (M-C1-CONT, M-C1-F/Th, M-G1-CONT and M-G1-F/Th) and Group 2 (M-C1-CONT, M-C1-CE, M-G1-CONT and M-G1-CE). The objective of Group 1 was to investigate the effect of the freeze-thaw cycles, while Group 2 was used to investigate the effect of the combined environmental cycles.

3.2.2.2 Materials used. The concrete with a target strength of 3,000 psi was provided by a local ready-mixed concrete plant; however, the average compressive strength of the concrete was determined to be 4,100 psi based on the test results of the standard cylinders ($\phi 6 \times 12$ in.) at the time of testing the mid-scale RC columns.

Number 3 and grade 60 reinforcing bars were used for longitudinal reinforcements, while number 2 steel wires were used for spiral reinforcements. Two types of FRP sheets (CFRP and GFRP) were used. The mechanical properties of steel reinforcements and FRP sheets were described in detail in Section 3.2.1.2.

3.2.2.3 Specimen detail and manufacturing. The schematic drawing of the mid-scale RC columns is illustrated in Figure 3.9. Mid-scale RC columns were prepared to simulate bridge piers. As shown in Figure 3.9, mid-scale RC columns consisted of a circular cross-section in the middle test region and larger square concrete blocks at both ends. The concrete blocks were included to avoid failure at the end of the column and simulate the case of the existing foundation or bridge cap. The diameter of the circular cross-section was 8 in. with a column length of 36 in. Eight number 3 reinforcing bars were used for longitudinal reinforcements. The spacing of the spiral reinforcement was 2 in. FRP sheets were applied using the wet-lay up technique. Since the width of FRP sheet provided by the manufacturer is 20 in., which is much less than the height of the mid-scale RC columns of 36 in., two individual FRP sheets (20 in. wide sheet and 16 in

wide sheet) were used to wrap one mid-scale column. There was no lap splice between these individual FRP sheets in longitudinal direction. Instead, 2.86 in. lap splice was applied in transverse direction. Figure 3.10 shows the mid-scale RC columns wrapped with CFRP and GFRP sheets.

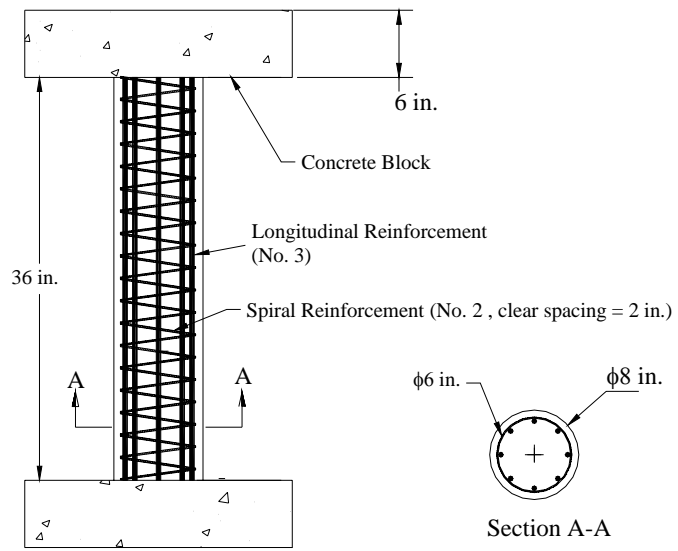


Figure 3.9. Detail of Mid-Scale Column



Figure 3.10. Mid-Scale RC Columns after FRP Sheet Wrapping

3.2.2.4 Test set-up and instrumentation. All the columns were tested under uni-axial compression. The load was applied using a hydraulic universal testing machine at a constant loading rate of approximately 0.5 kips/sec. Two string transducers were used to measure the longitudinal deformation. The gage length was 30 in. To monitor the radial strain of the columns, strain gages were attached to the surface of the FRP sheets at the mid-height of the columns. Applied load was measured by a load cell with a capacity of 500 kips. All the data were collected automatically by the computer operated data acquisition system. The schematic drawing of the test set-up of the mid-scale RC columns is presented in Figure 3.11.

3.2.2.5 Environmental conditioning. Environmental conditioning of the mid-scale RC columns was performed using the same environmental cycles used in the small-scale RC column tests. A detailed description regarding the environmental cycles can be found in Section 3.2.1.4.

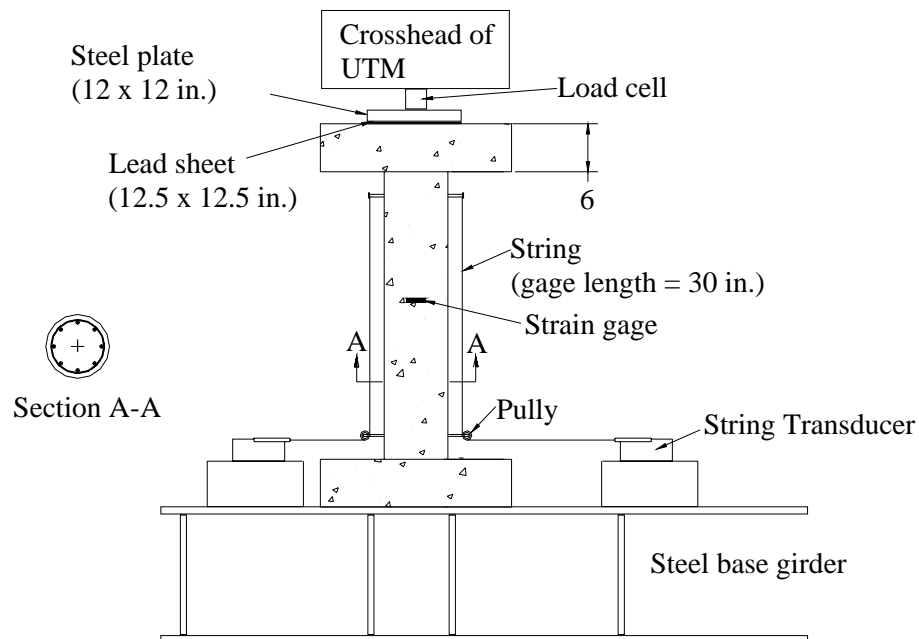


Figure 3.11. Test Set-Up and Instrumentation of Mid-Scale Column

3.3. CORROSION TESTS

3.3.1. Small-Scale RC Column Tests. The objective of this test was to investigate how effectively FRP sheet wrapping protect RC columns from the corrosion of steel reinforcements embedded in the columns. The test results were also used to develop design guidelines.

3.3.1.1 Test matrix. A total of thirty-six small-scale RC columns were fabricated for the corrosion tests, as summarized in Table 3.7. Test parameters include types of concretes, times of FRP wrapping, types of environmental conditions, and types of repair methods.

Some columns (R-series in the test matrix) were made out of regular concrete and the others (C-series) were made out of chloride-contaminated concrete. By comparing these two different series of columns, the effect of chloride ions in concrete on the initial speed to break down the passive film of steel reinforcements was investigated.

Column R-CONT was the control column of the R-series columns and was conditioned under the accelerated corrosion process. Column R-COV was conditioned under the accelerated corrosion process, but it was repaired after a certain period of accelerated corrosion process by the conventional method. The conventional repair method used in this test consisted of removing the corrosion-damaged cover and patching new concrete with low permeability. After the repair, the columns were conditioned under 300 freeze-thaw cycles, as specified previously in Figure 3.5 before the failure test. Column R-CFRP was conditioned by the same method as the columns R-COV. However, this column was repaired by CFRP wrapping instead of the conventional repair method, without removing the corrosion-damaged concrete cover.

Column C-CONT was used as the control column of C-series columns and was kept at room temperature until the failure test. Columns C-CON2 and C-CON3 were conditioned by wet-dry cycles in which the columns were immersed in 5 % saline solution during the wet-cycles. The purpose of these columns was to simulate the natural corrosion process of RC columns under severe corrosive environment.

Column C-CON4 was not strengthened with CFRP wrapping and conditioned under the accelerated corrosion process to serve as corrosion-damaged RC columns. Columns C-CFRP1, C-CFRP2, C-CFRP3 and C-CFRP4 were strengthened with CFRP

sheets and were conditioned under the accelerated corrosion process; Columns C-CFRP1 and C-CFRP3 were strengthened with CFRP sheets before the starting of the accelerated corrosion process, while Columns C-CFRP2 and C-CFRP4 were strengthened with CFRP sheet after a certain period of the accelerated corrosion process to induce corrosion-damage. These columns were then conditioned again under the accelerated corrosion process. In addition, it has been hypothesized that micro-cracks between fibers and matrix can develop due to the freeze-thaw cycles, eventually resulting in the increase in corrosion rate because of the moisture ingress through the micro-cracks. Thus, Columns

Table 3.7. Test Matrix of Small-Scale RC Columns for Corrosion Tests

Regular concrete			
Specimen	FRP Layer	Test Program (see note below)	# of Specimen
R-CONT	0	(CL+FP)-FA: Control	2
R-COV	1	(CL+FP)-RE-FT-(CL+FP)-FA	2
R-CFRP	1	(CL+FP)-AF-FT-(CL+FP)-FA	2
Chloride concrete			
Specimen	FRP Layer	Test Program (see note below)	# of Specimen
C-CONT	0	None -FA: Control	4
C-CON2	0	CL-FA	3
C-CON3	1	AF-CL-FA	3
C-CON4	0	(CL+FP)-FA	4
C-CFRP1	1	AF-(CL+FP)-FA	4
C-CFRP2	1	(CL+FP)-AF-(CL+FP)-FA	4
C-CFRP3	1	AF-(CL+FP)-FT-(CL+FP)-FA	4
C-CFRP4	1	(CL+FP)-AF-FT-(CL+FP)-FA	4
Total			36

* Key:

CL: Chloride solution attack FP: Fixed electric potential

(CL+FP): Chloride solution attack and fixed electric potential simultaneously

RE: Repair by conventional method

AF: Apply FRP sheet FT: Freeze-thaw cycles FA: Failure test

C-CFRP3 and C-CFRP4 were conditioned under the 300 freeze-thaw cycles before the starting of the second accelerated corrosion process; the test programs of Columns C-CFRP3 and C-CFRP4 are identical to those of the columns C-CFRP1 and C-CFRP2, respectively, except for the freeze-thaw cycles.

3.3.1.2 Materials used. The concrete used for R-series columns was produced using the mixture proportion, previously detailed in Table 3.3, which was also used for the small-scale RC columns for the ambient environmental effect tests. The chloride contaminated concrete was also produced according to the same mixture proportion, except that 5 % of salt was mixed with mixing water by weight. The compressive strengths of the concretes were determined based on the test results of standard cylinders ($\phi 6 \times 12$ in.) as presented in Table 3.8. For steel reinforcements and FRP sheets, the same kinds of materials that were used for the ambient environmental tests were used. Their mechanical properties are described in Section 3.2.1.2.

Table 3.8. Compressive Strength of Concrete Used for Small-Scale RC Columns for Corrosion Tests

	Regular Concrete	Chloride Contaminated Concrete
Compressive Strength f'_c (psi)	3,049	3,110

3.3.1.3 Specimen detail and manufacturing. The small-scale RC columns used in the corrosion tests are identical to the small-scale RC columns used in the ambient environmental effect tests, except that there is a longitudinal steel reinforcement at the center, which acted as the cathode during the accelerated corrosion process. The details of the columns are presented in Figure 3.12. These columns were also manufactured at the materials laboratory at the University of Missouri-Rolla and were cured at the ambient environmental condition until the accelerated corrosion process started.

3.3.1.4 Accelerated corrosion process. It is well known that the corrosion of steel reinforcements in RC structures is primarily caused by chloride attacks since

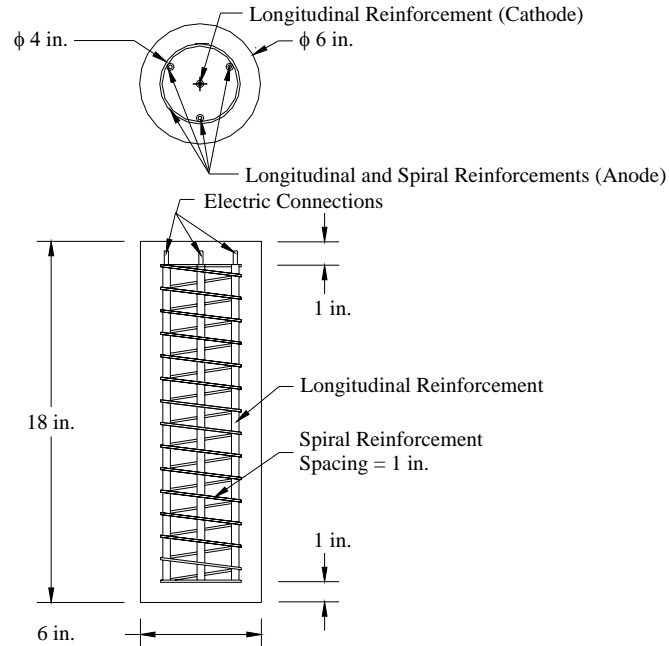
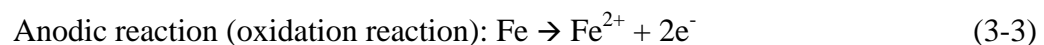


Figure 3.12. Details of Small-Scale RC Columns for Corrosion Test

chloride ions destroys the passive film forming on the surface of steel. Even if the mechanism of the passive film is not theoretically understood at this time, it is well known from experience that steel can be well protected in the concrete because of the high alkaline characteristic of normal concrete (pH of normal concrete is 12 ~ 13). A chloride attack, such as de-icing salt, can decrease the pH of the concrete, resulting in the damage of the passive film. Once the passive film breaks down, corrosion of steel can occur if oxygen and moisture are readily available to the steel. Concrete can breathe, which means that concrete is porous and permeable so that it can contain oxygen and moisture. Thus, corrosion continuously occurs unless the steel is repassivated. The full corrosion process is illustrated in Figure 3.13.

As shown in Figure 3.13, when steel in concrete corrodes, it dissolves in the pore water and gives up electrons; this is called anodic reaction.



The two electrons ($2e^-$) created in the anodic reaction must be consumed somewhere else on the steel surface to preserve electrical neutrality. This reaction is called cathodic reaction; it consumes oxygen and water as well as electrons, generating hydroxyl ion.

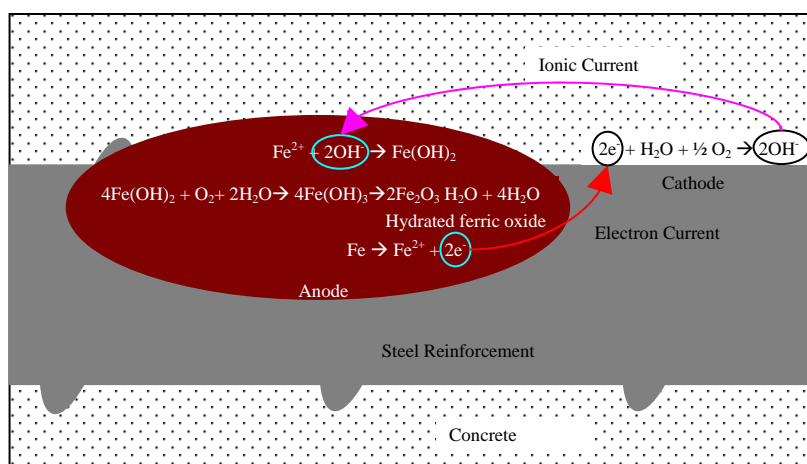
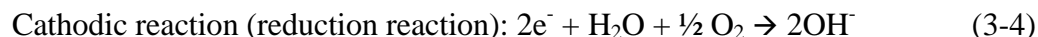
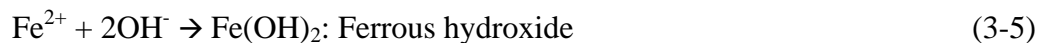


Figure 3.13. Schematic Drawing of Corrosion Process of Steel Reinforcement in Concrete

These two reactions are only the first step in the process of creating rust, which is the by-product of corrosion process. If the steel were dissolved in the pore water (the ferrous ion Fe^{2+} is soluble), cracking and spalling of cover concrete would not be seen. Thus, several more steps must occur for rust to form. The hydroxyl ions created in the cathodic reaction migrate to the anodic area through the ionic path in the concrete, and then finally forms ferrous hydroxide $\text{Fe}(\text{OH})_2$ by combining with ferrous ion (Fe^{2+}) created in anodic reaction as shown in Equation (3-5). By the two more chemical reactions in the anode areas, as shown Equations (3-6) and (3-7), hydrated ferric oxide (rust) is created.



The volume of unhydrated ferric oxide Fe_2O_3 is about two times greater than that of the steel. When it becomes hydrated, it swells even more. Thus, the rust generates the internal pressure around the steel and concrete interface, eventually causing the cracks and spalling of the concrete cover.

Since the corrosion of steel reinforcements in RC structures occurs over several years in the real world until cracking and spalling of concrete occur, it was necessary to establish an accelerated corrosion process to induce the corrosion of steel reinforcements in a laboratory within a relatively short period. In this study, the concept of electrolyte cell was adapted, as shown in Figure 3.14.

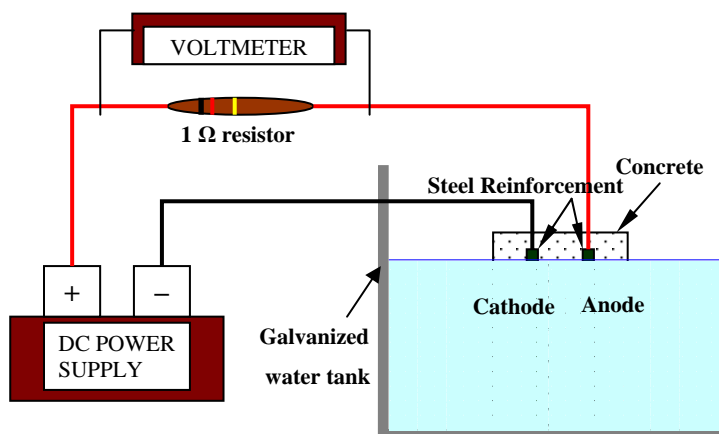


Figure 3.14. Schematic Drawing of the Accelerated Corrosion Process

The columns were placed in the water tank filled with a 5 % saline solution in order to destroy the passive film of steel reinforcements and supply water and oxygen. In addition, it was possible for the anode to lose a large amount of electrons by imposing

fixed electric potential. The fixed electric potential was supplied by a DC power supply. The corrosion rate was monitored by means of checking the electric voltage drop between the anode and the cathode using a voltmeter. Then, the corrosion current was calculated based on the measured voltage drop by Ohm's law as shown Equation (3-8),

$$\text{Ohm's law: } I=V/R \quad (3-8)$$

where I is current (Amp), V is voltage drops (V), and R is electric resistivity (Ω). Thus, an electric resistor of 1Ω was installed between the anode and the cathode to measure the voltage drop and the electric current. Figure 3.15 shows the laboratory set-up for the accelerated corrosion process.

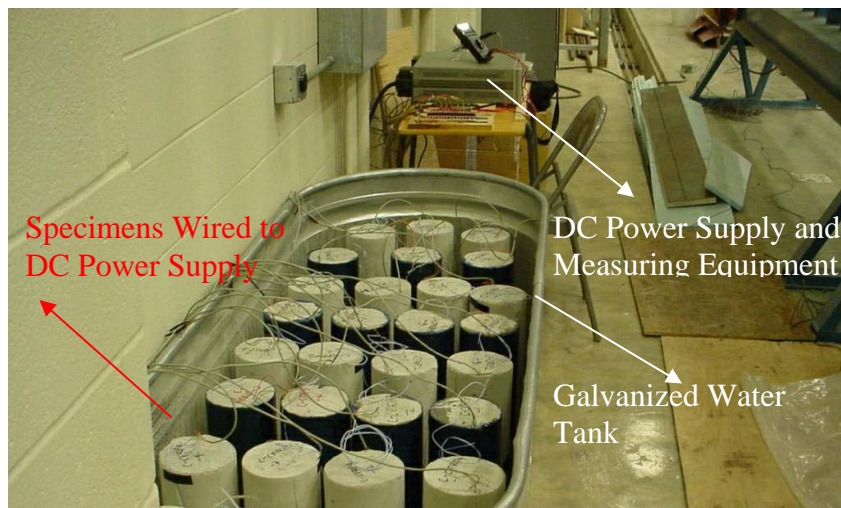


Figure 3.15. Laboratory Set-Up of the Accelerated Corrosion Process

The accelerated corrosion process in this study was separated into three stages, as shown in Table 3.9. During the first stage, the corrosion rate of the unwrapped and the CFRP wrapped columns was investigated. During the second stage, the evaporation rate of the entrapped moisture of the CFRP wrapped columns was investigated. After the

completion of the second stage, corrosion damaged columns were repaired either by the CFRP sheet wrapping or by the conventional method, and some of the columns were conditioned by 300 freeze-thaw cycles. The third stage was identical to the first stage.

Table 3.9. Stages of Accelerated Corrosion Process

Stages	Duration	Conditions of Accelerated Corrosion Process
1	1~63	Wet-dry cycles and fixed potential of 6V
2	64~249	Dry condition and fixed potential of 6V
3	250~316	Wet-dry cycles and fixed potential of 6V

3.3.1.5 Repair of the columns damaged by the accelerated corrosion process.

Columns R-CONT, C-CONT, C-CON2, and C-CON4 were unwrapped RC columns. Columns C-CON3, C-CFRP1 and C-CFRP3 were strengthened by CFRP sheet wrapping before the beginning of the accelerated corrosion process. The above mentioned columns were not repaired by any methods during the accelerated corrosion process. The remaining columns, R-COV, R-CFRP, C-CFRP2, and C-CFRP4, were repaired using the following methods.

3.3.1.5.1 Conventional method. Columns R-COV were repaired by the conventional method, which consisted of removing damaged concrete and patching a new low-permeable concrete after the second stage of the accelerated corrosion process. As shown in Figure 3.16, Columns R-COV were severely damaged by the accelerated corrosion process. The surface was stained by the rust and salt crystals, and longitudinal and transverse cracks were formed along the longitudinal and spiral reinforcements. The maximum width of the longitudinal cracks was 1/8 in.

Removal of the corrosion-damaged concrete cover was conducted using a pneumatic hand-held hammer, as shown in Figure 3.17. During the removal, it was also

noticed that there was a significant amount of rust around the longitudinal and spiral reinforcements underneath the cover concrete, as shown in Figure 3.17.



Figure 3.16. Column R-COV after the Second Stage of the Accelerated Corrosion Process



Figure 3.17. Removing of Corrosion-Damaged Concrete Cover by Pneumatic Hammer

Figure 3.18 shows Columns R-COV after the removal of the corrosion-damaged concrete cover. As illustrated in Figure 3.18, the spiral reinforcements of both columns, especially for Column R-COV-1, were severely damaged by the accelerated corrosion. Furthermore, the core concrete inside the spiral reinforcement of Column R-COV-1 was damaged by the pneumatic hammering, and thus the core concrete was all removed as shown in Figure 3.18. Therefore, the spiral reinforcement and concrete of Column R-COV-1 was replaced with new ones. Meanwhile, the core concrete and spiral reinforcement of Column R-COV-2 were used again as they were. In addition, the electric connection for the accelerated corrosion process was destroyed



Figure 3.18. Column R-COV after Removing of Corrosion-Damaged Concrete Cover

The concrete used for the repair was produced according to the mixture proportion as shown in Table 3.10. The compressive strength was determined as 3,049 psi based on the test results of standard cylinders ($\phi 6 \times 12$ in.) at the time of the failure test of Column R-COV.

Table 3.10. Mixture Proportion of the Concrete for the Repair of Column R-COV

							Unit lb/yd ³
W/C	Slump(in.)	Air (%)	S/a (%)	Cement	Water	Fine Aggregate	Course Aggregate
0.44	3.0	2.0	45	311	710	1282	1568

3.3.1.5.2 CFRP sheet wrapping after epoxy injection into cracks. Columns C-CFRP2 and C-CFRP4 were repaired by the CFRP sheet wrapping after the second stage of the accelerated corrosion process. Among them, four columns (C-CFRP2-3, C-CFRP2-4, C-CFRP4-3 and C-CFRP4-4) were wrapped with CFRP sheets after the cracks were sealed with epoxy injection. The procedure of the epoxy injection is presented in Figure 3.19.

3.3.1.5.3 CFRP sheet wrapping without epoxy injection into cracks. The remaining four columns of C-CFRP2 and C-CFRP4 were repaired by CFRP sheet wrapping after the second stage of the accelerated corrosion process without epoxy injection.

3.3.1.6 Test set-up and instrumentation. The test set-up and instrumentation was identical to that used in the ambient environmental effect tests, and it is described in Section 3.2.1.5.

	<p>(a) Step 1 Clean the surface and place the plastic ports on top of the cracks.</p>
	<p>(b) Step 2 Apply high-viscosity and quick-set epoxy resin along the cracks and wait for at least a day until it is cured.</p>
	<p>(c) Step 3 (1) Using a chalk gun, inject low-viscosity epoxy resin into one of the plastic ports until it comes out of other ports, (2) cover the plastic ports, (3) allow at least 3 day curing, and then (4) remove the plastic ports and clean the surface using a hand grinder.</p>

Figure 3.19. Procedure of Epoxy Injection Method

3.3.2. Mid-Scale RC Column Tests. The test results of the mid-scale RC columns were used to verify the performance of the design guidelines developed based on the test results of the small-scale RC columns.

3.3.2.1 Test matrix. A total of four columns were tested, as shown in Table 3.11. Column M-CONT was the control column. Column M-CFRP-COR was strengthened with CFRP sheet wrapping before the beginning of the accelerated corrosion process. Columns M-COR-CFRP and M-COR-CFRP-COR were conditioned first under the accelerated corrosion process and then strengthened with the CFRP sheet wrapping. However, Column M-COR-CFRP-COR was conditioned again under the accelerated corrosion process after it was strengthened with the CFRP sheet wrapping.

Table 3.11. Test Matrix of Mid-Scale RC Columns for Corrosion Tests

Specimen	FRP Layer	Test Program	# of Specimen
M-CONT	0	None -FA	1
M-CFRP-COR	1	AF-(CL+FP)-FA	1
M-COR-CFRP	1	(CL+FP)-AF-FA	1
M-COR-CFRP-COR	1	(CL+FP)-AF-(CL+FP)-FA	1
Total			4

3.3.2.2 Materials used. The concrete with a target strength of 3,000 psi was provided by a local ready-mixed concrete company; the compressive strength was, however, determined as 4,907 psi based on the test results of standard cylinders ($\phi 6 \times 12$ in.) at the time of the failure test of the columns.

Number 3 and grade 60 reinforcing bars were used for longitudinal reinforcements, while, number 2 steel wires were used for spiral reinforcements. CFRP sheets were used. Mechanical properties of the steel reinforcements and CFRP sheets are presented in detail in Section 3.2.1.2.

Aluminum pipes, made of Aluminum 6061-T6, were used as an internal cathode during the accelerated corrosion process. The inside and outside diameter of the pipe was 1.063 in. and 1.313 in., respectively and the thickness was 0.125 in. Tensile tests were

performed to obtain stress vs. strain relationship of the aluminum pipes, and the results are presented in Figure 3.20. A bi-linear stress-strain model for this aluminum was derived based on the experimental results as shown in Equations (3-9) and (3-10),

$$f_s = E_s \varepsilon_s \text{ when } f_s \leq f_y \quad (3-9)$$

$$f_s = f_y + 84.7 \left(\varepsilon_s - \frac{f_y}{E_s} \right) \text{ ksi when } f_s \geq f_y \quad (3-10)$$

where, yield strength, f_y , is 40 ksi, tensile strength, f_u , is 45 ksi, and elastic modulus, E_s , is 10,000 ksi.

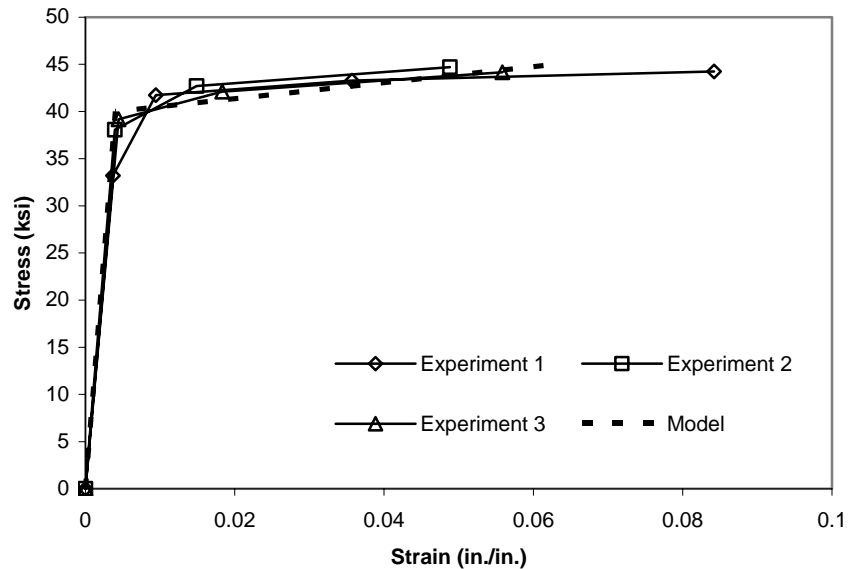


Figure 3.20. Experimental Results of Tensile Test of Aluminum 6061-T6 Bars and Bi-Linear Model

3.3.2.3 Specimen detail and manufacturing. The schematic drawing of the mid-scale RC columns for the corrosion tests is illustrated in Figure 3.21. The mid-scale

RC columns for the corrosion tests were identical to those of the ambient environmental effect tests, except that the aluminum pipe, shown in Figure 3.22, was installed at the center of the column.

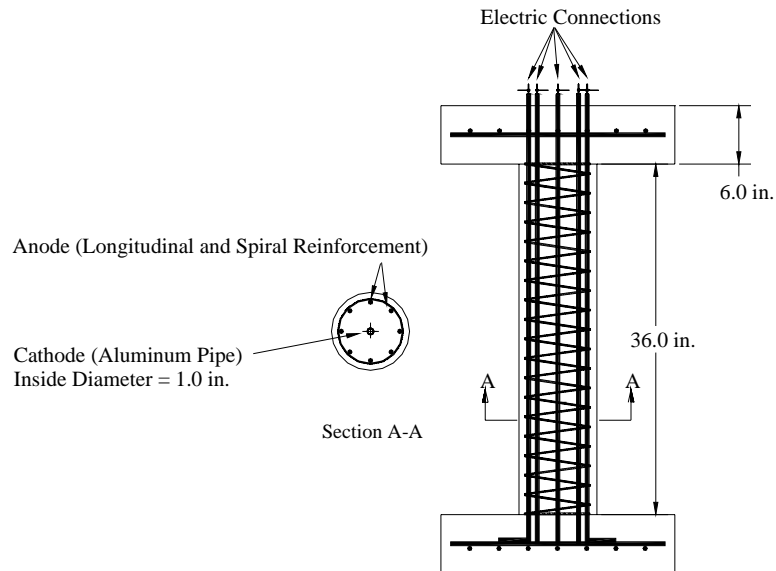


Figure 3.21. Details of Mid-Scale RC Columns for Corrosion Tests



Figure 3.22. Steel Cages and Aluminum Pipes Used for the Mid-Scale RC Columns of Corrosion Tests

3.3.2.4 Accelerated corrosion process. The accelerated corrosion process of mid-scale RC columns was achieved by imposing fixed electric potential of 6V between the steel reinforcements (anode) and the aluminum pipe (cathode). Water and oxygen were supplied through the drilled holes of the aluminum pipes, as shown in Figure 3.22.

3.3.2.5 Repair of the columns damaged by the accelerated corrosion process. The mid-scale RC columns damaged by the accelerated corrosion process were repaired by the CFRP sheet wrapping. Column M-COR-CFRP was strengthened with CFRP sheets after the accelerated corrosion process and then it was tested up to failure in uniaxial compression. Meanwhile, Column M-COR-CFRP-COR was conditioned again under the accelerated corrosion process after it was strengthened with the CFRP sheet wrapping.

3.3.2.6 Environmental conditioning. All the mid-scale RC columns, except for the control column M-CONT, were conditioned by 300 freeze-thaw cycles after the completion of the accelerated corrosion process. The profile of the freeze-thaw cycles is presented in Figure 3.5.

3.3.2.7 Test set-up and instrumentation. Failure tests were conducted in uniaxial compression as described in Section 3.2.2.4. Figure 3.23 shows the photograph of the mid-scale RC column in the test.



Figure 3.23. Column M-CONT in Testing

4. TEST RESULTS AND DISCUSSIONS

4.1. GENERAL

The test results are discussed in detail in this section. Discussions on the axial compressive behavior of the test columns were made, based on the definitions of mechanical properties of FRP confined columns, defined in Section 4.2. Other test results such as load vs. strain curves are provided in Appendices A and B.

4.2. DEFINITIONS OF MECHANICAL PROPERTIES OF FRP CONFINED COLUMNS

Figure 4.1 presents a typical load vs. axial strain curve of FRP wrapped RC columns. As shown in Figure 4.1, the curve is essentially composed of two parts with a transition zone. The initial portion of the curve is referred to as the elastic region and the portion to the right of the transition zone as the plastic region.

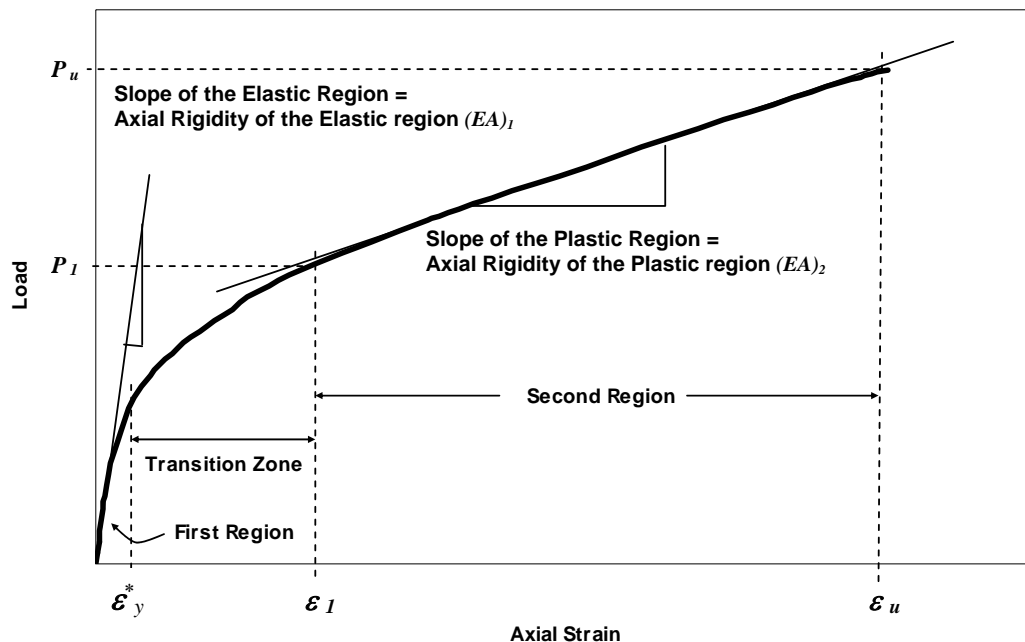


Figure 4.1. Typical Load - Axial Strain Curve of FRP Wrapped Columns

The failure of FRP wrapped RC columns is mainly due to the rupture of FRP sheets, and thus failure load, P_u , is defined as the load at which the column does not resist the applied load any further because of the rupture of FRP sheets.

The slope of the elastic region of the curve is almost identical to that of the unwrapped RC columns because of the passive nature of the FRP sheet wrapping system. In other words, in the elastic region, concrete undergoes little lateral expansion, which actually causes a small confinement pressure. During the transition zone, the core concrete inside FRP wrap exhibits cracking and expands rapidly and thus the FRP sheet wrapping system is fully activated. The response in the plastic region is dependent on the stiffness of the FRP sheet wrapping. Thus, the slope of the curve in the plastic region is an important indicator of the effectiveness of FRP wrapped RC columns and is referred to as axial rigidity in the plastic region, $(EA)_2$, throughout this report. If the concrete is well confined by FRP sheet wrapping, then the slope is positive at every point in the plastic region and is usually quite linear. Thus, the axial rigidity in the plastic region, $(EA)_2$, can be determined by Equation (4-1),

$$(EA)_2 = \frac{P_u - P_1}{\varepsilon_u - \varepsilon_1} \quad (4-1)$$

where P_u and P_1 are the load at axial strains ε_u and ε_1 , respectively, as shown in Figure 4.1.

Ductility was evaluated using ductility index, μ , as defined in Equation (4-2),

$$\mu = \frac{\varepsilon_u}{\varepsilon_y^*} \quad (4-2)$$

where ε_u is the axial strain at failure and ε_y^* is the axial strain at which transition zone begins, as shown in Figure 4.1. In this test, axial strain, ε_y^* , was approximately 0.002 for all the tested columns, which usually corresponds to the yield strain of longitudinal reinforcements used in the columns.

4.3. AMBIENT ENVIRONMENTAL EFFECT TESTS

4.3.1. Small-Scale RC Column Tests. A total of 36 small-scale RC columns were tested in uni-axial compression after exposure to various environmental conditions. The obtained results are summarized in Tables 4.1 through 4.3. In-depth discussions about the effects of the environmental conditions used in this study are presented in Sections 4.3.1.1 through 4.3.1.7.

Table 4.1. Failure Load, P_u , of Small-Scale RC Columns

Specimen	Failure load, P_u (kips)				COV (%)
	1	2	3	average	
S-C0-CONT	49	63	54	55	11
S-C1-CONT	146	138	144	143	3
S-C2-CONT	218	210	224	217	4
S-G1-CONT	139*	165	145	155	9
S-C1-F/Th	148	151	157	152	3
S-C1-CE	133	147	152	144	6
S-G1-F/Th	156	162	167	162	3
S-G1-CE	119	168	144	144	14
S-C2-CE	226	219	191	212	10
S-C1-Na-F/Th	135	143	156	145	8
S-G1-Na-F/Th	116	138	162	139	17
S-C1-Na-CE	142	132	152	142	9

* This column was discarded when calculating average failure load P_u because this column failed at a very low applied load out of the test region due to the stress concentration at the interface between the test region and the end of the column strengthened with the additional layer of CFRP sheets.

Table 4.2. Axial Rigidity in the Plastic Region, $(EA)_2$, of Small-Scale RC Columns

Specimens		First Point		Second Point		$(EA)_2$ (kips)	average $(EA)_2$ (kips)
		P_u (kips)	ϵ_u	P_l (kips)	ϵ_l		
S-C1-CONT	1	146	0.0217	105	0.0079	2942	2588
	2	138	0.0244	100	0.0085	2354	
	3	144	0.0245	107	0.0091	2468	
S-G1-CONT	1	138	0.0187	120	0.0113	2406*	1841
	2	164	0.0363	115	0.0105	1904	
	3	144	0.0350	98	0.0094	1778	
S-C2-CONT	1	217	0.0399	135	0.0116	2903	2960
	2	209	0.0349	140	0.0125	3087	
	3	223	0.0421	135	0.0116	2889	
S-C1-F/Th	1	147	0.0201	105	0.0071	3251	2891
	2	151	0.0248	105	0.0082	2792	
	3	156	0.0250	110	0.0076	2631	
S-C1-CE	1	132	0.0233	95	0.0081	2430	2588
	2	146	0.0201	115	0.0092	2850	
	3	151	0.0261	110	0.0095	2483	
S-G1-F/Th	1	156	0.0390	106	0.0118	1831	2026
	2	161	0.0278	125	0.0113	2162	
	3	167	0.0363	115	0.0115	2085	
S-G1-CE	1	119	0.0195	105	0.0125	1924	1773
	2	168	0.0395	120	0.0133	1814	
	3	143	0.0383	107	0.0150	1581	
S-C2-CE	1	225	0.0450	140	0.0141	2745	2890
	2	218	0.0413	140	0.0138	2814	
	3	190	0.0313	125	0.0105	3112	
S-C1-Na-F/Th	1	135	0.0204	105	0.0090	2608	2688
	2	142	0.0221	105	0.0090	2802	
	3	155	0.0238	115	0.0087	2654	
S-G1-Na-F/Th	1	115	0.0219	90	0.0081	1755	2038
	2	137	0.0250	105	0.0090	2021	
	3	161	0.0290	115	0.0093	2340	
S-C1-Na-CE	1	141	0.0183	115	0.0090	2829	2363
	2	131	0.0270	95	0.0088	1995	
	3	151	0.0254	115	0.0096	2263	

* This column was discarded when calculating average $(EA)_2$ because this column failed at a very low applied load out of the test region due to the stress concentration at the interface between the test region and the end of the column strengthened with the additional layer of CFRP sheets. As a result, the slope of the plastic region was not linear.

Table 4.3. Ductility Index, μ , of Small-Scale RC Columns

Specimens	Ductility Index, $\mu = \varepsilon_u / \varepsilon_y = \varepsilon_u / 0.002$						
	1		2		3		average
	ε_u	μ	ε_u	μ	ε_u	μ	
S-C1-CONT	0.0217	10.9	0.0244	12.2	0.0245	12.3	11.8
S-C2-CONT	0.0399	19.9	0.0349	17.5	0.0421	21.1	19.5
S-G1-CONT	0.0187*	9.4*	0.0363	18.1	0.0350	17.5	17.8
S-C1-F/Th	0.0201	10.1	0.0249	12.5	0.0250	12.5	11.7
S-C1-CE	0.0233	11.6	0.0201	10.0	0.0261	13.1	11.6
S-G1-F/Th	0.0390	19.5	0.0278	13.9	0.0363	18.1	17.2
S-G1-CE	0.0195	9.8	0.0395	19.8	0.0383	19.1	16.2
S-C2-CE	0.0450	22.5	0.0413	20.6	0.0313	15.7	19.6
S-C1-Na-F/Th	0.0204	10.2	0.0221	11.0	0.0238	11.9	11.0
S-G1-Na-F/Th	0.0219	11.0	0.0250	12.5	0.0290	14.5	12.7
S-C1-Na-CE	0.0183	9.2	0.0270	13.5	0.0254	12.7	11.8

* This column was discarded when calculating average ductility index μ because this column failed at a very low applied load out of the test region due to the stress concentration at the interface between the test region and the end of the column strengthened with the additional layer of CFRP sheets. As a result, the axial strain at failure ε_u was significantly lower when compared to the other similar columns.

4.3.1.1 Behavior of the control columns. Group 1 Columns (S-CONT, S-C1-CONT, S-C2-CONT, and S-G1-CONT) were used to evaluate the behavior of the control columns kept at room temperature. Column S-CONT were unwrapped RC columns while Columns S-C1-CONT, S-C2-CONT, and S-G1-CONT were wrapped with 1 layer of CFRP, 2 layers of CFRP and 1 layer of GFRP sheets, respectively.

As shown in Figure 4.2, which presents load vs. axial strain curves of Group 1 Columns, the load carrying capacity of the unwrapped columns was greatly increased by FRP sheet wrapping; however, the initial behavior of the columns wrapped with FRP sheets was not different from that of the unwrapped columns because of the passive nature of the FRP wrapping system.

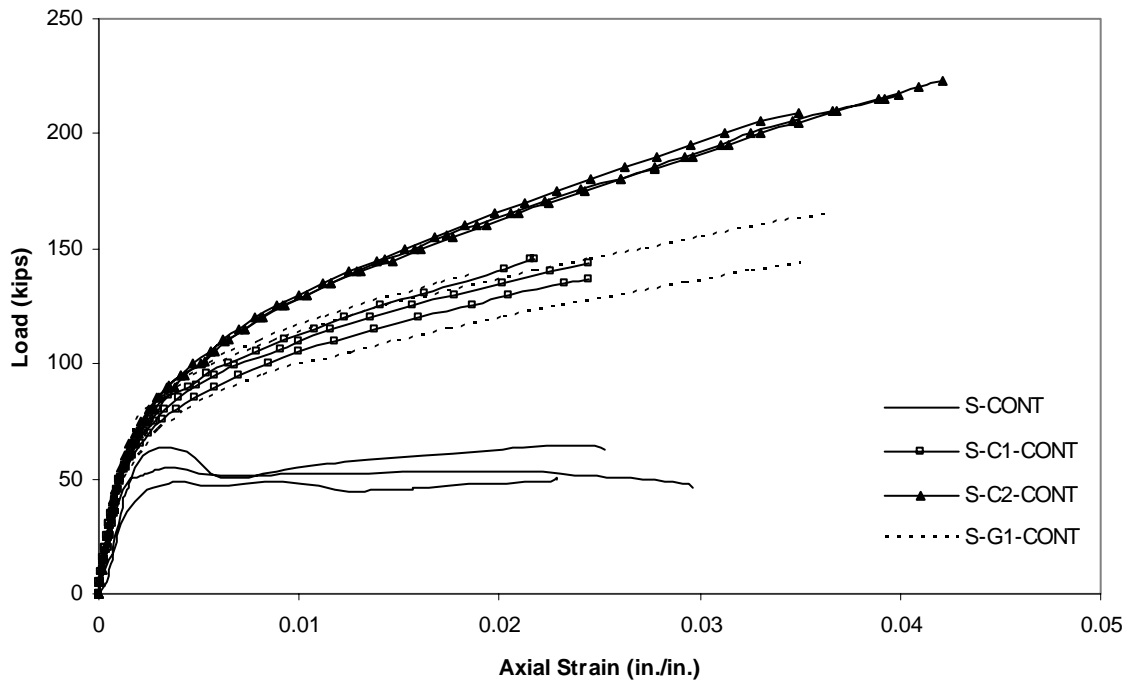


Figure 4.2. Applied Load vs. Axial Strain Curves of the Group 1 Columns

4.3.1.1.1 Failure load, P_u . In Figure 4.3, the average failure load, P_u , of Group 1 Columns is presented. The average failure load, P_u , of Column S-C1-CONT was 2.58 times higher than that of Column S-CONT while the average failure load, P_u , of Column S-G1-CONT was 2.80 times higher than that of Column S-CONT. In addition, as the number of layers of FRP sheets increased, the average failure load, P_u , increased; for example, the average failure load, P_u , of Column S-C2-CONT was 1.52 times higher than that of Column S-C1-CONT. This is because the confining pressure provided by the FRP sheet used for the wrapping of the columns increased as the number of layers increased.

4.3.1.1.2 Failure modes. The unwrapped columns S-CONT did not fail immediately after the cover concrete cracked and spalled off, since the strength of the core concrete had been enhanced by the tri-axial stresses resulting from the spiral reinforcement. As a result, the columns could undergo large deformations until the spiral reinforcement yielded, reaching the second peak load. The failure of the columns wrapped with FRP sheets was directly due to the rupture of the FRP sheets. Sometimes

the collapse was very violent and even explosive. The failure at the lap splice of FRP sheets was not observed. FRP sheets ruptured in the form of a small band at one or more locations as shown in Figure 4.4, which presents Columns S-C-CONT, S-C1-CONT and S-G1-CONT after failure.

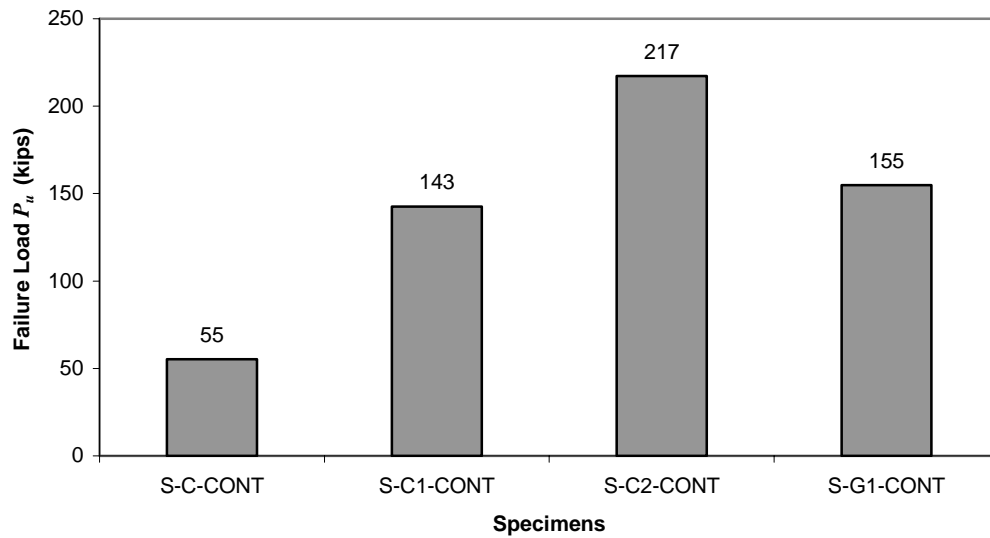


Figure 4.3. Average Failure Load, P_u , of Group 1 Columns



Figure 4.4. Columns S-C-CONT, S-C1-CONT, and S-G1-CONT after Failure
(From Left to Right)

4.3.1.2 Effects of freeze-thaw cycles on the FRP wrapped columns. Group 2 Columns (S-C1-CONT, S-C1-F/Th, S-G1-CONT and S-G1-F/Th) were used to investigate the effects of freeze-thaw cycles. The control columns S-C1-CONT and S-G1-CONT were kept at room temperature; while Columns S-C1-F/Th and S-G1-F/Th were conditioned under the freeze-thaw cycles. Columns S-C1-CONT and S-C1-F/Th were wrapped with 1 layer of CFRP sheet; while Columns S-G1-CONT and S-G1-F/Th were wrapped with 1 layer of GFRP sheet.

The freeze-thaw cycles used in this study did not adversely affect the behavior of the RC columns wrapped with FRP sheets. Rather, the failure load, P_u , slightly increased after the exposure to the freeze-thaw cycles. Figure 4.5 shows the average failure load, P_u , of Group 2 Columns. As shown in Figure 4.5, the average failure load, P_u , of Columns S-C1-F/Th and S-G1-F/Th was 7 % and 4 % higher than that of Columns S-C1-CONT and S-G1-CONT, respectively.

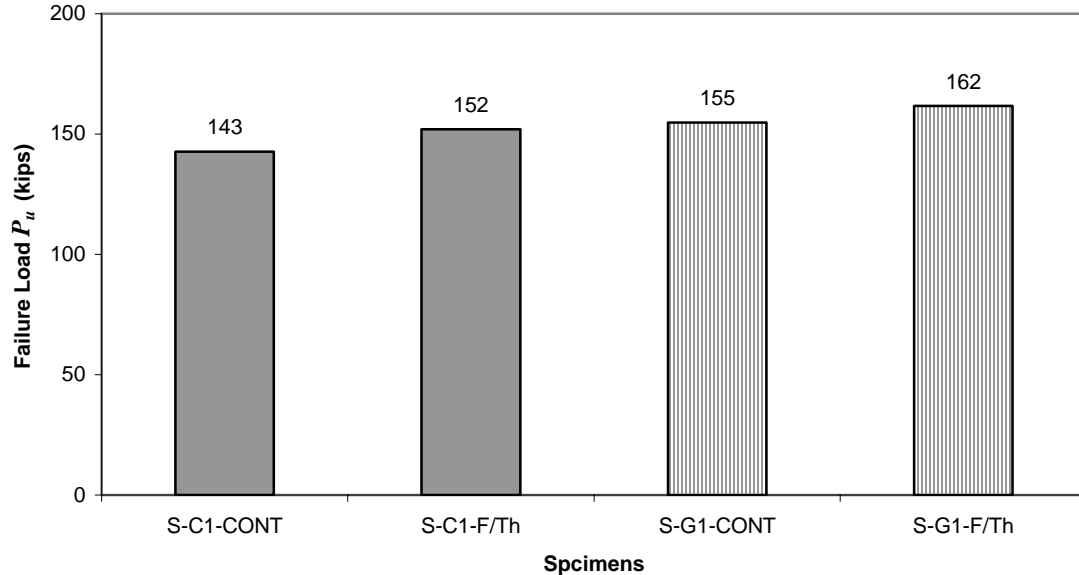


Figure 4.5. Average Failure Load, P_u , of Group 2 Columns

One possible reason for the increase in failure load, P_u , was the matrix hardening effect due to the extremely low temperature used in the freeze-thaw cycles. As a result, the axial rigidity in the plastic region, $(EA)_2$, of the columns conditioned by the freeze-thaw cycles was higher than that of control columns kept at room temperature. The average axial rigidity in the plastic region, $(EA)_2$, of Group 2 Columns is presented in Figure 4.6. As shown in Figure 4.6, the average axial rigidity in the plastic region, $(EA)_2$, of Column S-C1-F/Th was 12 % higher than that of Column S-C1-CONT and the average axial rigidity in the plastic region, $(EA)_2$, of Column S-G1-F/Th was 10 % higher than that of Column S-G1-CONT.

However, ductility index, μ , as defined in Equation (4-2), was decreased very slightly by 1 % and 4 % for both the GFRP and CFRP wrapped columns, respectively, as shown in Figure 4.7. It was probably due to the loss of bond due to the micro-cracking at the matrix-fiber interface induced by the freeze-thaw cycles, as previously reported by Karbhari et al. (2000).

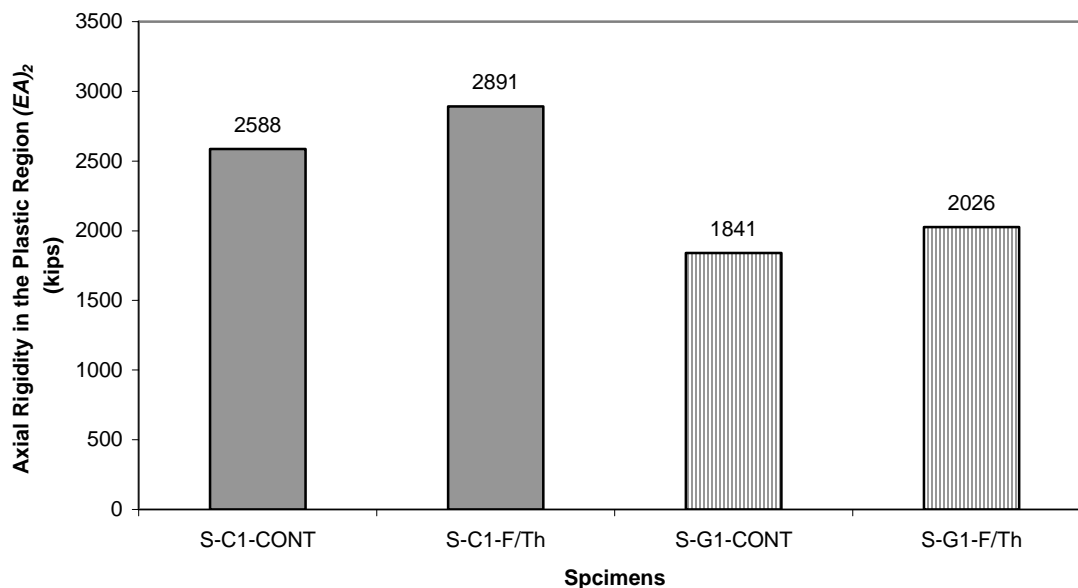


Figure 4.6. Average Axial Rigidity in the Plastic Region, $(EA)_2$, of Group 2 Columns

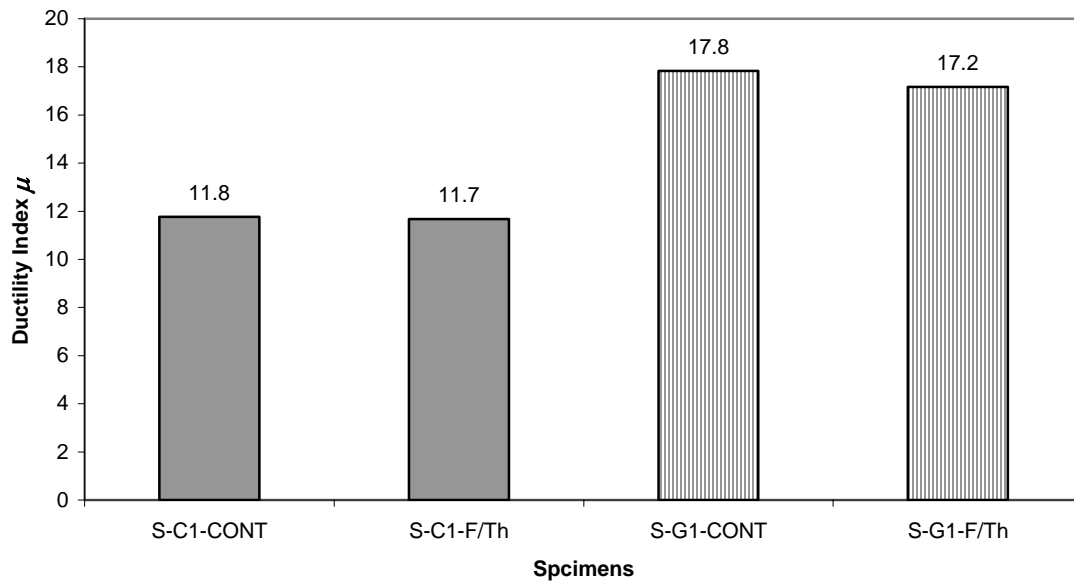


Figure 4.7. Average Ductility Index, μ , of Group 2 Columns

4.3.1.3 Effects of combined environmental cycles on the FRP wrapped columns. Group 3 Columns (S-C1-CONT, S-C2-CONT, S-C1-CE, S-C2-CE, S-G1-CONT and S-G1-CE) were used to investigate the effects of combined environmental cycles. The control columns S-C1-CONT, S-C2-CONT, and S-G1-CONT were kept at room temperature; while Columns S-C1-CE, S-C2-CE, and S-G1-CE were conditioned under the combined environmental cycles. Columns S-C1-CONT and S-C1-CE were wrapped with 1 layer of CFRP sheet; while Columns S-C2-CONT and S-C2-CE were wrapped with 2 layers of CFRP sheets. Columns S-G1-CONT and S-G1-CE were wrapped with 1 layer of GFRP sheet.

The effect of the combined environmental cycles was insignificant in both cases of the CFRP and GFRP wrapped columns. The average failure load, P_u , of Group 3 Columns are presented in Figure 4.8. As shown in Figure 4.8, the average failure load, P_u , of the CFRP wrapped columns was not significantly changed. For the GFRP wrapped columns, the failure load, P_u , of Column S-G1-CE was 7 % lower than that of Column S-G1-CONT.

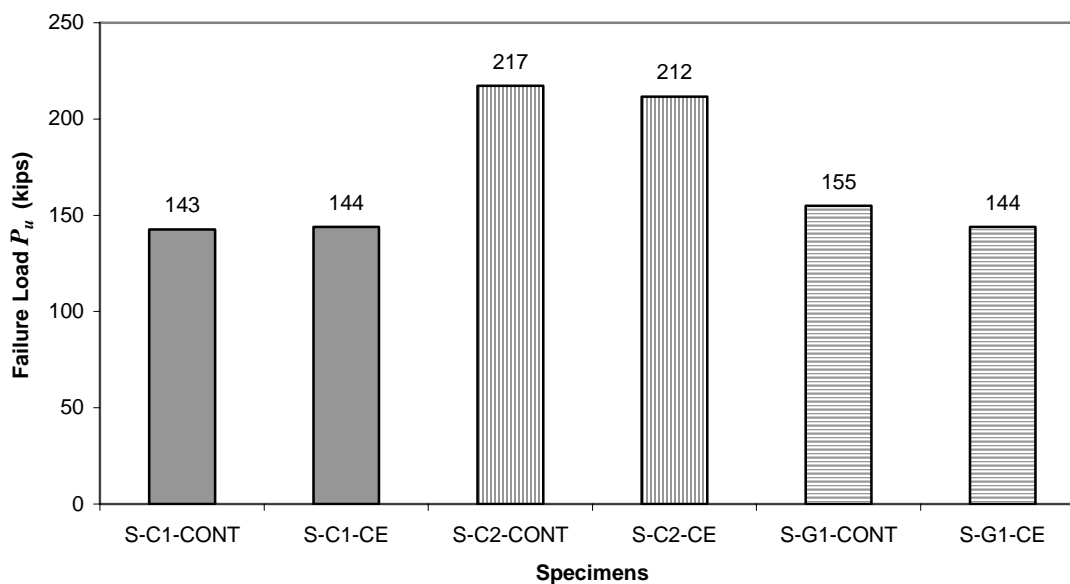


Figure 4.8. Average Failure Load, P_u , of Group 3 Columns

One possible reason for the decrease in failure load, P_u , could be attributed in large part to the plasticization of matrix, which could make the polymer softer. Plasticization is known to be induced by moisture and high temperature. The combined environmental cycles used in this study were composed of high-temperature cycles with UV radiation and high-humidity cycles, along with freeze-thaw cycles. Thus, the high-temperature cycles and high-humidity cycles could affect the change in matrix properties, resulting in plasticization. However, considering that the freeze-thaw cycles slightly increased the failure load due to the matrix hardening effect, as described in the previous section, it can be said that the combined effects of high-temperature cycles and high-humidity cycles compromised the effect of the freeze-thaw cycles. The plasticization was evidenced by the decrease in axial rigidity in the plastic region, $(EA)_2$, and the decrease in ductility index, μ , as shown in Figures 4.9 and 4.10, respectively. As shown in Figure 4.9, the average axial rigidity in the plastic region, $(EA)_2$, of the CFRP wrapped columns was not changed while that of Column S-G1-CE showed a 4 % decrease, when compared to the control specimens.

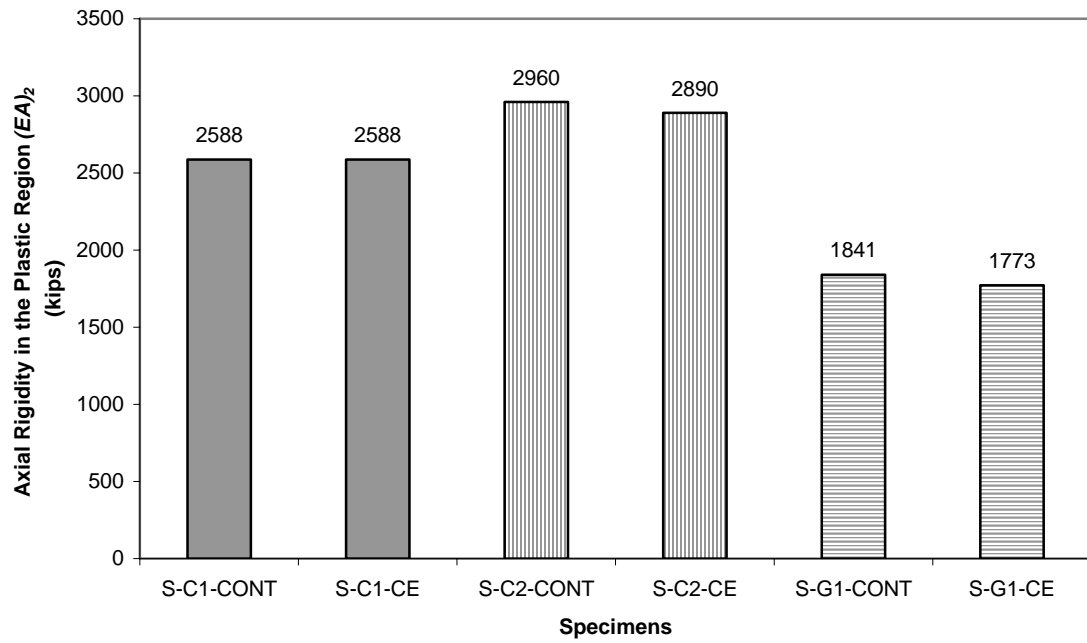


Figure 4.9. Average Axial Rigidity in the Plastic Region, $(EA)_2$, of Group 3 Columns

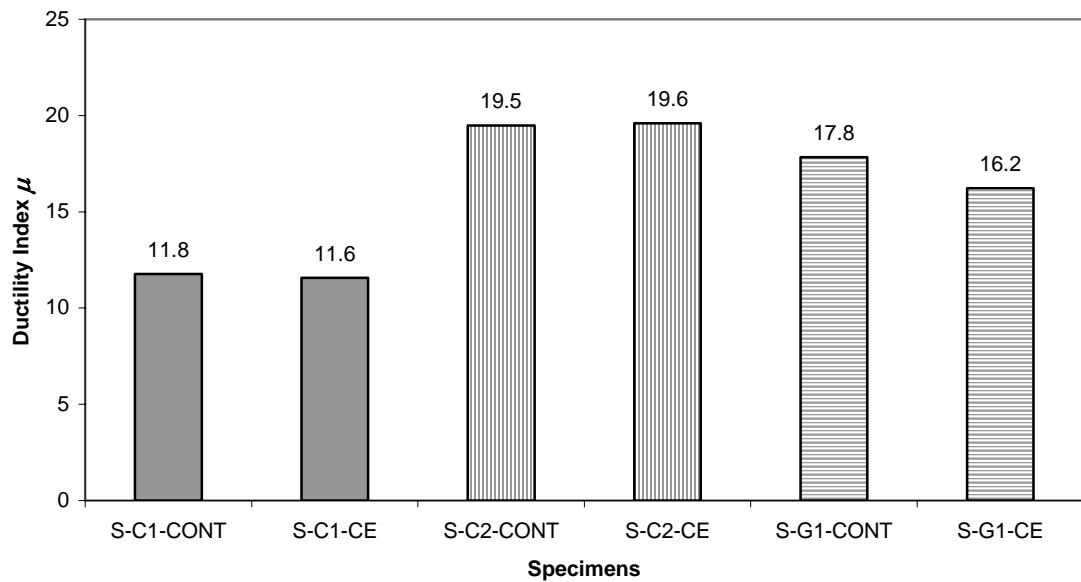


Figure 4.10. Average Ductility Index, μ , of Group 3 Columns

Another reason for the decrease in failure load, P_u , might be due to the micro cracking at the matrix-fiber interface. The micro-cracking could be induced by the variation of temperature and relative humidity. Because the thermal coefficients of the matrix and fibers were different, thermal variation caused shear stress between the matrix and fibers. Volume changes or swelling due to the moisture absorption also caused the stress between the matrix and fibers. As a result, micro-cracks were formed, and, in turn, moisture could reach the fibers by ingress through the micro-cracks. Moreover, it was possible that the surface damage due to the UV radiation used during the high-temperature cycles might accelerate either the moisture ingress through the micro-cracks at the matrix-fiber interface or diffusion via the matrix.

It should be noted now that the extent of decrease in failure load, P_u , of the GFRP wrapped columns was noticeable, while that of CFRP wrapped columns was not. This was probably due to the effect of moisture on the fibers. Glass fibers are prone to damage resulting from moisture effects because moisture extracts ions from the fibers, resulting in the degradation of the fibers, such as cracks on the fiber surface; however, carbon fibers are not susceptible to such a degradation mechanism. This phenomenon was evidenced by the decrease in ductility as shown in Figure 4.10. The ductility index, μ , of Column S-G1-CE decreased by 9 % when compared to the control column S-G1-CONT; while the CFRP wrapped columns showed no change.

4.3.1.4 Effects of saline solution on the FRP wrapped columns. Group 4 Columns (S-C1-F/Th, S-C1-Na-F/Th, S-C1-CE, S-C1-Na-CE, S-G1-F/Th and S-G1-Na-F/Th) were used to investigate the effects of saline solution during the freeze-thaw cycles and the combined environmental cycles. Columns S-C1-F/Th and S-G1-F/Th were conditioned under the freeze-thaw cycles, while Columns S-C1-Na-F/Th and S-G1-Na-F/Th were immersed in 5 % NaCl solution during the freeze-thaw cycles. Column S-C1-CE was conditioned under the combined environmental cycles, while Column S-C1-Na-CE was immersed in 5 % NaCl solution during the combined environmental cycles. Columns S-C1-F/Th, S-C1-Na-F/Th, S-C1-CE, and S-C1-Na-CE were wrapped with 1 layer of CFRP sheet, and Columns S-G1-F/Th and S-G1-Na-F/Th were wrapped with 1 layer of GFRP sheet.

The saline solution showed the most significant adverse effect among the environmental conditions used in this study, especially for the GFRP wrapped columns. Figure 4.11 presents the average failure load, P_u , of Group 4 Columns. As shown in Figure 4.11, the average failure load, P_u , of Column S-G1-Na-F/Th was 14 % lower than that of Column S-G1-F/Th; while, the average failure load, P_u , of Columns S-C1-Na-F/Th and S-C1-Na-CE was 5 % and 1 % lower than that of Columns S-C1-F/Th and S-C1-Na-CE, respectively.

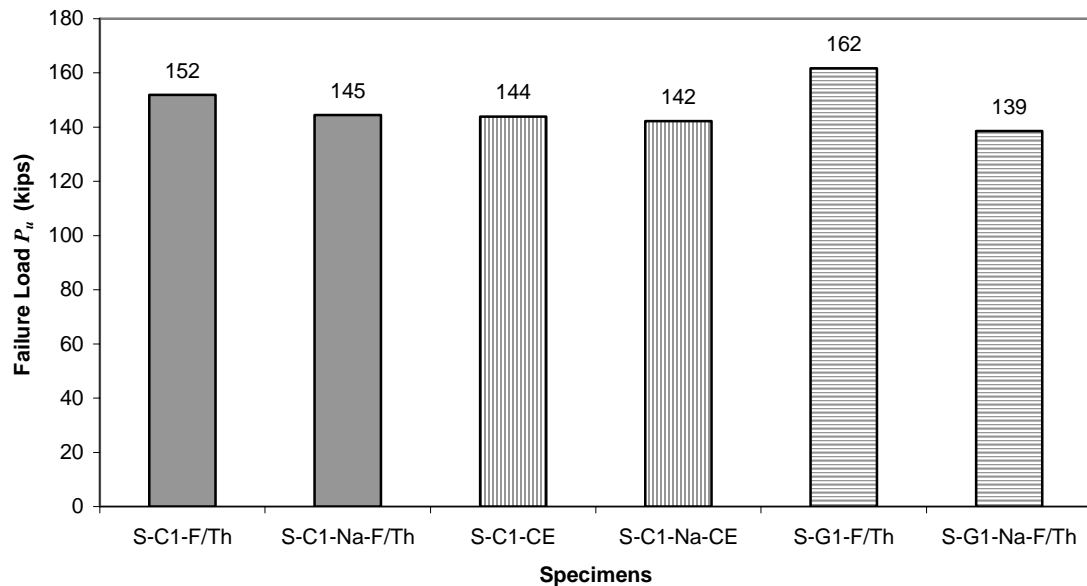


Figure 4.11. Average Failure Load, P_u , of Group 4 Columns

The decrease in failure load, P_u , of the CFRP wrapped columns was more likely due to the decrease in the axial rigidity in the plastic region, $(EA)_2$, induced by the combined effect of moisture and salt crystals. The moisture plasticized the matrix and caused micro-cracks at the matrix-fiber interface. In turn, salt crystals formed and expanded the micro-cracks, resulting in a decrease of stiffness of the CFRP composite. Figure 4.12 presents the average axial rigidity in the plastic region, $(EA)_2$, of Group 4 Columns. As shown in Figure 4.12, the axial rigidity in the plastic region, $(EA)_2$, of

Columns S-C1-Na-F/Th and S-C1-Na-CE was 7 % and 9 % lower than that of Columns S-C1-F/Th and S-C1-CE.

Unlike the CFRP wrapped columns, the axial rigidity in the plastic region, $(EA)_2$, of the GFRP wrapped columns was not affected; the axial rigidity in the plastic region, $(EA)_2$, of Column S-G1-Na-F/Th was 1 % higher than that of Column S-G1-F/Th, as shown in Figure 4.12. This was possibly could be due to the difference in the thickness of the CFRP and GFRP sheets. The thickness of the GFRP sheets was much larger than that of the CFRP sheets; and almost the same amount of matrix resin (primer and saturant) was used to apply the sheets to the concrete, therefore, the volumetric ratio of matrix of the GFRP wrapped columns to fiber were smaller than that of the CFRP wrapped columns. Thus, the total damage to the composite action induced by matrix degradation and micro-cracking of the GFRP wrapped columns could be smaller than that of the CFRP wrapped columns. In other words, the effect of the reduction in failure load, P_u , of the GFRP wrapped columns was somewhat different from that of the CFRP wrapped columns. It was mainly due to the damage of the glass fiber itself in the case of GFRP wrapped columns. As previously described, moisture could degrade the glass fiber, causing cracks in the fiber. As a result, the GFRP sheet can fail at a lower strength and there would be a decrease in ductility. Figure 4.13 presents the average ductility index, μ , of Group 4 Columns. As shown in Figure 4.13, the ductility index, μ , of Column S-G1-Na-F/Th was 26 % lower than that of Column S-G1-F/Th, while the ductility index, μ , of Columns S-C1-Na-F/Th and S-C1-Na-CE were not different from that of Columns S-C1-F/Th and S-C1-CE.

At this point, it should be noted that the moisture effects by immersing the columns in pure water throughout the environmental conditioning would be insignificant when compared to the high-humidity cycles, which induced the moisture effect by the continuous change of the relative humidity from 60 % to 100 %. The former might be limited to the effect of plasticization of the matrix and the lesser possibility of micro-cracks while the latter might induce micro-cracks due to the repeated volume change during the humidity change in addition to the plasticization. Thus, without formation and expansion of the salt crystals, the moisture effects by immersing the columns in pure

water, instead of saline solution, might have showed a smaller decrease in the axial compression capacity of the columns wrapped with FRP sheets.

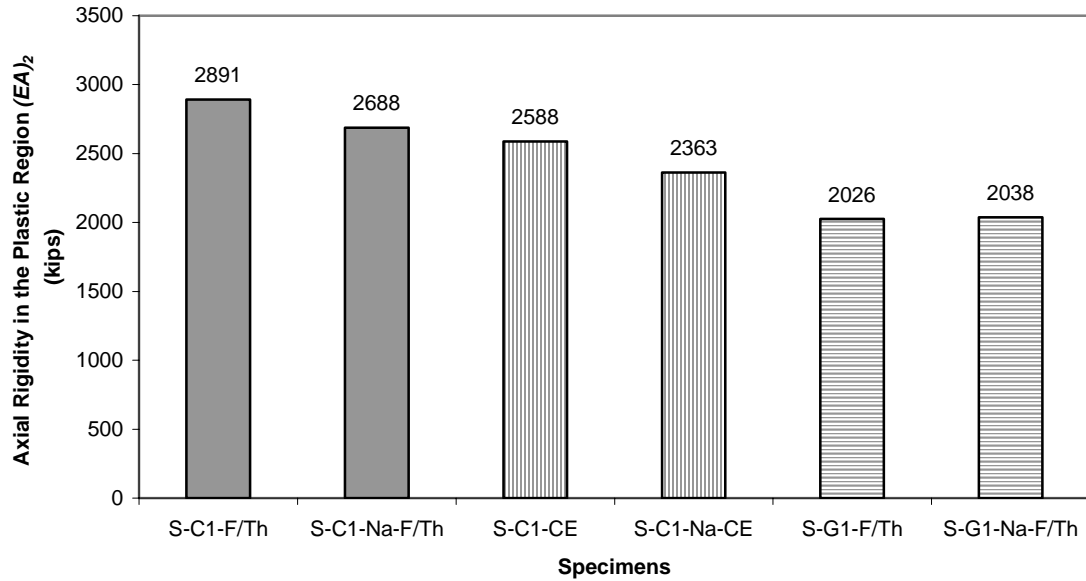


Figure 4.12. Average Axial Rigidity in the Plastic Region, $(EA)_2$, of Group 4 Columns

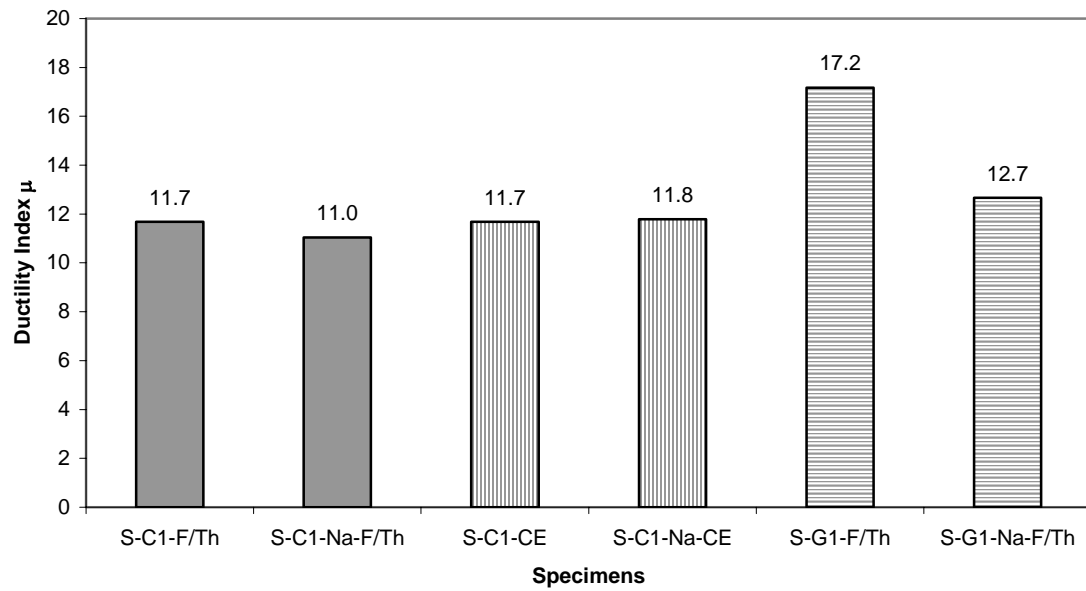


Figure 4.13. Average Ductility Index, μ , of Group 4 Columns

4.3.1.5 Effects of high-temperature cycles with UV radiation and high-humidity cycles on the FRP wrapped columns. Group 5 Columns (S-C1-F/Th, S-C1-CE, S-G1-F/Th and S-G1-CE) were used to investigate the effect of high-temperature cycles with UV radiation and high-humidity cycles. Columns S-C1-F/Th and S-G1-F/Th were conditioned under the freeze-thaw cycles, while Columns S-C1-CE and S-G1-CE were conditioned under the combined environmental cycles. Columns S-C1-F/Th and S-C1-CE were wrapped with 1 layer of CFRP sheet and Columns S-G1-F/Th and S-G1-CE were wrapped with 1 layer of GFRP sheet.

It was possible to investigate the combined effect of the high-temperature cycles with UV radiation and high-humidity cycles by comparing the test results of Columns S-C1-CE and S-G1-CE with the test results of Columns S-C1-F/Th and S-G1-F/Th, since the combined environmental cycles included the freeze-thaw cycles as well as the high-temperature cycles with UV radiation and high-humidity cycles. According to the comparative study, it was found that the high-temperature cycles with UV radiation and high-humidity cycles decreased the failure load, P_u , axial rigidity in the plastic region, $(EA)_2$, and ductility index, μ , for both the CFRP and GFRP wrapped columns.

Figure 4.14 presents the average failure load, P_u , of Group 5 Columns. As shown in Figure 4.14, the average failure load, P_u , of Columns S-C1-CE and S-G1-CE was 5 % and 11 % less than that of Columns S-C1-F/Th and S-G1-F/Th, respectively. The reason the GFRP wrapped columns showed larger decrease in failure load, P_u , was due to the effects of moisture on glass fiber itself, as described in the previous sections, resulting in the decrease in axial rigidity in the plastic region, $(EA)_2$, and ductility index, μ . Figure 4.15 presents the average axial rigidity in the plastic region, $(EA)_2$, of Group 5 Columns. As shown in Figure 4.15, the axial rigidity in the plastic region, $(EA)_2$, of Columns S-C1-CE and S-G1-CE was 11 % and 12 % lower than that of Columns S-C1-F/Th and S-G1-F/Th, respectively.

Figure 4.16 presents the average ductility index, μ , of Group 5 Columns. As shown in Figure 4.16, the ductility index, μ , of Column S-G1-CE was 6 % smaller than that of Column S-G1-F/Th. For the CFRP wrapped columns, the ductility index, μ , was

not affected significantly. The ductility index, μ , of Column S-C1-CE was just 1 % less than that of Column S-C1-F/Th.

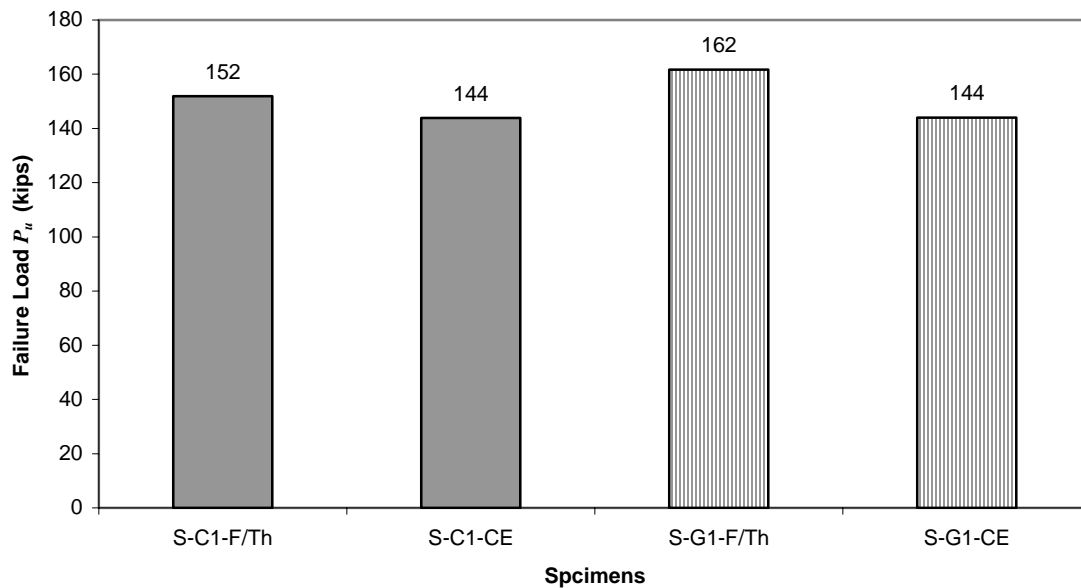


Figure 4.14. Average Failure Load, P_u , of Group 5 Columns

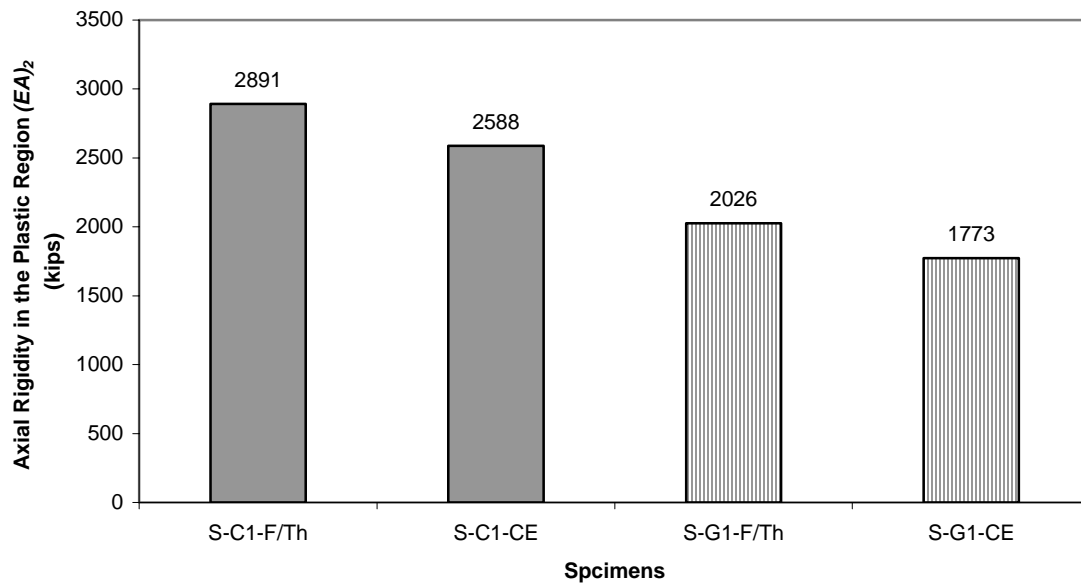


Figure 4.15. Average Axial Rigidity in the Plastic Region, $(EA)_2$, of Group 5 Columns

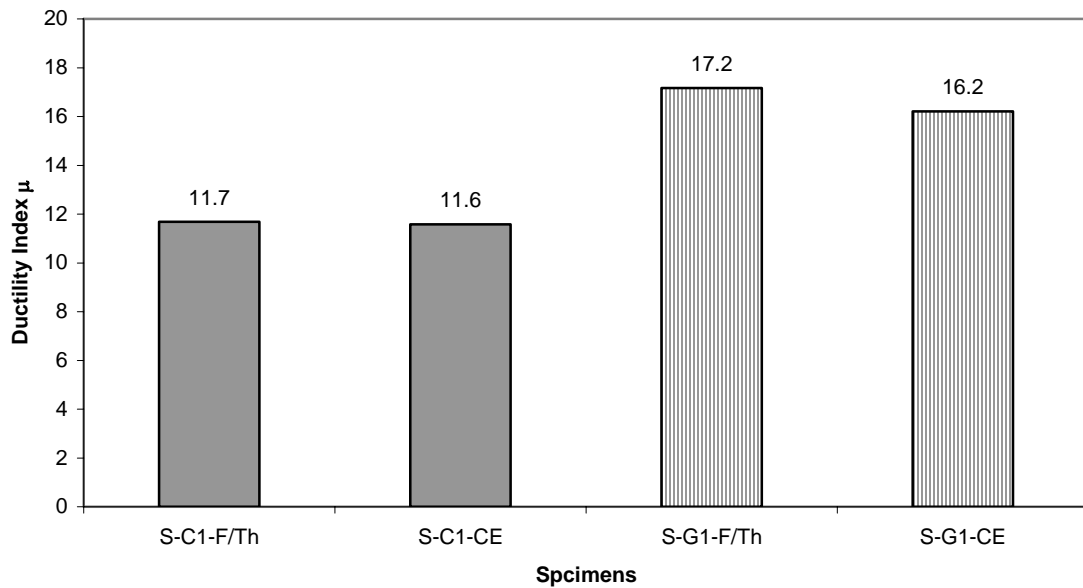


Figure 4.16. Average Ductility Index, μ , of Group 5 Columns

Consequently, it can be stated that both the high-temperature cycles and high-humidity cycles caused the micro-cracks at the matrix-fiber interface by repeated changing of the volume of the matrix and the fiber, and plasticization of the matrix, resulting in the decrease in stiffness and ductility of the FRP composite. In addition, moisture that reached the fibers by ingress through micro-cracks and diffusion via the matrix, during the high-humidity cycles, could degrade the glass fibers in the case of the GFRP wrapped columns. Furthermore, the surface damage due to UV radiation could make the damage even more severe for both CFRP and GFRP wrapped columns. The average axial rigidity in the plastic region, $(EA)_2$, average ductility index, μ , and in turn failure load, P_u , of the GFRP wrapped columns decreased more significantly than those of the CFRP wrapped columns.

4.3.1.6 Strain reduction factor, R_c . During the failure tests of the small-scale RC columns, the tensile strains of the FRP sheets were measured using strain gages. Figures 4.17 and 4.18 show the ratio of the measured ultimate tensile strains of the CFRP and GFRP sheets in the small-scale RC columns to the ultimate tensile strain of the CFRP

and GFRP sheets provided by manufacturer, respectively.

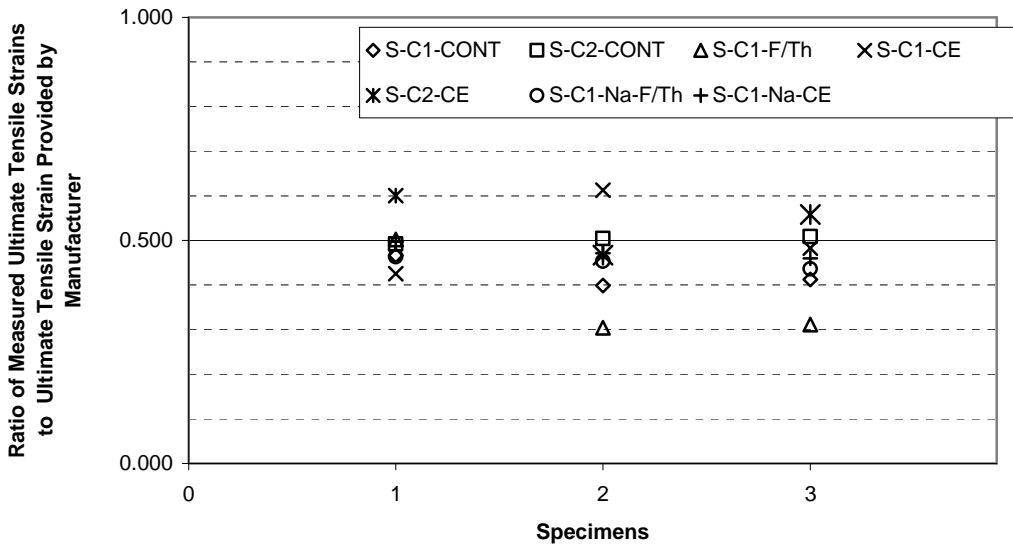


Figure 4.17. Ratio of Measured Ultimate Tensile Strains to Ultimate Tensile Strain Provided by Manufacturer (CFRP Sheet)

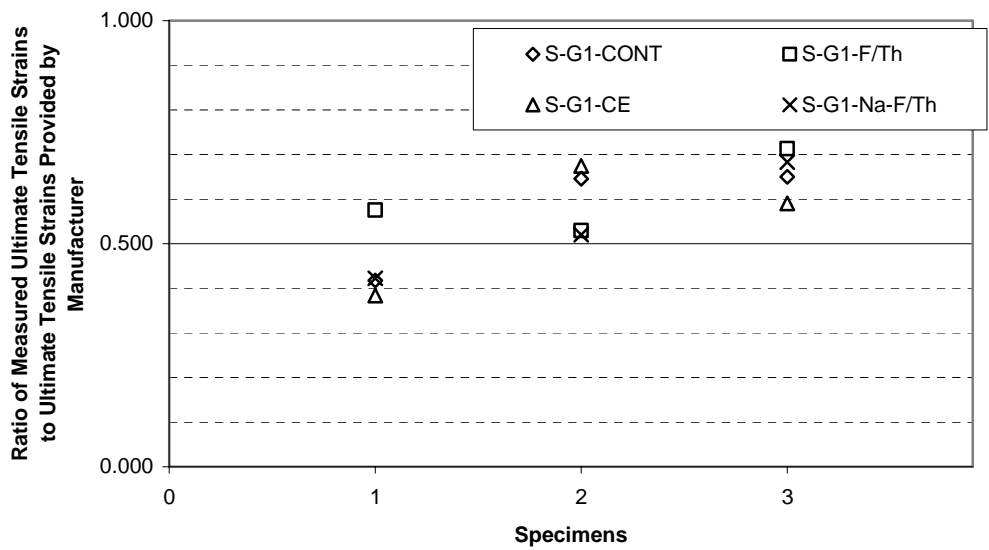


Figure 4.18. Ratio of Measured Ultimate Tensile Strains to Ultimate Tensile Strain Provided by Manufacturer (GFRP Sheet)

As shown in Figure 4.17, the ratio of the measured ultimate tensile strains of the CFRP sheets to the ultimate tensile strain provided by the manufacturer ranged from 0.31 to 0.61, and most of them were close to 0.5. Similarly, as shown in Figure 4.18, the ratio of the measured ultimate tensile strains of the GFRP sheet of the small-scale RC columns to the ultimate tensile strain provided by the manufacturer ranged from 0.38 to 0.71 and most of them were slightly over 0.5. Xiao and Wu (2000) also reported similar test results that the measured ultimate tensile strains were 50 % to 80 % of the ultimate tensile strain provided by manufacturers.

This is likely due to various reasons. First, in spite of using the same materials, the process of making flat coupons, which is usually used to obtain the ultimate tensile strain and strength by manufacturers, is easier than that of making the FRP wrapping system. As a result, the FRP composite in the form of a flat coupon may have a higher quality than the FRP wrapping system. Second, due to the existence of the confining pressure acting on the internal surface of the FRP sheet, as well as the axial stress in the FRP sheets transferred by the bond between the concrete and FRP sheets, the FRP sheets are in a tri-axial stress state instead of pure tension as in the flat coupon test. Third, cracking and crushing of the concrete core inside the FRP sheet cause local stress concentrations in the various locations of the FRP sheet. Finally, the radial strain of the FRP sheets was measured using strain gages. As a result, the measured strain could be localized strains, which might be smaller than the average strain.

Thus, it is suggested that the mechanical properties of the FRP sheets used in the design of the RC columns wrapped with FRP sheets should be determined by Equations (4-3) and (4-4), in order to account for the differences between the mechanical properties provided by manufacturer and the actual values:

$$\varepsilon_{fu}^* = R_c \varepsilon_{fu} \quad (4-3)$$

$$f_{fu} = E_f \varepsilon_{fu}^* \quad (4-4)$$

where, R_c is strain reduction factor, ε_{fu}^* is design ultimate tensile strain of FRP sheets, ε_{fu} is ultimate tensile strain provided by the manufacturer, f_{fu} is design tensile strength

of FRP sheets, and E_f is elastic modulus of FRP sheets. In Equation (4-3), R_c was determined to be 0.5 for both CFRP and GFRP wrapped RC columns, based on the experimental results of this study as shown in Figures 4.17 and 4.18.

4.3.1.7 Strength reduction factor, ϕ_{env} . In this section, a strength reduction factor, ϕ_{env} , was proposed in an attempt to consider the environmental effects when designing RC columns wrapped with FRP sheets. The strength reduction factor, ϕ_{env} , consists of three sub-factors ϕ_{FT} , ϕ_{Na} and ϕ_H . ϕ_{FT} accounts for the effects of the freeze-thaw cycles, ϕ_{Na} accounts for the effects of the saline solution, and ϕ_H accounts for the effects of the high-temperature with UV radiation and high-humidity cycles. The strength reduction factor, ϕ_{env} can be determined by combining through multiplication of three sub-factors, as shown in Equation (4-5):

$$\phi_{env} = \phi_{FT} \phi_{Na} \phi_H \quad (4-5)$$

In the previous sections, it was found that the failure load, P_u , of RC columns wrapped with FRP sheets was affected by exposure to various environmental conditions. Such a change in failure load, P_u , however, was due to the changes of the mechanical properties of concrete and FRP sheets; while steel reinforcements were not affected by environmental conditions. Thus, the strain reduction factor needed to be developed based on the changes of mechanical properties of concrete and FRP sheets.

FRP sheets and concrete act as FRP concrete system. Thus, in an attempt to evaluate the effects of environmental conditions on FRP-confined concrete, the compressive strength of the concrete, f'_{cc} , was calculated, excluding the contribution of the steel reinforcements, as shown in Equation (4-6):

$$f'_{cc} = \frac{P_u - f_y A_{st}}{A_g - A_{st}} \quad (4-6)$$

where, f'_{cc} is compressive strength of FRP confined concrete, f_y is yield strength (70 ksi) of steel reinforcements determined from tensile tests as described previously in Section 3.2.1.2, P_u is failure load, A_g is gross cross-sectional area of column, and A_{st} is cross-sectional area of longitudinal steel reinforcements. The compressive strength, f'_{cc} , of the small-scale RC columns, calculated by Equation (4-6) is presented in Tables 4.4 through 4.6. The three sub-factors ϕ_{FT} , ϕ_{Na} and ϕ_H are developed based on the test results provided in Tables 4.4 through 4.6.

4.3.1.7.1 Strength reduction factor, ϕ_{FT} . The Strength reduction factor, ϕ_{FT} , was determined based on the results provided in Table 4.4, which presents the compressive strength, f'_{cc} , of the control columns (S-C1-CONT and S-G1-CONT) and the freeze-thaw conditioned columns (S-C1-F/Th and S-G1-F/Th).

Table 4.4. Strength Reduction Factor, ϕ_{FT}

FRP types	Specimens	Compressive strength, f'_{cc} (ksi)				Ratio	ϕ_{FT}
		1	2	3	average		
CFRP	S-C1-CONT	4.38	4.09	4.33	4.27	1.08	1.00
	S-C1-F/Th	4.47	4.57	4.77	4.60		
GFRP	S-G1-CONT	4.14*	5.07	4.34	4.71	1.05	1.00
	S-G1-F/Th	4.74	4.96	5.15	4.95		

* This column was discarded when calculating average compressive strength f'_{cc} because this column failed at a very low applied load out of the test region due to the stress concentration at the interface between test region and the end of the columns strengthened with additional CFRP sheets.

As shown in Table 4.4, the ratio of average compressive strength, f'_{cc} , of freeze-thaw conditioned columns, S-C1-F/Th and S-G1-F/Th, to those of the control columns, S-C1-CONT and S-G1-CONT, were 1.08 and 1.10, respectively. Thus, the strength

reduction factor, ϕ_{FT} , of 1.08 and 1.10 had to be assigned to the CFRP and GFRP wrapped columns, respectively. However, conservatively, the value of 1.0 was assigned to both the CFRP and GFRP wrapped columns.

4.3.1.7.2 Strength reduction factor, ϕ_{Na} . The Strength reduction factor, ϕ_{Na} , was determined based on the results provided in Table 4.5, which presents compressive strength, f'_{cc} , of the columns conditioned under the freeze-thaw cycles or the combined environmental cycles (S-C1-F/Th, S-C1-CE, and S-G1-F/Th) and the columns immersed in saline solution during the environmental conditioning (S-C1-Na-F/Th, S-C1-Na-CE and S-G1-Na-F/Th).

Table 4.5. Strength Reduction Factor, ϕ_{Na}

FRP types	Specimens	Compressive strength, f'_{cc} (ksi)				Ratio	ϕ_{Na}
		1	2	3	average		
CFRP	S-C1-F/Th	4.47	4.57	4.77	4.60	0.94	0.95
	S-C1-Na-F/Th	4.01	4.27	4.73	4.34		
	S-C1-CE	3.91	4.42	4.61	4.31	0.99	
	S-C1-Na-CE	4.26	3.90	4.60	4.25		
GFRP	S-G1-F/Th	4.75	4.96	5.15	4.95	0.83	0.85
	S-G1-Na-F/Th	3.30	4.11	4.97	4.13		

As shown in Table 4.5, for the CFRP wrapped columns, the ratio of average compressive strength, f'_{cc} , of Columns S-C1-F/Th and S-C1-CE to that of Columns S-C1-Na-F/Th and S-C1-Na-CE were and 0.94 and 0.99, respectively. For the GFRP wrapped columns, the ratio of average compressive strength, f'_{cc} , of Columns S-G1-F/Th to that of Columns S-G1-Na-F/Th were 0.83. Thus, the strength reduction factor, ϕ_{Na} , of 0.95 and 0.85 were assigned to the CFRP and GFRP wrapped columns, respectively.

4.3.1.7.3 Strength reduction factor, ϕ_H . The Strength reduction factor, ϕ_H , was determined based on the results provided in Table 4.6, which presents compressive strength, f'_{cc} , of the freeze-thaw conditioned columns (S-C1-F/Th and S-G1-F/Th) and the combined environment conditioned columns (S-C1-CE and S-G1-CE).

As shown in Table 4.6, the ratio of average compressive strength, f'_{cc} , of the combined environment conditioned columns, S-C1-CE and S-G1-CE, to those of the freeze-thaw conditioned columns, S-C1-F/Th and S-G1-F/Th, were 0.94 and 0.87 for the CFRP and GFRP wrapped columns, respectively. Thus, the strength reduction factor, ϕ_H , of 0.95 and 0.85 were assigned to CFRP and GFRP wrapped columns.

Table 4.6. Strength Reduction Factor, ϕ_H

FRP types	Specimens	Compressive strength, f'_{cc} (ksi)				Ratio	ϕ_H
		1	2	3	average		
CFRP	S-C1-F/Th	4.47	4.57	4.77	4.60	0.94	0.95
	S-C1-CE	3.91	4.42	4.61	4.31		
GFRP	S-G1-F/Th	4.75	4.96	5.15	4.95	0.87	0.85
	S-G1-CE	3.43	5.19	4.33	4.32		

4.3.2. Mid-Scale RC Column Tests. A total of 6 mid-scale RC columns were tested in uni-axial compression after exposure to the freeze-thaw cycles and combined environmental cycles. The test results, such as applied load vs. axial strain curves and failure load P_u , are presented in Table 4.7 and Figures 4.19 through 4.20.

4.3.2.1 Failure mode. Similar to the small-scale RC column tests, the failure of the mid-scale RC columns wrapped with FRP sheets was directly due to the rupture of the FRP sheets, as shown in Figure 4.21. The failure mode of the columns conditioned under the environmental cycles was not different from that of the control columns.

Table 4.7. Failure Load, P_u , of Mid-Scale RC Columns

	Failure load P_u (kips)
M-C1-CONT	346
M-G1-CONT	365
M-C1-F/Th	349
M-G1-F/Th	363
M-C1-CE	352
M-G1-CE	336

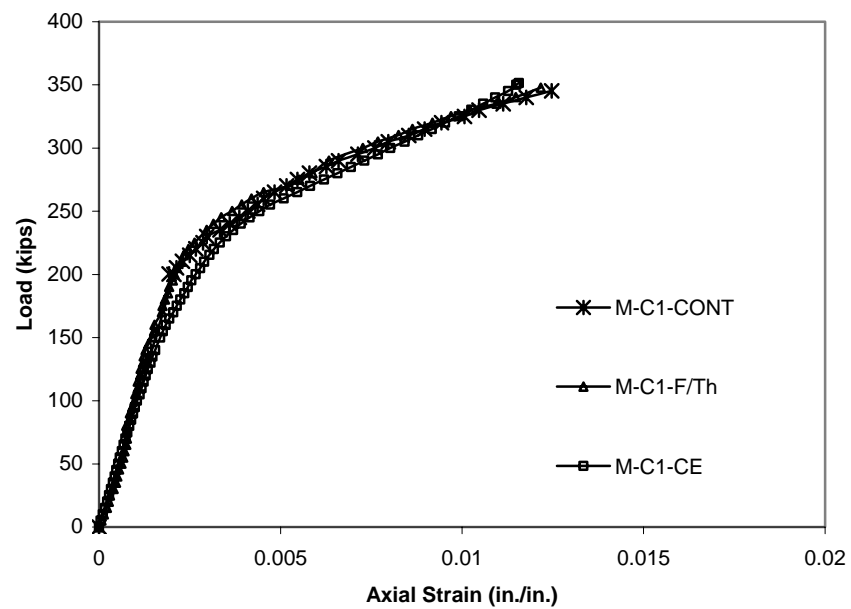


Figure 4.19. Applied Load vs. Axial Strain Curves of Mid-Scale RC Columns Wrapped with CFRP Sheets

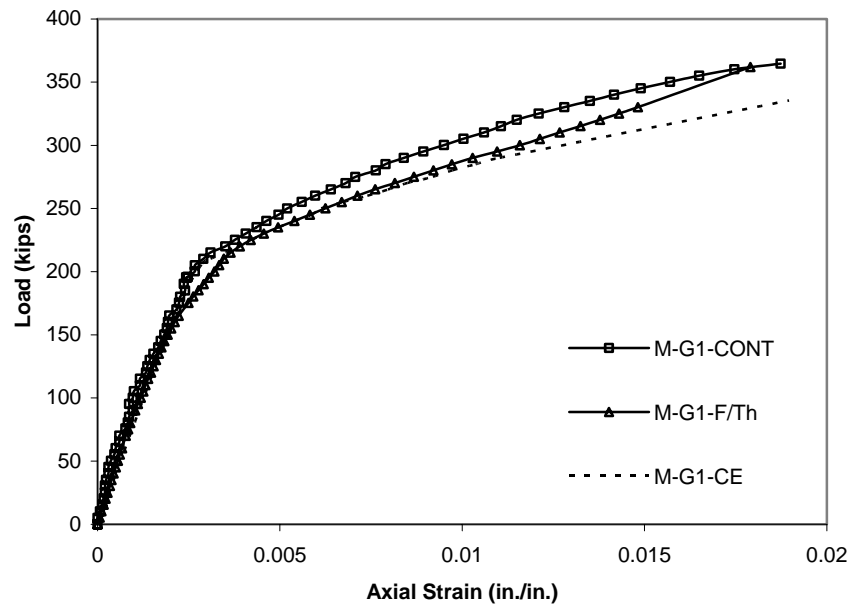


Figure 4.20. Applied Load vs. Axial Strain Curves of Mid-Scale RC Columns Wrapped with GFRP Sheets



(a) GFRP wrapped column



(b) CFRP wrapped column

Figure 4.21. Typical Failure Mode of Mid-Scale Columns

4.3.2.2 Effects of freeze-thaw cycles on the FRP wrapped columns. The failure load, P_u , of the freeze-conditioned columns M-C1-F/Th and M-G1-F/Th were almost same as that of the control columns M-C1-CONT and M-G1-CONT, as shown in Table 4.8. This is different from the results of the small-scale RC column tests. In the small-scale RC column tests, failure load, P_u , increased by 7 % and 4 % for CFRP and GFRP wrapped columns, respectively. This was a result of the matrix hardening effect due to the extremely low temperature. Thus, it could be said that the matrix hardening effect in the mid-scale RC column tests was not as significant as the small-scale RC column tests because of their different confining modulus, E_j , defined in Equation (5-6) of the following section. The confining modulus, E_j , is a function of the geometry of a column and the stiffness of the FRP sheets, and thus, it can define the relative amount of the FRP sheets used in wrapping with respect to a certain size of column. The confining modulus, E_j , of the CFRP wrapped small-scale RC columns was 143 ksi while that of the CFRP wrapped mid-scale RC columns was 54 ksi. For GFRP wrapped columns, the confining modulus, E_j , was 46 ksi and 37 ksi for the small-scale and mid-scale RC columns, respectively. Therefore, the matrix hardening effect on the mid-scale RC columns might be smaller than that of small-scale RC columns since the confining modulus, E_j , of the mid-scale RC columns was less than that of the small-scale RC columns. In addition, the differences in the properties of concretes used in making the small-scale and mid-scale RC columns should be considered. Since the small-scale RC columns were made of the concrete with high air content, they were not vulnerable to freeze-thaw damages. However, the mid-scale RC columns, which were made of normal strength ready-mixed concrete, could be degraded by the freeze-thaw cycles. As a result, although there was an increase in failure load, P_u , due to the matrix hardening effect on the FRP sheets, the increase might be compromised with the degradation of the concrete due to the freeze-thaw cycles. The axial rigidity in the plastic region, $(EA)_2$, and ductility were not changed significantly, as shown in Figures 4.19 and 4.20.

Table 4.8. Comparison of Failure Load, P_u , of Freeze-Thaw Conditioned Mid-Scale RC Columns with Control Columns

	Failure load P_u (kips)	Ratio
M-C1-CONT	346	
M-C1-F/Th	349	1.01
M-G1-CONT	365	
M-G1-F/Th	363	0.99

4.3.2.3 Effects of combined environmental cycles on FRP wrapped columns.

The failure load, P_u , of the CFRP wrapped columns was not significantly changed, while the failure load, P_u , of the GFRP wrapped columns decreased by 8 %, as shown in Table 4.9. This was because the GFRP sheet was more vulnerable to the high-temperature cycles with UV radiation and high-humidity cycles than the CFRP sheet, as discussed in the small-scale RC column tests. The axial rigidity in the plastic region, $(EA)_2$, and ductility were not changed significantly, as shown in Figures 4.19 and 4.20.

Table 4.9. Comparison of Failure Load, P_u , of Mid-Scale RC Columns Conditioned under the Combined Environmental Cycles with Control Columns

	Failure load P_u (kips)	Ratio
M-C1-CONT	346	
M-C1-CE	352	1.02
M-G1-CONT	365	
M-G1-CE	336	0.92

4.3.3. Summary and Conclusions. From the compressive failure tests, conducted on the small-scale and mid-scale RC columns wrapped with CFRP and GFRP sheets, and exposed to various environmental cycles, the effects of the environmental

cycles were quantified as summarized in Table 4.10 and the following conclusions were drawn:

1. The freeze-thaw cycles used in this test did not show any adverse effects on the CFRP and GFRP wrapped RC columns. Rather, failure load, P_u , and axial rigidity in the plastic region, $(EA)_2$, slightly increased. This was probably due to the matrix hardening effects at the extremely low temperature, causing the increase in stiffness of the matrix resin. However, the matrix hardening effect was compromised with the degradation of concrete itself due to the freeze-thaw cycles, when the confining modulus, E_j , was relatively low.
2. The combined environmental cycles used in this test did not show any significant effects on the CFRP wrapped RC columns. This is because in the case of the CFRP wrapped RC columns, the negative effects, such as plasticization of matrix, micro-cracking at matrix-fiber interface, were compromised with the positive effects, such as matrix hardening effect. On the other hand, the GFRP wrapped RC columns were significantly affected, resulting in a remarkable decrease in failure load, P_u . This decrease was due, in large part, to the degradation of the glass fiber itself induced by moisture effects during the high-humidity cycles. The CFRP wrapped RC columns, however, were not susceptible to such damage.
3. Among the environmental cycles used in this test, the saline solution had the most deteriorate environmental effect on the GFRP wrapped RC columns, resulting in a significant decrease in failure load, P_u , and ductility. On the other hand, the CFRP wrapped RC columns exhibited a slight decrease in failure load, P_u . The primary reason for the decrease in failure load, P_u , of the GFRP wrapped columns was attributed in large part to the damage of the glass fiber itself, such as cracking in the fiber induced by moisture. Furthermore, formation and expansion of salt crystal in the micro-cracks at the matrix-fiber interface increased the degradation.
4. The combined effects of the high-temperature cycles with UV radiation and high-humidity cycles was the second most deteriorate environmental conditions for GFRP wrapped RC columns, resulting in a decrease in failure load, P_u . For the CFRP wrapped RC columns, the decrease in failure load, P_u , was much smaller than that of

- the GFRP wrapped RC columns. The primary reason for this was that the variation of temperature and relative humidity during the high-temperature cycles and high-humidity cycles caused the plasticization of matrix, micro-cracking at matrix-fiber interface. In addition, the reason the GFRP wrapped columns showed more significant reduction of failure load, P_u , was again due to the moisture effect on glass fiber itself.
5. Strain reduction factor, R_c , was proposed to account for the difference between the ultimate tensile strain of the FRP sheets used for wrapping the RC columns and the ultimate tensile strain provided by manufacturers.
 6. Strength reduction factor, ϕ_{env} , was proposed to account for the effects of various environmental conditions based on the small-scale RC column tests. The strength reduction factor, ϕ_{env} , consists of three sub-factors ϕ_{FT} , ϕ_{Na} , and ϕ_H . ϕ_{FT} accounts for the effects of the freeze-thaw cycles, ϕ_{Na} accounts for the effects of the saline solution, and ϕ_H accounts for the effects of the high-temperature with UV radiation and high-humidity cycles.
 7. Overall, RC columns wrapped with FRP sheets were affected by environmental conditions, resulting in a decrease in failure load, P_u . The extent of the decrease was dependent on the types of FRP sheets and on the types of environmental conditions. This must be considered in the design of RC columns wrapped with FRP under severe environments by using knock-down factors, such as the strength reduction factor, ϕ_{env} , proposed in this section.

Table 4.10. Percentile Changes in Mechanical Properties Due to the Environmental Conditioning Used in this Study

Types of Environmental Conditioning		Percentile Changes in Mechanical Properties (%)								
		CFRP Wrapped RC Columns						GFRP Wrapped Columns		
		1-Layer			2-Layer			1-Layer		
		P_u	$(EA)_2$	μ	P_u	$(EA)_2$	μ	P_u	$(EA)_2$	μ
Freeze-Thaw Cycles		7	12	-1	-	-	-	4	10	-4
Combined Environmental Cycles		1	0	-2	-3	-2	1	-7	-4	-9
Saline Solution	During Freeze-Thaw Cycles	-5	-7	-5	-	-	-	-14	1	-26
	During Combined Environmental Cycles	-1	-9	1	-	-	-	-	-	-
High-Temperature Cycles with UV Radiation and High-Humidity Cycles		-5	-11	-1	-	-	-	-11	-12	-6

In this table, positive values represent the percentile increase in the mechanical properties while negative values represent the percentile decrease in the mechanical properties.

4.4. CORROSION TESTS

4.4.1. Definition of Corrosion Rate. The Corrosion rate was evaluated by measuring corrosion current. The measured corrosion current, in turn, was converted into steel loss using Faraday's Law, as shown in Equation (4-7):

$$\Delta w(g) = \frac{A_m \cdot I \cdot t}{z \cdot F} \quad (4-7)$$

where, $\Delta w(g)$ is incremental steel loss (grams), A_m is atomic mass (for iron 55.85 g), I is uniform current (Am) applied over time increment t (second), z is valency (assuming that most of rust product is $\text{Fe}(\text{OH})_2$, it is taken as 2), and F is Faraday's constant (96487 C/eq). In Equation (4-7), it was assumed that all of the current resulting from the accelerated corrosion process is used to produce rust.

Thus, the total accumulated steel loss over the period of the accelerated corrosion process was determined from the area under the corrosion current vs. time curve by integration, as shown in Equation (4-8):

$$w = \frac{A_m}{z \cdot F} \sum \Delta t \cdot I_{ave} \quad (4-8)$$

Typical corrosion current vs. time curves are presented in Figure 4.22, and the corresponding steel losses calculated by Faraday's Law are presented in Figure 4.23. Using corrosion vs. time curves, as shown in Figure 4.22, it is somewhat difficult to understand that Example 1 has a higher corrosion rate than Example 2. However, steel loss vs. time curves provides an efficient way to define corrosion rate, as shown in Figure 4.23; that is, the slopes of the steel loss vs. time curves can be defined as corrosion rate. In Figure 4.23, the corrosion rate (i.e., the slope) of Example 1 is 4.16 g/day, while that of Example 2 is 1.94 g/day for the period from day 15 to day 90. Thus, it can be said that the corrosion rate of Example 1 is about twice higher than that of Example 2 for the period. This definition for corrosion rate will be used throughout this section.

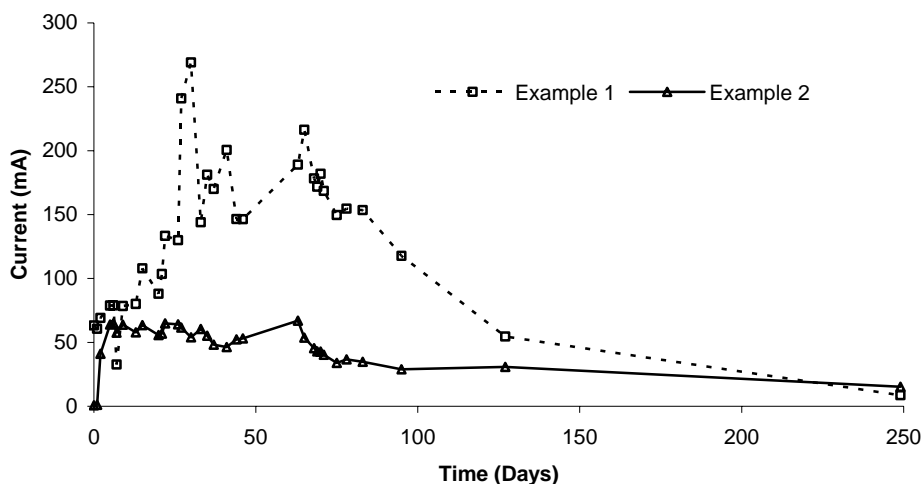


Figure 4.22. Typical Corrosion Current vs. Time Curves

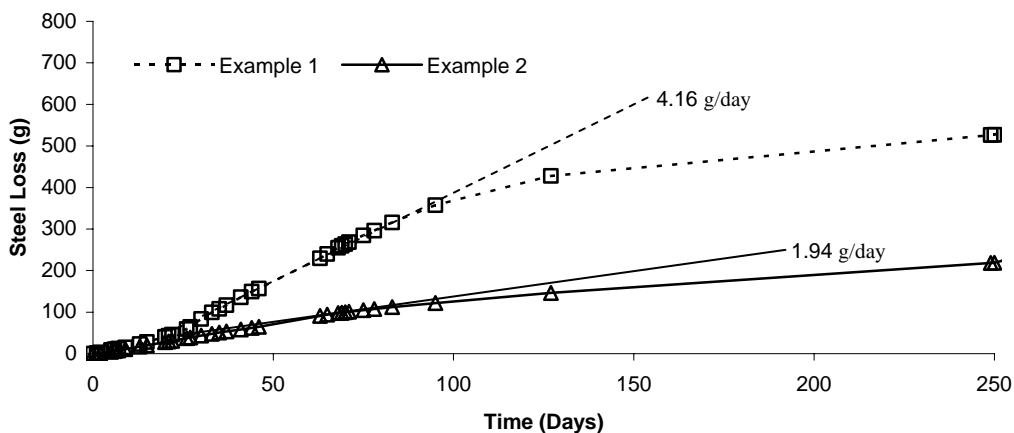


Figure 4.23. Typical Steel Loss vs. Time Curves

4.4.2. Small-Scale RC Column Tests. A total of 36 small-scale RC columns were fabricated for the extensive parametric study. Among them, 26 columns were tested in uni-axial compression after the accelerated corrosion process. The remaining 8 columns were used to investigate the internal damages induced by the accelerated corrosion process without failure tests. Discussions about the obtained results are made in two different categories: the results of accelerated corrosion process and the results of

failure tests.

4.4.2.1 Results of accelerated corrosion process. In this section, discussions on the results obtained during the accelerated corrosion process are made with focus on the corrosion rate and corrosion damages.

4.4.2.1.1 Corrosion rate. Factors affecting the corrosion rate of RC columns wrapped with CFRP sheets are discussed in this section.

(a) Effect of sodium chloride in concrete mix water. In order to inspect whether chloride contaminated concrete could initiate the corrosion process by breaking down the passive film of the steel reinforcements earlier than regular concrete, the test results of Columns R-CON and C-CON4 were compared to each other. Column R-CON was fabricated from regular concrete as described in Section 3.3.1.2, while Column C-CON4 was fabricated from chloride contaminated concrete. Both columns were conditioned by the same procedure.

The measured corrosion currents and the corresponding steel losses of the columns throughout the accelerated corrosion process are presented in Figures 4.24 and 4.25, respectively. In Figure 4.24, it is difficult to determine which one has a higher

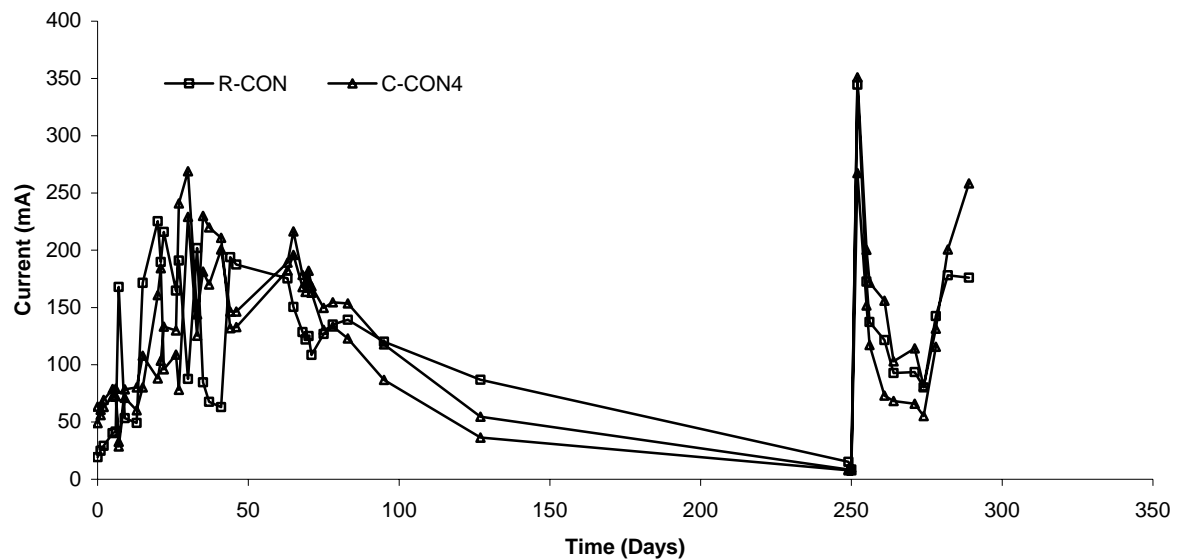


Figure 4.24. Corrosion Current vs. Time Curves of Columns R-CON and C-CON4

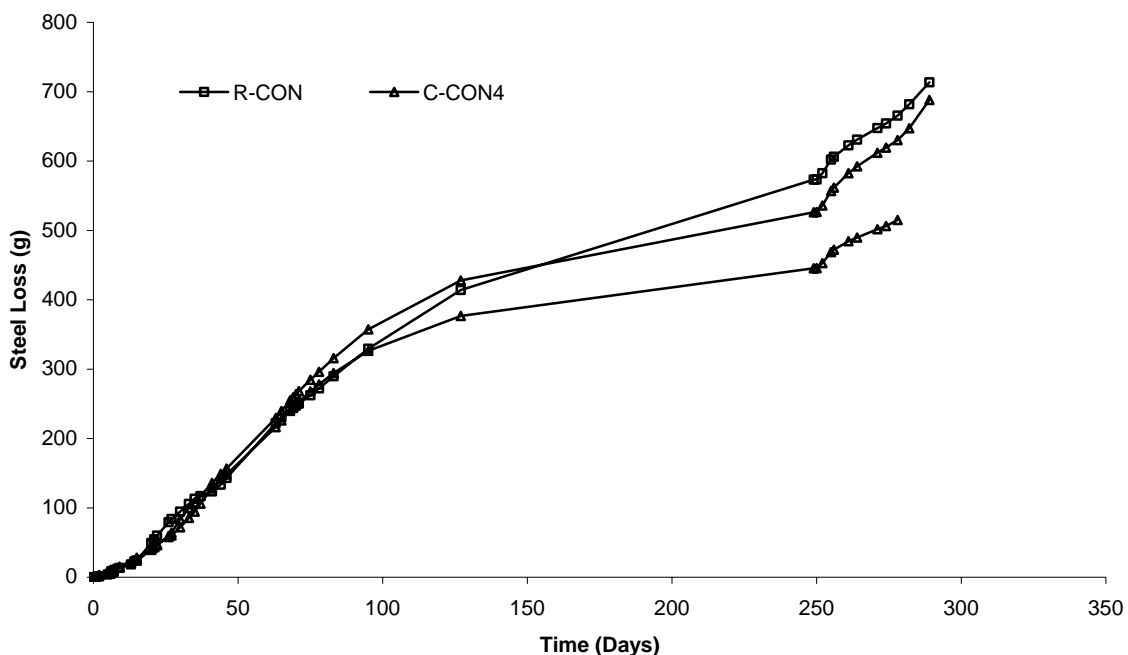


Figure 4.25. Steel Loss vs. Time Curves of Columns R-CON and C-CON4

corrosion rate. The variations of the corrosion currents of the columns seem to be similar throughout the accelerated corrosion process. However, it is more clearly seen from Figure 4.25 that the initial slopes of the columns are quite similar up to about 100 days. Thus, adding sodium chloride into the mix water could not increase the initial corrosion rate. This is most likely because the regular concrete used for making Column R-CON had very high air content, which consequently makes the concrete highly permeable. Thus, when Column R-CON was immersed in 5 % saline solution for the wet-dry cycles, it was possible that the chloride ions in the solution reached the steel reinforcements easily so as to destroy the passive film as quickly as the chloride ion in the chloride contaminated concrete did.

It should be noted, however, that this situation was intentionally designed in order to evaluate the accelerated corrosion regime rather than to evaluate the actual effects of the sodium chloride ion in the mix water. In the real construction, such a highly air-entrained concrete is not commonly used and the permeability of the concrete is usually much lower than that of the concrete used for Column R-CON in this test. Furthermore,

it is well known that the sodium chloride ions in the mix water can cause severe corrosion damage in the long run.

(b) Effect of CFRP wrapping. In order to investigate how effectively CFRP sheet wrapping could decrease corrosion rate, the test results of Columns C-CON4 and C-CFRP4 were compared to each other. Column C-CON4 was unwrapped columns, while Column C-CFRP4 was wrapped with CFRP sheets before the beginning of the accelerated corrosion process. The measured corrosion currents and the corresponding steel losses of the columns are presented in Figures 4.26 and 4.27.

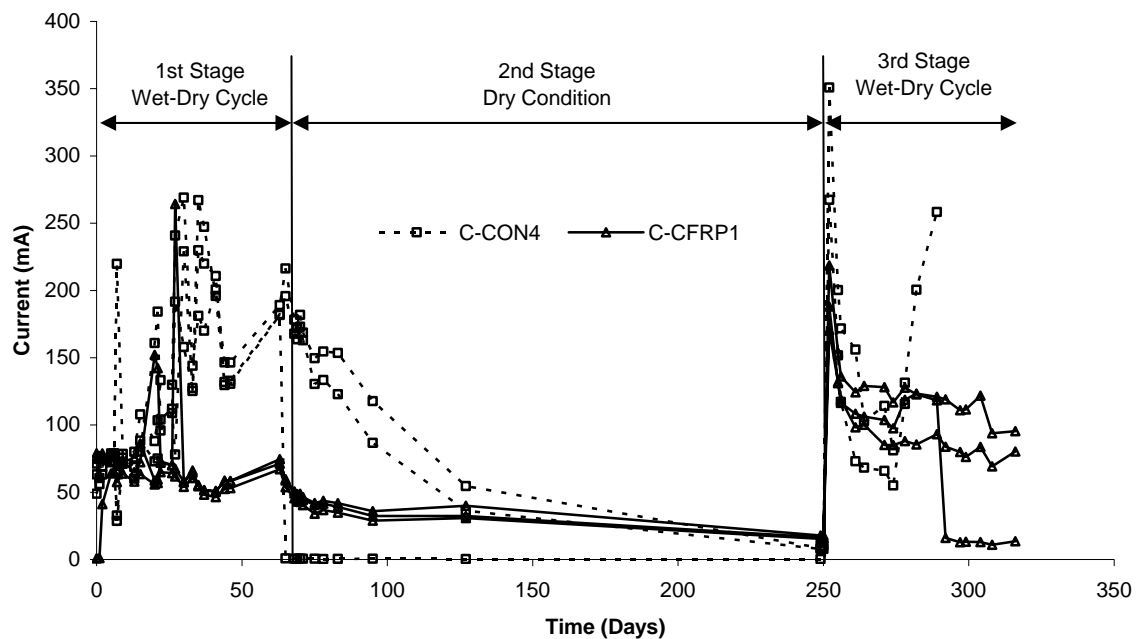


Figure 4.26. Corrosion Current vs. Time Curves of Columns C-CON4 and C-CFRP1

In Figure 4.26, it was observed that the corrosion currents of the unwrapped columns C-CON4, gradually increased during the first stage of the accelerated corrosion process (wet-dry cycles), while the corrosion currents of the CFRP wrapped columns C-CFRP1, seemed to be somewhat constant. In the second stage (dry condition), the

unwrapped columns C-CON4, exhibited a rapid decrease in corrosion current, while the decrease in the corrosion currents of the CFRP wrapped columns C-CFRP1, was not significant. This implies that the evaporation of the moisture inside the CFRP wrapped columns C-CFRP1 was inhibited by the CFRP sheets, and therefore the corrosion of steel reinforcements of the CFRP wrapped columns may continue to occur even after the elimination of moisture sources. This hypothesis was supported by comparing the corrosion rates of the columns, as shown in Figure 4.27.

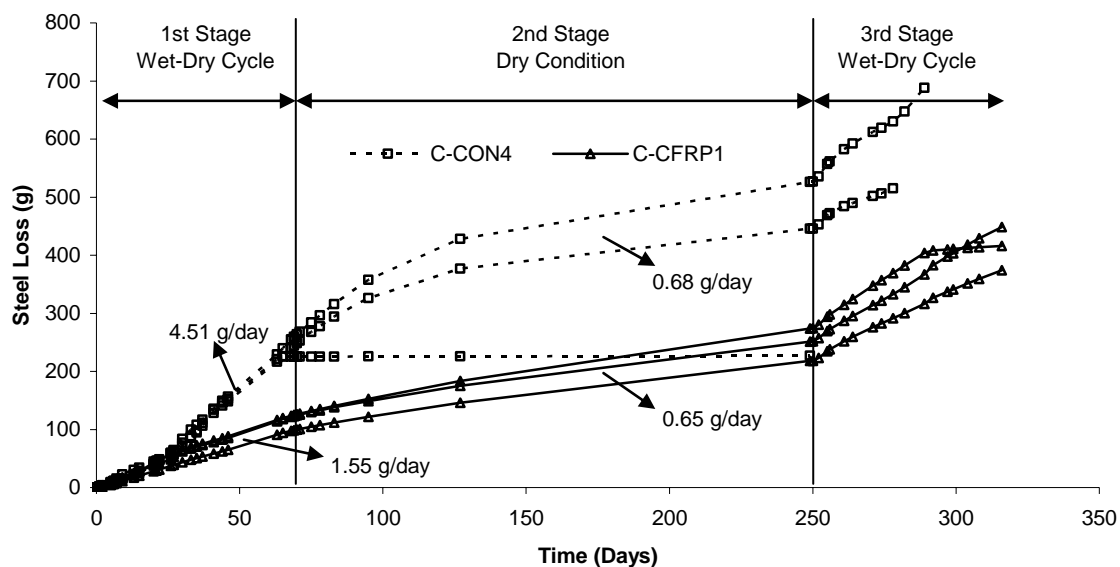


Figure 4.27. Steel Loss vs. Time Curves of Columns C-CON4 and C-CFRP1

As shown in Figure 4.27, the average corrosion rate of the unwrapped columns C-CON4 began to decrease from 4.51 g/day, as soon as the second stage (dry condition) started, and eventually reached 0.68 g/day. Meanwhile, the average corrosion rate of the CFRP wrapped columns C-CFRP1 was changed from 1.55 g/day to 0.65 g/day. Eventually, at the end of the second stage (dry condition), the average corrosion rate of the CFRP wrapped columns C-CFRP1 became larger than that of the unwrapped columns C-CON4.

In the third stage, the dramatic increase in the corrosion rate was observed in the case of the CFRP wrapped columns C-CFRP1. This increase in the corrosion rate of the CFRP wrapped columns C-CFRP1 during the third stage was due to the cracks in the CFRP sheets, as shown in Figure 4.28, which caused by the expansion of the column in the longitudinal direction due to the corrosion of spiral reinforcement. The cracks were in the fiber direction and the width was over 1/8 in; thus, moisture could directly reach the concrete surface and the steel reinforcements. Discussion regarding the cracks is presented in detail in the following sections.



Figure 4.28. Cracks in the CFRP Sheets Due to the Accelerated Corrosion Process

Therefore, it can be said that although CFRP sheet wrapping can decrease the corrosion rate, the corrosion may continue to occur even after the removal of the source of moisture because of the entrapped moisture. Furthermore, once cracks develop in the CFRP sheets, it can not be expected that the CFRP sheets will act as a diffusion barrier of moisture to decrease the corrosion rate.

(c) Effect of freeze-thaw cycles. As briefly discussed in the previous section, cracks significantly affected the corrosion rate of the CFRP wrapped columns. In this section, micro-cracks at fiber matrix interface which could be developed by the freeze-thaw cycles were the focus of the discussion.

The CFRP wrapped columns C-CFRP1 and C-CFRP3 were identical and were conditioned in the same way throughout the accelerated corrosion process. However, Column C-CFRP3 was conditioned by 300 freeze-thaw cycles between the completion of the second stage and the beginning of the third stage of the accelerated corrosion process, while Column C-CFRP1 were not. The measured corrosion currents and the corresponding steel losses of the columns are presented in Figures 4.29 and 4.30.

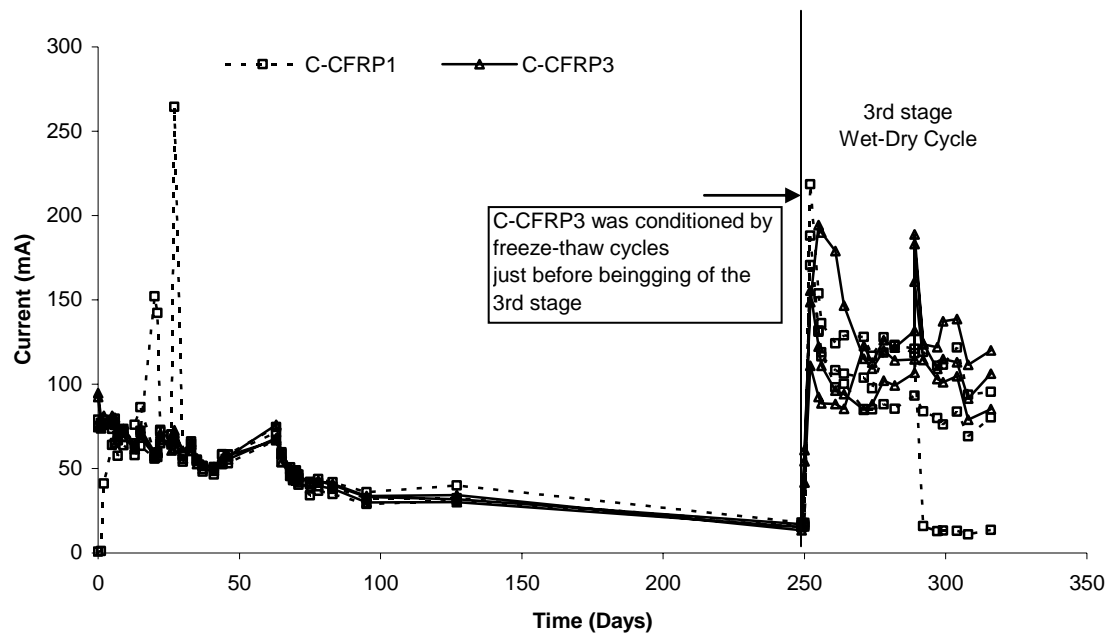


Figure 4.29. Corrosion Current Variations of Columns C-CFRP1 and C-CFRP3 during the Accelerated Corrosion Process

As shown in Figures 4.29 and 4.30, it was observed that the measured corrosion currents and the corrosion rates of all columns during the third stage were much higher than during the previous two stages. This was due to the existence of wide cracks in the CFRP sheets developed during the first and second stages of the accelerated corrosion process. Column C-CFRP3 was conditioned under the freeze-thaw cycles after the completion of the second stage of the accelerated corrosion process. Thus, even if micro-cracks developed in the CFRP sheets due to the freeze-thaw cycles, the effects of the

micro-cracks could not be seen because of the wide cracks, as shown in Figure 4.28. Consequently, the effect of the micro-cracks could not be investigated.

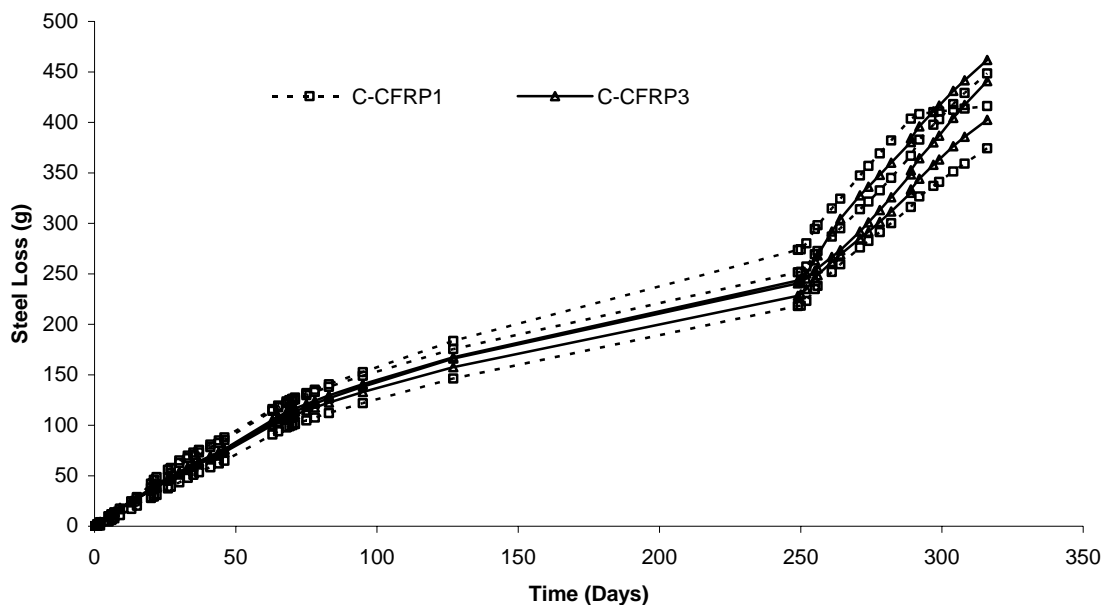


Figure 4.30. Calculated Steel Loss of Columns C-CFRP1 and C-CFRP3 during the Accelerated Corrosion Process

(d) Comparison between repair methods. Three different repair methods are discussed in this section. Column R-COV-1 was repaired by the conventional method after the second stage of the accelerated corrosion process. Columns C-CFRP2 and C-CFRP4 were repaired by CFRP sheet wrapping after the second stage of the accelerated corrosion process. Among Columns C-CFRP2 and C-CFRP4, the cracks of Columns C-CFRP2-3 and C-CFRP4-3 were sealed with the epoxy injection technique, while others were not. In Figure 4.31, the steel loss vs. time curves of the columns in the third stage of the accelerated corrosion process are presented.

As shown in Figure 4.31, it was proven that the CFRP wrapping could decrease the corrosion rate significantly when compared to the conventional method. The corrosion rate of the column repaired by the conventional method was significantly

higher than those of the other columns repaired by CFRP wrapping. However, the effect of the epoxy injection was not observed; the corrosion rates of Columns C-CFRP2-3 and C-CFRP4-3, of which cracks were sealed with epoxy injection, were not significantly different from those of unsealed columns C-CFRP2-1, C-CFRP2-2, C-CFRP4-1 and C-CFRP4-2.

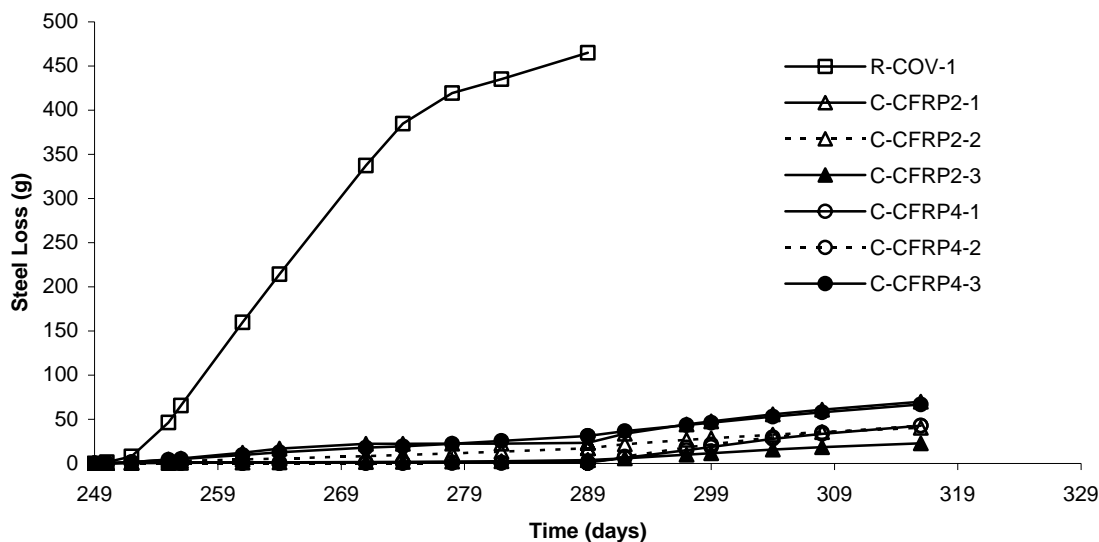


Figure 4.31. Steel Loss vs. Time Curves during the Third Stage

4.4.2.1.2 Corrosion damages due to the accelerated corrosion process.

Among the thirty-six small-scale RC columns used in the corrosion tests, eight columns were used to investigate the damage induced by the accelerated corrosion process.

(a) **Loss of cross-sectional area of steel reinforcements.** The cross-sectional area of the steel reinforcements of both the unwrapped and CFRP wrapped columns was reduced due to the accelerated corrosion process, as shown in Figure 4.32.

As shown in Equation (4-8), it was possible to predict the decrease rate of the cross-sectional area of steel reinforcements due to the accelerated corrosion process, using the accumulated steel loss calculated by Faraday's Law. The calculated steel loss

and the predicted decrease rate of the cross-sectional area of steel reinforcements of all the columns are presented in Table 4.11.



Figure 4.32. Corrosion Damaged Longitudinal and Spiral Reinforcements

Table 4.11. Percentile Loss of Cross-Sectional Area of Steel Reinforcement Determined by Faraday's Law

Specimen	Steel Loss (g)				$A_{st} Loss_{Faraday}$
	1	2	3	Average	
C-CON4	688	515	227	477	34 %
C-CFRP1	372	444	414	410	29 %
C-CFRP2	516	470	523	503	35 %
C-CFRP3	399	458	437	431	30 %
C-CFRP4	425	507	572	501	36 %

In Table 4.11, the percentile loss of the cross-sectional area of steel reinforcements, $A_{st} Loss_{Faraday}$, was calculated by dividing the average steel loss (g), calculated by Faraday's Law, by the original weight of 1,397.4 (g) of the steel reinforcements (i.e., 3 longitudinal reinforcements and spiral reinforcement). As shown in Table 4.11, the percentile loss of the cross-sectional area of steel reinforcements,

$A_{st} Loss_{Faraday}$, of the CFRP wrapped columns C-CFRP1 and C-CFRP3 was slightly less than that of the unwrapped column C-CON4. However, it should be noted that the average percentile loss of the cross-sectional area of steel reinforcements, $A_{st} Loss_{Faraday}$, of the CFRP wrapped columns was about 30 %. This implies that even if the CFRP wrapping could decrease the corrosion rate of the RC columns, it could not perfectly protect the steel reinforcements from the corrosion. In order to investigate whether it was accurate to predict the percentile loss of the cross-sectional area of steel reinforcements using Faraday's Law, tensile tests of the steel reinforcements were performed and the results were summarized in Table 4.12.

Table 4.12. Comparison of the Percentile Loss of Cross-Sectional Area of Steel Reinforcement Determined by Tensile Test with that Determined by Faraday's Law

Tensile Test					Calculation by Faraday's Law			$\frac{A_{st} Loss_{Faraday}}{A_{st} Loss_{Test}}$
Specimen	Load at Failure P_u (lb)			Average	$A_{st} Loss_{Test}$ *	Steel Loss: (g)	$A_{st} Loss_{Faraday}$ **	
	1	2	3					
Control	9863	9927	10064	9951	-	1397.4***	-	
C-CON4-4	7930	7607	6849	7462	25 %	305	22 %	0.88
C-CFRP1-4	5118	6821	7110	6350	36 %	487	35 %	0.97
C-CFRP2-4	6822	6146	3340	5436	45 %	626	45 %	1.00
C-CFRP3-4	6812	7281	8223	7439	25 %	440	31 %	1.24
C-CFRP4-4	2288	5602	6849	4913	51 %	514	37 %	0.72
R-CON-1	5244	5326	5964	5511	45 %	714	51 %	1.13
Average								0.99

* $A_{st} Loss_{Test}$: Percentile loss of the cross-sectional area determined by tensile test

** $A_{st} Loss_{Faraday}$: Percentile loss of the cross-sectional area determined by Faraday's Law

***1397.4: Original weight of steel cage (three longitudinal rebars and spiral reinforcement, see Figure 3.12)

In Table 4.12, the results of the tensile tests are compared to the calculations by Faraday's Law. The rebar specimens for the tensile test were taken out from each one of the columns, as listed in Table 4.12. The percentile loss of the cross-sectional area determined by tensile test, $A_{st} Loss_{Test}$, was calculated by dividing the average failure load of the corrosion damaged steel reinforcements by the average failure load of the control reinforcements (i.e., undamaged reinforcements). Comparisons between $A_{st} Loss_{Test}$ and $A_{st} Loss_{Faraday}$ are given in the last column in Table 4.12, and it was shown that $A_{st} Loss_{Faraday}$ reasonably in good agreement with $A_{st} Loss_{Test}$.

(b) Cracking. Figures 4.33 shows typical cracks developed in the unwrapped columns and the CFRP wrapped columns. As shown in Figure 4.33(a), longitudinal cracks occurred along the locations of longitudinal reinforcements and transverse cracks occurred along the spiral reinforcement in the unwrapped columns. As shown in Figure 4.33(b), transverse cracks in the CFRP sheets occurred about 1.5 in. from the bottom in the case of the CFRP wrapped columns. The CFRP wrapped columns were strengthened



(a) longitudinal and transverse cracks on the unwrapped columns



(b) transverse crack near the bottom surface of the column strengthened by CFRP sheet wrapping before beginning of the accelerated corrosion process

Figure 4.33. Cracks of Unwrapped and CFRP Wrapped Columns Due to the Accelerated Corrosion Process

with CFRP sheets before the beginning of the accelerated corrosion process, and the cracks were found at the end of the second stage of the accelerated corrosion process. The cracks developed due to the expansion of the concrete in the longitudinal direction of the columns, induced by the internal pressure generated by the corrosion of steel reinforcements. The widths of the cracks were up to 0.125 in.

It should be noted that the fiber direction was at 90 degree angle relative to the longitudinal direction of the columns and thus the FRP sheet wrapping system could not resist the force in the longitudinal direction. On the other hand, the expansion of concrete due to the steel reinforcements could be in any direction. As a result, transverse cracks developed, as shown in Figure 4.33(b); however, such wide cracks will not be seen in the field. This is because the columns and bridge piers are restrained by foundations, cap beams, or slabs, and thus the deformation of the columns and bridge piers will not be large enough to develop such a wide crack. Nonetheless, this phenomenon should be considered in the design of the strengthening of RC structures facing possible corrosion problems.

Cross-sectional cuts were taken to investigate the internal damages, as shown in Figure 4.34. As a result, it was found that cracks occurred even in the CFRP wrapped columns C-CFRP1 and C-CFRP3 as shown in Figures 4.33(c) and (d). However the crack widths of the CFRP wrapped columns C-CFRP1 and C-CFRP3 were relatively smaller than those of the unwrapped column C-CON4 and the repaired columns C-CFRP2 and C-CFRP4, as shown in Table 4.13. In addition, the concrete cover was

Table 4.13. Crack Width Measured with Crack Scope

Unit: milli inches

Specimen	Circumferential				longitudinal			
	1	2	3	average	1	2	3	average
C-CON4	40	20	25	28	40	40	30	37
C-CFRP1	10	10	15	12	10	7	10	9
C-CFRP2	20	15	10	15	20	40	15	25
C-CFRP3	10	20	10	13	15	10	5	10
C-CFRP4	25	30	15	23	15	15	15	15

totally delaminated from the core concrete because cracks formed a continuous ring around the spiral reinforcement for both the unwrapped and the CFRP wrapped columns.

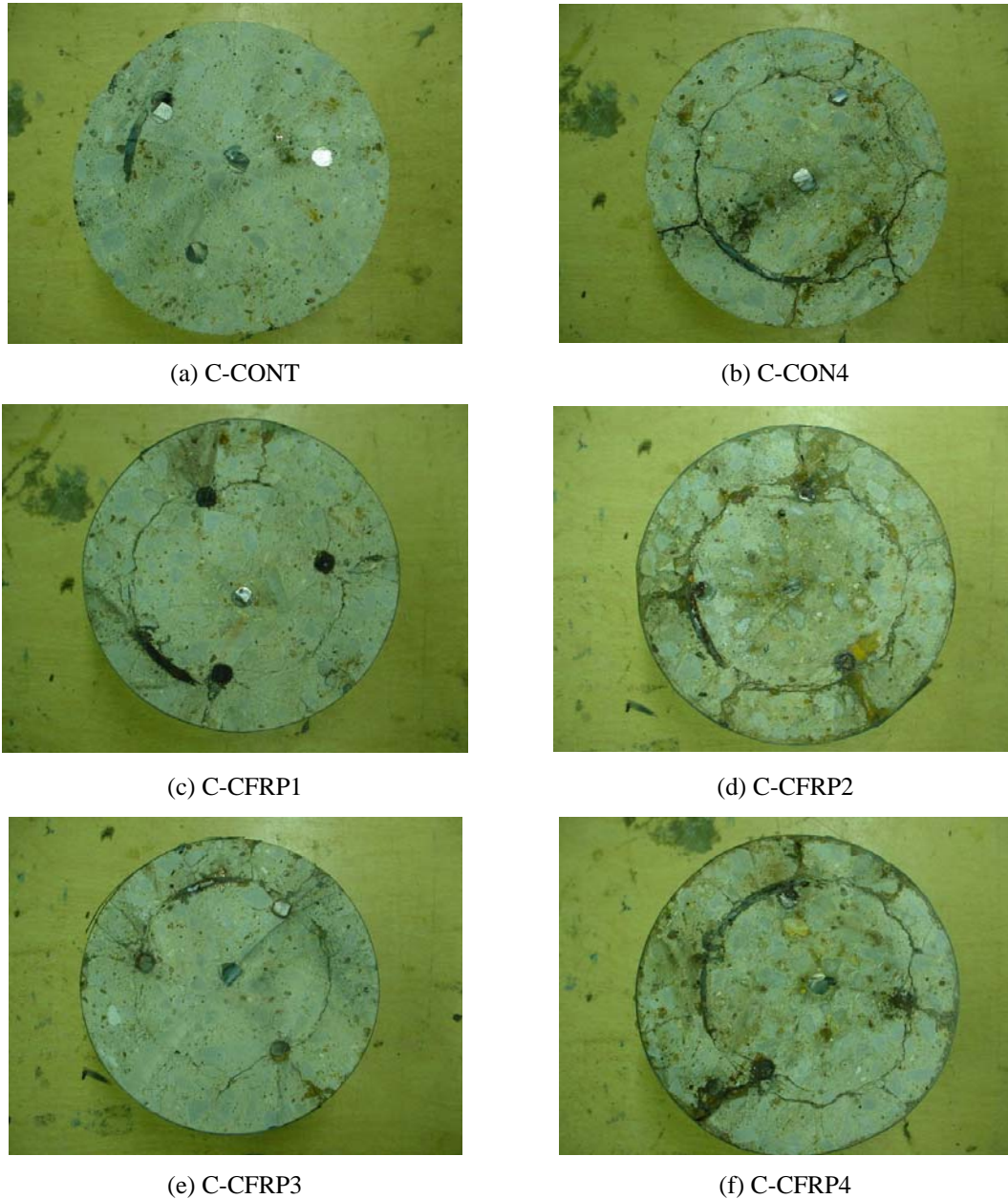


Figure 4.34. Internal Crack Patterns of Control Column and Corrosion Damaged Columns

(c) **Radial strain.** The radial strains of the CFRP wrapped columns C-CFRP1 and C-CFRP2 were monitored throughout the accelerated corrosion process, and the obtained results are plotted in Figure 4.35. At the end of the accelerated corrosion process, the radial strains were approximately 0.00476 to 0.00813 which are 28 % to 48 % of the ultimate tensile strain of the CFRP sheet provided by the manufacturer, ϵ_{fit} , 0.017.

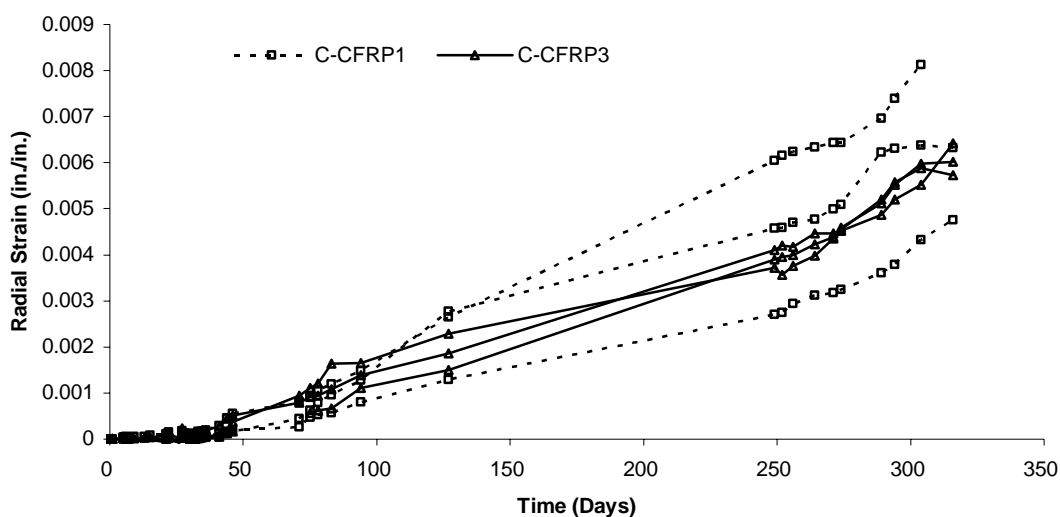


Figure 4.35. Radial Strain vs. Time Curves of Columns C-CFRP1 and C-CFRP3

Figure 4.36 shows the radial strains plotted against the percentile loss of the steel reinforcements. As shown in Figure 4.36, the radial strains did not increase until 5 % loss of the cross-sectional area. After the 5 % loss of the cross-sectional area, the radial strains exhibited a rapid increase up to about 20 % loss of the cross-sectional area. After the 20 % loss of the cross-sectional area, the increase rate of the radial strain slowed down. This implies that the radial strain did not increase until the rust, which is a by-product of the corrosion process, filled in the void of the concrete. Once the void was filled with the rust, concrete started to expand, resulting in the rapid increase in the radial

strain. However, if internal cracks formed around the spiral cracks, the increase rate was reduced.

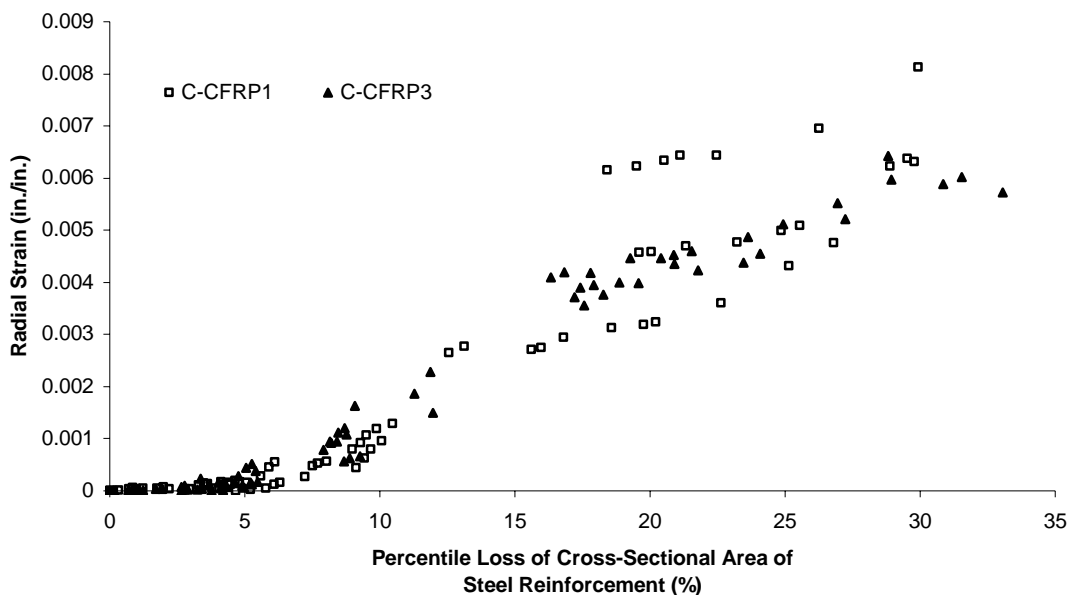


Figure 4.36. Radial Strain vs. Percentile Loss of Cross-Sectional Area of Steel Reinforcements

4.4.2.2 Results of failure tests. A total of 26 small-scale RC columns were tested in uni-axial compression after the accelerated corrosion process. The obtained results are summarized in Table 4.14. Discussions about the effects of the corrosion of steel reinforcements resulting from the accelerated corrosion process are addressed in the following sections.

4.4.2.2.1 Failure modes. The failure modes of the CFRP wrapped columns were significantly affected by the accelerated corrosion process. The failure mode of each column is presented in Table 4.11.

(a) Unwrapped columns. Failure of the unwrapped columns occurred due to the cracking and spalling of the concrete cover, as shown in Figure 4.37. However, it was noticeable that the spalling of the concrete cover of the corrosion damaged columns C-

CON4 occurred along the height of the column almost at the same time and the failure load was much lower when compared to that of the undamaged columns C-CONT and C-CON2. This occurred because the concrete cover of the corrosion damaged columns C-CON4 was already delaminated, prior to the failure test, due to the cracks formed around the spiral reinforcement as discussed in the previous section.

Table 4.14. Failure Load, P_u , and Failure Modes of Small-Scale RC Columns of Corrosion Tests

Specimen	Failure Load P_u (kips)			
	(Failure Mode*)			
	1	2	3	Average
C-CONT	110	109	99	106
C-CON2	122	126	119	122
C-CON3	195 (I)	204 (I)	190 (I)	196
C-CON4	58	72	67	66
C-CFRP1	169 (I)	139 (I)	179 (I)	174**
C-CFRP2	147 (II)	165 (II)	173 (II)	162
C-CFRP3	163 (I)	167 (I)	173 (I)	168
C-CFRP4	153 (II)	147 (I)	134 (II)	145
R-CFRP	165 (I)	153 (II)		159

* Failure Mode

(I): Rupture of the CFRP sheet

(II): Debonding of lap splice

** When calculating the average, the failure load of the column C-CFRP1-2 was excluded because this column was failed at significantly low load due to the transverse crack as shown in Figure 4.32(b).



(a) C-CONT

(b) C-CON2

(c) C-CON4

Figure 4.37. Failure Modes of Unwrapped Columns

(b) Columns strengthened by CFRP sheet wrapping before beginning of the accelerated corrosion process. The failure of the columns strengthened with CFRP sheet wrapping before the beginning of the accelerated corrosion process (C-CFRP1 and C-CFRP3) was due to the rupture of the CFRP sheets, as shown in Figure 4.38. This is the common type of the failure mode of RC columns wrapped with FRP sheets.

(c) Corrosion-damaged columns repaired by CFRP sheet wrapping after the accelerated corrosion process. The failure of the corrosion-damaged columns repaired by CFRP sheet wrapping (C-CFRP2 and C-CFRP4) was mainly due to the debonding of the lap splice of the CFRP sheets, as shown in Figure 4.39. Of the 6 columns repaired by CFRP sheet wrapping, 5 columns were failed in this manner. The remaining one was failed due to the rupture of the CFRP sheets. This phenomenon was probably due to the delamination of the concrete cover which already existed, prior to strengthening with CFRP sheets.

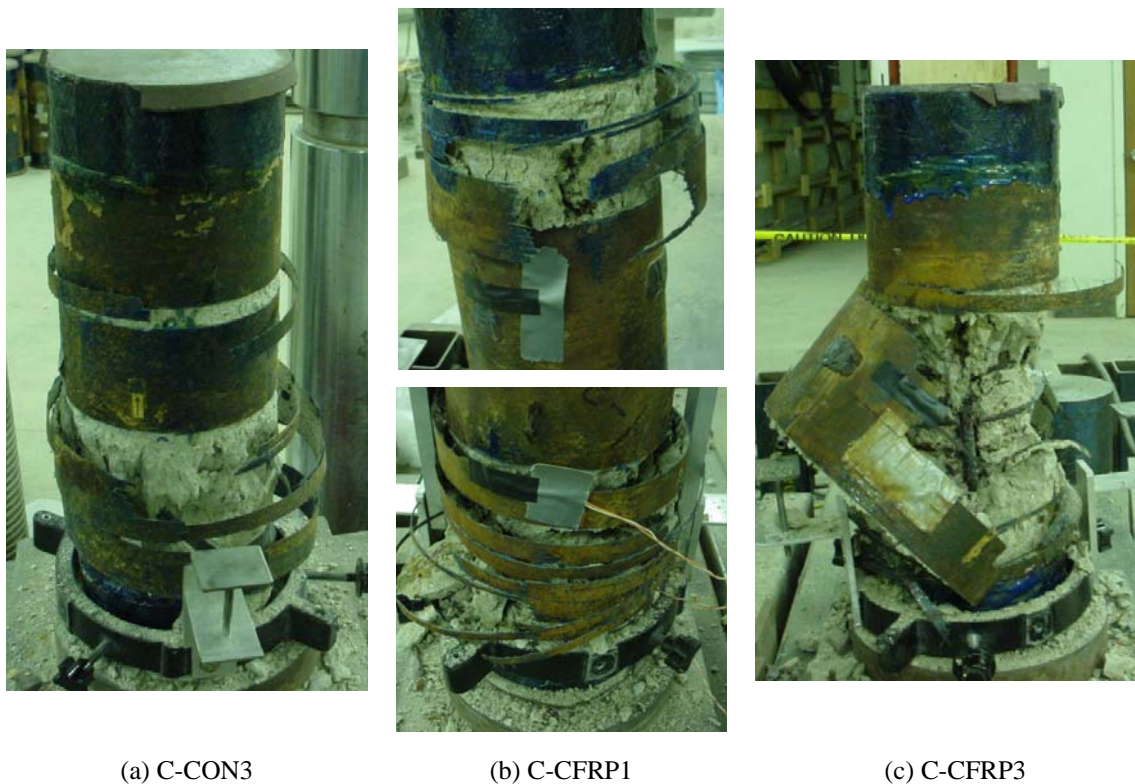


Figure 4.38. Failure Modes of the Columns Strengthened by CFRP Sheet Wrapping before Beginning of the Accelerated Corrosion Process

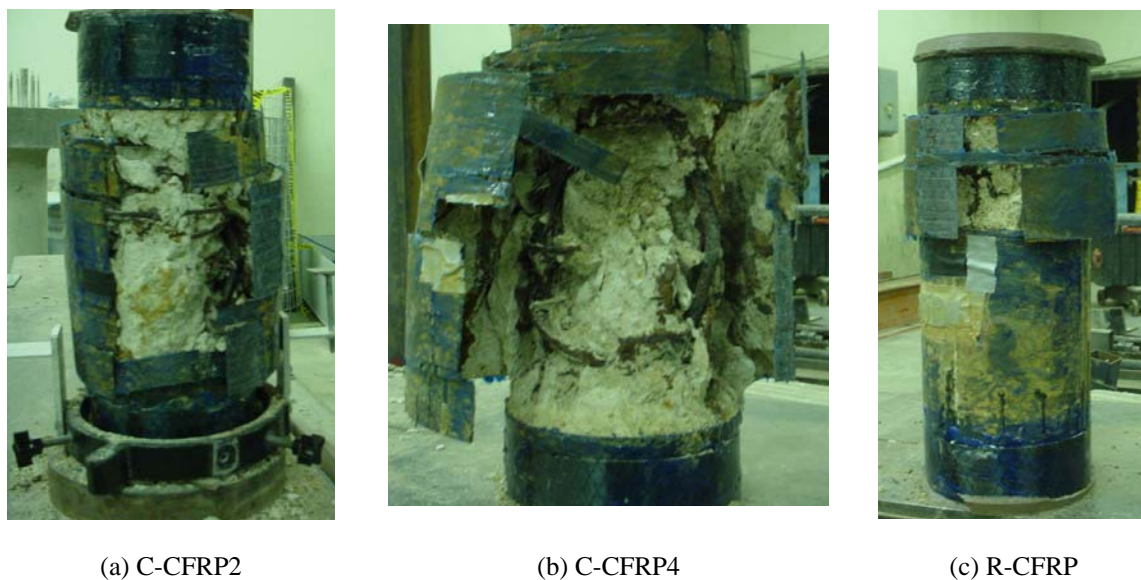


Figure 4.39. Failure Modes of the Corrosion-Damaged Columns Repaired by CFRP Sheet Wrapping after the Accelerated Corrosion Process

4.4.2.2.2 Failure load. Load vs. axial strain curves of all the tested columns are shown in Figures 4.40. The failure load of the corrosion-damaged columns C-CON4, C-CFRP1, C-CFRP2, C-CFRP3, and C-CFRP4 was smaller than that of the corresponding control columns (i.e., C-CONT for C-CON4 and C-CON3 for C-CFRP1, C-CFRP2, C-CFRP3, and C-CFRP4).

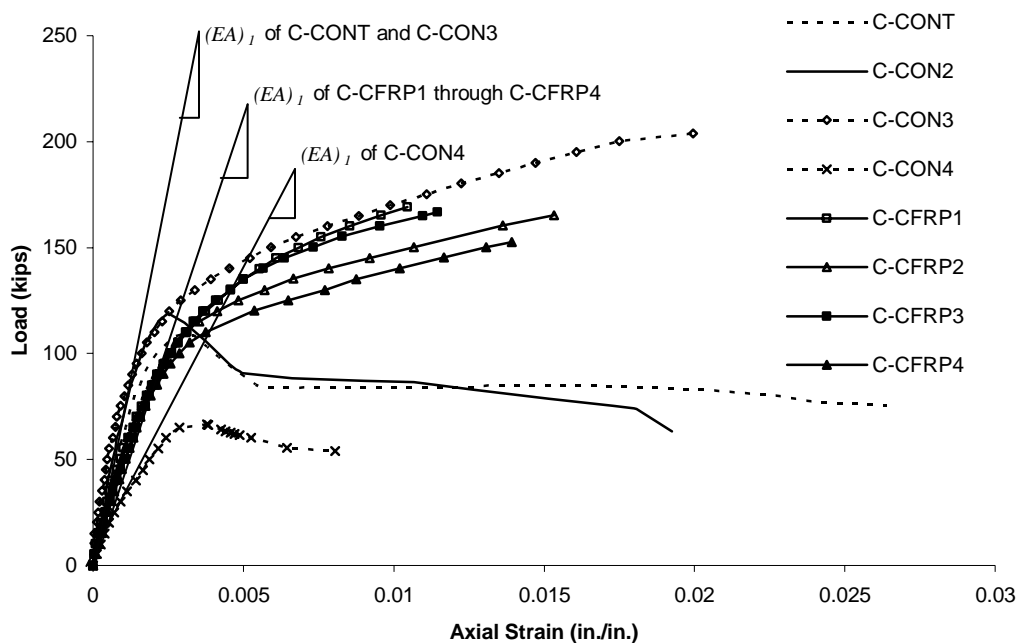


Figure 4.40. Typical Load vs. Axial Strain Curves of all Tested Columns

One reason for the decrease in the failure load is definitely attributed to the loss of the cross-sectional area of steel reinforcements; while the other reason could be attributed to the loss of the structural integrity resulting from the cracking. The loss of the structural integrity appeared to decrease in the axial rigidity in the elastic region, $(EA)_1$, (definition is given in Section 4.2), as shown in Figure 4.40. In order to quantify the extent of decrease in the axial rigidity in the elastic region, $(EA)_1$, due to corrosion damage, a concept of the equivalent area, A_{eqv} , is introduced in the following section.

(a) **Equivalent area of corrosion damaged RC columns, A_{eqv} .** The equivalent area, A_{eqv} , can be determined based on the assumption that elastic modulus, E_c , and compressive strength, f'_c , are not affected by corrosion damage, such as deposition of corrosion by-product in the void of concrete, cracking, and corrosion of steel reinforcements. With these assumptions, the equivalent area, A_{eqv} , are calculated by Equation (4-9):

$$A_{eqv} = \frac{P_u - f_s A_{st}}{f'_c} \quad (4-9)$$

where P_u is failure load measured during the failure tests, f'_c is strength of concrete (f'_{cc} in case of CFRP wrapped RC columns), A_{st} is cross-sectional area of longitudinal steel reinforcements, and f_s is stress of longitudinal steel reinforcements at failure determined by the bi-linear model proposed in Section 3.2.1.2.

However, it was impossible to determine the equivalent area, A_{eqv} , using Equation (4-9), since f'_c and f'_{cc} were unknown. Instead, the ratio of the equivalent area, A_{eqv} , of the corrosion-damaged columns to those of the control columns could be determined, based on the assumption that f'_c (or f'_{cc}) remains unaffected even after the corrosion of steel reinforcements occur. The ratio is called area reduction factor throughout this report and expressed as ϕ_{cor2} . Since it can be assumed that the equivalent area, A_{eqv} , of the control columns is a known value (i.e., $A_g - A_{st}$ in which A_g is the gross area of the cross-section of the column), the equivalent area, A_{eqv} , of the corrosion damaged columns can be determined by multiplying the area reduction factor, ϕ_{cor2} , by the equivalent area, A_{eqv} , of the control columns. The obtained results are presented in Table 4.15 and the ratio is expressed as ϕ_{cor2} .

Table 4.15. Ratio of the Equivalent Area of Corrosion-Damaged Columns to those of Control Columns

Specimen		P_u (kips)	A_{st} (in ²)	$f_s A_{st}$ (kips)	$f'_c A_{eqv}$ * (kips)	Average (kips)	ϕ_{cor2} **	A_{eqv} (in ²)
C-CONT	1	110.36	0.44	30.86	79.50			27.83
	2	109.48	0.44	30.90	78.59			
	3	99.37	0.44	30.85	68.52	75.53		
C-CON3	1	195.05	0.44	33.29	161.76			27.83
	2	203.91	0.44	33.03	170.88			
	3	190.32	0.44	32.49	157.83	163.49		
C-CON4	1	58.05	0.22	15.65	42.40		0.56	15.58
	2	71.84	0.28	-	-	-	-	-
	3	66.76	0.37	25.95	40.81		0.54	15.03
C-CFRP1	1	169.19	0.32	23.36	145.83		0.89	24.77
	2	139.05	0.30	-	-	-	-	-
	3	179.48	0.31	22.59	156.89		0.96	26.72
C-CFRP2	1	146.83	0.28	20.53	126.30		0.77	21.43
	2	165.19	0.29	21.53	143.66		0.88	24.49
	3	172.62	0.28	20.45	152.17		0.93	25.88
C-CFRP3	1	162.81	0.31	22.88	139.93		0.86	23.93
	2	166.70	0.30	21.48	145.22		0.89	24.77
	3	173.14	0.30	22.03	151.12		0.92	25.61
C-CFRP4	1	152.65	0.31	22.45	130.20		0.80	22.26
	2	147.19	0.28	20.32	126.87		0.78	21.71
	3	133.70	0.26	18.66	115.04		0.70	19.48

$$* f'_c A_{eqv} = P_u - f_s A_{st}$$

$$** \phi_{cor2} = \frac{f'_c A_{eqv}}{(f'_c A_{eqv})_{control}}$$

In Table 4.15, the area reduction factors, ϕ_{cor2} , of the unwrapped columns C-CON4 were 0.56 and 0.5, which were determined by dividing $f'_c A_{eqv}$ of Column C-CON4

(42.40 and 40.81 kips) by $f'_c A_{eqv}$ of the control columns C-CONT (75.53 kips). For the CFRP wrapped columns, $f'_c A_{eqv}$ of the corrosion-damaged columns C-CFRP1 through C-CFRP4 was divided by $f'_c A_{eqv}$ of the control columns C-CON3, which is 163.49 kips.

In addition, the area reduction factor, ϕ_{cor2} , of 0.56 and 0.5 for the corrosion-damaged unwrapped columns C-CON4 in Table 4.15 means that the equivalent area, A_{eqv} , of Column C-CON4 are 56 % and 54 % of the cross-sectional area of the concrete of the control column C-CONT. Furthermore, the area reduction factor, ϕ_{cor2} , of 0.56 and 0.54 of Column C-CON4 are very close to the ratio of the area of the core concrete inside the spiral reinforcement to the cross-sectional area of concrete of the control column, 0.52. It is usually thought that the concrete outside the spiral reinforcement of the corrosion damaged RC columns does not take part in resisting the applied load. Thus, the area reduction factor, ϕ_{cor2} , and the equivalent area, A_{eqv} , could be a proper measure to predict the decrease in the axial rigidity in the elastic region, $(EA)_1$, of CFRP wrapped RC columns as well as the decrease in the axial rigidity in the elastic region, $(EA)_1$, of the unwrapped RC columns. Based on the concept of equivalent area, A_{eqv} , introduced in this section, discussions about the behavior of the corrosion damaged RC columns are made in the following sections.

(b) Behavior of unwrapped RC columns. In order to investigate the behavior of the unwrapped columns, the test results of the unwrapped columns C-CONT and C-CON4 were compared. The control column C-CONT was conditioned under room temperature, while Column C-CON4 was the corrosion-damaged column conditioned by the accelerated corrosion process. The average failure load, P_u , and average equivalent area, A_{eqv} , of the columns are presented in Figure 4.41, and the load vs. axial strain curves of the columns are presented in Figure 4.42. As shown in Figure 4.41, the average failure load, P_u , of the corrosion-damaged column C-CON4 was 66 kips which was just 62 % of the average failure load, P_u , of the control columns C-CONT, 106 kips. The decrease in the failure load, P_u , was due to the corrosion damages, such as spalling of the concrete and loss of the cross-sectional area of the steel reinforcements. The in-depth

discussions about the steel loss were presented previously in Section 4.4.2.1. The spalling of the concrete resulted in the reduction of the equivalent area by 54 %, as shown in Figure 4.41. As a result, the axial rigidity in the elastic region was significantly decreased, as shown in Figure 4.42.

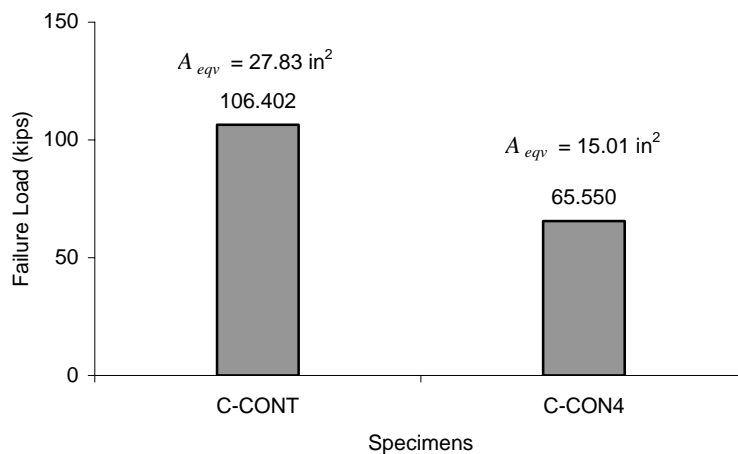


Figure 4.41. Average Failure Load, P_u , and Equivalent Area, A_{eqv} , of Columns C-CONT and C-CON4

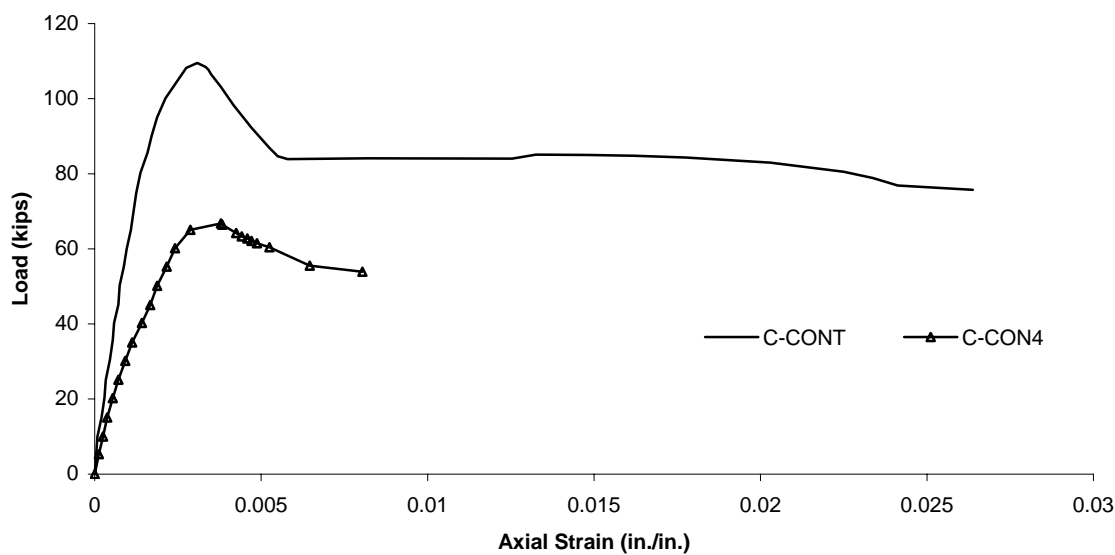


Figure 4.42. Typical Load vs. Axial Strain Curves of Columns C-CONT and C-CON4

(c) Effect of repair by CFRP sheet wrapping. In order to investigate the effect of the repair of the corrosion-damaged RC columns by CFRP sheet wrapping, the test results of Columns C-CON4 and C-CFRP2 were compared in this section. Column C-CON4 was severely damaged by the accelerated corrosion process as discussed in the previous section, resulting in a decrease in the failure load, P_u , by approximately 40%. Column C-CFRP2 was conditioned by the accelerated corrosion process, and thus the extent of the corrosion damage was considered almost the same as that of Column C-CON4. Then, Column C-CFRP2 was strengthened with CFRP sheet wrapping. The average failure load, P_u , and average equivalent area, A_{eqv} , of the columns are presented in Figure 4.43 and the load vs. axial strain curves of the columns are presented in Figure 4.44.

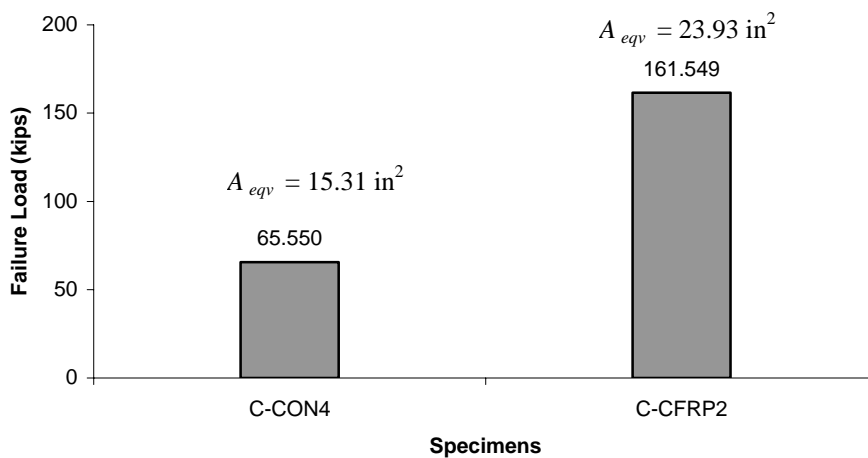


Figure 4.43. Average Failure Load, P_u , and Equivalent Area, A_{eqv} , of Columns C-CON4 and C-CFRP2

As shown in Figure 4.43, the average failure load, P_u , of Column C-CFRP2 was 162 kips which was 2.32 times higher than that of Column C-CON4. In addition, the average failure load, P_u , of Column C-CFRP2 was 1.52 times higher even when compared to the control column C-CONT. Thus, it can be concluded that the CFRP sheet

wrapping significantly improves the axial compression capacity of the corrosion-damaged RC columns.

The increase in the failure load, P_u , was due to the confinement effect of the CFRP sheet wrapping, resulting in an increase in the axial rigidity in the elastic region $(EA)_1$ and the strength of concrete. The increase in the axial rigidity in the elastic region $(EA)_1$ is clearly shown in Figure 4.44. The increase in the axial rigidity in the elastic region $(EA)_1$ could be due to the increase in the equivalent area, A_{eqv} . The equivalent area, A_{eqv} , of Column C-CFRP2 was 24 in² which was 156 % higher than that of Column C-CON4 and was about 86 % of that of Column C-CONT. It implies that the corrosion-damaged concrete cover outside the spiral reinforcement was restored to a significant extent by the CFRP sheet wrapping.

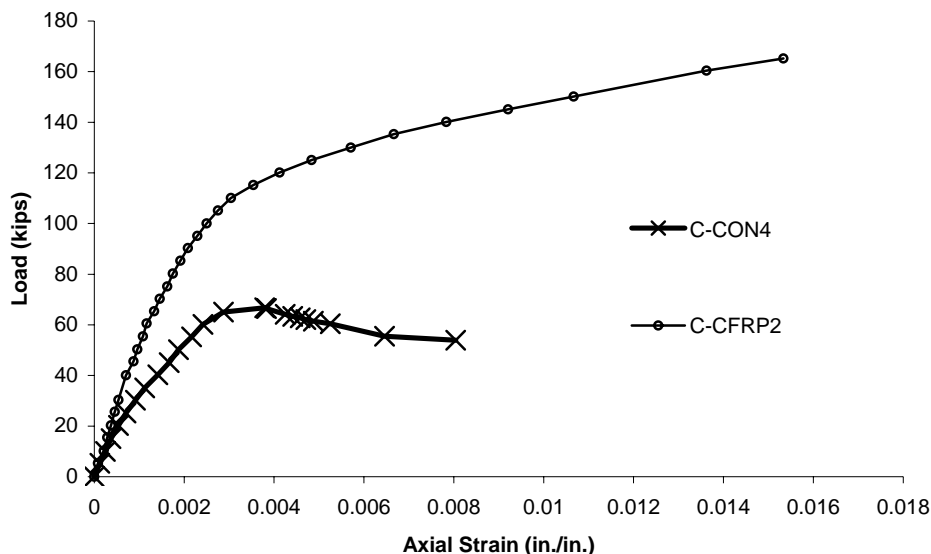


Figure 4.44. Typical Load vs. Axial Strain Curves of Columns C-CON4 and C-CFRP2

(d) Decrease in failure load, P_u , of the CFRP wrapped RC columns due to the corrosion of steel reinforcement. In order to investigate the decrease in the failure load,

P_u , of the CFRP wrapped columns due to the corrosion of steel reinforcements, Columns C-CON3 and C-CFRP1 were compared. Both C-CON3 and C-CFRP were strengthened with CFRP sheets before the beginning of the accelerated corrosion process. However, only Column C-CFRP1 was conditioned under the accelerated corrosion process. The average failure load, P_u , and average equivalent area, A_{eqv} , of the columns are presented in Figure 4.45 and the load vs. axial strain curves of the columns are presented in Figure 4.46.

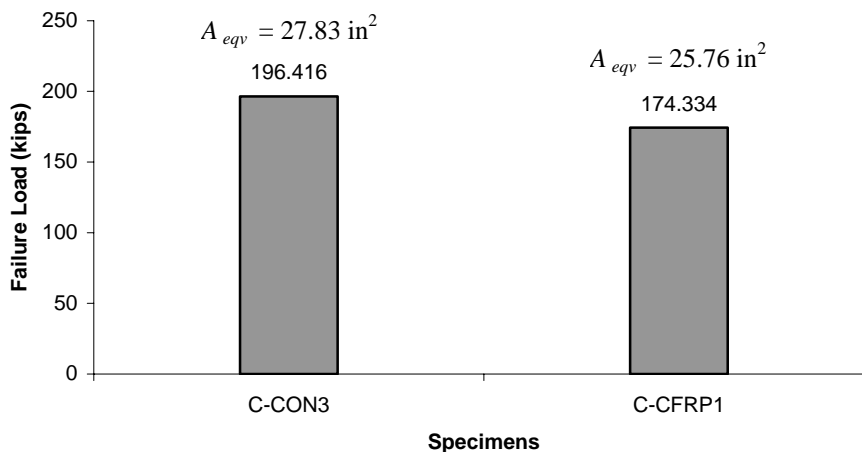


Figure 4.45. Average Failure Load, P_u , and Equivalent Area, A_{eqv} , of Columns C-CON3 and C-CFRP1

As shown in Figure 4.45, the average failure load, P_u , of Column C-CFRP1 was 89 % of that of Column C-CON3. The decrease in the failure load, P_u , was due to several reasons; loss of the cross-sectional area of the steel reinforcements, passive confinement of the CFRP sheets induced by the expansion of concrete, and decrease in the axial rigidity resulting from the cracking. Discussions regarding the loss of the cross-sectional area of the steel reinforcements and radial strain induced by the corrosion of steel were addressed previously in Section 4.4.2.1.

As shown in Figure 4.46, the axial rigidity in the elastic region $(EA)_1$ of Column C-CFRP1 was smaller than that of Column C-CON3; while the axial rigidity in the plastic region $(EA)_2$ of both columns are similar. This is because the behavior of the plastic region is dependent on the stiffness of the FRP sheets, while the behavior of the elastic region is affected by the properties of concrete. The decrease in the axial rigidity $(EA)_1$ in the elastic region was quantified by the equivalent area, A_{eqv} . The equivalent area, A_{eqv} of Column C-CFRP1 was 26 in.² which was 93 % of that of Column C-CON3, 28 in.².

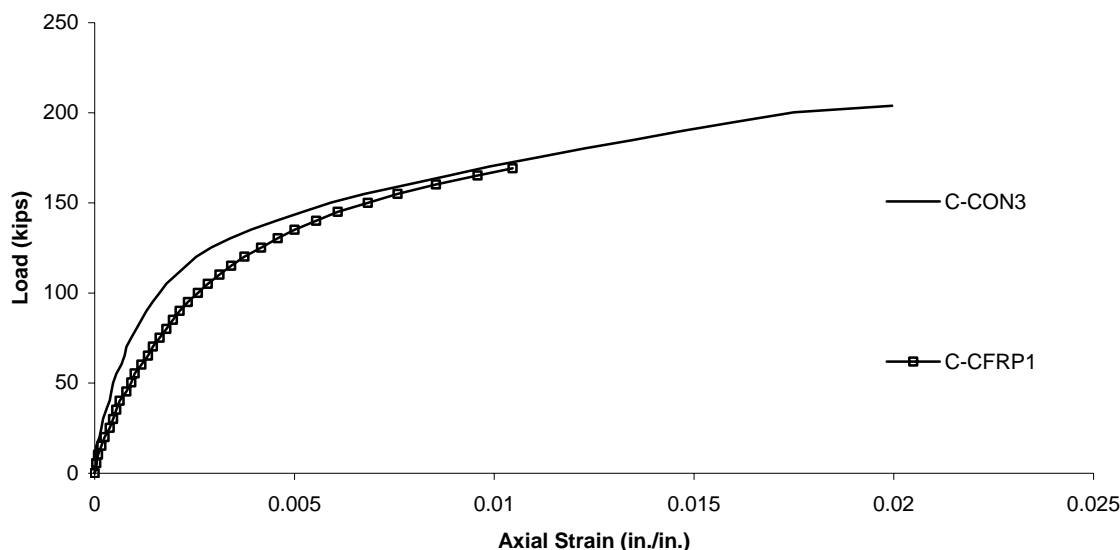


Figure 4.46. Typical Load vs. Axial Strain Curves of Columns C-CON3 and C-CFRP1

(e) Effect of freeze-thaw cycles. In order to investigate the freeze-thaw effect, the test results of Columns C-CFRP1, C-CFRP2, C-CFRP3, and C-CFRP4 were compared. Columns C-CFRP1 and C-CFRP2 were unconditioned columns, while Columns C-CFRP3 and C-CFRP4 were conditioned by the freeze-thaw cycles. Columns C-CFRP1 and C-CFRP3 were strengthened with CFRP sheet wrapping before the beginning of the accelerated corrosion process, while Column C-CFRP2 and C-CFRP4

were strengthened with CFRP sheet wrapping after the second stage of the accelerated corrosion process. The average failure load, P_u , and average equivalent area, A_{eqv} , of the columns are presented in Figure 4.47.

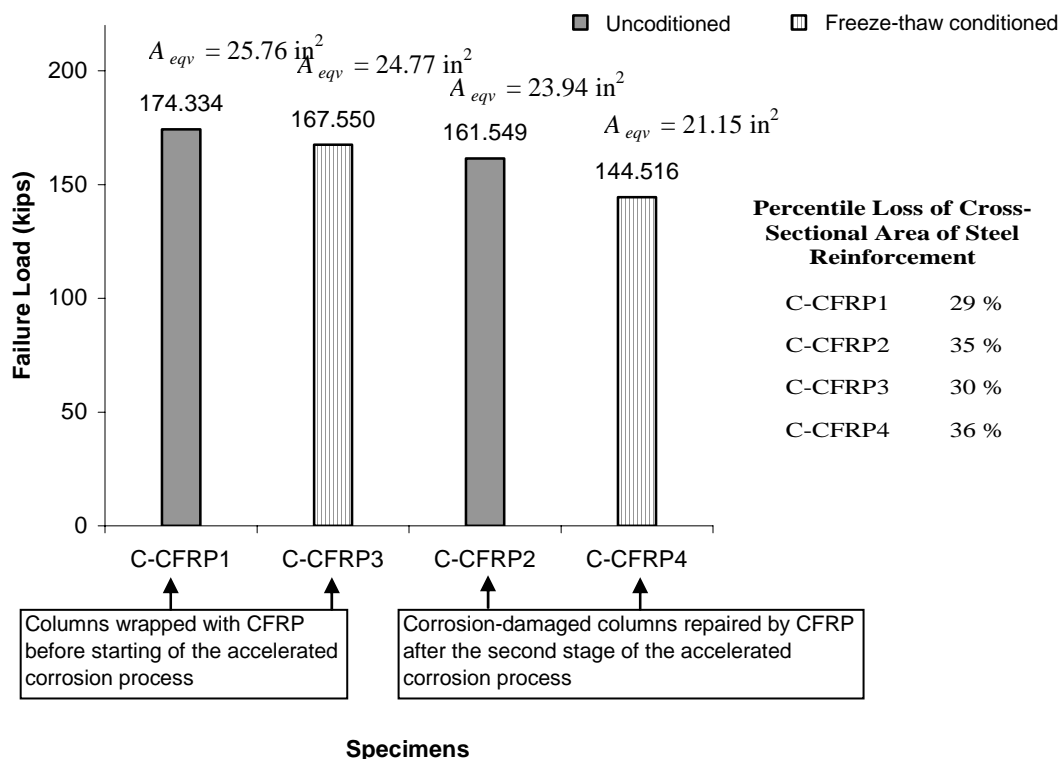


Figure 4.47. Average Failure Load, P_u , and Equivalent Area, A_{eqv} , of Columns C-CFRP1, C-CFRP2, C-CFRP3 and C-CFRP4

As shown in Figure 4.47, the average failure load, P_u , of the freeze-thaw conditioned columns was slightly smaller than that of the unconditioned columns. In addition, the cross-sectional area loss of the steel reinforcement of the columns conditioned by the freeze-thaw cycles was slightly higher than that of the unconditioned columns. As a result, the equivalent area, A_{eqv} , of the freeze-thaw conditioned columns was slightly smaller than that of the unconditioned columns. These results imply that freeze-thaw cycles could result in more severe corrosion damages since the micro-cracks

at fiber-matrix interface could allow moisture ingress into the inside concrete, accelerating the corrosion process of steel reinforcement.

4.4.2.3 Area reduction factor, ϕ_{cor} . The area reduction factor, ϕ_{cor} , was proposed in an effort to consider the effects of corrosion of steel reinforcement in the design of the RC columns wrapped with CFRP sheets. The area reduction factor, ϕ_{cor} , is separated into two different factors: ϕ_{cor1} and ϕ_{cor2} . Discussions on these factors are presented in the following three sections.

4.4.2.3.1 Area reduction factor, ϕ_{cor1} . It has been found that the cross-sectional area of the steel reinforcements was reduced by the accelerated corrosion process, even if RC columns were wrapped with CFRP sheets. Thus, it could be assumed that if CFRP wrapped RC columns were in a severe corrosive environment, the cross-sectional area of the steel reinforcement would be reduced due to the corrosion process in the long term. In order to consider this phenomenon in the design of the RC columns wrapped with CFRP sheets, area reduction ϕ_{cor1} was introduced as shown in Equation (4-10):

$$(A_{st})_{cor} = \phi_{cor1} A_{st} \quad (4-10)$$

where $(A_{st})_{cor}$ is the reduced cross-sectional area of longitudinal steel reinforcement and A_{st} is cross-sectional area of longitudinal steel reinforcement.

4.4.2.3.2 Area reduction factor, ϕ_{cor2} . Area reduction factor, ϕ_{cor2} , was proposed to account for the degradation of the concrete due to the cracking induced by the corrosion of steel reinforcement, mainly resulting in the decrease in the axial rigidity in the elastic region, $(EA)_1$. In order to account for the decrease in the axial rigidity in the elastic region, $(EA)_1$, the concept of the equivalent area, A_{eqv} , was introduced in the previous section, and it is formulated as shown in Equation (4-11).

$$A_{eqv} = \phi_{cor2} [A_g - (A_{st})_{cor}] = \phi_{cor2} (A_g - \phi_{cor1} A_{st}) \quad (4-11)$$

4.4.2.3.3 Relationship between area reduction factors, ϕ_{cor1} and ϕ_{cor2} . The relationship between the area reduction factors, ϕ_{cor1} and ϕ_{cor2} is illustrated in Figure 4.47 based on the test results of this study.

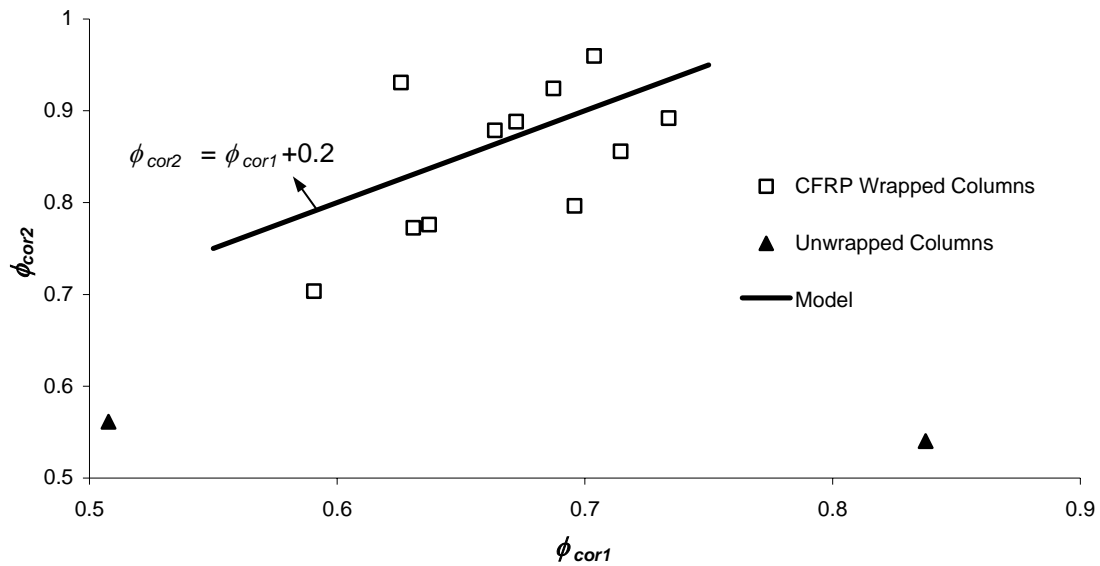


Figure 4.48. Relationship between ϕ_{cor1} and ϕ_{cor2}

Triangular solid dots in Figure 4.48 are data of the unwrapped RC columns, and rectangular dots are data of the CFRP wrapped columns. Figure 4.48 shows that, the area reduction factor, ϕ_{cor2} , for unwrapped RC columns did not change even if the area reduction factor, ϕ_{cor1} , significantly changed. This implies that once the spalling of concrete cover occurs, the equivalent area, A_{eqv} , of the corrosion-damaged columns is limited to the area of the core concrete inside the spiral reinforcement. However, in the case of the CFRP wrapped columns, it can be observed that as the area reduction factor, ϕ_{cor1} , decreases, the area reduction factor, ϕ_{cor2} , decreases. In other words, the CFRP wrapped columns with greater loss of the cross-sectional area of steel reinforcements have smaller axial rigidity (or equivalent area, A_{eqv}) due to the cracking. However, it

should be noticed that all the values of the area reduction factor, ϕ_{cor2} , of the CFRP wrapped RC columns were much higher than those of the unwrapped RC columns in all cases.

4.4.2.3.4 Determination of area reduction factor, ϕ_{cor} . Assigning a number to the area reduction factor, ϕ_{cor} is a difficult task because not only corrosion of steel reinforcements includes complex electrochemical reaction, but also the damage of RC structures induced by the corrosion of steel reinforcement vary according to the extent of the corrosion rate, the geometry of steel reinforcement, the reinforcement ratio, and the properties of concrete such as permeability and strength. Especially for RC columns wrapped with CFRP sheets, the degree of corrosion damage is also affected by the level of confinement provided by the CFRP sheets. Thus, it was difficult to carry out the tests which include all the parameters in this study. Instead, it was the intention of this study to construct the worst case scenario throughout the experimental program by using high permeable and low strength concrete, with a low reinforcement ratio of 0.016 (usually higher reinforcement ratio result in more severe corrosion damages to concrete), a small-depth of concrete cover of 1 in. Therefore, assigning numbers to area reduction factors ϕ_{cor1} and ϕ_{cor2} based on the test results of this study would result in a conservative outcome in most cases, although they are not always highly accurate.

In Table 4.16, the area reduction factor, ϕ_{cor2} , of Columns C-CFRP1, C-CFRP2, C-CFRP3, and C-CFRP4 and the experimental programs applied to the columns are summarized. The area reduction factor, ϕ_{cor2} , as shown in Table 4.16, is the averages of three identical columns. Calculations of all the columns were previously presented in Table 4.15. Based on the test results of this study as shown in Table 4.16, the area reduction factor, ϕ_{cor2} , of the CFRP wrapped RC columns in different environments were proposed in Table 4.17, which can be used for the design of RC columns wrapped with CFRP sheets; while the area reduction factor, ϕ_{cor1} , in Table 4.17 were calculated based on the relationship between ϕ_{cor1} and ϕ_{cor2} , as shown in Figure 4.47. For example, Column C-CFRP1 in Table 4.16 was wrapped with CFRP sheets before the beginning of

Table 4.16. Area Reduction Factors, ϕ_{cor2} , of Columns C-CFRP1, C-CFRP2, C-CFRP3, and C-CFRP4 and Experimental Programs Applied to the Columns

Specimen	ϕ_{cor2}	Experimental Program
C-CON3	1.00	Control
C-CFRP1	0.93	CFRP sheet were applied before beginning of the accelerated corrosion process
C-CFRP2	0.86	CFRP sheet were applied after the columns were severely damaged by corrosion of steel reinforcement as a repair method
C-CFRP3	0.89	Same as C-CFRP1 but conditioned by 300 freeze-thaw cycles after CFRP sheet wrapping
C-CFRP4	0.76	Same as C-CFRP1 but conditioned by 300 freeze-thaw cycles after CFRP sheet wrapping

Table 4.17. Proposed Area Reduction Factor, ϕ_{cor2}

ϕ_{cor1}	ϕ_{cor2}	Conditions of RC Columns
0.75	0.95	Newly constructed RC columns with CFRP wrapping
0.65	0.85	Corrosion-damaged RC columns repaired by CFRP sheet wrapping
0.70	0.90	Newly constructed RC columns with CFRP wrapping placed where possible freeze-thaw damages are anticipated
0.55	0.75	Corrosion-damaged RC columns repaired by CFRP sheet wrapping placed where possible freeze-thaw damages are anticipated

the accelerated corrosion process, thus it could represent the newly constructed RC columns wrapped with CFRP sheets in a corrosive environment as shown in Table 4.17. Similarly, Column C-CFRP2 as shown in Table 4.16 could represent the corrosion damaged RC columns repaired by CFRP sheet wrapping as shown in Table 4.17. Columns C-CFRP3 and C-CFRP4 were conditioned in the same procedure as Columns C-CFRP1 and C-CFRP2, respectively. However, only Columns C-CFRP3 and C-CFRP4

were freeze-thaw conditioned before the third stage of the accelerated corrosion process. Thus, Column C-CFRP3 as shown in Table 4.16 could represent the newly constructed RC columns with CFRP wrapping placed where possible freeze-thaw damages are anticipated, and Column C-CFRP4 as shown in Table 4.16 could represent the corrosion-damaged RC columns repaired by CFRP sheet wrapping placed where possible freeze-thaw damages are anticipated.

Because the reduction factors ϕ_{cor1} and ϕ_{cor2} as shown in Table 4.17 were developed based on the test results of this study, it was assumed in all cases that the corrosion sources such as water and de-icing salt were not removed, even after the CFRP sheet wrapping (i.e., all the tested columns were re-conditioned by the accelerated corrosion process after CFRP sheet wrapping). In the fields, corrosion sources can be removed after repair of corrosion damaged RC columns with CFRP wrapping in order to prevent further corrosion. However, the test results of this study showed that corrosion of steel reinforcement continued to occur, even after the removal of the corrosion source as previously shown in Figures 4.26 and 4.27. Therefore, it is suggested that the area reduction factors ϕ_{cor1} and ϕ_{cor2} be used, even if corrosion sources are removed after repair of corrosion-damaged RC columns with CFRP sheet wrapping.

4.4.2.4 Decrease in ultimate tensile strain of CFRP sheets. Strain reduction factor, R_c , was proposed in Section 4.3.1.6, as shown in Equation (4-3), in order to account for the difference between the ultimate tensile strain provided by manufacturer and the actual ultimate tensile strain measured during the compressive tests. Equation (4-3) was modified in this section to account for the effect of the corrosion of steel reinforcement. In Table 4.18, the radial strains measured at the end of the accelerated corrosion process, $(\epsilon_r)_{corrosion}$, and the radial strains measured at failure during the compressive test, $(\epsilon_r)_{failure\ test}$, were presented. Using the data shown in Table 4.18, Figure 4.49 was drawn based on the average values.

As shown in Figure 4.49, the ultimate tensile strain of CFRP sheet of the CFRP wrapped columns decreased if the columns were conditioned by the accelerated corrosion process. This was due to the fact that there was pre-strain induced by the expansion of

Table 4.18. Radial Strains, ϵ_r , Measured during the Accelerated Corrosion Process and during the Compressive Failure Test

		Radial Strain ϵ_r (in./in.)				$(\epsilon_r)_{total} / \epsilon_{fu}$
		1	2	3	Average	
C-CON3	$(\epsilon_r)_{failure\ test}^*$	0.009356	0.011013	0.008882	0.009750	0.57
	$(\epsilon_r)_{corrosion}^{**}$	0	0	0	0	0
	$(\epsilon_r)_{total}^{***}$	0.009356	0.011013	0.008882	0.009750	0.57
C-CFRP1	$(\epsilon_r)_{failure\ test}$	0.003771	0.001509	0.004547	0.003275	0.19
	$(\epsilon_r)_{corrosion}$	0.004762	0.008132	0.006318	0.006404	0.38
	$(\epsilon_r)_{total}$	0.008533	0.009641	0.010865	0.009679	0.57
C-CFRP2	$(\epsilon_r)_{failure\ test}$	0.006995	0.008865	0.004851	0.006903	0.41
	$(\epsilon_r)_{corrosion}$	0.001554	0.000826	0.000934	0.001105	0.06
	$(\epsilon_r)_{total}$	0.008549	0.009691	0.005785	0.008008	0.47
C-CFRP3	$(\epsilon_r)_{failure\ test}$	0.003716	0.003617	0.003108	0.003480	0.20
	$(\epsilon_r)_{corrosion}$	0.006420	0.005726	0.006020	0.006055	0.36
	$(\epsilon_r)_{total}$	0.010136	0.009343	0.009128	0.009535	0.56
C-CFRP4	$(\epsilon_r)_{failure\ test}$	0.007331	0.007033	0.005017	0.006460	0.38
	$(\epsilon_r)_{corrosion}$	0.001216	0.001138	0.000970	0.001108	0.07
	$(\epsilon_r)_{total}$	0.008547	0.008171	0.005987	0.007568	0.45

* $(\epsilon_r)_{failure\ test}$: radial strain due to the mechanical loading measured at failure during the failure test

** $(\epsilon_r)_{corrosion}$: radial strain due to the corrosion of steel reinforcement measured at the end of the accelerated corrosion process.

*** $(\epsilon_r)_{total} = (\epsilon_r)_{failure\ test} + (\epsilon_r)_{corrosion}$

the columns due to the corrosion of steel reinforcement. Thus, Equation (4-3) was modified into Equation (4-12) and the design ultimate strain of CFRP sheet must be determined by Equation (4-12):

$$\epsilon_{fu}^* = R_c \epsilon_{fu} - (\epsilon_r)_{corrosion} \quad (4-12)$$

where ϵ_{fu}^* is design ultimate tensile strain of FRP sheets, R_c is strain reduction factor

(0.5 for both CFRP and GFRP wrapped RC column), ε_{fu} is ultimate tensile strain provided by the manufacturer, and $(\varepsilon_r)_{corrosion}$ is pre-strain induced by the corrosion of steel reinforcement.

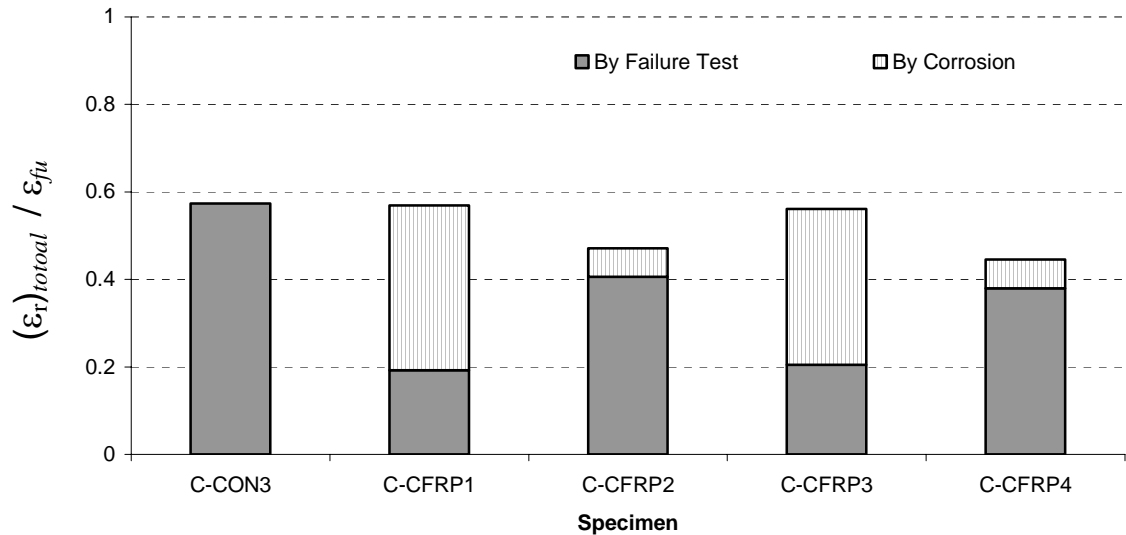


Figure 4.49. Ratio of $(\varepsilon_r)_{total} / \varepsilon_{fu}$

4.4.3. Mid-Scale RC Column Tests. A total of 4 mid-scale RC columns were tested in uni-axial compression after the accelerated corrosion process. The obtained results and discussions are presented in the following sections.

4.4.3.1 Results of accelerated corrosion process. In this section, the results obtained during the accelerated corrosion process are discussed.

4.4.3.1.1 Corrosion rate. Corrosion rates were monitored by measuring the corrosion current throughout the accelerated corrosion process. Corrosion currents vs. time curves of all the mid-scale RC columns, except for the control column M-CONT, are presented in Figure 4.50. For Columns M-COR-CFRP and M-CFRP-COR, the accelerated corrosion process was stopped at the end of the first stage. For Column M-COR-CFRP-COR, the accelerated corrosion process was continued until the end of the

second stage of the accelerated corrosion process. Thus, during the second stage of the accelerated corrosion process, only data of Column M-COR-CFRP-COR were recorded, as shown in Figure 4.50.

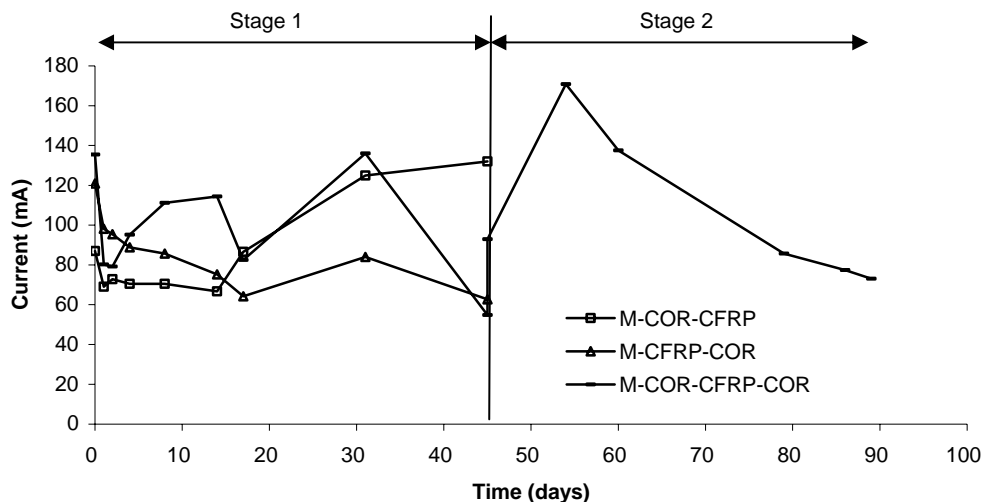


Figure 4.50. Current vs. Time Curves of Columns M-COR-CFRP, M-CFRP-COR and M-COR-CFRP-COR

At this point, it should be noted that the purpose of the accelerated corrosion process of the mid-scale RC column tests was not to evaluate the corrosion rate of the columns, since it was already investigated using small-scale RC columns. Rather, the purpose was to introduce same corrosion-damage to all the columns by means of controlling the amount of the cross-sectional area loss of steel reinforcement.

Figure 4.51 shows the steel loss vs. time curves of the columns. The corrosion rates (i.e., slope of the curves) of all the columns appeared to be very close to each other. As a result, the accumulated steel loss of Column M-COR-CFRP was almost the same as that of Column M-CFRP-COR.

4.4.3.1.2 Corrosion damages due to the accelerated corrosion process. Figure 4.52 shows the picture of Columns M-COR-CFRP and M-COR-CFRP-COR after the completion of the first stage of the accelerated corrosion process. At the end of the first

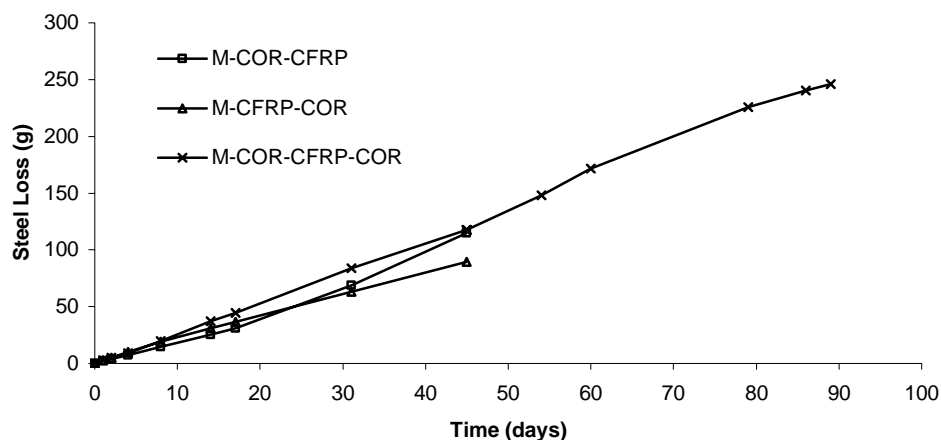


Figure 4.51. Steel Loss vs. Time Curves of Columns M-COR-CFRP, M-CFRP-COR and M-COR-CFRP-COR

stage of the accelerated corrosion process, the percentile loss of the cross-sectional area of the steel reinforcement of each column was calculated by Faraday's Law. The calculated average percentile loss appeared to be just 0.6%. However, there were many cracks along the locations of longitudinal and spiral reinforcements at that time, as shown in Figure 4.52. In addition, the crack widths ranged from 0.02 to 0.05 in. In the field, repairs are motivated usually by concrete damages such as cracking, spalling, and delamination. Thus, the decision was made to stop the accelerated corrosion process and repair the damaged mid-scale RC columns, even if the calculated percentile loss of the cross-sectional area of the steel reinforcement was very small.

4.4.3.1.3 Radial strains. Radial strains of the CFRP sheet of the two columns, M-CFRP-COR and M-COR-CFRP-COR, were measured using strain gages during the accelerated corrosion process and the obtained results are presented in Figure 4.53. Column M-CFRP-COR showed a rapid increase in radial strain, while Column M-COR-CFRP-COR showed a gradual increase. It should be noted that Column M-CFRP-COR was strengthened with CFRP sheets before the beginning of the accelerated corrosion process, while Column M-COR-CFRP-COR was strengthened with CFRP sheets after the accelerated corrosion process. As a result, Column M-COR-CFRP-COR had several cracks before the strengthening with CFRP sheets. Thus, the gradual increase in radial

strain of Column M-COR-CFRP-COR was probably due to the existence of the cracks. The corrosion by-product, rust, was deposited in the cracks, and thus the expansion due to the accelerated corrosion process was not significant.

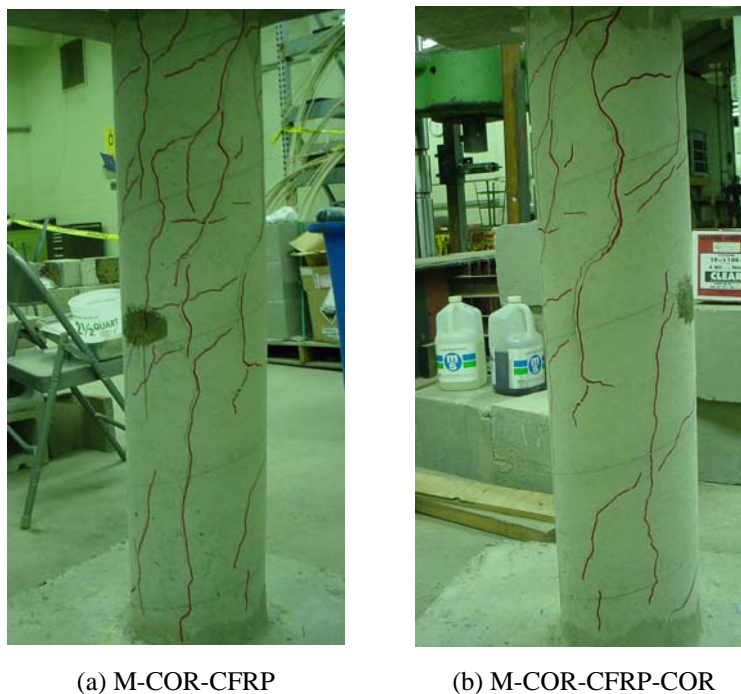


Figure 4.52. Cracks Due to the Accelerated Corrosion Process

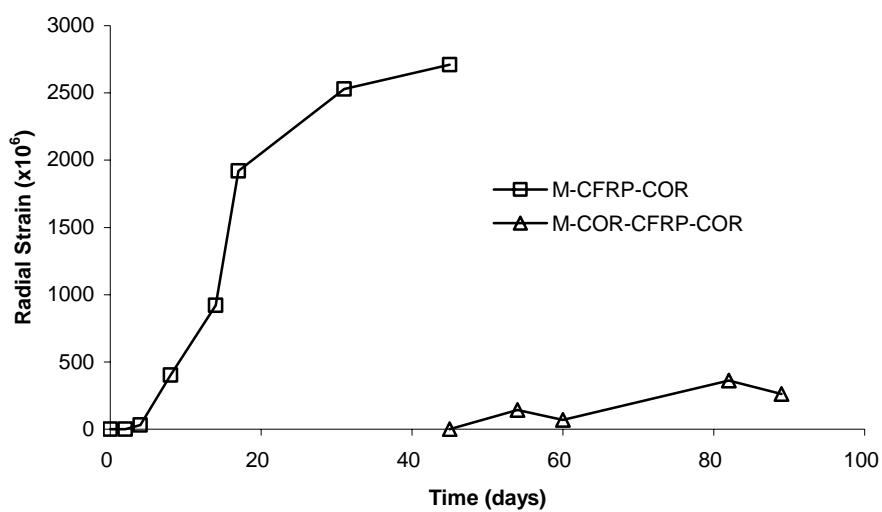


Figure 4.53. Radial Strain of CFRP Wrapped Mid-Scale RC Columns

4.4.3.2 Results of failure tests. All mid-scale RC columns were tested in uni-axial compression after the accelerated corrosion process. The results are discussed in this section.

4.4.3.2.1 Failure modes. Figure 4.54 shows the failure modes of the mid-scale RC columns. The unwrapped column M-CONT failed due to the concrete spalling. For the CFRP wrapped columns, M-CFRP-COR and M-COR-CFRP, the failure occurred directly due to the rupture of CFRP sheets. However, Column M-COR-CFRP-COR failed because of the debonding of the lap splice of CFRP sheets, as shown in Figure 4.54. This phenomenon of lap splice debonding was also observed in the test of the



(a) M-CONT: Concrete spalling and buckling of longitudinal rebar



(b) M-CFRP-COR and M-COR-CFRP: rupture of CFRP sheet



(c) M-COR-CFRP-COR: debonding of lap splice and delamination

Figure 4.54. Failure Modes of Mid-Scale RC Columns

small-scale RC columns (in the case of Columns C-CFRP2 and C-CFRP4). Columns M-COR-CFRP-COR, C-CFRP2 and C-CFRP4 were conditioned by the accelerated corrosion process before the strengthening with CFRP sheet wrapping. As a result, there were cracks and concrete cover was delaminated before the wrapping of the CFRP sheets. Therefore, the pre-existing cracks and the delaminated concrete cover probably are the

primary reasons for the debonding failure. Consequently, when repairing the corrosion-damaged RC columns with CFRP sheet wrapping, the length of lap splice must be longer than the length of lap splice used for the wrapping of RC columns without corrosion damages. Further research must be conducted on this subject because this kind of failure leads to a decrease in failure load to a significant degree.

4.4.3.2.2 Failure load, P_u . Failure load, P_u , of all the tested columns are summarized in Table 4.19 and the load vs. axial strain curves of the columns are presented in Figure 4.55.

Table 4.19. Failure Load P_u and Failure Modes

	Failure Load P_u	Failure Mode
M-CONT	270	
M-CFRP-COR	433	Rupture of CFRP sheet
M-COR-CFRP	379	Rupture of CFRP sheet
M-COR-CFRP-COR	211	Lap splice debonding and delamination

As shown in Figure 4.55, Columns M-CONT and M-COR-CFRP-COR were loaded monotonically up to failure. For Columns M-CFRP-COR and M-COR-CFRP, loading was stopped since the top and bottom concrete blocks were broken before the columns failed. This occurred because the concrete blocks were also damaged by the accelerated corrosion process and had large cracks on the top and bottom surface. Thus, Columns M-CFRP-COR and M-COR-CFRP were re-loaded after the broken block had been fixed.

Similar to the results of the small-scale RC column tests, it was found that corrosion-damaged columns could be repaired by CFRP sheet wrapping, resulting in increase in failure load, P_u . The failure load, P_u , of Column M-COR-CFRP was 379

kips which was 1.40 times higher than that of the control column M-CONT. It is important to remember that Column M-CONT was undamaged and cured at room temperature until the compressive test, while the column M-COR-CFRP was severely damaged before the CFRP wrapping due to the corrosion, as shown in Figure 4.52. Thus, if the failure load of Column M-COR-CFRP were compared to a corrosion-damaged column, the ratio would be much higher than 1.40. Another important remark in comparing Columns M-CONT and M-COR-CFRP is the decrease in the axial rigidity in the elastic region $(EA)_1$, as shown in Figure 4.54.

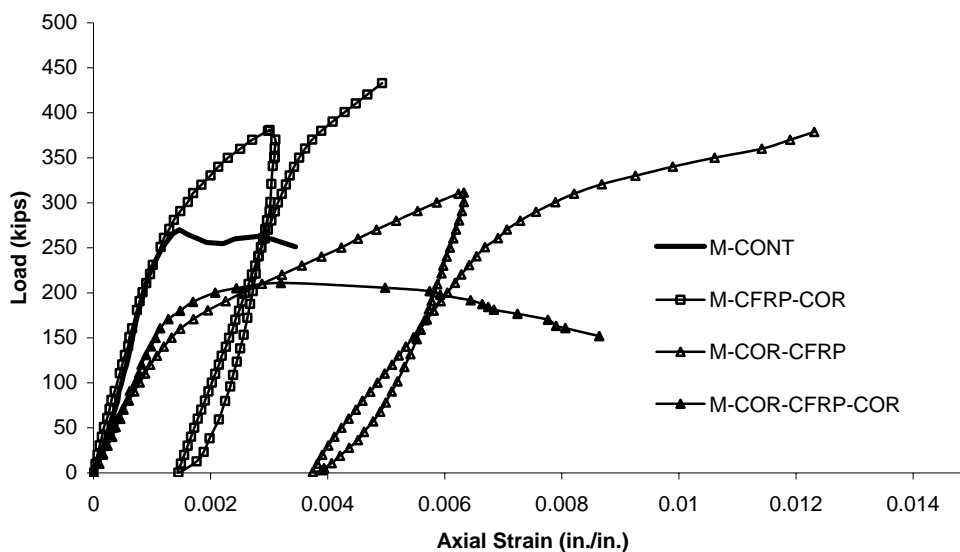


Figure 4.55. Axial Load vs. Axial Strain Curves of Mid-Scale RC Columns

When the column was conditioned again after the repair with CFRP sheet wrapping under the accelerated corrosion process (i.e., in case of Column M-COR-CFRP-COR), the failure load, P_u , was smaller than that of the control column M-CONT. The failure load, P_u , of Column M-COR-CFRP-COR was 211 kips, which was just 78 % of that of the control column M-CONT. Moreover, it was just 56 % of the failure load of Column M-COR-CFRP. Columns M-COR-CFRP and M-COR-CFRP-COR were

conditioned under the same procedure before the CFRP wrapping. After the CFRP wrapping, Column M-COR-CFRP was conditioned under room temperature until the compressive tests, while Column M-COR-CFRP-COR was conditioned again by the accelerated corrosion process. Thus, internal damages of Column M-COR-CFRP-COR might be greater than that of Column M-COR-CFRP. However, the primary reason for the significantly lower failure load, P_u , must be due to the failure modes created by lap splice debonding, as shown in Figure 4.54.

4.4.4. Summary and Conclusions. From the accelerated corrosion process and the compressive failure tests on small-scale and mid-scale RC columns wrapped with CFRP sheets, the effects of the corrosion of steel reinforcement were quantified and the following conclusions were drawn:

1. Although wrapping an RC column with CFRP sheets could decrease the corrosion rate, the corrosion of steel reinforcement continued to occur because of the entrapped moisture. This is especially true if the cracks in the CFRP sheets occurred due to the expansion of the columns induced by the corrosion of steel reinforcements. In this case, the effect of CFRP sheets on decreasing corrosion rate was not significant because moisture could ingress through the cracks, directly reaching the concrete and the steel reinforcement.
2. Repair of corrosion damaged RC columns by CFRP sheet wrapping could greatly improve the axial compression capacity by increasing the axial rigidity of the elastic region, $(EA)_1$. It would also increase the compressive strength of the concrete due to the confinement effect.
3. In the case where the CFRP wrapped RC columns were conditioned by the accelerated corrosion process, the failure load, P_u , was slightly decreased. This was due to the corrosion of steel reinforcement, resulting in the decrease in axial rigidity in the elastic region, $(EA)_1$, in addition to the loss of the cross-sectional area of steel reinforcement.
4. The failure of RC columns strengthened with CFRP sheet wrapping before the beginning of the accelerated corrosion process was directly due to the rupture of the CFRP sheets. However, in the case where the RC columns were severely damaged

- by the accelerated corrosion process and then strengthened with CFRP sheet wrapping, the failure occurred because of the debonding at the lap splice, resulting in the decrease in failure load at a significant degree. The failure mode of lap splice debonding might be due to the pre-existing cracks and delaminations of concrete cover.
5. In order to quantify the decrease in axial rigidity in the elastic region, $(EA)_1$, a concept of the equivalent area, A_{eq} , was introduced. It was proven to be a proper measure to predict the degradation of concrete due to cracking, induced by the corrosion of steel reinforcement.
 6. Area reduction factor, ϕ_{cov1} , was proposed to account for the loss of the cross-sectional area of steel reinforcements based on the test results of small-scale RC columns. In addition, area reduction factor, ϕ_{cov2} , was proposed to account for the degradation of concrete due to the corrosion of steel reinforcement.
 7. An equation was proposed to account for the decrease in the ultimate tensile strain of the CFRP sheets due to the corrosion of steel reinforcement.
 8. Overall, RC columns wrapped with CFRP sheets could be affected by the corrosion of steel reinforcement, if they were placed in a severe corrosive environment, resulting in decrease of failure load, P_u . The reasons for the decrease were attributed to the loss of cross-sectional area of steel reinforcement, decrease in axial rigidity in the elastic region, $(EA)_1$, and decrease in ultimate tensile strain of the CFRP sheets. These effects could be considered in the design of the RC columns wrapped CFRP sheet by using the area reduction factors ϕ_{cov1} and ϕ_{cov2} and the equations proposed in the design guidelines.

5. ANALYTICAL MODEL

5.1. GENERAL

An analytical model was proposed in this section to predict the behavior of the axially loaded circular concrete columns confined by FRP sheets. The proposed model was developed based on Mander et al. (1988)'s model for steel confined concrete and the concept of variable Poisson's ratio proposed by Fam and Rizkalla (2001). The performance of the proposed model was validated through the comparison with the experimental results available in the literatures and the test results of the small-scale RC column tests in this study.

5.2. ELASTIC BEHAVIOR OF CONCRETE CONFINED BY FRP SHEET

It is impossible to analyze the entire behavior of concrete confined by FRP sheets up to failure by the elastic theory because of its plastic behavior beyond elastic limit. However, it could provide a basic concept for developing an analytical model.

The cylindrical coordinates system in Figure 5.1 is adapted to describe the stress-strain relationship of concrete confined by FRP sheets. The following assumptions were also made:

- (1) Concrete is isotropic and homogeneous.
- (2) There are perfect bond between concrete surface and FRP sheet.
- (3) Load is applied only to the ends of concrete.
- (4) Tri-axial stress status in FRP sheet is not considered.

This is a case that an axial load is applied to the end of the concrete member confined by FRP sheets. As shown in Figure 5.1, concrete would be subjected to the tri-axial stress condition due to the existence of the lateral pressure in radial direction developed by the FRP composite sheet when the load is applied. The strain of concrete, ε_a , and corresponding stress, f_a , in z-direction can be expressed by Equations (5-1) and (5-2), respectively, by the generalized Hooke's Law:

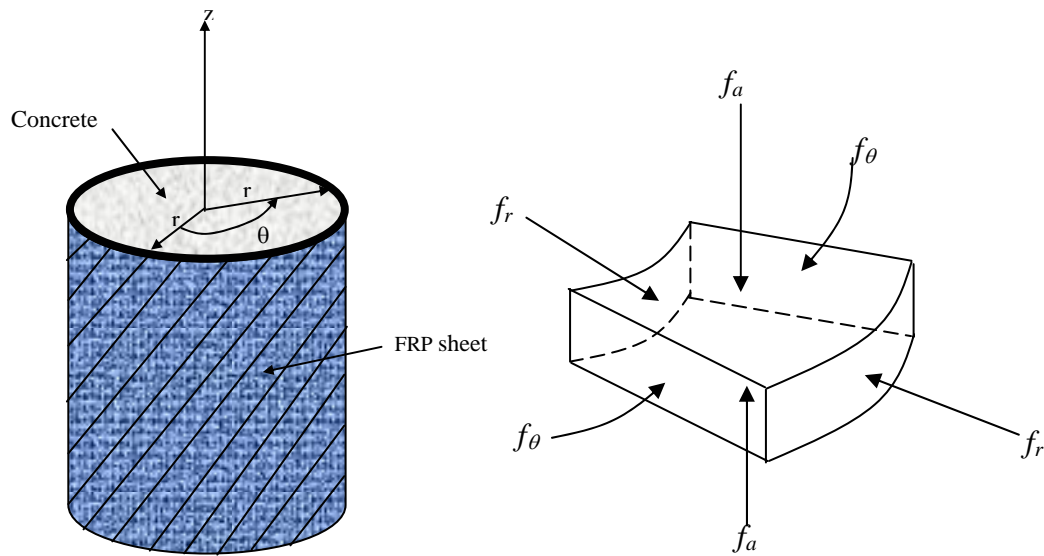


Figure 5.1. Coordinate System of Concrete Cylinder Confined by FRP Sheet along with Stress and Strain Components

$$\varepsilon_a = \frac{1}{E_c} [f_a - \nu_c (f_\theta + f_r)] \quad (5-1)$$

$$f_a = \frac{E_c}{(1 + \nu_c)(1 - 2\nu_c)} [(1 - \nu_c)\varepsilon_a + \nu_c(\varepsilon_\theta + \varepsilon_r)] \quad (5-2)$$

where, ε_a is strain in z-direction, ε_θ is strain in θ -direction, ε_r is strain in r-direction, f_a is stress in z-direction, f_θ is stress in θ -direction, f_r is stress in r-direction, E_c is elastic modulus of concrete, and ν_c is Poisson's ratio of concrete.

In this case, the hoop stress, f_θ , and radial stress, f_r , are the same and the corresponding hoop strain, ε_θ , and radial strain, ε_r , are the same. Thus, Equations (5-1) and (5-2) can be re-written in Equations (5-3) and (5-4) as:

$$\varepsilon_a = \frac{1}{E_c} (f_a - \nu_c 2f_r) \quad (5-3)$$

$$f_a = \frac{E_c}{(1+\nu_c)(1-2\nu_c)} [(1-\nu_c)\varepsilon_a + 2\nu_c\varepsilon_r] \quad (5-4)$$

The radial stress f_r in Equation (5-3) can be determined by the equilibrium of the forces as shown in Figure 5.2, resulting in Equations (5-5) to (5-7) as:

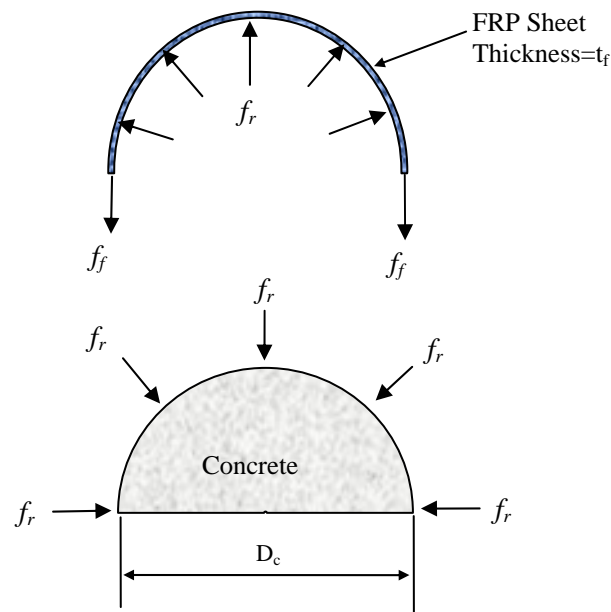


Figure 5.2. Equilibrium of Forces in Concrete Cylinder Wrapped with FRP Jacket

$$f_r = \frac{2t_f}{D_c} f_f = \frac{2t_f}{D_c} E_f \varepsilon_f = E_j \varepsilon_f = E_j \varepsilon_r \quad (5-5)$$

$$E_j = \frac{2t_f}{D_c} E_f \quad (5-6)$$

$$f_r = -E_j \varepsilon_r \quad (5-7)$$

where, f_r is radial stress of FRP sheet, t_f is thickness of FRP sheet, D_c is diameter of concrete cylinder, f_f is hoop stress of FRP sheet, ε_f is hoop strain of FRP sheet, E_f is elastic modulus of FRP sheet, and E_j is confining modulus of the concrete confined by FRP sheet. In Equation (5-5), the hoop strain of FRP composite jacket, ε_f , equals to the radial strain, ε_r ($=\varepsilon_\theta$), based on the assumption of perfect bond between the concrete surface and FRP composite jacket. Thus, the radial stress, f_r , applied to concrete is expressed as a function of confinement modulus, E_j , and radial strain, ε_r , as in Equation (5-7).

Substituting Equations (5-4) and (5-7) into Equation (5-3) and expressing in terms of the radial strain, ε_r , yields Equation (5-8), which correlate the radial strain, ε_r , with the axial strain, ε_a , as:

$$\varepsilon_r = -\frac{E_c}{E_c + E_j(1 + \nu_c)(1 - 2\nu_c)} \nu_c \varepsilon_a \quad (5-8)$$

Substituting Equations (5-7), and (5-8) into Equation (5-3) leads the following formula as shown in Equation (5-9), which can be used to predict the axial stress, f_a , of concrete confined by FRP sheet at a given axial strain, ε_a as follow:

$$f_a = \left[1 + \frac{2\nu_c^2 E_j}{E_c + E_j(1 + \nu_c)(1 - 2\nu_c)} \right] E_c \varepsilon_a \quad (5-9)$$

From the observation of Equation (5-9), it was found that with much smaller value of E_j than that of E_c in the elastic limit, the value of the fractions in the bracket would be almost zero. It implies that FRP composite does not have much effect on the concrete cylinder under elastic limit, explaining the passive nature of the FRP composite jacket confining system. As the load increases beyond the elastic limit, the Poisson's ratio of concrete, ν_c , increases but the modulus of elasticity of concrete, E_c , decreases.

As a result, the value of the fractions in the bracket would become larger, which implies that the effect of FRP sheet on the concrete cylinder would be fully activated.

5.3. VARIABLE POISSON'S RATIO OF CONCRETE CONFINED BY FRP SHEET

The relationship between the radial strain, ε_r , and the axial strain, ε_a , was expressed in Equation (5-8) by the elastic theory. However, the Poisson's ratio, ν_c , and elastic modulus, E_c , of concrete become variables after elastic limit because of internal damage such as micro-cracking and can not be defined theoretically. Thus, the relationship between radial strain, ε_r , and axial strain, ε_a , was proposed by Fam and Rizkalla (2001) based on the experimental study of Gardner (1969), in which normal strength concrete cylinders were tested under different hydrostatic pressures. It was found from the Gardner (1969)'s study that the relationship between radial strain and axial strain followed a second-order polynomial as shown in Equation (5-10) as:

$$\varepsilon_r = A\varepsilon_a^2 + B\varepsilon_a \quad (5-10)$$

Dividing Equation (5-10) by the axial strain, ε_a , a simplified linear relationship for the variable Poisson's ratio, ν_c' , was proposed by Fam and Rizkalla (2001) as shown in Equation (5-11):

$$\nu_c' = \frac{\varepsilon_r}{\varepsilon_a} = A\varepsilon_a + B \quad (5-11)$$

Equation (5-11) was normalized with respect to the initial Poisson's ratio, ν_c , and the peak strain, ε_{cc} , of confined concrete as shown in Equation (5-12):

$$\frac{\nu_c'}{\nu_c} = C \left(\frac{\varepsilon_a}{\varepsilon_{cc}} \right) + D \quad (5-12)$$

In Equation (5-12), strain, ε_{cc} , of confined concrete can be determined by Equation (5-13) proposed by Richart et al. (1929) (referring Figure 5.3) as:

$$\varepsilon_{cc} = \varepsilon_{co} \left[1 + 5 \left(\frac{f'_{cc}}{f'_{co}} - 1 \right) \right] \quad (5-13)$$

where, ε_{co} is peak strain of unconfined concrete, ε_{cc} is peak strain of confined concrete, f'_{co} is compressive strength of unconfined concrete, and f'_{cc} is compressive strength of confined concrete.

The constant D in Equation (5-10) was determined to be 1.0 so that Poisson's ratio is equal to the initial Poisson's ratio when the axial strain is zero. The constant C and D were proposed by Fam and Rizkalla (2001) as follows based on the regression study:

$$C = 1.914 \frac{f_r}{f'_{co}} + 0.719 \quad (5-14)$$

$$D = 1.0 \quad (5-15)$$

Substituting Equation (5-13), (5-14), and (5-15) into (5-12) and simplifying in terms of v'_c yield Equation (5-16), which can be used to determine variable Poisson's ratio of confined concrete, v'_c :

$$v'_c = v_c \left(1.914 \frac{f_r}{f'_{co}} + 0.179 \right) \left(\frac{\varepsilon_a}{\varepsilon_{cc}} \right) + v_c \quad (5-16)$$

5.4. MANDER ET AL.'S MODEL FOR STEEL CONFINED CONCRETE

The model, as shown in Figure 5.3, was developed by Mander et al. (1988) to determine the axial stress vs. strain relationship of concrete confined by steel

reinforcements. The compressive strength of confined concrete, f'_{cc} , as shown in Figure 5.3 is calculated by Equation (5-17):

$$f'_{cc} = f'_{co} \left(-1.254 + 2.254 \sqrt{1 + \frac{7.94 f'_r}{f'_{co}} - 2 \frac{f'_r}{f'_{co}}} \right) \quad (5-17)$$

where, f'_{co} is compressive strength of unconfined concrete, f'_{cc} is compressive strength of confined concrete, and f'_r is ultimate confining stress provided steel reinforcements.

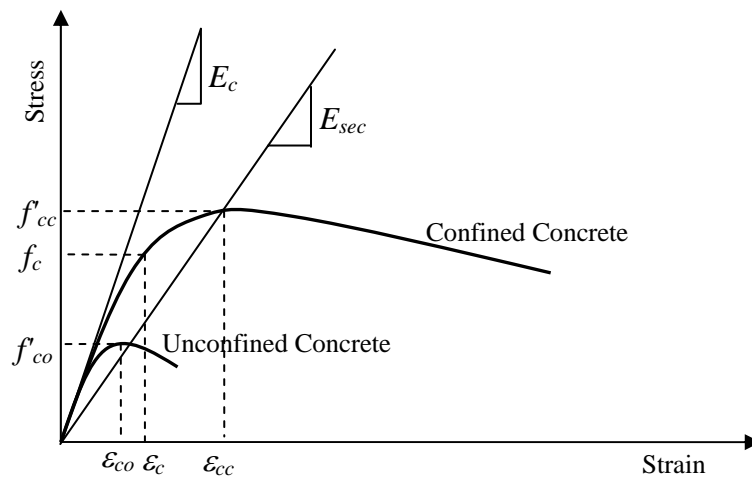


Figure 5.3. Steel Confinement Model by Mander et al. (1988)

The stress of confined concrete f_c at a given axial strain ϵ_c is determined by Equations (5-18) through (5-21):

$$f_c = \frac{f'_{cc} x r}{r - 1 + x} \quad (5-18)$$

$$x = \epsilon_c / \epsilon_{cc} \quad (5-19)$$

$$r = \frac{E_c}{E_c - E_{\text{sec}}} \quad (5-20)$$

$$\varepsilon_{cc} = \varepsilon_{co} \left[1 + 5 \left(\frac{f'_{cc}}{f'_{co}} - 1 \right) \right] \quad (5-21)$$

where, ε_{co} is peak strain of unconfined concrete, ε_{cc} is peak strain of confined concrete, and E_{sec} is secant elastic modulus of confined concrete

Since this model was based on the assumption of constant ultimate confining pressure, f'_r , Mander et al.'s model is valid only for concrete confined by steel reinforcements, which yield and show large plastic deformation after elastic limit. However, FRP composite materials behave elastically up to failure. As a result, the confining pressure provided by FRP sheet is not constant at all. Thus, it is necessary to modify Mander et al.'s model so as to fit to the concrete confined by FRP sheets. The modification of Mander et al.'s model is discussed in detail in the following section.

5.5. A STEP BY STEP APPLICATION OF MANDER ET AL.'S MODEL TO FRP CONFINED CONCRETE

Figure 5.4 shows the concept of the proposed model. As shown in Figure 5.4, the final response of this model crosses through a family of curves, which represent the response of the Mander et al.'s model under different levels of confining pressures. In order to utilize Mander et al.'s model, Equations (5-17) and (5-21) were modified into Equations (5-22) to (5-23), respectively:

$$(f'_{cc})_i = f'_{co} \left(-1.254 + 2.254 \sqrt{1 + \frac{7.94(f_r)_i}{f'_{co}}} - 2 \frac{(f_r)_i}{f'_{co}} \right) \quad (5-22)$$

$$(\varepsilon_{cc})_i = \varepsilon_{co} \left[1 + 5 \left(\frac{(f'_{cc})_i}{f'_{co}} - 1 \right) \right] \quad (5-23)$$

where, $(f_r)_i$ is confining pressure provided by FRP sheet at strain $(\varepsilon_c)_i$, $(f'_{cc})_i$ is compressive strength of FRP confined concrete at a confining pressure $(f_r)_i$, and $(\varepsilon_{cc})_i$ is

peak strain of FRP confined concrete at a given $(f'_{cc})_i$ and $(f_r)_i$.

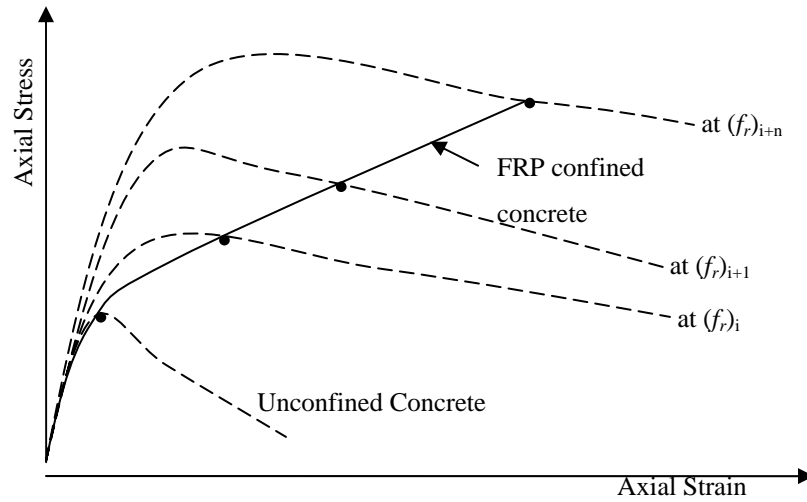


Figure 5.4. Proposed Axial Stress-Strain Response Model

In Equation (5-22), confining pressure, $(f_r)_i$, can be determined using the variable Poisson's ratio as shown in Equations (5-24) through (5-26).

$$(\nu'_c)_i = \nu_c \left(1.914 \frac{(f_r)_{i-1}}{f'_{co}} + 0.719 \right) \left(\frac{(\varepsilon_c)_i}{(\varepsilon_{cc})_{i-1}} \right) + \nu_c \quad (5-24)$$

$$(\varepsilon_r)_i = (\nu'_c)_i (\varepsilon_c)_i \quad (5-25)$$

$$(f_r)_i = -E_j (\varepsilon_r)_i \quad (5-26)$$

A flow chart of a step-by-step application of this model is presented in Figure 5.5. As shown in the flow chart, the calculations are completed when the calculated radial strain, ε_r , reaches the design ultimate tensile strain of FRP sheets, ε_{fu}^* .

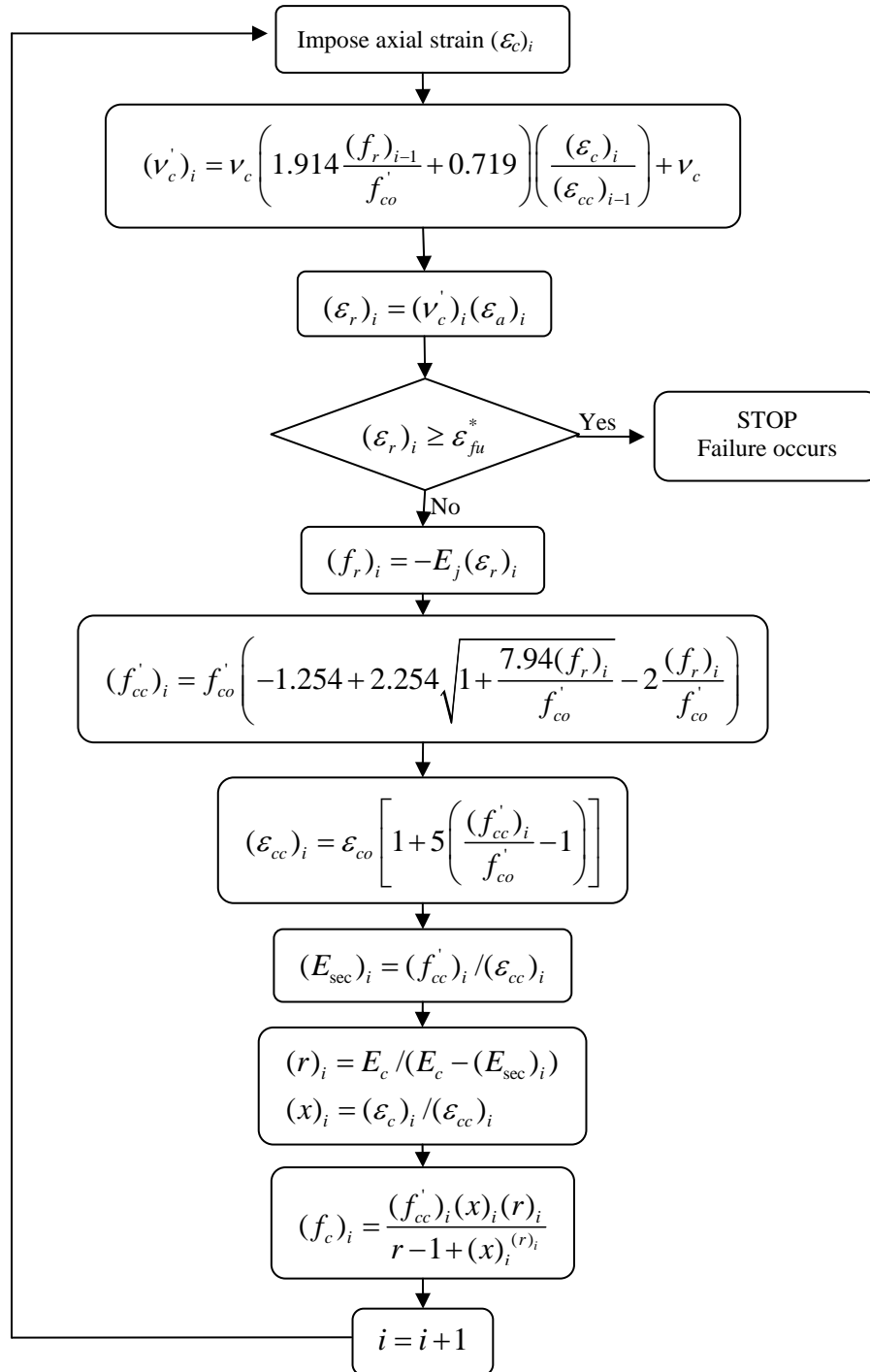


Figure 5.5. Flow Chart for the Proposed FRP Confined Model

5.6. COMPARISON OF THE PREDICTIONS BY THE PROPOSED ANALYTICAL MODEL WITH EXPERIMENTAL RESULTS

5.6.1. Small-Scale RC Columns in this Study. The test results of control columns S-C1-CONT and S-G1-CONT of small-scale RC column tests in this study were compared to the predictions by the proposed analytical model. The mechanical properties of the columns are presented in Table 5.1. In Table 5.1, the compressive strength, f'_{co} , is the average of the compressive test results of standard cylinders ($\phi 6 \times 12$ in.) and the initial tangent modulus was calculated using the Equation (5-27) proposed by ACI 318-02.

$$E_c = 57,000\sqrt{f'_{co}} \text{ (psi)} \quad (5-27)$$

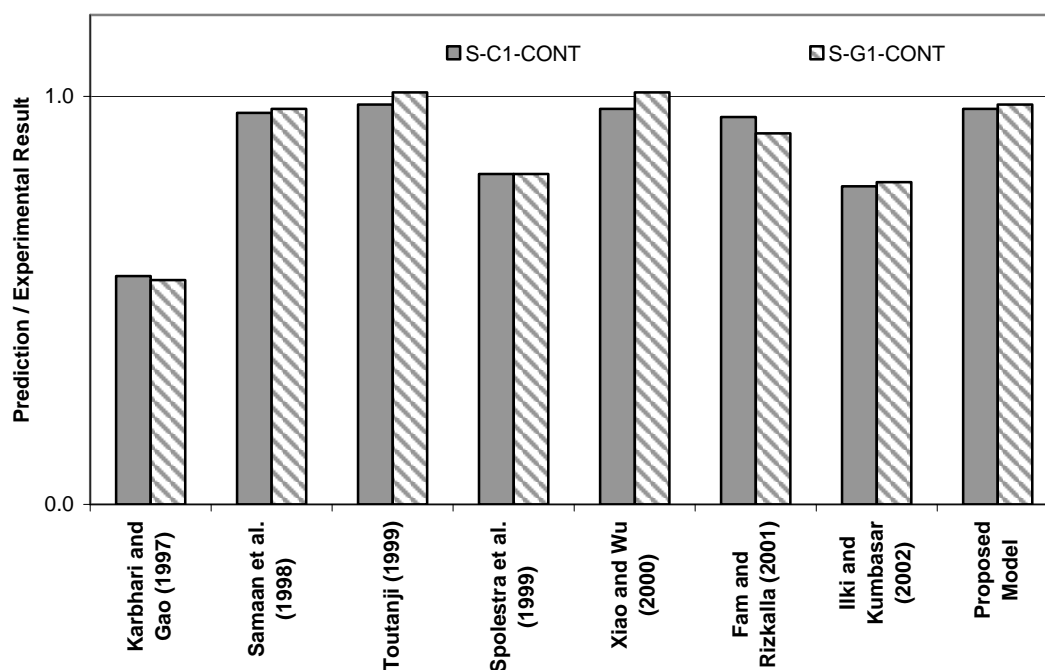
Table 5.1. Mechanical Properties of Small-Scale RC Columns

	Confining Modulus E_j (ksi)	Compressive Strength of Unconfined Concrete f'_{co} (ksi)	Initial Tangent Modulus E_c (ksi)	Initial Poisson's Ratio ν_c
S-C1-CONT	71.5	1.8	2401	0.18
S-G1-CONT	48.7	1.8	2401	0.18

The experimentally obtained compressive strength, $f'_{cc,exp}$, and predictions, $f'_{cc,pre}$, by analytical models proposed by other researches and this study are compared in Table 5.2 and Figure 5.6. In addition, the axial stress vs. strain curves obtained from the experiment and the analytical model proposed in this study are presented in Figures 5.7 and 5.8. As seen in Table 5.2 and Figures 5.6 through 5.8, the proposed model could predict the axial stress-strain response and the compressive strength very well within an error range of 3 %.

Table 5.2. Comparison of the Compressive Strength between Experimental Results and Predictions by Analytical Models

	S-C1-CONT		S-G1-CONT	
	$f'_{cc,pre}$ (ksi)	$f'_{cc,exp} / f'_{cc,pre}$	$f'_{cc,pre}$ (ksi)	$f'_{cc,exp} / f'_{cc,pre}$
Experimental result ($f'_{cc,exp}$)	4.205	1.00	4.433	1.00
Karbhari and Gao (1997)	2.371	0.56	2.459	0.55
Samaan et al. (1998)	4.046	0.96	4.314	0.97
Toutanji (1999b)	4.129	0.98	4.469	1.01
Spolestra et al. (1999)	3.411	0.81	3.569	0.81
Xiao and Wu (2000)	4.080	0.97	4.466	1.01
Fam and Rizkalla (2001)	4.002	0.95	4.041	0.91
Ilki and Kumbasar (2002)	3.288	0.78	3.511	0.79
Present Study	4.110	0.97	4.340	0.98

Figure 5.6. Comparison of Compressive Strength, f'_{cc} , between Experimental Results and Predictions by Analytical Models

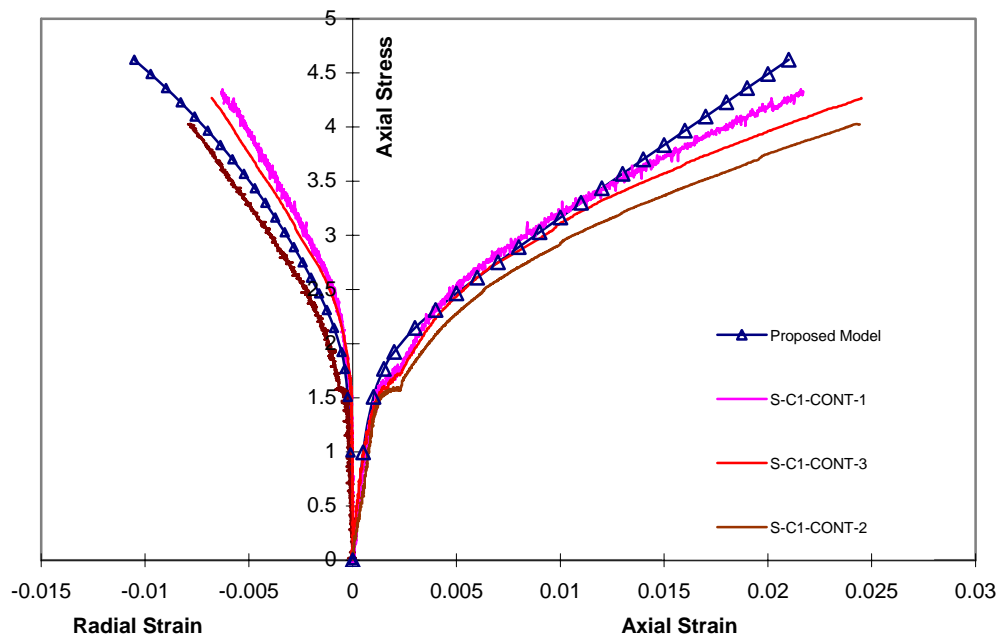


Figure 5.7. Comparison of Axial Stress vs. Strain Curve of Column S-C1-CONT Obtained from Experiments and the Proposed Analytical Model

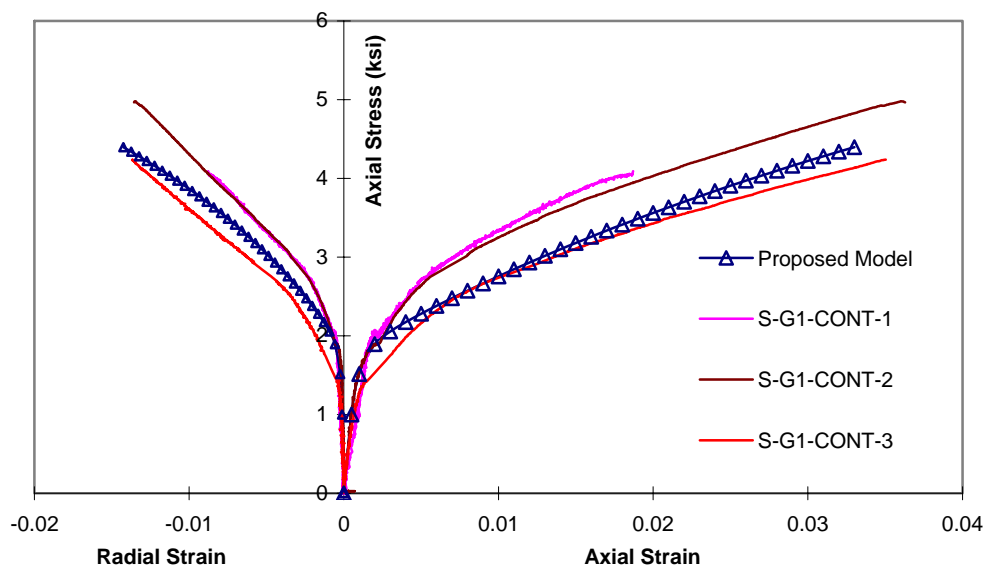


Figure 5.8. Comparison of Axial Stress vs. Strain Curve of Column S-G1-CONT Obtained from Experiments and the Proposed Analytical Model

5.6.2. Xiao and Wu (2000). Xiao and Wu (2000) tested 36 concrete cylinders with a diameter of 6 in. and a height of 12 in., confined by CFRP sheets with three different layers. The specimens were fabricated using three different strength of concrete (4.9 ksi, 6.4 ksi, and 8.0 ksi). CFRP sheets were applied using the wet-lay up technique, which was also used in this study. Some of the test results were compared to the values predicted by the proposed analytical model in Table 5.3. In Table 5.3, specimens LC, MC and HC were made of low, medium, high strength concrete, respectively. The specimens 1L, 2L and 3L were wrapped with 1-ply, 2-ply, and 3-ply CFRP sheet.

Table 5.3. Comparison of Experimental Results of Xiao and Wu (2000) and Predictions by the Proposed Analytical Model

Specimen	$\epsilon_{cc,exp}$	$f'_{cc,exp}$ (ksi)	$\epsilon_{cc,pre}$	$f'_{cc,pre}$ (ksi)	$f'_{cc,pre}/f'_{cc,exp}$	$\epsilon_{cc,pre}/\epsilon_{cc,exp}$
LC1L	0.0140	7.252	0.0174	8.105	1.12	1.24
LC2L	0.0250	10.153	0.0187	10.800	1.06	0.75
LC3L	0.0275	12.618	0.0177	12.164	0.96	0.64
MC2L	0.0150	12.183	0.0200	13.164	1.08	1.33
MC3L	0.0180	13.489	0.0175	14.264	1.06	0.97
HC2L	0.0115	11.168	0.0100	11.367	1.02	0.87
HC3L	0.0145	15.229	0.0172	16.316	1.07	1.19
Average					1.05	1.00
S.D.					0.05	0.24
COV					5 %	24 %

The predicted compressive strength, $f'_{cc,pre}$, in the Table 5.3 was determined using the radial failure strain measured in the test. As shown in Table 5.3, the proposed model predicted the strength accurately with an average ratio, $f'_{cc,pre}/f'_{cc,exp}$, of 1.05 and a COV of 5 %. Meanwhile, the prediction of ultimate axial strain is not as accurate as that of compressive strength, but relatively in good agreement with the experimental results

except for specimen LC3L and MC2L. The average ratio $\varepsilon_{cc,pre} / \varepsilon_{cc,exp}$ was 1.0, but the COV was 24 %.

5.6.3. Toutanji (1999b). A total of 18 cylindrical specimens were tested in a study by Toutanji (1999b). The diameter and height of the specimens were 3 in. and 12 in., respectively. Two types of FRP sheets were used to confine the specimens (GFRP and CFRP) and normal strength of concrete was used (4.4 ksi). Two layers of FRP sheets were applied to the specimen using the wet-lay up technique. Their experimental results are presented in Table 5.4 and compared to the predicted values. In Table 5.4, specimen C1 and C5 were strengthened with CFRP sheet while GE was strengthened with GFRP sheet. The predicted compressive strength, $f'_{cc,pre}$, as shown in Table 5.4 was determined using the radial failure strain measured in the test. As shown in Table 5.4, the proposed model accurately predicted the compressive strength of FRP confined concrete. In addition, the prediction of the ultimate axial strain was relatively accurate except for specimen GE.

Table 5.4. Comparison of Experimental Results of Toutanji (2000) and Predictions by the Proposed Analytical Model

Specimen	$\varepsilon_{cc,exp}$	$f'_{cc,exp}$ (ksi)	$\varepsilon_{cc,pre}$	$f'_{cc,pre}$ (ksi)	$f'_{cc,pre}/f'_{cc,exp}$	$\varepsilon_{cc,pre}/\varepsilon_{cc,exp}$
GE	0.0153	8.821	0.0266	8.958	1.02	1.74
C1	0.0245	13.781	0.0232	13.077	0.95	0.95
C5	0.0155	13.635	0.0140	12.825	0.94	0.90
Average					0.97	1.20
S.D.					0.04	0.38
COV					4 %	32 %

5.6.4. Ilki and Kumbasar (2002). Twenty-seven standard cylinders ($\phi 6 \times 12$ in.) were tested in a study by Ilki and Kumbasar (2002). The specimens were made of normal strength concrete (4.6 ksi) and were confined with three different layers of CFRP sheet (1-ply, 3-ply and 5-ply) using the wet-lay up technique.

Some of the test results were compared to the predicted values in Table 5.5. In Table 5.5, specimen 3-14-S and 3-15-S were confined by 1-ply CFRP sheet and 3-ply CFRP sheet, respectively while 3-17-S and 3-18-S were confined by 5-ply CFRP sheet. The predicted compressive strength, $f'_{cc,pre}$, as shown in Table 5.5 were determined using the radial failure strain measured in the test. As shown in Table 5.5, the proposed model accurately predicted the compressive strength. However, the predicted ultimate axial strains, $\epsilon_{cc,pre}$, were not close to the experimental results, $\epsilon_{cc,exp}$, except for specimen 3-14-S.

Table 5.5. Comparison of Experimental Results of Ilki and Kumbasar (2002) and Predictions by the Proposed Analytical Model

Specimen	$\epsilon_{cc,exp}$	$f'_{cc,exp}$ (ksi)	$\epsilon_{cc,pre}$	$f'_{cc,pre}$ (ksi)	$f'_{cc,pre}/f'_{cc,exp}$	$\epsilon_{cc,pre}/\epsilon_{cc,exp}$
3-14-S	0.0144	6.846	0.0159	7.451	1.09	1.10
3-15-S	0.0343	12.154	0.0208	12.768	1.05	0.61
3-17-S	0.0496	15.534	0.0201	15.074	0.97	0.41
3-18-S	0.0432	15.621	0.0201	15.074	0.97	0.47
Average					1.02	0.65
S.D.					0.05	0.27
COV					5 %	42 %

5.6.5. Samaan et al. (1998). Samaan et al. (1998) tested 30 concrete-filled FRP tubes. The inside diameter of the tube was 6 in. and the height was 12 in.. The tubes were made of polyester resin with unidirectional E-glass fibers at $\pm 75^\circ$ winding angle. The thickness of the tubes was 0.0568 in. for specimen DA11, 0.0868 in. for specimen DA21, and 0.1168 in. for DA31, respectively. The concrete used to make the specimens had a compressive strength of 4.5 ksi. The test results are presented in Table 5.6. The predicted compressive strength, $f'_{cc,pre}$, as shown in Table 5.6 was determined using the radial failure strain measured in the test.

Table 5.6. Comparison of Experimental Results of Samaan et al. (1998) and Predictions by the Proposed Analytical Model

Specimen	$\epsilon_{cc,exp}$	$f'_{cc,exp}$ (ksi)	$\epsilon_{cc,pre}$	$f'_{cc,pre}$ (ksi)	$f'_{cc,pre}/f'_{cc,exp}$	$\epsilon_{cc,pre}/\epsilon_{cc,exp}$
DA11	0.0306	7.783	0.0227	9.794	1.26	0.74
DA21	0.0407	10.576	0.0258	12.887	1.22	0.63
DA31	0.0435	12.433	0.0243	13.998	1.13	0.56
Average					1.20	0.64
S.D.					0.05	0.07
COV					4 %	11 %

As shown in Table 5.6, the proposed model overestimates the compressive strength; the average ratio $f'_{cc,pre} / f'_{cc,exp}$ was 1.20 and the COV was 4 %. The overestimation of the compressive strength by the proposed model might be due to two reasons. First, mechanical properties of the FRP tubes obtained by the coupon test was not close to the actual values since fiber were wound at $\pm 75^\circ$ so that bi-axial stress could be introduced in the tubes when applying the load. Second, the proposed model was developed based on the assumption of the perfect bond between the FRP composite and concrete surface. However, in case of concrete-filled tube system, the bond between the tube and concrete substrate might be lower than that of the FRP sheet wrapping system, in which FRP sheet is usually applied by the wet-lay up technique using epoxy-based resins. Thus, lower bond could cause lower confining pressure in this test.

5.6.6. Karbhari and Gao (1997). Karbhari and Gao (1997) tested concrete cylinders with two different FRP application techniques. The first set of FRP wraps were applied with unidirectional fiber sheets using the wet lay-up technique in various configurations. The test results of the first set are presented in Table 5.7. In Table 5.7, the specimen denomination tells the configuration of fibers, for example, $[0]_3$ means that three layers of FRP sheet are aligned in hoop direction (0° direction) while $[0/90/0]$ means that three layers of FRP sheet are applied in 0° , 90° and 0° directions, respectively. The second set was fabricated using the wet lay-up technique but there are resin rich layers next to concrete and on the outer surface for the purpose of environmental

protection. In addition, the fiber direction of the second set is hoop direction (0° direction) only. The test results of the second set are presented in Table 5.8. The predicted compressive strength $f'_{cc,pre}$ as shown in Tables 5.7 and 5.8 was stress at the axial failure strain measured in the test since they did not report the radial failure strain in their paper.

As shown in Table 5.7, the proposed model predicted the compressive strength of the specimens wrapped with 1 layer of CFRP sheet very accurately (in the case of [0]). However, as the number of layers increases, the accuracy decreases. In addition as fiber angle increases, the accuracy decreases. This is due to the variation of the mechanical properties of FRP composites; the difference between material properties obtained from flat coupon tests and the real values could increase as the configuration of fibers became complex.

Table 5.7. Comparison of Experimental Results 1 of Karbhari and Gao (1997) and Predictions by the Proposed Analytical Model

Specimen	$\epsilon_{cc,exp}$	$f'_{cc,exp}$ (ksi)	$f'_{cc,pre}$ (ksi)	$f'_{cc,pre}/f'_{cc,exp}$
[0]	0.0110	6.508	6.239	0.96
[0] ₂	0.0130	8.656	10.287	1.19
[0] ₃	0.0220	11.267	12.595	1.12
[0] ₄	0.0240	12.978	16.127	1.24
[0/90]	0.0080	7.002	6.029	0.86
[0/90/0]	0.0170	9.687	9.664	1.00
[+45/-45]	0.0060	6.145	3.322	0.54
[+45/-45] ₂	0.0050	5.997	4.222	0.70
[90/45/-45/0]	0.0090	7.472	6.822	0.91
Average				0.95
S.D.				0.21
COV				22 %

According to Table 5.8, the proposed model predicted relatively well the compressive strength when compared to the test results of the first set. This is due to the fact that the fibers are aligned in hoop direction only, and thus the mechanical properties obtained from the flat coupon test were more compatible to the model assumptions than those of the first set, as previously described.

Table 5.8. Comparison of Experimental Results 2 of Karbhari and Gao (1997) and Predictions by the Proposed Analytical Model

Specimen	$\epsilon_{cc,exp}$	$f'_{cc,exp}$ (ksi)	$f'_{cc,pre}$ (ksi)	$f'_{cc,pre}/f'_{cc,exp}$
A	0.0240	11.926	10.357	0.87
B	0.0130	10.237	9.256	0.90
C	0.0240	11.929	10.277	0.86
D	0.0220	11.529	9.801	0.85
Average				0.87
S.D.				0.02
COV				2 %

5.7. SUMMARY AND CONCLUSIONS

An analytical model was proposed to predict the behavior of the axially loaded circular concrete confined by FRP sheet and the performance was investigated through comparisons with several experimental studies including the test results of this study. Based on all discussions presented here, it can be concluded that the proposed analytical model can accurately predict the compressive strength, f'_{cc} , of FRP wrapped concrete with 10 % error range when the FRP sheet is applied uni-directionally. However, the proposed analytical model is not intended to predict other FRP wrapping configurations.

6. DESIGN GUIDELINES

6.1. GENERAL

The purpose of the design guidelines presented in this section is to provide designers with ways how to deal with the effects of various environmental conditions on the long-term performance of RC columns wrapped with FRP sheets. As a result, the design guidelines provide reduction factors to account for the reduction of axial compression capacity of RC columns wrapped with FRP sheets due to various environmental conditions. The reduction factors are utilized in the design equations to determine axial compression capacity of RC columns wrapped with FRP sheets, subjected to long-term environmental effects.

6.2. SCOPE AND LIMIT

The proposed design equations are based on the traditional RC column design method specified by ACI 318-02 and the design recommendations of ACI committee 440. Further information regarding the material properties, quality control, installation, and maintenance of FRP system can be found elsewhere in the above mentioned documents.

The reduction factors utilized in the proposed design guidelines were developed based on the test results of this study, in which two different types of FRP sheets, i.e., CFRP and GFRP sheets, were bonded to concrete substrate by the wet-lay up technique using epoxy based primer and saturant. Thus, the design guidelines may not be applicable to other types of FRP sheets, adhesives, or installation techniques, which were not considered in this study. In addition, the proposed design equations would not cover RC columns wrapped with FRP sheet subjected to the combined axial and bending forces unless further research verifies the flexural behavior of RC columns wrapped with FRP sheets.

6.3. DESIGN EQUATIONS

A design equation to determine the axial compression capacity of RC columns wrapped with FRP sheets under various environmental conditions was proposed in Equation (6-1). This design equation is the modification of the equation specified in ACI

318-02, which is used to compute the axial load capacity of non-prestressed members with spiral reinforcements. Thus, the load factors and strength reduction factors stated in ACI 318-02 should be used when using Equation (6-1):

$$\phi P_n = 0.85\phi \left[0.85\psi_f \phi_{env} f'_{cc} (A_g - A_{st}) + f_y A_{st} \right] \quad (6-1)$$

where, ϕ is strength reduction factor, ψ_f is strength reduction factor recommended by ACI 440 in order to account for the uncertainty of new technology (0.95), ϕ_{env} is strength reduction factor proposed by this study in order to account for the effects of various environmental conditions, f'_{cc} is compressive strength of concrete confined by FRP sheet, A_g is gross area of the cross-section of the member, A_{st} is cross-sectional area of longitudinal steel reinforcements, and f_y is yield strength of the longitudinal steel reinforcements. This equation is applicable only to the RC columns with a circular cross-section.

The modifications in Equation (6-1) when compared to the original equation in ACI 318-02 are additional strength reduction factors ψ_f , ϕ_{env} , and compressive strength of concrete confined by FRP sheet, f'_{cc} . The strength reduction factor, ψ_f , of 0.95 is recommended by ACI 440 to account for the limited knowledge of FRP systems as compared to reinforced concrete or prestressed concrete. Discussions about the strength reduction factor, ϕ_{env} , the compressive strength of concrete confined by FRP sheet, f'_{cc} , and other details are made in the following sections.

6.4. MATERIAL PROPERTIES

6.4.1. Concrete. The mechanical properties of concrete used in design of the RC columns wrapped with FRP sheets are provided herein. The mechanical properties should be determined in accordance with ACI 318-02. If necessary, for strengthening of existing RC columns, in-place compressive strength of concrete and soundness of the concrete, especially the concrete cover should be investigated to ensure the proper bond

strength between concrete substrate and FRP sheets.

f'_{co} : compressive strength of unconfined concrete

E_c : elastic modulus of concrete

ν_c : initial Poisson's ratio of concrete within elastic region

6.4.2. Steel Reinforcement. The following mechanical properties of steel reinforcements are used to design the RC columns wrapped with FRP sheets. The mechanical properties should be determined in accordance with ACI 318-02. However, it is recommended that the location and extent of corrosion of steel reinforcements be surveyed if corrosion-damaged RC columns are repaired by FRP wrapping system.

f_y : yield strength of steel reinforcements

E_s : elastic modulus of steel reinforcements

6.4.3. FRP Sheet. The mechanical properties of FRP sheet should be determined by Equations (6-2) and (6-3) to account for the differences between the mechanical properties provided by manufacturer and the actual values:

$$\varepsilon_{fu}^* = R_c \varepsilon_{fu} - (\varepsilon_r)_{corrosion} \quad (6-2)$$

$$f_{fu} = E_f \varepsilon_{fu}^* \quad (6-3)$$

where, ε_{fu}^* is design ultimate tensile strain of FRP sheets, R_c is reduction factor (0.5 for both CFRP and GFRP wrapped RC column), ε_{fu} is ultimate tensile strain provided by the manufacturer, $(\varepsilon_r)_{corrosion}$ is pre-strain induced by the corrosion of steel reinforcement, f_{fu} is design tensile strength of FRP sheet and E_f is elastic modulus of FRP sheets. The pre-strain in Equation (6-2) induced by the corrosion of steel reinforcement, $(\varepsilon_r)_{corrosion}$, is

considered only when the RC columns wrapped with FRP sheets are placed in a corrosive environment.

6.5. STRENGTH REDUCTION FACTOR, ϕ_{env}

The strength reduction factor, ϕ_{env} , in Table 6.1 should be used to reflect the effects of various environmental conditions and consequently to obtain the required reliability of the RC columns wrapped with FRP sheets under severe environmental conditions.

Table 6.1. Strength Reduction Factor, ϕ_{env}

FRP Sheet type /Adhesive types	Strength Reduction Factor $\phi_{env} = \phi_{FT}\phi_H\phi_{Na}$			Remark
	ϕ_{FT}	ϕ_H	ϕ_{Na}	
CFRP/Epoxy	1.00*	0.95	0.95	If one of the environmental conditions can be ignored, the strength reduction factor for the environmental conditions can be taken as unity
GFRP/Epoxy	1.00*	0.85	0.85	

* Reduction factor based on non-moist freeze-thaw cycles

6.6. COMPRESSIVE STRENGTH OF FRP CONFINED CONCRETE, f'_{cc}

Compressive strength of concrete, f'_{cc} , of circular RC column wrapped with FRP sheets can be computed by the analytical model proposed in Section 5. The material properties necessary for the calculation can be determined in accordance with the guidelines presented in Section 6.4.

6.7. REDUCED CROSS-SECTIONAL AREA OF STEEL REINFORCEMENTS, $(A_{st})_{cor}$, AND AREA REDUCTION FACTOR, ϕ_{cor1}

The cross-sectional area of steel reinforcement, A_{st} , in Equation (6-1) can be replaced with $(A_{st})_{cor}$ according to Equation (6-4) if RC columns wrapped with CFRP

sheet are located in a corrosive environment or corrosion-damaged RC columns are repaired by CFRP sheet wrapping in order to account for the loss of the cross-sectional area of the steel reinforcements due to corrosion process:

$$(A_{st})_{cor} = \phi_{cor1} A_{st} \quad (6-4)$$

where $(A_{st})_{cor}$ is the reduced cross-sectional area of longitudinal steel reinforcement, A_{st} is cross-sectional area of longitudinal steel reinforcement, and ϕ_{cor1} is area reduction factor for steel reinforcement.

The area reduction factor, ϕ_{cor1} , can be determined from Table 6.2. However, if there is additional information (e.g., field survey) such that engineers can determine the extent of the loss of cross-sectional area of steel reinforcements, the area reduction factor, ϕ_{cor1} , can be determined based on that information.

Table 6.2. Area Reduction Factors, ϕ_{cor1} and ϕ_{cor2}

	ϕ_{cor1}	ϕ_{cor2}	Conditions of RC Columns
CASE 1	0.75	0.95	Newly constructed RC columns with CFRP wrapping
CASE 2	0.65	0.85	Corrosion-damaged RC columns repaired by CFRP sheet wrapping
CASE 3	0.70	0.90	Newly constructed RC columns with CFRP wrapping placed where possible freeze-thaw damages are anticipated
CASE 4	0.55	0.75	Corrosion-damaged RC columns repaired by CFRP sheet wrapping placed where possible freeze-thaw damages are anticipated

6.8. EQUIVALENT AREA, A_{eqv} , AND AREA REDUCTION FACTOR, ϕ_{cor2}

The area of concrete in Equation (6-1), $(A_g - A_{st})$, can be replaced with the equivalent area, A_{eqv} , according to Equation (6-5) in case where RC columns wrapped

with CFRP sheets are placed in a corrosive environment or corrosion-damaged RC columns are repaired by CFRP sheet wrapping in order to account for the decrease in axial rigidity due to the damages of concrete such as cracking, spalling, and delamination resulting from the corrosion of steel reinforcement.

$$A_{eqv} = \phi_{cor2} [A_g - (A_{st})_{cor}] = \phi_{cor2} (A_g - \phi_{cor1} A_{st}) \quad (6-5)$$

where A_g is gross area of the cross-section of CFRP wrapped RC column, A_{st} is cross-sectional area of longitudinal steel reinforcements, $(A_{st})_{cor}$ is reduced cross-sectional area of longitudinal steel reinforcements, ϕ_{cor1} is area reduction factor for longitudinal steel reinforcements and ϕ_{cor2} is area reduction factor for area of concrete.

The area reduction factor ϕ_{cor1} and ϕ_{cor2} in Equation (6-5) can be determined from Table 6.2; however, if there is specific information (e.g., field survey) such that engineers can determine the extent of the loss of cross-sectional area of steel reinforcements, the area reduction factors, ϕ_{cor1} and ϕ_{cor2} , can be determined based on that information.

6.9. COMPARISON OF EXPERIMENTAL RESULTS AND PREDICTIONS CALCULATED BY THE PROPOSED DESIGN GUIDELINES

It should be noted that the proposed reduction factors were developed based on limited data obtained from the small-scale RC column tests of this study. Thus, in order to obtain more reliable reduction factors, not only more intensive tests for this specific purpose should be conducted, but also more extensive statistical data should be gathered. This is beyond the scope of this study. Instead, a rather simple attempt was made herein to verify the reliability of the reduction factors proposed in this study through comparative studies. In the comparative studies, predictions calculated by the proposed design guidelines are compared to experimental results of RC columns of which scale was different from the small-scale RC columns used to develop the design guidelines. For that purpose, mid-scale RC columns were used in this study. Of course, it is better to perform full-scale test to verify the performance of the proposed design guidelines.

However, it was difficult to conduct full-scale tests due to laboratory limitations. Thus, the mid-scale RC columns were fabricated and tested for this purpose. The details of mid-scale RC column test were presented in Section 3.

6.9.1. Mid-Scale RC Columns of Ambient Environmental Effect Tests. The performance assessment of the proposed model was conducted by the comparison of compressive strength, f'_{cc} , instead of failure load, P_u , since the design equation as presented in Equation (6-1) includes many reductions factors such as 0.85, ϕ and ψ_f , and therefore direct comparison for the evaluation of strength reduction factor, ϕ_{env} , could not be achieved.

6.9.1.1 Material properties of mid-scale RC columns wrapped with FRP sheets. The following material properties were used to calculate the compressive strength, f'_{cc} , of mid-scale RC columns.

6.9.1.1.1 Concrete. The compressive strength of unconfined concrete, f'_{co} , was determined based on the compressive test of standard cylinders ($\phi 6 \times 12$ in.) and initial tangent modulus of concrete was calculated by Equation (5-27) which is specified in ACI 318-02. The obtained mechanical properties of the concrete used in mid-scale RC columns for the ambient environmental tests are presented in Table 6.3.

Table 6.3. Mechanical Properties of Concrete for Mid-Scale RC Columns

	Confining Modulus E_j (ksi)	Compressive Strength of Unconfined Concrete f'_{co} (ksi)	Initial Tangent Modulus E_c (ksi)	Initial Poisson's Ratio ν_c
M-C1-CONT M-C1-F/Th M-C1-CE	53.6	4.1	3649	0.18
M-G1-CONT M-G1-F/Th M-G1-CE	36.5	4.1	3649	0.18

6.9.1.1.2 Steel reinforcements. The yield strength, f_y , of the steel reinforcements was determined as 70 ksi, based on tensile tests as described in Section 3.2.1.2, and the nominal area, A_{sr} , of 0.88 in² was used for the calculation.

6.9.1.1.3 FRP sheets. The design ultimate tensile strains, ε_{fu}^* , of CFRP and GFRP sheets were determined based on Equation (6-2). In Table 6.4, ultimate tensile strains, ε_{fu} , provided by manufacturer and rupture strains, ε_f , measured during the failure tests were presented. As shown in Table 6.4, the design ultimate tensile strain, ε_{fu}^* , of CFRP wrapped mid-scale RC columns were 57 % higher than that of the measured rupture strain, ε_f . As for GFRP wrapped mid-scale RC columns, the design ultimate tensile strain, ε_{fu}^* , were 12 % lower that of the measured rupture strain, ε_f .

Table 6.4. Radial Strains of FRP Sheet

FRP Types	Measured Rupture Strains ε_f	Ultimate Tensile Strains Provided by Manufacturer ε_{fu}	Design Ultimate Tensile Strains $\varepsilon_{fu}^* = R_c \varepsilon_{fu} = 0.5 \varepsilon_{fu}$	$\varepsilon_{fu}^* / \varepsilon_f$
CFRP	0.00542	0.017	0.0085	1.57
GFRP	0.0119	0.021	0.0105	0.88

6.9.1.2 Compressive strength, f'_{cc} , of the mid-scale RC columns. As a first step to determine the compressive strength of the mid-scale RC columns conditioned under the various environmental conditions, the compressive strength of the control columns, i.e., the mid-scale RC columns kept at room temperature (M-C1-CONT and M-G1-CONT) was calculated. Then, strength reduction factor, ϕ_{env} , was multiplied by the compressive strength of concrete of the control columns in order to consider the effects of the environmental conditions; this was done in the following section.

Using the material properties presented in the previous sections, the compressive strengths, f'_{cc} , of concrete of the control columns were calculated using the analytical

model proposed in Section 5. Then, the calculated compressive strengths were compared to the experimental results in Table 6.5. In Table 6.5, the experimental results were calculated by Equation (6-4) as:

$$f'_{cc} = \frac{P_u - f_s A_{st}}{A_g - A_{st}} \quad (6-4)$$

where P_u is failure load of the mid-scale RC columns, measured during the tests, f_s is stress of longitudinal steel reinforcement determined based on bi-linear stress-strain model as detailed in Section 3.2.1.2, A_g is gross cross-sectional area of mid-scale RC column, and A_{st} is cross-sectional area of steel reinforcement.

Table 6.5. Compressive Strengths of Concrete Confined by FRP Sheets of Mid-Scale RC Columns

	M-C1-CONT		M-G1-CONT	
	f'_{cc} (ksi)	Ratio	f'_{cc} (ksi)	Ratio
Experimental Results	5.709		6.119	
Prediction 1	5.510	0.97	5.819	0.95
Prediction 2	6.244	1.10	5.599	0.92

Predictions 1 and 2 in Table 6.5 were calculated using the proposed analytical model as detailed in Section 5.6. The difference between predictions 1 and 2 was the design ultimate strains, ε_{fu}^* , of FRP sheets when calculating compressive strength, f'_{cc} . Prediction 1 used the measured rupture strains, ε_f , (see Table 6.4) as the design ultimate strain, ε_{fu}^* , while Prediction 2 was calculated using the design ultimate tensile strains, ε_{fu}^* , calculated by Equation (6-2). As a result, Prediction 2 was slightly higher than Prediction

1 in case of M-C1-CONT; while Prediction 2 was slightly lower than that of Prediction 1 in case of M-G1-CONT. However, since the differences between the two cases were not significant, it can be concluded that the design ultimate tensile strain, ε_{fu}^* , of FRP sheets determined by Equation (6-2) can be used to calculate the compressive strength, f'_{cc} . In addition, Predictions 2 were reasonably in good agreement with the experimental results; in case of M-C1-CONT; the ratio of Prediction 2 to the experimental results was 1.10, while it was 0.92 in case of M-G1-CONT, as shown in Table 5.6. Thus, it was also concluded that the analytical model is accurate enough to be used for the prediction of the compressive strength of the concrete of RC columns wrapped with FRP sheets.

6.9.1.3 Performance of strength reduction factor, ϕ_{env} . In table 6.6, strength reduction factor, ϕ_{env} , for all mid-scale RC columns was determined according to values of Table 6.1. For the control columns (M-C1-CONT and M-G1-CONT), ϕ_{env} is unity since there was no environmental conditioning. For freeze-thaw conditioned columns (M-C1-F/Th and M-G1-F/Th), ϕ_{env} is also unity since ϕ_{FT} is 1.0 for freeze-thaw cycles. For the columns conditioned under combined environmental cycles (M-C1-CE and M-G1-CE), ϕ_{FT} was taken as 1.0 and ϕ_H was taken as 0.95 for CFRP and 0.85 for GFRP wrapped column. For ϕ_{Na} , 1.0 was used for all the mid-scale RC columns since saline solution was not used during the environmental conditioning.

Using the strength reduction factor, ϕ_{env} , presented in Table 6.6, the compressive strength, $\phi_{env}f'_{cc}$, of the columns conditioned under environmental cycles were calculated and were compared to the experimental results, $f'_{cc,exp}$, in Table 6.7.

As shown in Table 6.7, the predictions calculated by the proposed design guidelines are in good agreement with the experimental results; the average ratio, $\phi_{env}f'_{cc,pre} / f'_{cc,exp}$, was 0.99 and the COV was 9 %. The 9 % COV may be because of differences of mechanical properties used in calculation of compressive strength, f'_{cc} , by the proposed analytical model. Particularly, the design ultimate tensile strain, ε_{fu}^* , is the primary reason as described in section 6.9.1.3. In addition, another reason is the scale effect. The effect of freeze-thaw cycles on mid-scale RC columns was not as significant

as small-scale RC columns due to the relatively smaller confining modulus of mid-scale RC columns when compared to small-scale RC columns. Consequently, the strength reduction factor developed based on small-scale RC column test was conservative in case of mid-scale RC column test.

Table 6.6. Strength Reduction Factors, ϕ_{env} , for Mid-Scale RC Columns Exposed to Environmental Cycles

Specimens	ψ_f	$\phi_{env} = \phi_{FT}\phi_H\phi_{Na}$				$\psi_f\phi_{env}$
		ϕ_{FT}	ϕ_H	ϕ_{Na}	ϕ_{env}	
M-C1-CONT	0.95	1.00	1.00	1.00	1.00	0.95
M-C1-F/Th	0.95	1.00	1.00	1.00	1.00	0.95
M-C1-CE	0.95	1.00	0.95	1.00	0.95	0.90
M-G1-CONT	0.95	1.00	1.00	1.00	1.00	0.95
M-G1-F/Th	0.95	1.00	1.00	1.00	1.00	0.95
M-G1-CE	0.95	1.00	0.85	1.00	0.85	0.81

Table 6.7. Comparison of Compressive Strengths between Experimental Results and Predictions by the Proposed Design Guidelines

	Compressive Strength		Ratio $\phi_{env}f'_{cc,pre} / f'_{cc,exp}$
	Experimental Results $f'_{cc,exp}$ (ksi)	Predictions $\phi_{env}f'_{cc,pre}$ (ksi)	
M-C1-CONT	5.709	6.244	1.10
M-C1-F/Th	5.744	6.244	1.09
M-C1-CE	5.832	5.932	1.02
M-G1-CONT	6.119	5.599	0.92
M-G1-F/Th	6.015	5.599	0.93
M-G1-CE	5.477	4.759	0.87
Average			0.99
S.D.			0.09
COV			9 %

6.9.2. Mid-Scale RC Columns of Corrosion Tests. In this section, the nominal axial capacity, P_n , of the mid-scale RC columns used for corrosion tests are calculated using the proposed design guidelines and the predictions are compared to the experimental results.

6.9.2.1 Material properties of mid-scale RC columns wrapped with CFRP sheets. The following material properties were used to calculate the compressive strength, f'_{cc} , of mid-scale RC columns.

6.9.2.1.1 Concrete. The compressive strength of unconfined concrete, f'_{co} , was determined based on the compressive test of standard cylinders ($\phi 6 \times 12$ in.) and initial tangent modulus of concrete was calculated by Equation (5-27), which is specified in ACI 318-02. The results are presented in Table 6.8.

Table 6.8. Mechanical Properties of Concrete for Mid-Scale RC Columns

Confining Modulus E_j (ksi)	Compressive Strength of Unconfined Concrete f'_{co} (ksi)	Initial Tangent Modulus E_c (ksi)	Initial Poisson's Ratio ν_c
53.6	4.9	3992	0.18

6.9.2.1.2 Steel reinforcement. The yield strength, f_y , was determined as 70 ksi, based on the results of the tensile tests as described in Section 3.2.1.2 and the nominal area, A_{st} , of 0.88 in^2 . was used for the calculation.

6.9.2.1.3 Aluminum pipe. For the aluminum pipe used as an internal cathode during the accelerated corrosion process, yield strength, $f_{y,alm}$, was determined as 40 ksi, based on tensile tests as described in Section 3.3.2.2. The cross-sectional area, A_{alm} , of the aluminum pipe was calculated based on the measured dimensions and taken as 0.47 in^2 .

6.9.2.1.4 FRP sheets. The design ultimate tensile strains, ϵ_{fu}^* , of CFRP sheets were determined based on Equation (6-2) and the results are presented in Table 6.9. In

Table 6.9, $(\varepsilon_r)_{corrosion}$ is the strain measured at the end of the accelerated corrosion process.

Table 6.9. Design Ultimate Tensile Strain of CFRP Sheet

Specimen	ε_{fu}	$(\varepsilon_r)_{corrosion}$	$\varepsilon_{fu}^* = R_c \varepsilon_{fu} - (\varepsilon_r)_{corrosion}$
M-CFRP-COR	0.017	0.0027	0.0058
M-COR-CFRP	0.017	-	0.0085
M-COR-CFRP-COR	0.017	0.000262	0.0082

6.9.2.2 Compressive strength, f'_{cc} , of mid-scale RC columns. The compressive strength, f'_{cc} , of mid-scale RC columns wrapped with CFRP sheet were calculated by the analytical model proposed in Section 5, and the results are presented in Table 6.10. The difference of the compressive strength, f'_{cc} , between the columns, as shown in Table 6.10, was due to the difference of the design ultimate strains, ε_{fu}^* , of the columns, as shown in Table 6.9.

Table 6.10. Compressive Strength, f'_{cc} , of Mid-Scale RC Columns Wrapped with CFRP Sheet Calculated by the Proposed Analytical Model

Specimen	f'_{cc} (ksi)
M-CFRP-COR	5.490
M-COR-CFRP	6.179
M-COR-CFRP-COR	6.087

6.9.2.3 Area reduction factors ϕ_{cor1} and ϕ_{cor2} . The area reduction factors, ϕ_{cor1} and ϕ_{cor2} used for the mid-scale RC columns are presented in Table 6.11. The area

reduction factor, ϕ_{cor1} , was taken as 1.0 since there was just 0.6 to 1.5 % of steel loss monitored at the end of the accelerated corrosion process as discussed in Section 4.

The area reduction factor, ϕ_{cor2} , was determined according to Table 6.2. Since Column M-CFRP-COR was wrapped with CFRP sheets before the beginning of the accelerated corrosion process and conditioned by 300 freeze-thaw cycles, it was corresponding to Case 3 in Table 6.2 (newly constructed RC columns with CFRP wrapping placed where possible freeze-thaw damages are anticipated). Column M-COR-CFRP was corrosion-damaged at the first stage of the accelerated corrosion process and was repaired by CFRP sheet wrapping. After CFRP sheet wrapping, Column M-COR-CFRP was not re-conditioned by the accelerated corrosion process. Only 300 freeze-thaw cycles were applied to Column M-COR-CFRP after CFRP sheet wrapping. Thus, Column M-COR-CFRP was corresponding to Case 4 in Table 6.2 (Corrosion-damaged RC columns repaired by CFRP sheet wrapping placed where possible freeze-thaw damages are anticipated). Column M-COR-CFRP-COR was conditioned in similar way as Column M-COR-CFRP was. However, after CFRP sheet wrapping and 300 freeze-thaw cycles, Column M-COR-CFRP-COR was re-conditioned by the accelerated corrosion process. Thus, Column M-COR-CFRP-COR was corresponding to Case 4 in Table 6.2 (Corrosion-damaged RC columns repaired by CFRP sheet wrapping placed where possible freeze-thaw damages are anticipated).

Table 6.11. Area Reduction Factors, ϕ_{cor1} and ϕ_{cor2} used for Mid-Scale RC Columns

Specimen	ϕ_{cor1}	ϕ_{cor2}
M-CFRP-COR	1.0	0.90
M-COR-CFRP	1.0	0.75
M-COR-CFRP-COR	1.0	0.75

6.9.2.4 Reduced cross-sectional area of steel reinforcement, $(A_{st})_{cor}$, and equivalent area, A_{eqv} . The reduced cross-sectional area of steel reinforcements, $(A_{st})_{cor}$, was calculated using Equations (6-4) and the equivalent area, A_{eqv} , was calculated using

Equation (6-6) as shown below, instead of using Equation (6-5), in order to subtract the cross-sectional area of aluminum pipe, $(A_{alm})_{out}$, that was calculated by the outside diameter of the aluminum pipe.

$$A_{eqv} = \phi_{cor2}(A_g - (A_{st})_{cor} - (A_{alm})_{out}) = \phi_{cor2}(A_g - \phi_{cor1}A_{st} - (A_{alm})_{out}) \quad (6-6)$$

6.9.2.5 Axial compressive capacity P_n . The axial compressive capacity P_n was calculated using Equation (6-7) instead of Equation (6-1), proposed in the design guidelines, in order to account for the existence of the aluminum pipe used as an internal cathode:

$$P_n = f_{cc}'A_{eqv} + f_y(A_{st})_{cor} + f_{y,alm}A_{alm} \quad (6-7)$$

Table 6.12. Reduced Cross-Sectional Area of Steel Reinforcement, $(A_{st})_{cor}$, and Equivalent Area, A_{eqv}

Specimen	$(A_{st})_{cor}$ (in ²)	A_{eqv} (in ²)
M-CFRP-COR	0.88	49.061
M-COR-CFRP	0.88	36.024
M-COR-CFRP-COR	0.88	36.024

In addition, strength reduction factors such as ϕ , ψ_f , and ϕ_{env} were excluded in the calculation since the purpose of this work is to access the performance of the area reduction factors ϕ_{cor1} and ϕ_{cor2} .

The calculated axial compressive capacity, P_n , are presented in Table 6.13 and compared to the failure load, P_u , obtained from tests. According to Table 6.13, the axial compressive capacity, P_n , of Columns M-CFRP-COR and M-COR-CFRP are about 80 %

of the failure load, P_u , obtained from the tests. This is probably because the area reduction factor, ϕ_{cor2} , used in the calculation was too large to assess the decrease in the axial rigidity in the elastic region, $(EA)_1$. Now, let us consider the ratio of the area of core concrete inside the spiral reinforcement to the gross area of the column. For small-scale RC columns used to develop the area reduction factor, ϕ_{cor2} , the ratio is 0.51 while it is 0.66 for mid-scale RC columns. Thus, the decrease rate of the axial rigidity in the elastic region, $(EA)_1$, of the mid-scale RC columns might be smaller than that of the small-scale RC columns. Other possible reasons for the difference between the calculated axial compressive capacity, P_n , and the failure load, P_u , might be resulting from the underestimation of the compressive strength of concrete, f'_{cc} , and the difference of material properties.

Table 6.13. Comparisons of Failure Load, P_u and Predictions by the Proposed Design Guidelines, P_n

Specimen	P_n (kips)	P_u (kips)	P_n / P_u (kips)
M-CFRP-COR	350	433	0.81
M-COR-CFRP	303	379	0.80
M-COR-CFRP-COR	300	211	1.42

For Column M-COR-CFRP-COR, the calculated axial compressive capacity, P_n , was 1.42 times higher than the failure load, P_u , obtained from the tests unlike the cases of Columns M-CFRP-COR and M-COR-CFRP. It is definitely because Column M-COR-CFRP-COR failed by lap splice debonding. As a result, the confinement effect provided by CFRP sheet wrapping was not fully activated.

6.10. SUMMARY AND CONCLUSIONS

This section proposed design guidelines for RC columns wrapped with FRP sheets and the performance of the proposed design guidelines were evaluated through the comparative study with mid-scale RC column tests. Summary and concluding remarks drawn from this section are as follows.

1. In order to account for the effects of various environmental conditions in the design, strength reduction factor, ϕ_{env} , as well as design equations to compute the axial compressive capacity of RC columns wrapped with FRP sheets were proposed. The strength reduction factor, ϕ_{env} , consisted of three sub-factors, ϕ_{FT} , ϕ_H and ϕ_{Na} , each of which was used to account for freeze-thaw cycles, high-temperature cycles with UV radiation and high-humidity cycles, and saline solution effect, respectively.
2. The concepts of reduced area of steel reinforcement, $(A_{st})_{cor}$, and equivalent area of concrete, A_{eqv} , were introduced in order to account for the effects of corrosion of steel reinforcement. The reduced area of steel reinforcement, $(A_{st})_{cor}$, and the equivalent area, A_{eqv} , were determined using area reductions factors, ϕ_{cor1} and ϕ_{cor2} .
3. An equation was proposed to determine the design ultimate tensile strain of FRP sheet, ε_{fu}^* . The equation included the strain reduction factor, R_c , that was used to account for the difference between the ultimate tensile strain provided by manufacturer and the actual ultimate tensile strain measured during the test.
4. According to the comparative study of the test results of mid-scale RC columns and the predictions, the proposed design guidelines were somewhat conservative. This might be due to the fact that the reduction factors proposed in the design guidelines were developed based on the small-scale RC column test, which was designed to induce severe damages due to the environmental conditions in order to access the effect of the environmental conditions; however, the mid-scale columns were made of normal concrete.
5. It is suggested to use the proposed design guidelines unless further research provides more statistically reliable and thus more accurate reduction factors.

7. CONCLUSIONS AND RECOMMENDATIONS FOR FUTURE RESEARCH

7.1. SUMMARY OF RESEARCH WORK

FRP composite materials have emerged as an efficient alternative to conventional construction materials because of their inherent advantages such as unique design flexibility, ease in manufacturing, fabrication, handling and installation, non-corrosive nature and excellent strength-to-weight ratio. Thus, there has been a rapid growth in their use for civil engineering applications.

Extensive research projects were conducted to investigate the behavior of the RC columns strengthened with FRP composites materials over the past decade and the information on the short-term performance is abundant. However, despite of the importance of these materials, limited research studies have been conducted on the durability of RC column wrapped with FRP composite materials. Thus, the primary purpose of this study was to evaluate the effects of various environmental conditions on the long-term behavior of RC columns wrapped with FRP sheets, and thus add further valuable information in this area.

This study is composed of three main parts; experimental program, development of analytical model and development of design guidelines for RC columns wrapped with FRP sheets. The experimental program was categorized into two parts; ambient environmental effect tests and corrosion tests. The experiments were conducted using two different scales of RC columns; small-scale and mid-scale RC columns. The test results of small-scale RC columns were used to develop design guidelines while the mid-scale RC column tests were conducted to verify the performance of the proposed design guidelines.

An analytical model was proposed to predict the compressive behavior of FRP confined concrete, based on the steel confined model proposed by Mander et al. (1988) and the variable Poisson's ratio proposed by Fam and Rizkalla (2001). The proposed model was verified through experimental corroboration of existing test results.

Design guidelines were developed based on the test results of the small-scale RC columns. The design guidelines included reduction factors to account for the effect of various environmental conditions and equations to compute the axial compression

capacity of RC columns wrapped with FRP sheet. In addition, equations to calculate the design material properties of FRP sheet were proposed. The performance was validated through a comparative study with the test results of mid-scale RC columns.

7.2. CONCLUSIONS

7.2.1. Ambient Environmental Effect Tests. The following conclusions are attributed to the ambient environmental effects tests.

1. The freeze-thaw cycles considered in this test did not adversely affect the compressive behavior of RC columns wrapped with both CFRP and GFRP sheets. Rather, the axial compression capacity of the columns conditioned under the freeze-thaw cycles slightly increased. The possible reason for the increase could be attributed in large part to the matrix-hardening effect resulting from the extremely low temperature during the freeze-thaw cycles.
2. The increase rate of axial compression capacity due to the matrix hardening effect, however, could be minimized by the degradation of concrete due to the freeze-thaw cycles when the confining modulus E_j of RC columns wrapped with FRP sheets is relatively small.
3. The combined environmental cycles, which included all the environmental cycles used in this test, such as freeze-thaw cycles, high-temperature cycles with UV radiation and high-humidity cycles, did not show any significant effect on CFRP wrapped RC columns. This was probably because the adverse effects, such as plasticization of matrix and micro-cracking at matrix-fiber interface, induced by the high-temperature cycles with UV radiation and high-humidity cycles, compromised the positive effect of freeze-thaw cycles, such as matrix hardening effect.
4. The axial compression capacity of GFRP wrapped columns, on the other hand, was reduced slightly due to the combined environmental cycles. The different results of CFRP and GFRP wrapped columns was probably due to the inherent difference of chemical properties; GFRP sheets could be degraded by the moisture which extracts ions from glass fiber, while CFRP sheets were not vulnerable to this kind of degradation mechanism. Thus, during the high-humidity cycles, GFRP sheets could be degraded by the moisture effects, resulting in the decrease in fiber strength

5. The saline solution appeared to have the most deteriorative effect on GFRP wrapped columns, resulting in a significant loss of axial compression capacity and ductility. The formation and expansion of salt crystals could accelerate the micro-cracking and thus the moisture could reach the glass fiber more easily, resulting in further damage of glass fiber. Meanwhile, CFRP wrapped RC columns showed an insignificant decrease in axial compression capacity due to the saline solution effect.
6. The combined effects of high-temperature cycles with UV radiation and high-temperature cycles was the second most deteriorative environmental conditions for GFRP wrapped columns, resulting in a significant loss of axial compression capacity; while CFRP wrapped columns exhibited a slight reduction of axial compression capacity. The primary reason for the significant loss of axial compression capacity of GFRP wrapped columns was moisture effects, resulting in damage of glass fiber, in addition to the plasticization and micro-cracking at the fiber-matrix interfaces due to the high-temperature and humidity variations during the environmental cycles. Furthermore, it was possible that the surface damage resulting from UV radiation could accelerate the moisture diffusion via matrix and the moisture ingress through the micro-cracks. As for CFRP wrapped RC columns, the loss of axial compression capacity was small since carbon fiber was not vulnerable to the moisture effects.
7. Strain reduction factor, R_c , of 0.5 was proposed for both CFRP and GFRP wrapped RC columns in order to account for the difference between the ultimate tensile strain provided by manufacturer and the actual value measured during the tests. This difference was likely due to the following reasons. First, despite same materials used, the process of making a flat coupon which is usually used to obtain ultimate tensile strain and strength by manufacturers is easier than that of making FRP wrapped RC columns. As a result, the quality of the coupon might be higher than that of FRP wrapped columns. Second, due to the existence of the lateral pressure created by confining action of FRP sheets in addition to the applied axial load, the FRP sheet in the RC columns was in the tri-axial stress state, instead of pure tension as in the flat coupon test. Third, cracking and crushing of the core concrete inside the FRP sheets could cause the stress-concentrations.

8. Strength reduction factor, ϕ_{env} , was proposed to consider the environmental effects on RC columns wrapped with FRP sheets in the design and thus to obtain the required reliability of the structure. The strength reduction factor, ϕ_{env} , is composed of three sub-factors ϕ_{FT} , ϕ_H , and ϕ_{Na} which account for the effects of freeze-thaw cycles, high-temperature cycles with UV radiation and high-humidity cycles, and saline solution, respectively.

7.2.2. Corrosion Tests. The following conclusions were drawn from the test results of corrosion tests.

1. The corrosion of steel reinforcement continues to develop even when RC columns were wrapped with CFRP sheets. This is because the moisture may ingress into the concrete inside the CFRP sheet wrapping through the unwrapped portion of the column, in addition to the moisture diffusion through the CFRP sheet wrapping. Furthermore, when cracks of the CFRP sheet wrapping developed due to the expansion of concrete induced by the corrosion of steel reinforcements, the effectiveness of CFRP sheet wrapping may not be expected.
2. The failure load, P_u , of the RC columns wrapped with CFRP sheets decreases due to the corrosion of steel reinforcements. The decrease in failure load, P_u , was resulting from the loss of the cross-sectional area of steel reinforcements and the degradation of the concrete, such as cracking.
3. In order to quantify the extent of degradation of concrete inside the CFRP sheet wrapping, a concept of the equivalent area, A_{eqv} , was proposed in this study. The equivalent area, A_{eqv} , utilizes the area reduction factors ϕ_{cor1} and ϕ_{cor2} , experimentally determined based on the test results of this study.
4. Wrapping a corrosion-damaged RC column with CFRP sheets can restore the structural integrity of the column, resulting in a significant increase in the failure load, P_u , depending on the confinement level provided by the CFRP sheet wrapping. However, if the column remains in the corrosive environment after the repair, it is expected that the corrosion of steel reinforcements continues to occur. In this case,

the failure mode of the column may change from the rupture of CFRP sheets to the debonding of lap splices, resulting in a significant decrease in the failure load P_u .

5. Although the mechanism of the failure mode of lap splice debonding is not yet fully resolved, it is suggested to increase the lap splice lengths when repairing corrosion-damaged RC columns by CFRP sheet wrapping.

7.2.3. Analytical Model. An analytical model was proposed in this study, which can be used to predict the compressive strength of the concrete confined by FRP sheets, based on the steel confined concrete model. The compressive strengths calculated by the proposed analytical model exhibited a reasonably good agreement with the experimental results.

7.2.4. Design Guidelines. Design guidelines were developed based on the test results of this study and the performance was evaluated through comparison with the experimental results. The following conclusions were obtained.

1. Equations to calculate the axial compressive capacity of FRP wrapped RC columns exposed to various environmental conditions, were proposed. The equations utilized the strength reduction factor, ϕ_{env} , accounting for the effects of various ambient environmental conditions, and the area reduction factors, ϕ_{cor1} and ϕ_{cor2} , accounting for the effects of corrosion of steel reinforcements.
2. The performance of the proposed design guidelines was evaluated through the comparative study with the test results of mid-scale RC columns. As a result, it was found that the predictions calculated by the proposed design guidelines were somewhat conservative. This was due to the reduction factors ϕ_{env} , ϕ_{cor1} and ϕ_{cor2} used in the design guidelines; the reduction factors were developed based on small-scale RC column tests, in which the columns were designed to be vulnerable to the environmental conditions. As a result, the effects of the environmental effects were easily detected; however, the mid-scale columns were not designed that way and were made of normal strength of concrete provided by local ready mixed concrete plant.

7.3. GENERAL CONCLUSION

This study aimed to investigate the effects of various environmental conditions on

long-term behavior of RC columns wrapped with FRP sheets. Through the experimental works, the effects of the environmental conditions considered in this study were quantified in order to propose design guidelines. Although the design guidelines were developed based on the limited data obtained only from this study, it is believed at least to provide engineers with appropriate concepts of how to deal with the effect of environmental conditions for the design of RC columns wrapped with FRP sheet. However, it is suggested to use the proposed design guidelines unless further research provides more statistically reliable and thus more accurate reduction factors.

7.4. RECOMMENDATIONS FOR FUTURE RESEARCH

It is recommended that the following research be pursued as an extension of this study.

1. In order to obtain more reliable strength reduction factor ϕ_{env} , it is recommended that further investigation be conducted with a particular attention to the level of confinement provided by FRP sheets, the properties of concrete and the size of columns.
2. Although the area reduction factors ϕ_{cor1} and ϕ_{cor2} were proposed in order to account for the damages induced by the corrosion of steel reinforcement, it is still necessary to develop an analytical model that can define the relationship between the radial strain of FRP sheet wrapping and the steel loss so that steel loss can be inferred by measuring radial strains when RC columns are wrapped with FRP sheets.
3. The failure modes of corrosion-damaged columns repaired by CFRP sheet was lap splice debonding in most cases, causing a significant decrease in axial compression capacity. However, the mechanism of this failure mode is not yet fully resolved. Thus, it needs to be verified and included in the future design guidelines.

APPENDIX A

Load vs. Axial Strain Curves of the Small-Scale RC Columns in Ambient Environmental Tests

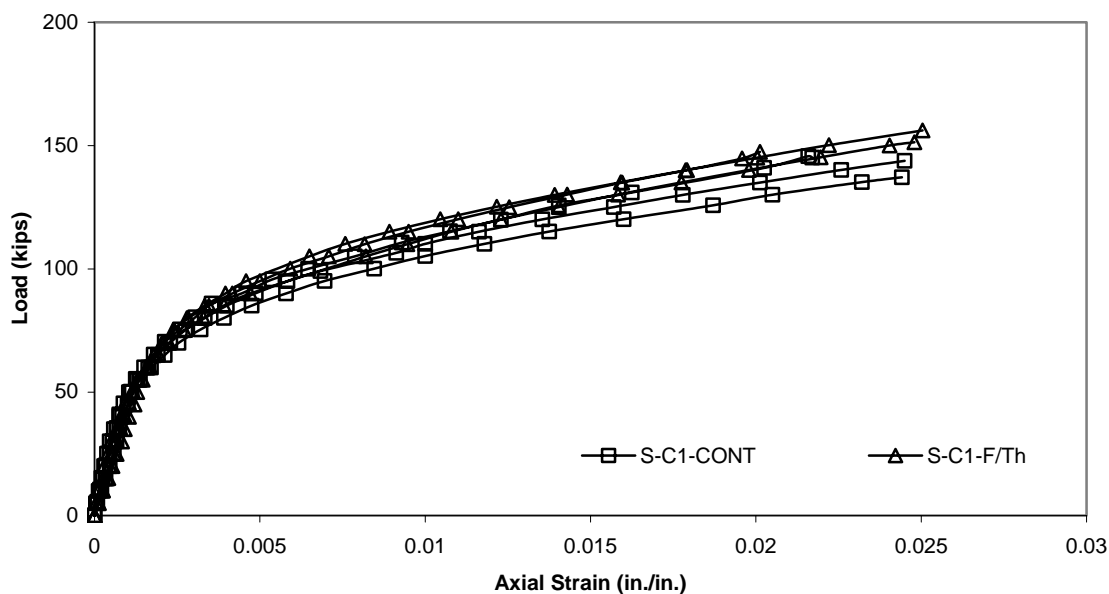


Figure A.1. Applied Load vs. Axial Strain Curves of Columns S-C1-CONT and S-C1-F/Th

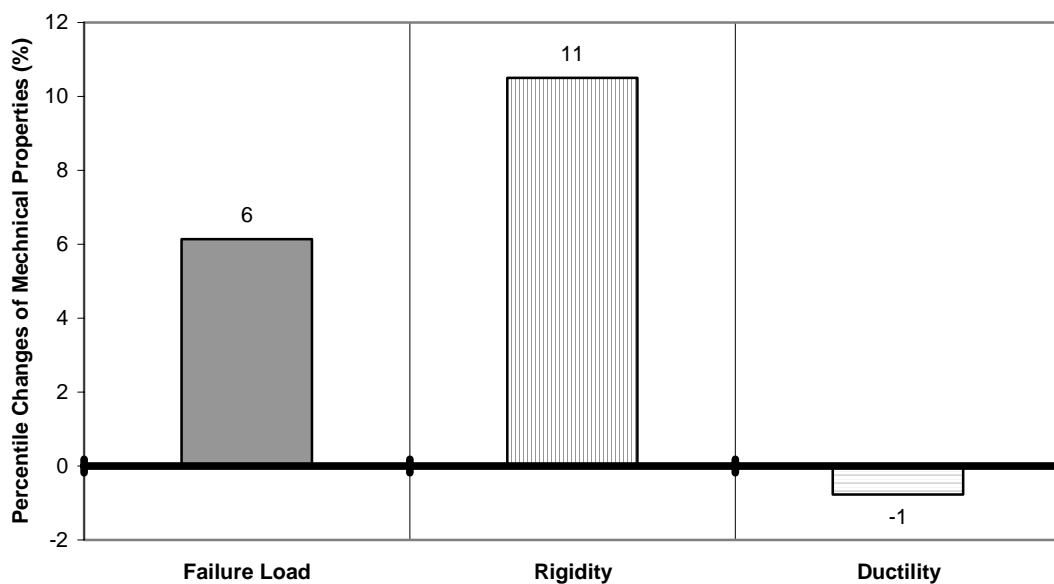


Figure A.2. Percentile Changes of Mechanical Properties of CFRP Wrapped RC Columns Due to the Freeze-Thaw Cycles

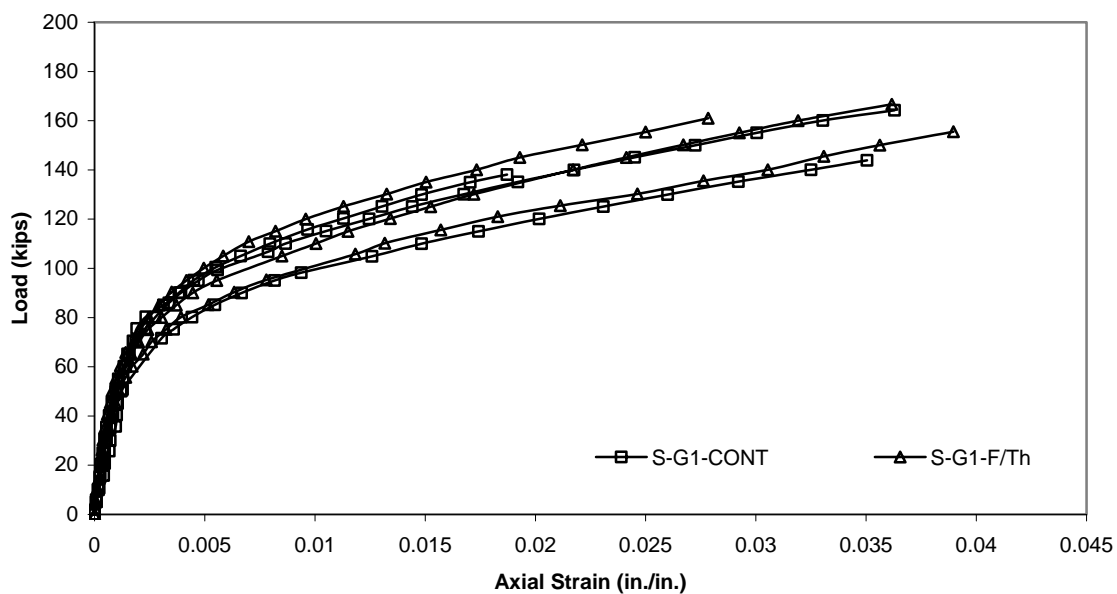


Figure A.3. Applied Load vs. Axial Strain Curves of Columns S-G1-CONT and S-G1-F/Th

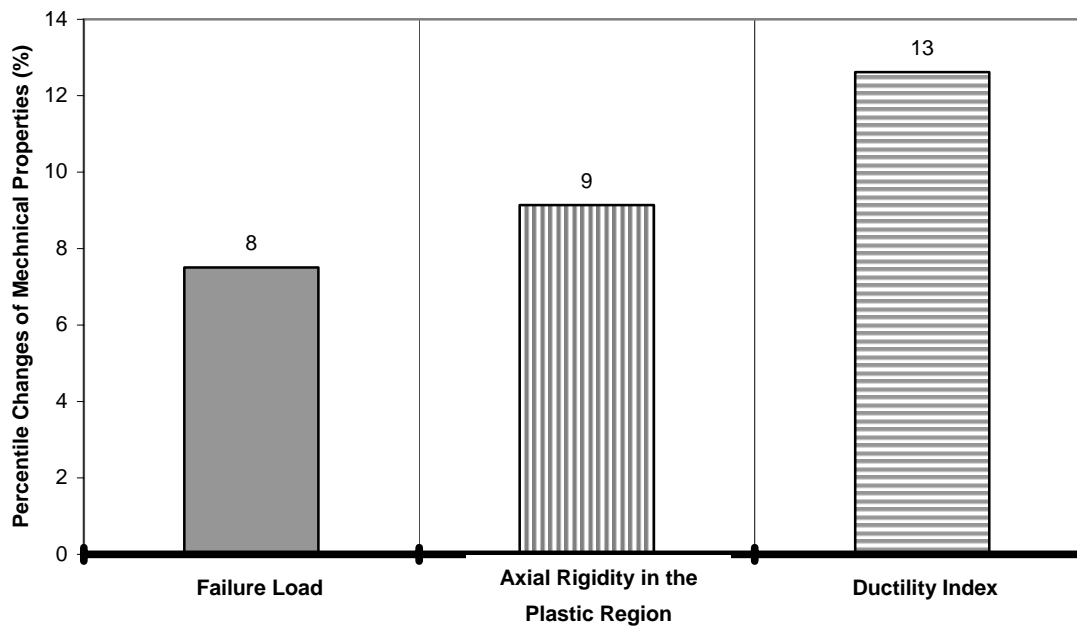


Figure A.4. Percentile Changes of Mechanical Properties of GFRP Wrapped RC Columns Due to the Freeze-Thaw Cycles

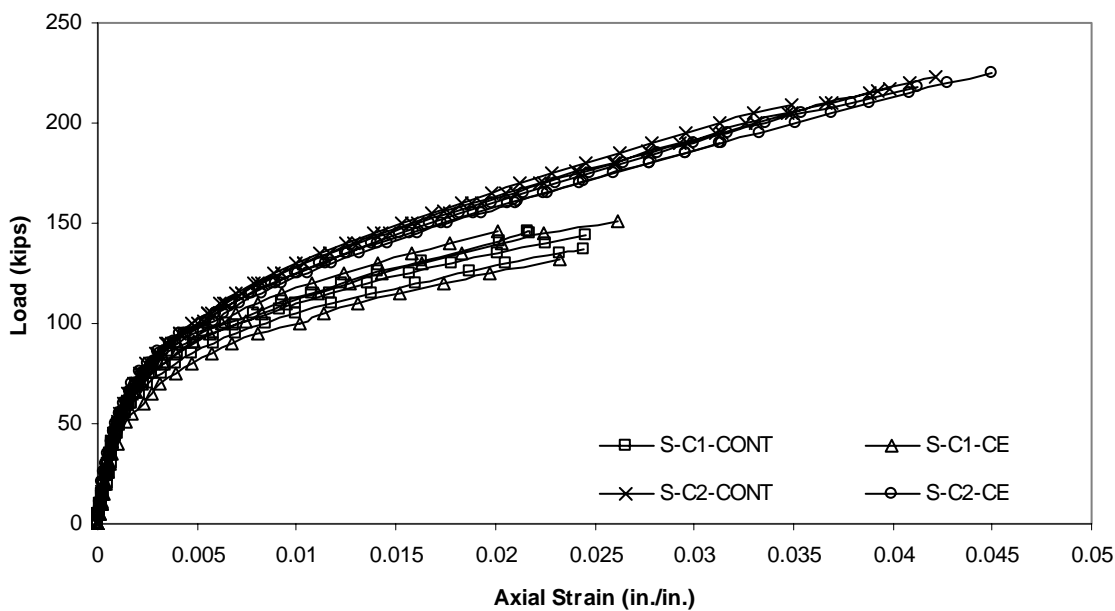


Figure A.5. Applied Load vs. Axial Strain Curves of Columns S-C1-CONT, S-C2-CONT, S-C1-CE, and S-C2-CE

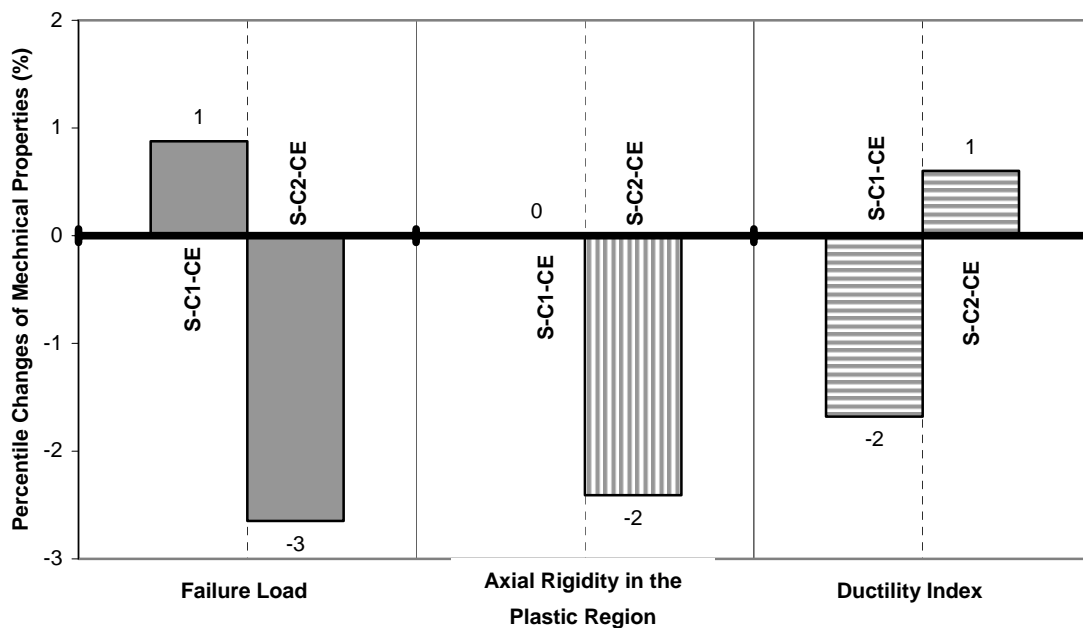


Figure A.6. Percentile Changes of Mechanical Properties of CFRP Wrapped RC Columns Due to the Combined Environmental Cycles

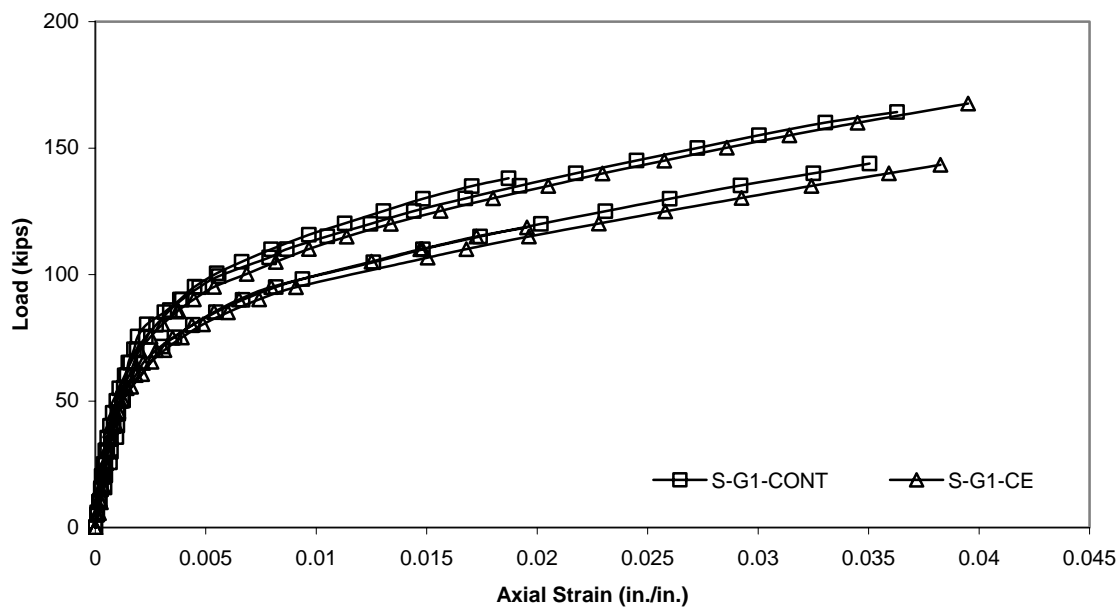


Figure A.7. Applied Load vs. Axial Strain Curves of Columns S-G1-CONT and S-G1-CE

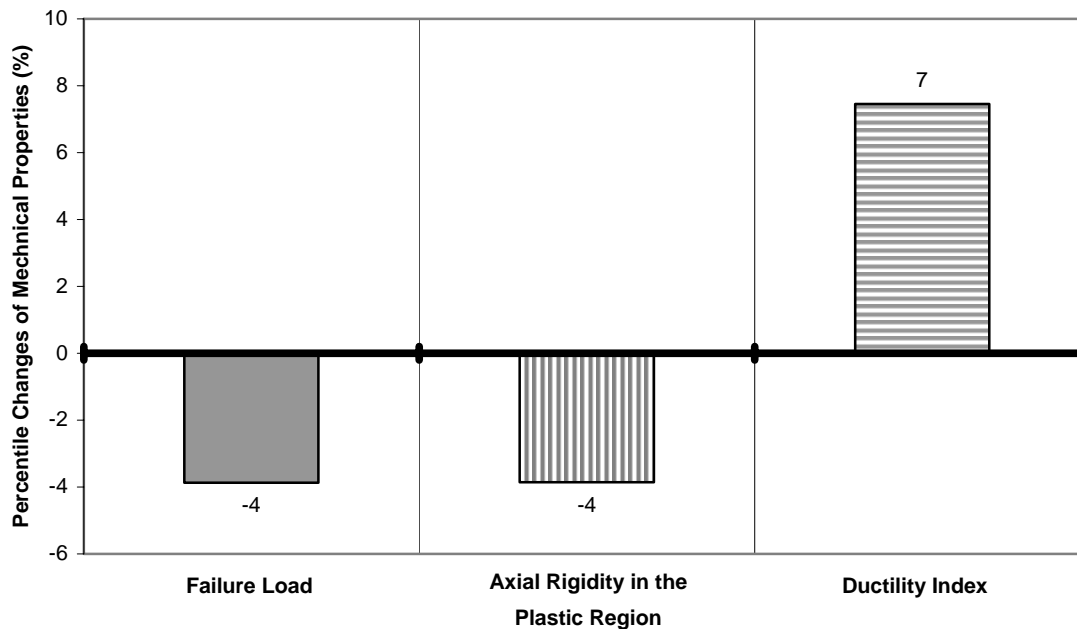


Figure A.8. Percentile Changes of Mechanical Properties of GFRP Wrapped RC Columns Due to the Combined Environmental Cycles

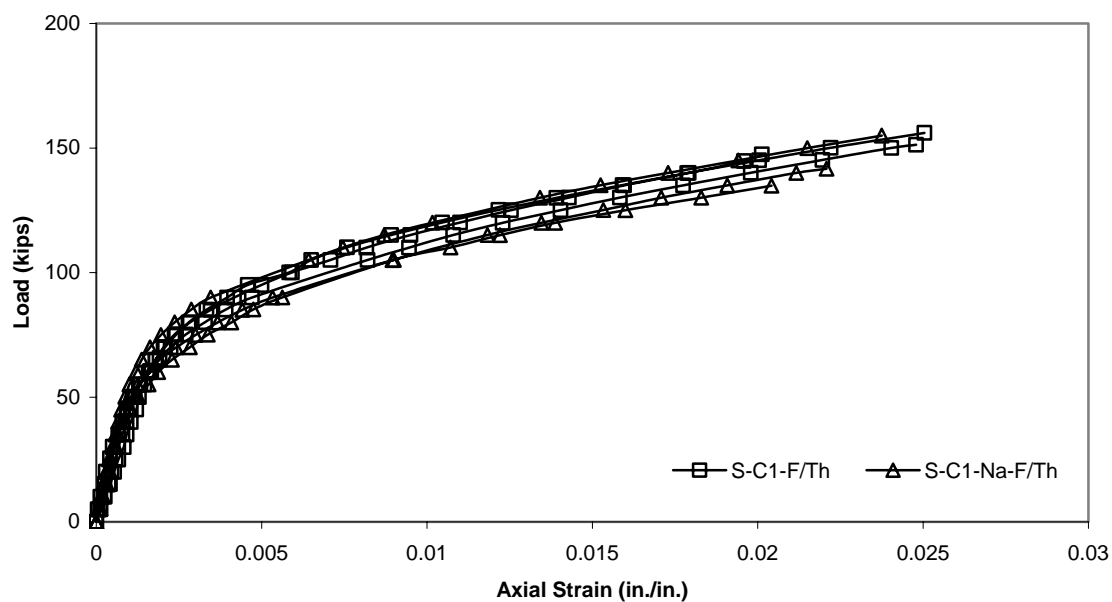


Figure A.9. Applied Load vs. Axial Strain Curves of Columns S-C1-F/Th and S-C1-Na-F/Th

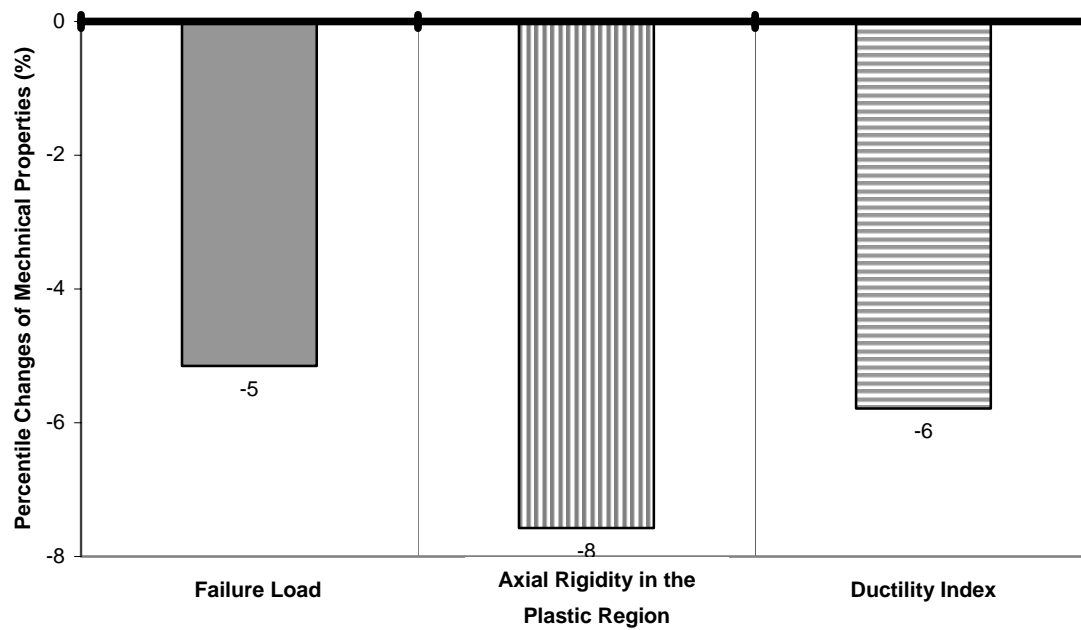


Figure A.10. Percentile Changes of Mechanical Properties of CFRP Wrapped RC Columns Due to the Saline Solution during Freeze-Thaw Cycles

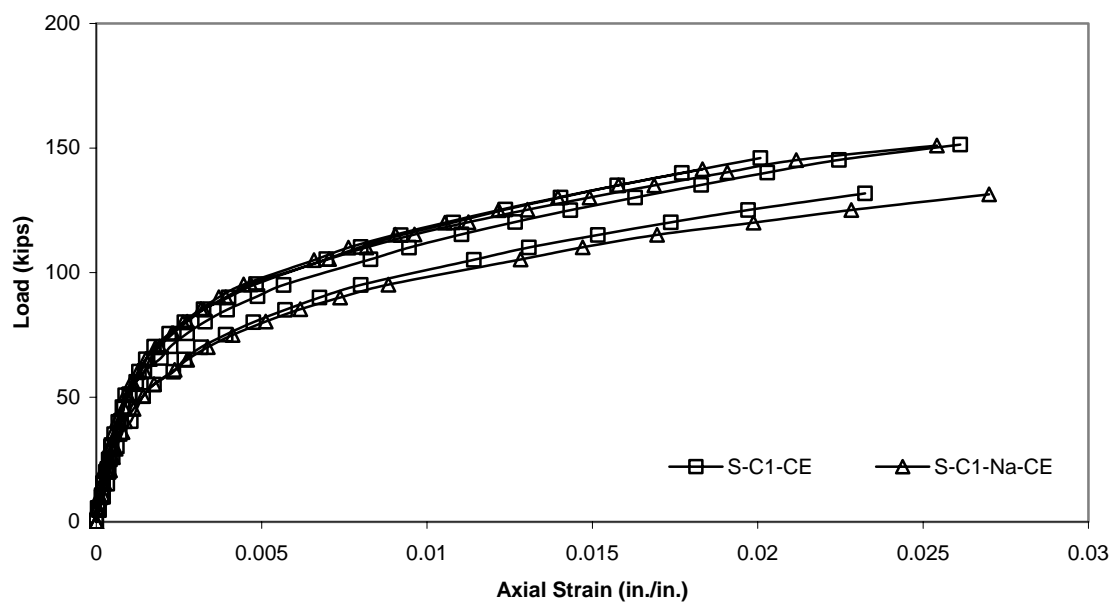


Figure A.11. Applied Load vs. Axial Strain Curves of Columns S-C1-CE and S-C1-Na-CE

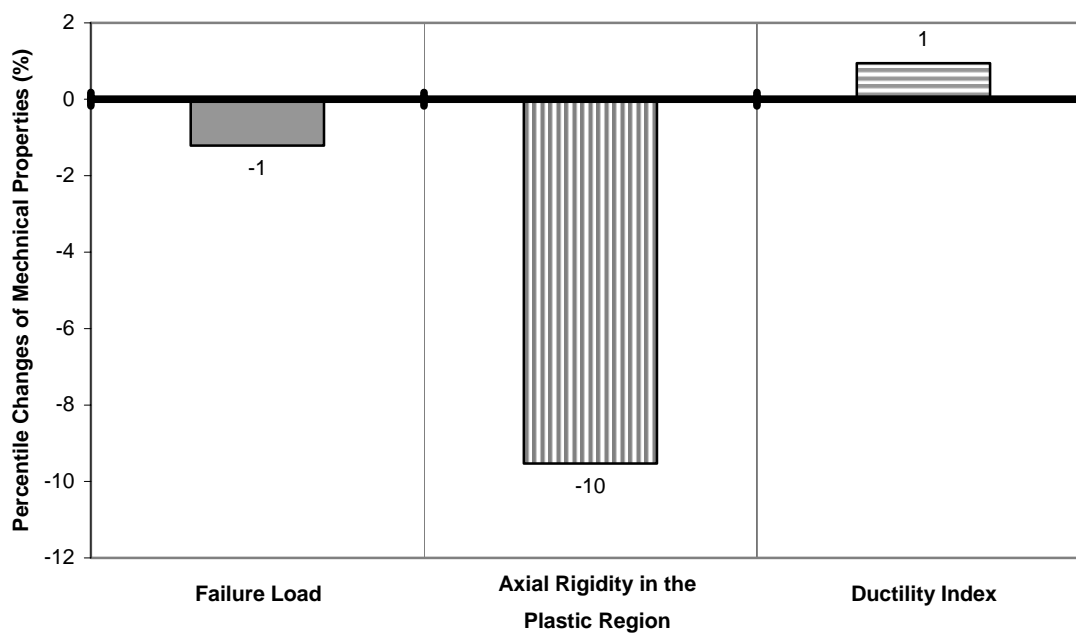


Figure A.12. Percentile Changes of Mechanical Properties of CFRP Wrapped RC Columns Due to the Saline Solution during Combined Environmental Cycles

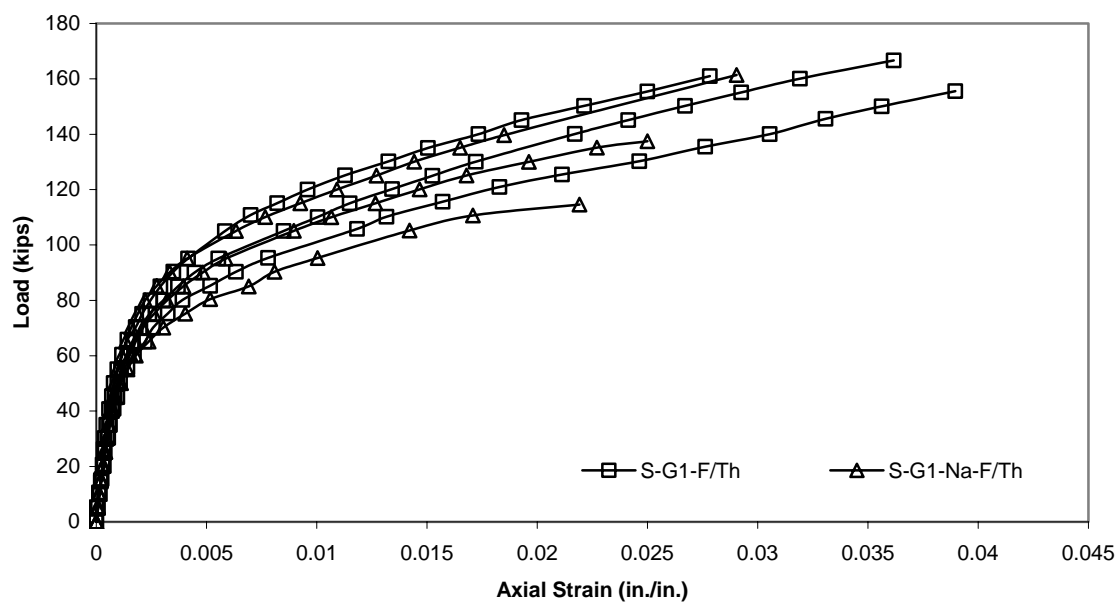


Figure A.13. Applied Load vs. Axial Strain Curves of Columns S-G1-F/Th and S-G1-Na-F/Th

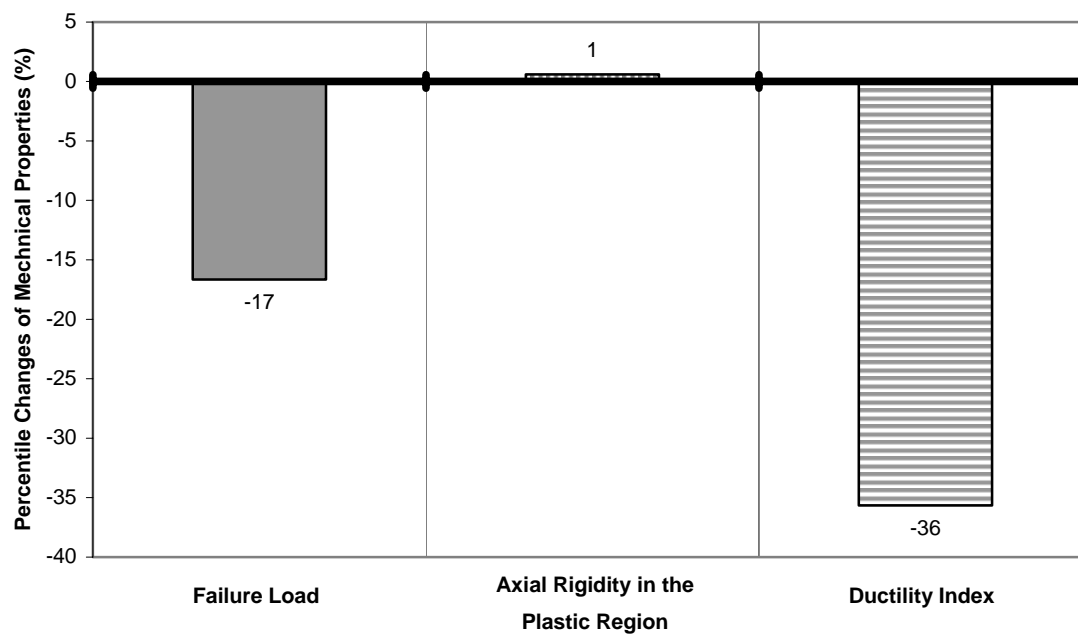


Figure A.14. Percentile Changes of Mechanical Properties of GFRP Wrapped RC Columns Due to the Saline Solution during Freeze-Thaw Cycles

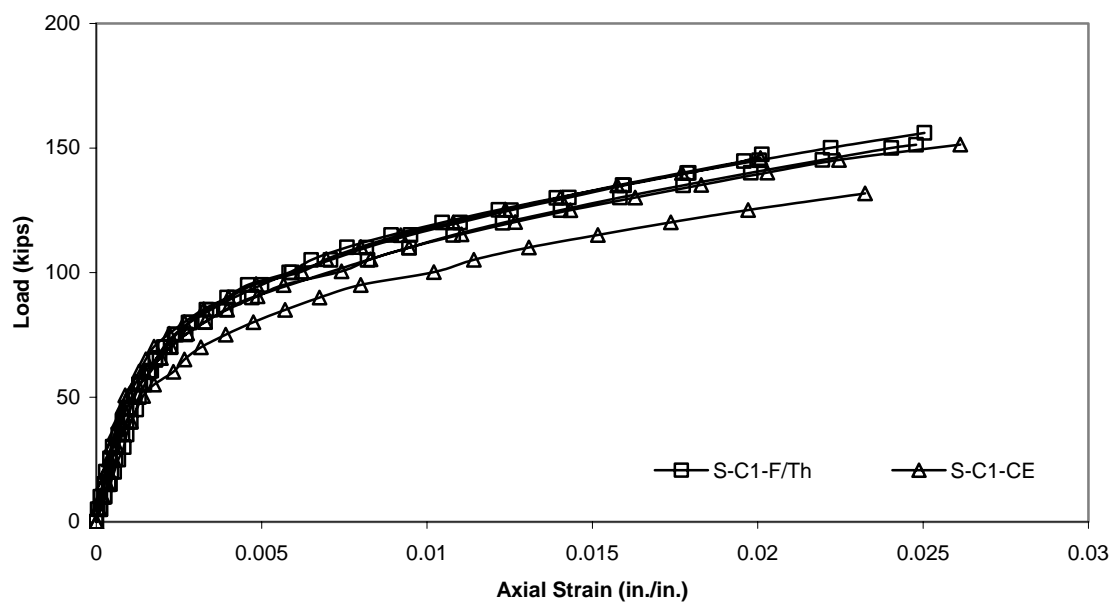


Figure A.15. Applied Load vs. Axial Strain Curves of Columns S-C1-F/Th and S-C1-CE

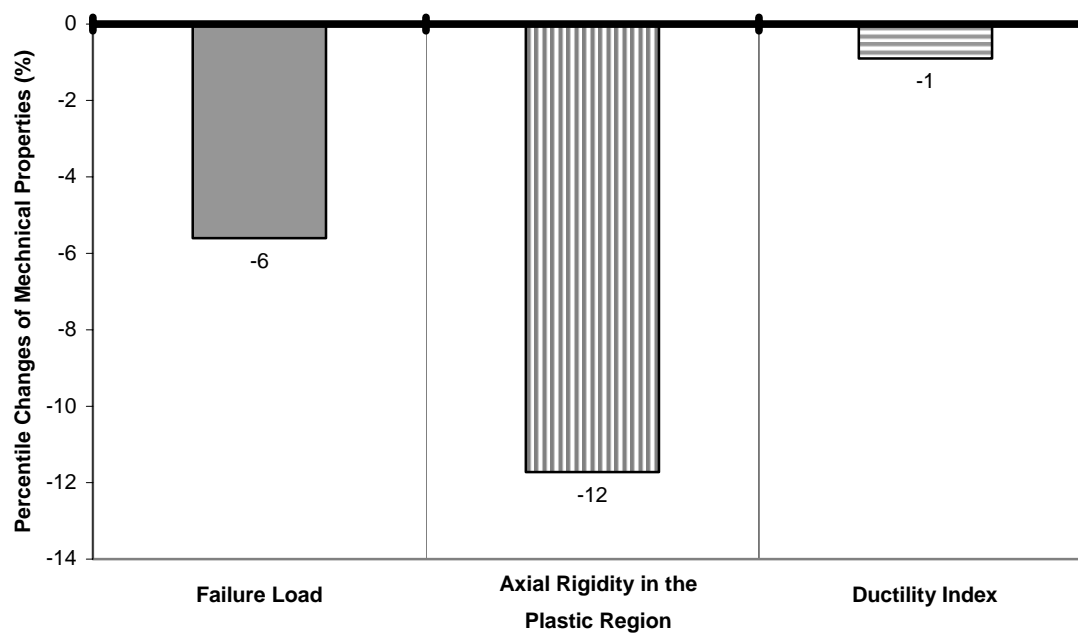


Figure A.16. Percentile Changes of Mechanical Properties of CFRP Wrapped RC Columns Due to High-Temperature Cycles and High-Humidity Cycles

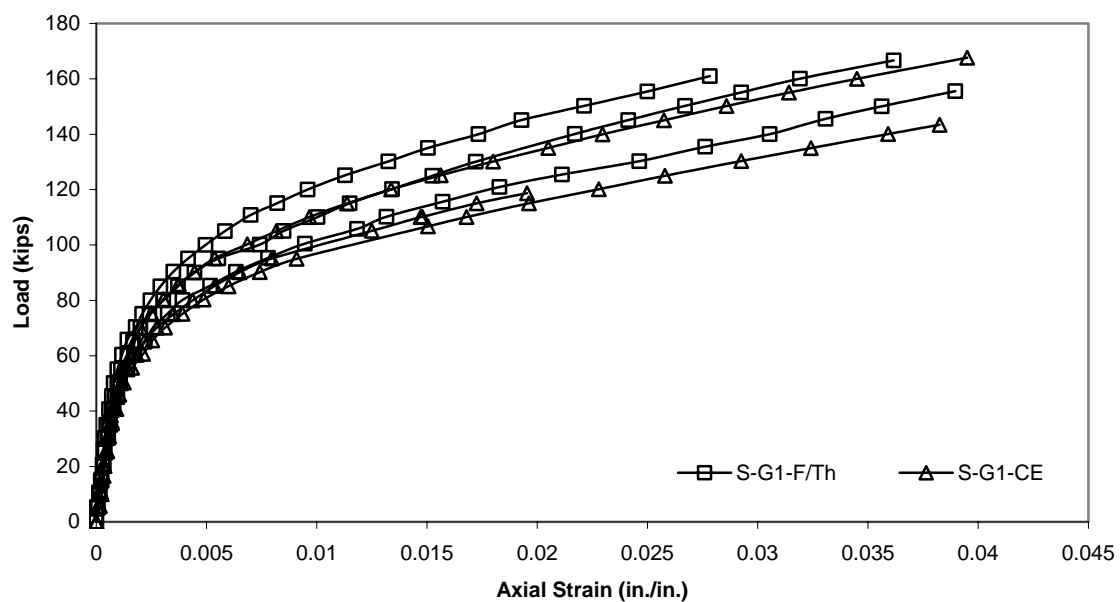


Figure A.17. Applied Load vs. Axial Strain Curves of Columns S-G1-F/Th and S-G1-CE

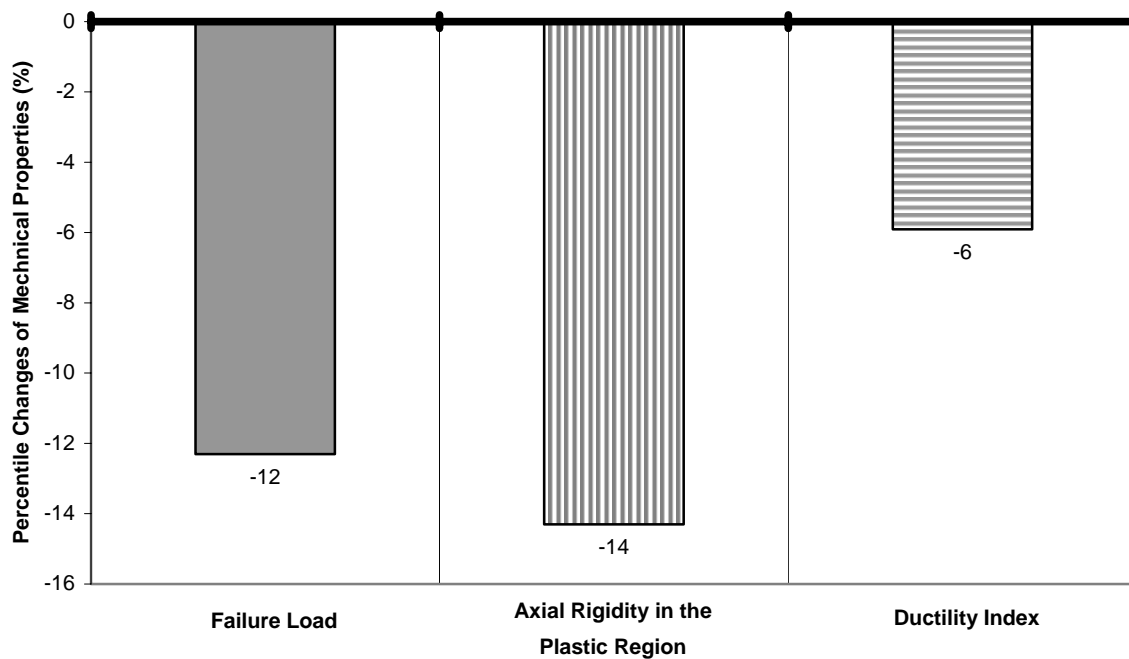


Figure A.18. Percentile Changes of Mechanical Properties of GFRP Wrapped RC Columns Due to High-Temperature Cycles and High-Humidity Cycles

APPENDIX B

Load vs. Axial Strain Curves of the Small-Scale RC Columns in Corrosion Tests

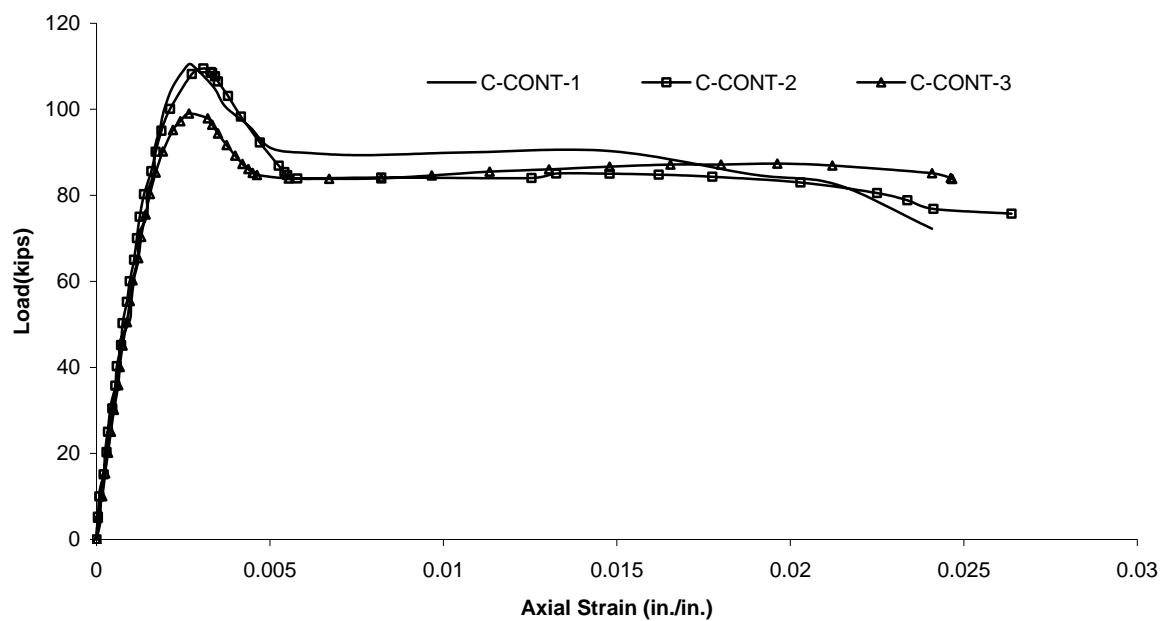


Figure B.1. Applied Load vs. Axial Strain Curves of Column C-CONT

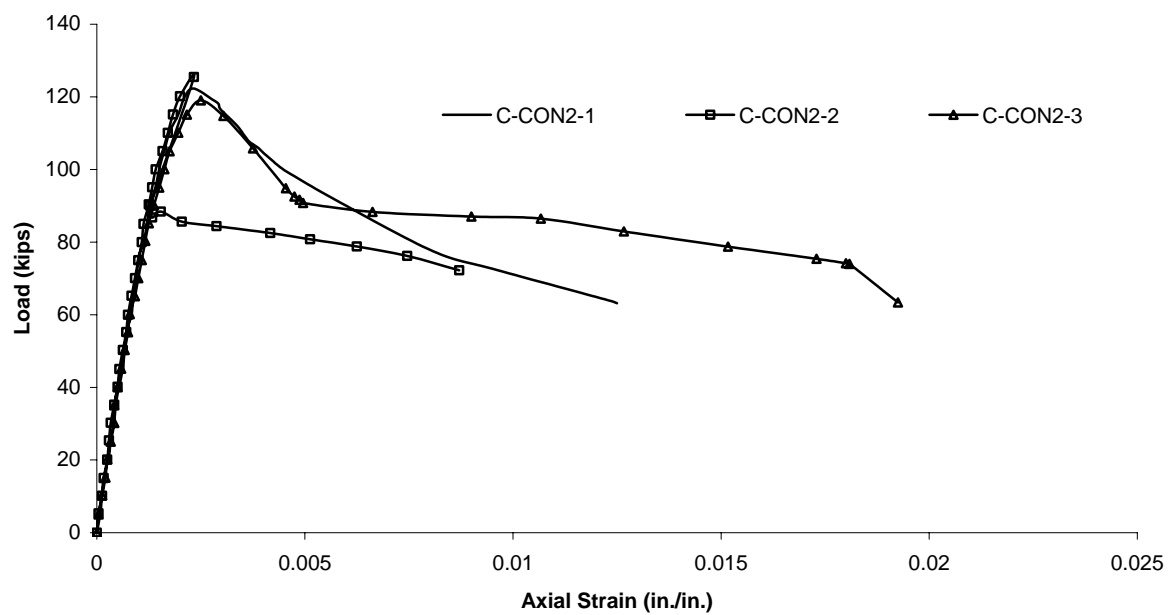


Figure B.2. Applied Load vs. Axial Strain Curves of Column C-CON2

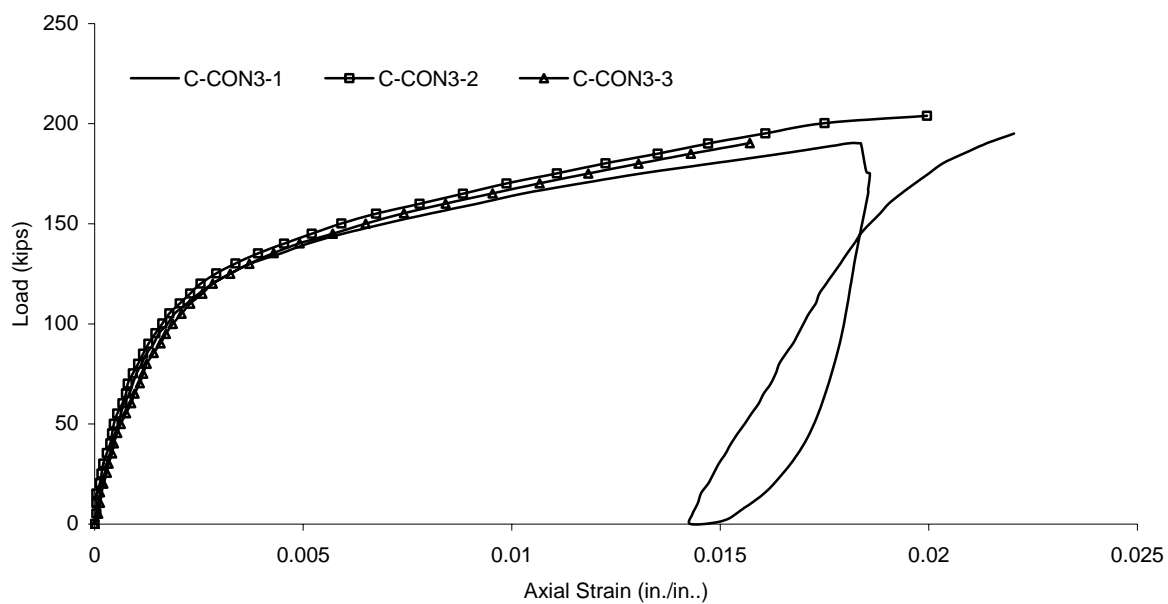


Figure B.3. Applied Load vs. Axial Strain Curves of Column C-CON3

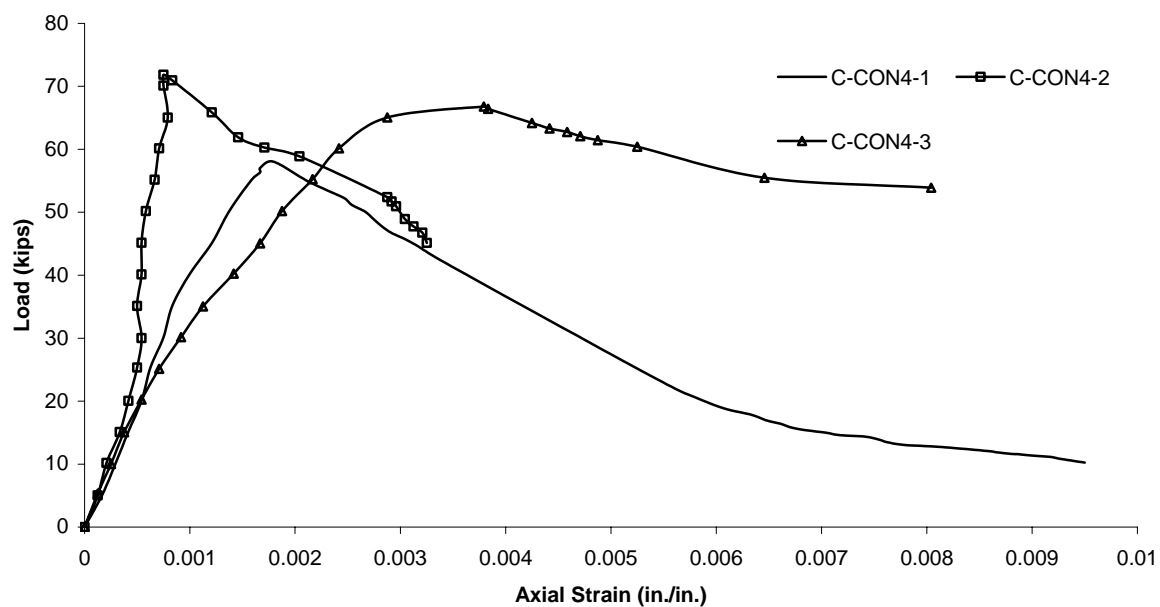


Figure B.4. Applied Load vs. Axial Strain Curves of Column C-CON4

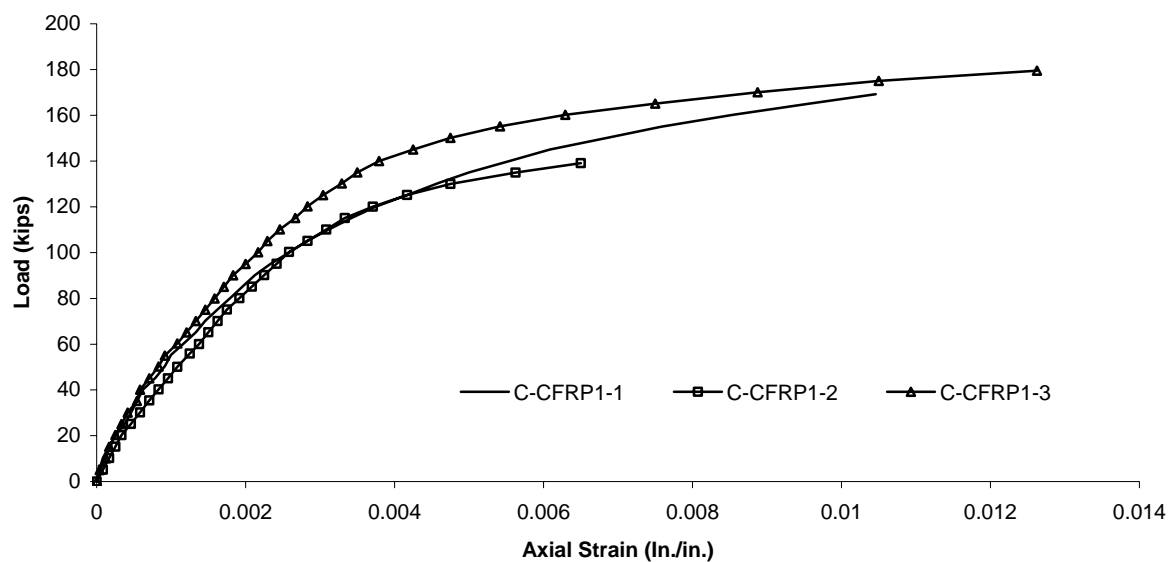


Figure B.5. Applied Load vs. Axial Strain Curves of Column C-CFRP1

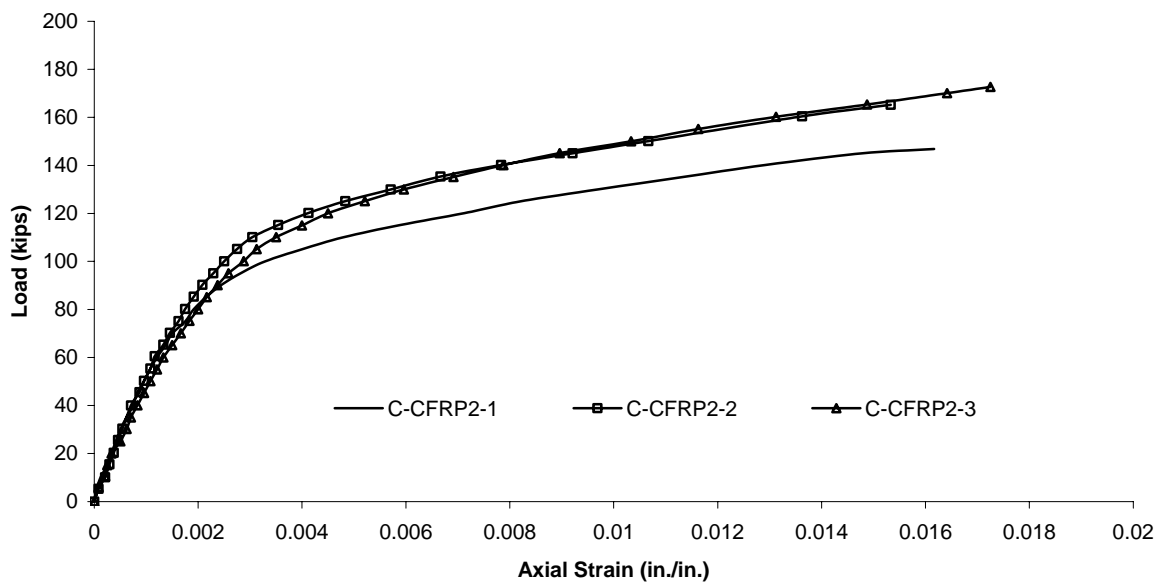


Figure B.6. Applied Load vs. Axial Strain Curves of Column C-CFRP2

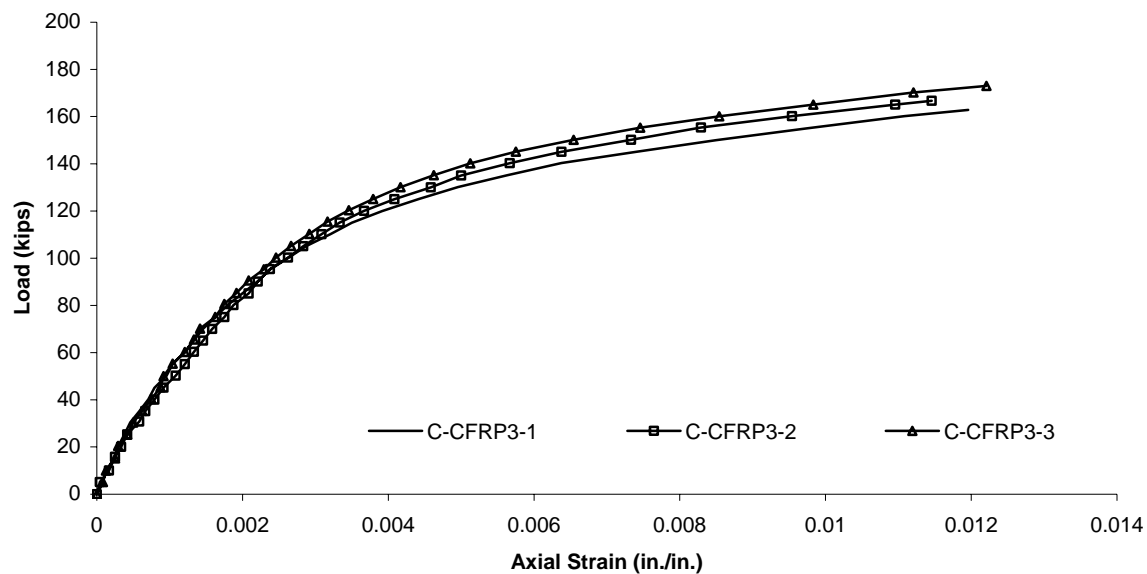


Figure B.7. Applied Load vs. Axial Strain Curves of Column C-CFRP3

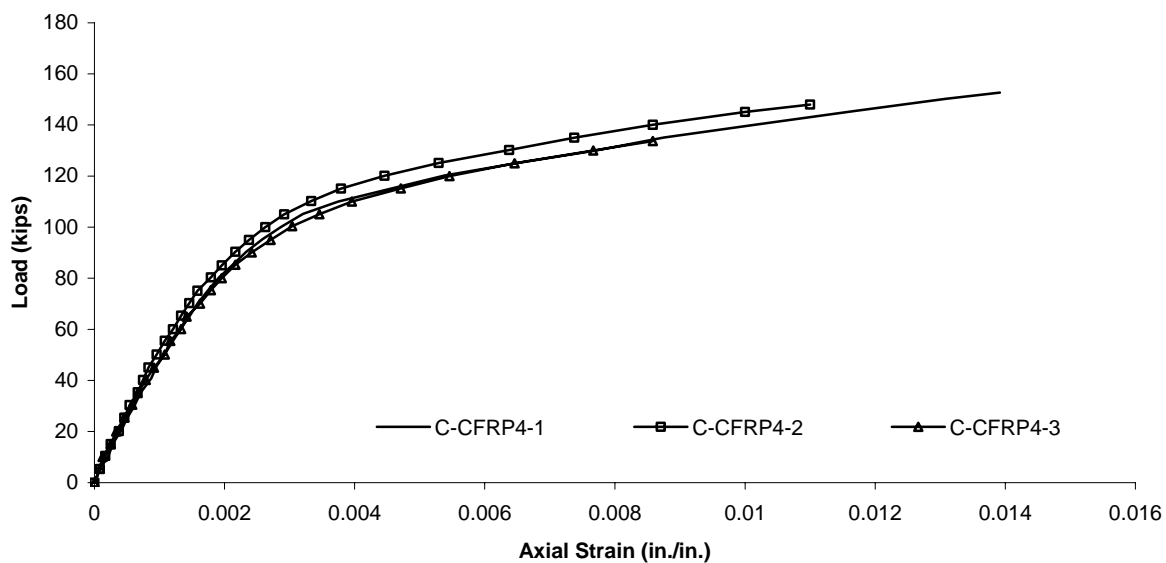


Figure B.8. Applied Load vs. Axial Strain Curves of Column C-CFRP4

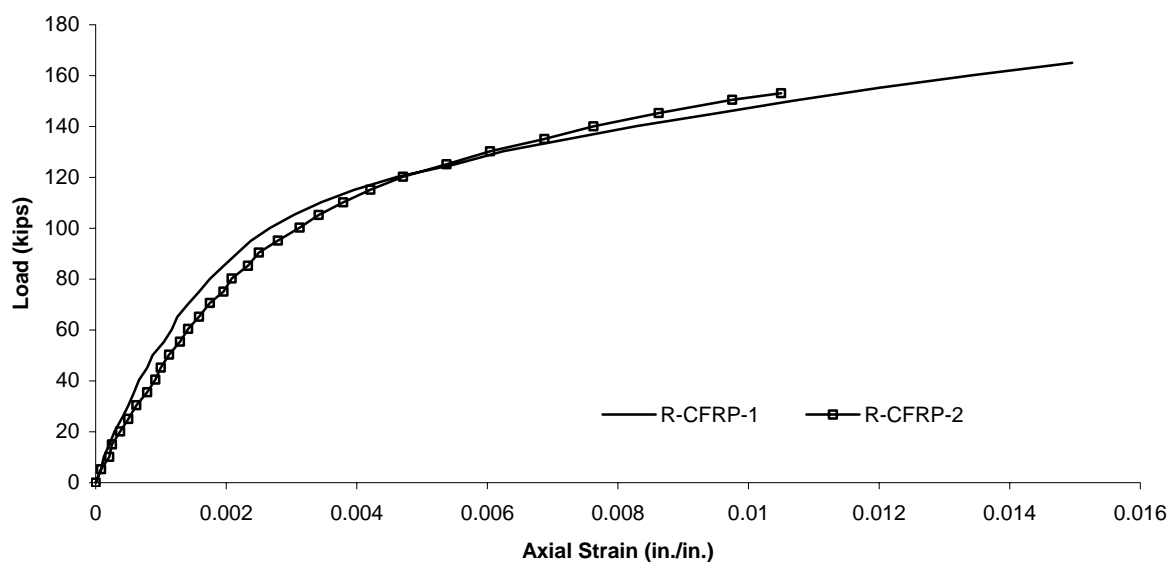


Figure B.9. Applied Load vs. Axial Strain Curves of Column C-CFRP4

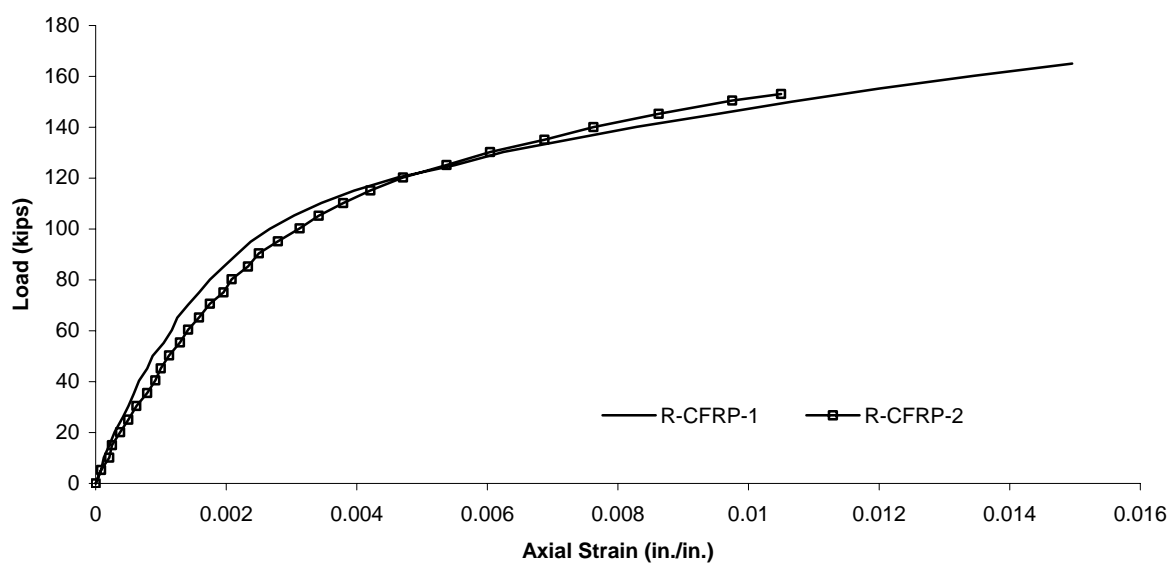


Figure B.10. Applied Load vs. Axial Strain Curves of Column C-CON4

BIBLIOGRAPHY

- ACI Committee 318 (2002). *Building Code Requirements for Structural Concrete and Commentary (ACI 318-02/ACI 318R-02)*. American Concrete Institute, Farmington Hills, Michigan.
- ACI Committee 440 (2002). *Guide for the Design and Construction of Externally Bonded FRP Systems for Strengthening Concrete Structures*. American Concrete Institute, Farmington Hills, Michigan.
- Adimi, M. R., Rahman, A. H., and Benmokrane, B. (2000). "New Method for Testing Fiber-Reinforced Polymer Rods under Fatigue," *Journal of Composites for Construction*, Vol. 4, No. 4, pp. 206-213.
- ASTM C 310 (1971). *Test for Resistance of Concrete Specimens to Slow Freezing in Air and Thawing in Water*. West Conshohocken, Pennsylvania.
- ASTM C 666 (2003). *Standard Test Method for Resistance of Concrete to Rapid Freezing and Thawing*. West Conshohocken, Pennsylvania.
- Baumert, M. E., Green, M. F. and Erki, M. A. (1996). "Low Temperature Behaviour of Concrete Beams Strengthened with FRP sheets," *CSCE Annual Conference*, Edmonton, Alberta, Canada, pp. 179-190, June.
- Breña, S. F., Wood, S. L., and Kreger, M. E. (2002). "Fatigue Tests of Reinforced Concrete Beams Strengthened Using Carbon Fiber Reinforced Polymer Composites," *Second International Conference on Durability of FRP Composites for Construction*, Montreal, Canada, pp. 575-586, May.
- Carino, N. J. (1999). "Nondestructive Techniques to Investigate Corrosion Status in Concrete Structures," *Journal of Performance of Constructed Facilities*, Vol. 13, No. 3, pp. 96-106.
- Fam, A. Z. and Rizkalla, S. H., (2001). "Confinement Model for Axially Loaded Concrete Confined by Circular Fiber-Reinforced Polymer Tubes," *ACI Structural Journal*, Vol. 98, No. 4, pp. 451-461.
- Gardner, N. J. (1969). "Triaxial Behavior of Concrete," *ACI Journal*, Vol. 66, No. 2, pp. 136-146.

- George, G. A., Sacher, R. E. and Sprouse, J. F. (1997). "Photo-Oxidation and Photoprotection of the Surface Resin of a Glass Fiber-Epoxy Composite," *Journal of Applied Polymer Science*, Vol. 21, pp. 2241-2245.
- Green, M. F., Bisby, L. A., Beaudoin, Y. and Labossiere, P. (2000). "Effect of Freeze-Thaw Cycles on the Bond Durability between Fibre Reinforced Polymer Plate Reinforcement and Concrete," *Canadian Journal of Civil Engineering*, Vol. 27, No. 5, pp. 949-959.
- Heffernan, P. J. (1997). *Fatigue Behavior of Reinforced Concrete Beams Strengthened with CFRP Laminates*. Ph.D. Thesis, Royal Military College of Canada, Kingston, Ontario, Canada.
- Ilki, A. and Kumbasar, N. (2002). "Behavior of Damaged and Undamaged Concrete Strengthened by Carbon Fiber Composite Sheets", *Structural Engineering and Mechanics*, Vol. 13, No. 1, pp. 75-90.
- Kajorncheappunngam, S., Gupta, R. K. and GangaRao, H. V. S. (2002). "Effect of Aging Environment on Degradation of Glass-Reinforced Epoxy," *Journal of Composites for Construction*, Vol. 6, No. 1, pp. 61-69.
- Karbhari, V. M., Chin, J. W., Hunston, D., Benmokrane, B., Juska, T., Morgan, R., Lesko, J. J., Sorathia, U. and Reynaud, D. (2003). "Durability Gap Analysis for Fiber-Reinforced Polymer Composites in Civil Infrastructure," *Journal of Composites for Construction*, Vol. 7, No.3, pp. 238-247.
- Karbhari, V. M. and Eckel II, D. A. (1994). "Effect of Cold Region Climate Composite Jacketed Concrete Columns," *Journal of Cold Region Engineering*, Vol. 8, No. 3, pp. 73-86.
- Karbhari, V. M. and Gao, Y. (1997). "Composite Jacketed Concrete under Uniaxial Compression-Verification of Simple Design Equation," *Journal of Materials in Civil Engineering*, Vol. 9, No. 4, pp. 185-193.
- Karbhari, V. M., Rivera, J. and Dutta, P.K. (2000). "Effect of Short-Term Freeze-Thaw Cycling on Composite Confined Concrete," *Journal of Composites for Construction*, Vol. 4, No. 4, pp. 191-197.

- Kumar, A. and Gupta, R. K. (1998). *Fundamentals of Polymers*. McGraw-Hill, New York.
- Lee, C. (1998). *Accelerated Corrosion and Repair of Reinforced Concrete Columns Using CFRP Sheet*. M.S. Thesis, Department of Civil Engineering, University of Toronto, Canada.
- Mallick, P. K. (1993). *Fiber-Reinforced Composites: Materials, Manufacturing, and Design*. 2nd Edition, Marcel Dekker, Inc, New York, New York.
- Mander, J. B., Priestley, J. N. and Park, R. (1988). "Observed Stress-Strain Behavior of Confined Concrete," *Journal of Structural Engineering*, Vol. 114, No. 8, pp. 1827-1849.
- Master Builders Inc. (1998). *MbraceTM Composite Strengthening System-Engineering Design Guidelines; Second Edition*. Cleveland, Ohio.
- Masoud, S., Soudki, K. and Topper, T. (2001). "CFRP Strengthened and Corroded RC Beams Under Monotonic and Fatigue Loads," *Journal of Composites for Construction*, Vol. 5, No. 4, pp. 228-236.
- Micelli, F., Myers, J. J. and Murthy, S. (2001). "Effect of Environmental Cycles on Concrete Cylinders Confined with FRP," *Project Report of Center for Infrastructure Engineering Studies (CIES) at the University of Missouri-Rolla*, Rolla, Missouri.
- Mohsen, S. and Thomas, E. B. (1999). "Static and Fatigue Performance of RC Beams Strengthened with CFRP Laminates," *Journal of Structural Engineering*, Vol. 125, No. 6, pp. 613-621.
- Moran, D. A., and Pantelides, C. P. (2002). "Stress-Strain Model for Fiber-Reinforced Polymer-Confined Concrete," *Journal of Composites for Construction*, Vol. 6, No. 4, pp. 233-240.
- Myers, J. J., Murthy, S., and Micelli, F. (2001). "Effect of Combined Environmental Cycles on the Bond of FRP sheet to Concrete," *Proceedings-Composites in Construction, 2001 International Conference*, Porto, Portugal, October.
- Nanni, A. (2000). "Carbon Fibers in Civil Structures: Rehabilitation and New Construction," *Proceedings - the Global Outlook for Carbon Fiber 2000*, Texas, December.

- Nanni, A., Norris, M. S., and Bradford, N. M. (1993). "Lateral Confinement of Concrete Using FRP Reinforcement," *ACI SP-138*, Farmington Hills, Michigan.
- Okba, S. H., El-Dieb, A. S., El-Shafle, H. M. and Rashad, A. (2003). "Evaluation of Corrosion Protection for Reinforced Concrete Wrapped by FRP," *Proceedings - A New Era of Building, ICPCM2003*, Cairo, Egypt, February.
- Pantazopoulou, S. J., Bonacci, J. F., Hearn, N., Sheikh, S. A. and, Thomas, M. D. A. (1996). "Repair of Corrosion Damaged Concrete Using Advanced Composite Materials," *Second International Conference on Advanced Composite Materials in Bridges and Structures*, Montreal, Canada, pp. 457-463, May.
- Pantazopoulou, S. J., Bonacci, J. F., Sheikh, S., Thomas, M. D. A. and Hearn, N. (2001). "Repair of Corrosion-Damaged Columns with FRP Wraps," *Journal of Composites for Construction*, Vol. 5, No. 1, pp. 3-11, 2001
- Richard, A. B., and Geoffrey, C. M. (1999). "Fatigue Performance of Concrete Beams Strengthened with CFRP Laminates," *Journal of Composites for Construction*, Vol. 3, No. 2, pp. 63-72.
- Richart, F. E., Brandtzaeg, A. and Brown, R. L. (1929). "The Failure of Plain and Spirally Reinforced Concrete in Compression," *Bulletin 190, University of Illinois Engineering Experimental Station*, Champaign, Illinois.
- Roylance, D. and Roylance, M. (1976). "Influence of Outdoor Weathering on Dynamic Properties of Glass/Epoxy Laminates," *ASTM STP 602*, ASTM, Philadelphia, Pennsylvania, pp. 85-94.
- Samaan, M., Mirmiran, A. and Shahawy, M. (1998). "Model of Concrete Confined by Composites," *Journal of Structural Engineering*, Vol. 124, No. 9, pp. 1025-1031.
- Santhilnath, S. P. (2001). *Performance of CFRP Strengthened Reinforced Concrete Beams in the Presence of Delamination and Lap Splice*. M.S. Thesis, Department of Civil Engineering, University of Missouri, Rolla, Missouri.
- Shahawy, M. and Beitelman, T. E. (1998). "Fatigue Performance of RC Beams Strengthened with CFRP Laminates," *Durability of Fiber Reinforced Polymer (FRP) Composites for Construction*, B. Benmokrane and H. Rahman, Eds., Department of Civil Engineering, University of Sherbrooke, pp. 169-178.

- Schutte, C. L. (1994). "Environmental Durability of Glass-Fiber Composites," *Materials Science and Engineering R-Report*, Vol. 13, No. 7, pp. 265-324.
- Soudki, K. A. and Green, M. F. (1997). "Freeze-Thaw Response of CFRP Wrapped Concrete," *Concrete International*, Vol. 19, No. 8, pp. 64-67.
- Spoelstra, M. and Monti, G. (1999). "FRP-Confined Concrete Model," *Journal of Composites for Construction*, Vol. 3, No. 3, pp. 143-65.
- Stone, D., Koenigsfeld, D., Myers, J. J. and Nanni, A. (2002). "Durability of GFRP Rods, Laminates and Sandwich Panels Subjected to Various Environmental Conditioning," *Proceedings - Second International Conference on Durability of Fiber-Reinforced Polymer (FRP) Composites for Construction*, Quebec, Canada, May.
- Toutanji, H. A. (1999a). "Durability Characteristics of Concrete Columns Confined with Advanced Composite Materials," *Composite Structures*, Vol. 44, No. 2, pp. 155-161.
- Toutanji, H. A. (1999b). "Stress-Strain Characteristics of Concrete Columns Externally Confined with Advanced Fiber Composite," *ACI Material Journal*, Vol. 96, No. 3, pp. 397-404.
- Toutanji, H. A. and Balaguru, P. (1999). "Effect of Freeze-Thaw Exposure on Performance of Concrete Columns Strengthened with Advanced Composites," *ACI Materials Journal*, Vol. 96, No. 5, pp. 605-610.
- Toutanji, H. A. and Gomez, W. (1997). "Durability Characteristics of Concrete Beams Externally Bonded with FRP Composite Sheets," *Cement and Concrete Composites*, Vol. 19, No. 4, pp. 351-358.
- Xiao, Y. and Wu, H. (2000). "Compressive Behavior of Concrete Confined by Carbon Fiber Composite Jackets," *Journal of Materials in Civil Engineering*, Vol. 12, No. 2, pp. 139-146.
- Yang, X. and Nanni, A. (2002). "Lap Splice Length and Fatigue Performance of FRP Laminates," *ACI Materials Journal*, Vol. 99, No. 4, pp. 386-392.

